"AN ASSESSMENT OF THE FRACTURE TOUGHNESS OF TWO CAST AND WROUGHT STAINLESS STEELS

by

C.R. STOCK B. Tech.

A thesis submitted as a partial requirement for the degrees of Doctor of Philosophy

Brunel University November, 1971

SYNOPSIS

The crack-tip displacement concept has been applied to austenitic steels at 25°C and in the temperature range 400-800°C. The measurement of a maximum load crack-tip displacement in a notch bend test, provided a good indication of fracture-toughness since it included a portion of slow crack-growth. The ability of these alloys to tolerate slow crack-growth, and even to arrest cracks without becoming unstable, is of considerable engineering importance since many service failures originate at stress concentrations produced by welding of poor design.

Slow crack-growth was intermittent and highly dependent upon microstructural irregularities in the immediate vicinity of the crack-tip. The stress concentration at the crack-tip could be relieved (and the fracture-toughness improved) by localized plastic deformation. The degree of stress relief depended upon the locality and proximity of the various microstructural features as determined by the alloy manufacturing process.

The temperature sensitivity of the bond strengths of the various interfaces particularly in cast alloys, had a marked effect on fracture-toughness. This may have been the result of segregation of trace elements e.g. lead to the interface.

Above the equicohesive temperature, the greatest contribution to fracture-toughness was associated with the presence of large amounts of second phase particles in the boundaries.

In many cases, and particularly cast alloys, more than

one crack formed at the notch root. Only one of these cracks propagated to failure. Heterogeneous cracking of this kind (itself an indication of fracture-toughness), lead to difficulties in correlating an initiation C.O.D. with the macroscopic plastic properties of the material. Similar correlations were however possible with the maximum load crack opening displacement.

ACKNOWLEDGEMENTS

During the execution of this work, I have received assistance from a variety of sources. I wish particularly to thank Lloyds (Burton) Ltd., and A.P.V. - Paramount (Crawley) Ltd., for the supply of centrispun tubing; Professor J. Nutting (University of Leeds) for making available a scanning electron microscope; and those members of the technical and academic staffs of the Metallurgy Department, Brunel University who have provided assistance in numerous ways over the past three years.

It is a pleasure also to record my thanks to Professor C. Bodsworth for his generous and expert supervision; his experience has been invaluable to me.

Finally, I am indebted to my wife for transcribing an almost illegible draft into typescript, for providing continual encouragement throughout the tenure of this research, and for assisting the Science Research Council with financial support.

CONTENTS

CONTENTS

Chapter 6

CONCLUSIONS AND IMPLICATIONS

CHAPTER 1

INTRODUCTORY

1.1. THE PROBLEM

The development and successful marketing of cast alloys for high temperature service of types more familiar as wrought stock, has been hindered not only by the diversity and fragmentation of the foundry industry, but also by a natural reluctance among users to change to the unfamiliar. The economic saving offered by castings is not enough on its own to promote their more widespread use if potential user confidence in them is low.

In recent years general confidence in high temperature casting alloys for critical applications has hardly advanced despite significant improvements in casting techniques, non-destructive testing procedures, and the specification of minimum defect sizes. The causes of this paradox are easy to identify, but more difficult to rectify. To begin with, the foundry industry could rationalize its efforts and take a more positive lead and impose a more rigid degree of standardization and control on the rapidly increasing multitude of cast grades available. Many existing specifications have overlapping property ranges which are comparable to one another Thus a fair number of these could be quite easily deleted following a rationalization of compositions without necessarily impairing the range of properties which can be offered The situation to aim for is one where the number of basic or general high tonnage grades is kept to a minimum, thereby alleviating materials' selection problems among potential users, and allowing castings to compete on more level terms with possible wrought alternatives.

A second factor which reduces a potential users' confidence in many castings is the presence of large gaps in knowledge of the physical metallurgy and long term service behaviour of many of these alloys, which when set alongside the considerable volume of literature available for comparable wrought grades acts as the final deterrent. In particular, only a sketchy picture is available of the influence of casting practice on subsequent service behaviour, and indeed by wrought alloy standards, high temperature casting alloys are underdeveloped and primitive.

As an illustration, consider the apparent variable quality of some cast products, particularly the macro-grain pattern. This can be equiaxed, columnar or more usually, a varying proportion of the two. A user will clearly wish to know what effect (if any) this grain pattern has on subsequent service behaviour; and the absence of sufficient and reliable data on this point must inevitably lead to potential users remaining suspicious of such castings. It is the foundry industry's responsibility to resolve the question. either by showing convincingly that the form of the macro-grain is immaterial, or if it is not, to modify casting techniques to consistently produce the grain pattern found to be most beneficial This point will be re-examined later.

It is frequently pointed out that wrought materials invariably display improved performances over equivalent cast grades for many applications. Whilst the truth of this statement is not disputed in principle, it does not dispel the unpalatable fact that a number of components

enter service "over designed", often because the cast alternative is not seriously considered. Rather it suggests the enormous potential field which may be opened to cast alloys once they have been more fully developed. On economic grounds alone, the importance of realizing this development potential is undeniable.

In particular there are large savings to be made in production costs and delivery times, and in addition the economic production unit is much smaller than that usually found in the wrought field. Thus small melt sizes can be viable and stock-holding costs can be low. To maintain these advantages, high tonnage general casting grades should rely on as few compositional changes as possible for their desired property ranges, whilst elaborate modifications to casting cycles should generally be reserved for specialist applications. This should present little difficulty in practice since compositional ranges are no longer restricted to those which can be hot worked. Indeed, certain properties may be easily obtainable which cannot be competitively offered by wrought grades.

Applications which require a particular combination of properties or property extremes, and which generally call for much smaller quantities of metal, should be equally attractive to the cast manufacturers. Here the smaller economic production unit ensures that more expensive modifications to the casting process to obtain the desired properties, can be contemplated without necessarily making the final product more expensive than any possible wrought equivalent Such modifications could include post-casting

heat-treatments, remelting cycles during cooling, and (where component geometry permitted it), cooling under restraint to promote uniform precipitation processes by imposing a measure of hot straining. Thus, where either a casting or forging could be used, availability, economy and adaptability of properties to engineering use, must all be very carefully examined.

1.2. CONCLUSION

Many worthwhile advantages may be obtained by a shift of emphasis from wrought to cast alloys for high temperature use. The problem is to establish castings as both realistic and reliable alternatives against the present lack of information about them. An answer is for the foundry industry as a body to grasp the initiative and continue rationalizing the number of its high tonnage standard products with essentially similar properties, and to capitalize more effectively on the remarkable flexibility of the much maligned casting process. It can only achieve this by engaging more actively in research and development, the final aim of which must be to provide customers with both good castings and evidence convincing enough to instil the necessary degree of confidence in their use.

1.3. SCOPE OF CURRENT RESEARCH

It has been suggested previously, that the possible use of cast alloys for certain high temperature applications is frequently not considered because of a lack of metallurgical knowledge about them, even though the geometrical shape required may be more economically produced by a casting process. Thick-walled tubes provide a good example. These

components are quite cheaply produced by a centrifugal-casting process, but require much additional expense to manufacture as wrought stock.

This study considers centrifugally-cast and derived wrought austenitic steels of the 18Cr/8Ni/1Nb formula, of the type employed as high temperature, tubular pressure-vessels in reformer plant. These plants, used extensively by chemical, gas and other industries, operate under conditions "extremely challenging to the materials of construction"(1) with temperatures in the range 650-750°C and higher, and pressures greater than $2MNm^{-2}$(app.300psi). Cast and wrought austenitic steels which can withstand these conditions are available, but the occurrence of costly failures in practice, demonstrates only to forcefully, that the behaviour of heat-resistant alloys under these conditions is far from understood.

The core of this study, is the development of a crack tolerance or toughness test based on the crack-opening-displacement concept. The test is designed to simulate crack initiation and crack propagation behaviour under conditions similar to those found in service. Thus crack propagation has been studied under conditions of stable or slow growth, and its measured contribution to toughness assessed fractographically and related to the microstructual features characteristic of each manufacturing process. The crack-opening-displacement test is used specifically to highlight differences in the cracking characteristics of each as-received microstructure, since the attainment of controlled amounts of slow crack growth in the more

conventional tensile test is difficult to achieve because of the intervention of a mechanical instability.

The work reported here forms part of a larger study[2] concerned with creep and stress relaxation behaviour, which includes a detailed study of the microstructural changes that occur after prolonged periods of exposure at elevated temperatures. These aspects are, therefore, not considered in detail in the present work, although summaries of such portions where pertinent to the discussion are included in the text and clearly acknowledged.

1.4. ALLOY CHOICE

The original casting grades for high temperature service, particularly for reformer tubes, were the more expensive high alloy types e.g. 18Cr/37Ni, and 25Cr/20Ni. The high carbon contents associated with these steels rendered them unsuitable for hot-working, so to facilitate a direct comparison with an equivalent wrought grade attention was focussed on the niobium stabilized 18Cr/8Ni base composition. These steels are not only easy to hot-work, but in accord with comments made earlier, the metallurgical response of the cast state is poorly documented, compared with that of the equivalent wrought grade, and thus they make an ideal choice for this study.

Heat-resistant steels of the 18/8 type were developed originally as corrosion-resistant alloys for use at temperatures below the creep range. They were available only as wrought grades with limits imposed on carbon content because of poor hot-workability and difficulties in welding. A major step in their development was the addition of niobium

or titanium, together with a reduced carbon content to improve corrosion-resistance and reduce susceptibility to intergranular attack by weld-decay. Over the years, as service requirements extended step by step into the creep range i.e. 600-750°C; it was discovered, almost by accident, that existing wrought low carbon 18/8 - Nb or Ti stabilized-steels were adequate for these applications. Thus they were established as high temperature service materials. Curiously, whilst considerable attention was devoted to the selection of alloy type, the method of manufacture was not given the consideration it warranted. However, evidence is now growing that an increased use of castings in the high temperature field, may be metallurgically as well as economically justified.

CHAPTER 2

REVIEW

2.1. INTRODUCTION

The operating requirements and response of high temperature alloys in steam-reformer plant have been well described elsewhere[3-6], and it is superfluous to repeat the details here. These sources[3,6] are unanimous in demonstrating that interdendritic regions in centrifugally (or statically) cast stainless-steels display pronounced tendencies for interfacial seperation of one kind or another, under a wide spectrum of load and temperature conditions. Thus the characteristics of the seperating interfaces are crucial factors affecting tube life. The same comments apply to wrought steels in and above the equicohesive temperature range. Thus it is important that a thorough understanding is achieved of the way in which these interfaces behave in service, and how they respond to changes in external conditions.

The review which follows is divided into two sections. Section A is an attempt to assess the metallurgical significance of the various types of interface present as reflected by their formation in manufacture and subsequent modification in service. In section B some mechanisms of interfacial seperation are discussed together with possible criteria for fracture.

SECTION A

INTERFACE FORMATION IN MANUFACTURE AND MODIFICATION IN SERVICE

A.1. GENERAL

The first section of this review begins with a discussion of the microstructural interfacial zones as they form during solidification, with particular reference to the problem of casting segregation and the macro-grain pattern. This is followed by a brief consideration of the effect of hot-working processes on the cast microstructure, in an attempt to highlight the major metallurgical differences between the two production processes. The review moves on to examine those processes and effects which could modify the character, number, size and distribution of interfaces in service. Included here are aspects of precipitate nucleation and growth, segregation and the relief of strain and surface-energy.

In this section of the review reasons are suggested as to why tubes of identical chemical composition produced by different manufacturing processes, should display such dissimilar behaviour. The treatment is generalized, but where examples from the literature to illustrate points are known for austenitic steels, these have been quoted.

A.2. FORMATION OF INTERFACES IN MANUFACTURE

A.2.1. Solidification

The solidification process in alloys is one of continual change, both physical and chemical. This, together with the complex chemical phase relationships in alloys with a finite freezing range, produces wide compositional

variations throughout a solid casting. Under commercial casting conditions, diffusion rates fail to maintain equilibrium proportions of solute and solvent at the reaction interface. In addition, the rejection of solute over the area of the interface is seldom uniform. Thus an accumulation of either solute or solvent at the reaction interface takes place, which is a characteristic of dendritic growth. Such heterogeneity is more marked as the freezing-rate increases. Concurrently, microsegregation occurs, promoted by the lateral transport of solute to the various growth fronts, thereby increasing the number of regions of varying solute composition. Some of these regions may be so far removed from equilibrium composition, that phases form which are not predicted by the equilibrium diagram. The final segregation profile, although complex, is classified according to the stage of its formation in the dendritic growth process(7).

a) Segregation between primary dendrite arms.

b) Segregation between secondary and tertiary arms different from a) above.

c) Differences in cross-section within an arm due to distortion in cross-section because of branching i.e. intradendritic segregation, and a gradual thickening of the structure with decreasing temperature.

d) Possible local areas within the various inter-arm spaces having differences in concentration as a result of interactions among the various branch orders.

Casting segregation of the kind described is not necessarily harmful and may possibly exert a beneficial influence, as for example on creep resistance. It has been pointed out[8] that dendritic segregation is unlikely to anneal out very rapidly at the service temperature, and is almost certain to be associated with differences in lattice parameter, thus providing an inherent hardening effect in the boundary regions vulnerable to creep rupture.

Macro-grain Size and Pattern:- The problem of the macro-grain size and pattern, with respect to its influence on high temperature service behaviour, is a difficult one to analyse since attempts to alter one variable inevitably produce many unquantifiable secondary interactions as well. Theoretically, a coarse cast grain-size for a high temperature application implies a decreased likelihood of having many grain-boundaries orientated transversely to the maximum applied stress. Presumably, this reduces both the creep rate and the probability of premature failure by creep rupture. On the other hand, altering the grain morphology changes the segregation pattern; whether adversely or not is at present unknown.

In the case of the centrifugal-casting the problem takes on an additional dimension. Bore porosity is probably the most odious feature of this type of casting and, since it is presumably reduced by unidirectional solidification, the type of structure required is that where little or no freezing occurs from the bore. In other words a predominantly columnar grain is needed.

It is important also to have at least some idea of the

effect on service behaviour of differences in the ratio of interdendritic to grain-boundary segregation. Again this depends very much on whether the grain pattern is equiaxed or columnar. Experimental observations[9,10] indicate that a non-dendritic interface displays a lower level of solute enrichment than that of a well developed dendritic one. Thus, in the final liquid to solidify between two approaching grains, interactions of the solute-rich layer associated with each grain, will vary according to the degree of dendritic growth present. Hence for fast growth rates which are primarily dendritic, segregation tends to be interdendritic rather than intergranular; where-as for the slow growth rates usually associated with a reduction in dendritic behaviour, there is more time for solute to diffuse away from the dendritic interface. The result is increased segregation in the last liquid layers to freeze.

The extent of the partitioning of segregate between dendrites and grain-boundaries is difficult to quantify, but must clearly depend on the type and amount of solute as well as the growth variables: rate, gradient and concentration. The practical effects of segregate partitioning are associated with its influence on the relative merits of columnar and equiaxed grain structures for high temperature applications. In the latter, grain-boundary segregation should be greater since growth is slower and takes place at a slightly higher temperature than that for columnar growth. In columnar structures, grains grow essentially parallel to one another so any interaction is between dendrites in neighbouring grains.

Role of Impurities:- Segregation in commercial alloys may also be influenced by the presence of impurities. Thus in an alloy steel, increasing carbon content increases chromium segregation, whilst in the same alloy the addition of 0.12% arsenic induces nickel segregation[11]. An anlysis of compositional effects on segregation is a difficult problem, but important factors must surely include interaction among solutes, the distribution coefficients of the various components and the proximity in composition of any terminal phase boundaries. This latter factor is significant, since it could lead to only slight differences between grain-boundary and interdendritic segregation once the limits of terminal composition have been exceeded within the dendrite arms.

Weld Metal:- Many of the comments made above could well apply to weld metal, although a full consideration of the welding process is beyond the scope of the present review.

A.2.2. Hot-working

Homogenization of cast alloys by high temperature annealing treatments, is easier to achieve when concentration gradients are high e g. in castings or ingots with a fine dendrite arm spacing. Hot-working may or may not assist the process. Most hot-working operations impart a fair degree of directionality to an alloy which only serves to re-distribute segregate rather than remove it, since compression of segregated regions in one direction e.g. the primary arms, produces a corresponding seperation in the secondary arm direction. Nevertheless, the high temperatures required for hot-working will tend to reduce segregation,

although they are generally not employed for sufficient lengths of time to eliminate all segregation effects. In allegedly single phase alloys, segregation of alloy elements may induce the formation of a second phase, or alternatively increase the proportion of the second phase already present in a duplex alloy. This may be especially significant in the context of the present work, when it is recalled that the ferrite contents of many cast duplex stainless-steels decrease on hot-working[12].

Further effects of hot-working include the dissolution and subsequent partial re-precipitation of most second phase particles in a random manner throughout the matrix, with or without directionality depending upon the hot-working process. There is usually the complete replacement of the cast grain-structure with a new and more regular one by recrystallization processes. Thus the grain-size of a wrought steel is usually finer than that of its cast counterpart. However, it is perhaps slightly ironic to record, that the various metallurgical and compositional features deliberately sought in high temperature service alloys for both deformation resistance and structural stability, are those which reduce hot-workability as well; though it is fair to add that many of these effects are minimized at the much higher temperatures required for successful hot-working.

As a result of these high working temperatures, and providing post-working cooling rates are fairly rapid, matrix supersaturation will be higher than that found in castings of the same composition. Subsequent ageing

treatments tend therefore to produce uniform dispersions of precipitates throughout the matrix, rather than promote the more extensive grain-boundary area precipitation common in cast grades.

A.3. INTERFACIAL CHANGES IN SERVICE

This analysis has so far considered the nature of the cast and wrought states, by contrasting the major differences between the two types of structure which are likely to affect elevated temperature behaviour in the as-received condition. However, structures are subject to a continual modification in service either by the formation of new interfaces or by changes to existing ones. The extent of these changes is determined by external factors such as temperature, time at temperature and loading condition, and by internal factors such as the level of matrix supersaturation and the degree and type of segregation. In this section some of these microstructural changes are considered together with possible rate-controlling influences. The influence of an externally applied load on the type and magnitude of these changes, although clearly relevant to high temperature service behaviour, is outside the scope of this dissertation, but is considered in the overall study[2] of which this forms a part.

A.3.1. Factors Affecting Interface Formation and Growth in Service

There are several modes of stable interface formation in solids, each requiring a definite energy to activate them. This energy may be reduced in the presence of non-equilibrium structural discontinuities such as grain-

boundaries and dislocations, which therefore become preferred sites for precipitation. Hence initial differences in cast and derived wrought alloys of the type, number and distribution of these irregularities, together with the influence of segregation upon them as effective precipitation sites, will have a profound effect on subsequent service behaviour. In addition, the significance of the dominating defect in the nucleation process is determined largely by its ability (if any) to nucleate a series of defects over a protracted period, or whether nucleation is in fact limited by site saturation or lack of local supersaturation.

A.3.1.1. Strain-energy

The uniqueness of the strain-energy term in solid-state reactions is of vital importance, and arises from any volumetric misfit between matrix and precipitate. The strain-energy largely governs the growth morphology of second phases and therefore the magnitude of the precipitate matrix interfacial area.

Its importance in many grain-boundary reactions is well illustrated by the precipitation of FCC niobium, titanium and vanadium carbides and nitrides in austenitic steels. Although these processes occur in a number of different ways, precipitates always form first at dislocations or grain-boundaries[12-18]. Precipitation occurs intra-granularly at dislocations, because the elastic energy produced by the large misfit between precipitate and matrix can be minimized[19]. The same argument applies to grain-boundary precipitation and thus surface-energy

effects become subordinate to the relief of strain-energy.

A further illustration of the strain-energy effect and the ability of a structural defect to nucleate a series of precipitates, is found in stainless-steels, and is the so-called "stacking-fault precipitation"[13,20,21]. Here, carbides precipitate on a moving partial dislocation by a process of repeated nucleation. There is a large increase in atomic volume when carbides of the NbC type precipitate from an austenite lattice, and the driving force (believed to be chemical in nature)[22], is associated with the resultant vacancy deficiency. This volume change must be accommodated before carbide growth takes place. On undissociated dislocations this occurs by the formation of prismatic dislocation loops, but in dissociated regions vacancy absorption causes the rapid climb of the Frank partial dislocation, leaving it available as a site for repeated nucleation. Thus the stacking-fault, although an obvious feature of this type of nucleation, is entirely incidental to the basic mechanism[13].

It appears then, that the stacking-fault energy and carbide type are important parameters influencing this kind of precipitation[23]. Stacking-fault energy reflects the degree of dissociation of dislocations and hence the ease of dislocation climb, whereas carbide type determines the degree of atomic misfit and thus the level of strain-energy. Austenite has only a slightly larger atomic volume than $M_{23}C_6$ type carbides, so the vacancy deficiency is insufficient to induce dislocation climb; but the precipitation of niobium carbide for example, with an atomic

volume about one-third greater than austenite[24], frequently leads to repeated nucleation on dislocations.

A.3.1.2. Surface-energy

The relief of strain-energy is of course only one consideration. The relief of suface-energy is important also, particularly in its vulnerability to segregation processes in its efforts to reach a minimum value. Thus grain-boundaries of the matrix phase become available as sites for precipitation when the surface-energy requirements for nucleation are less in that boundary. This becomes increasingly important as the surface-energy component of the free-energy of nucleation increases; for example at low supersaturation or where structural barriers inhibit the formation of a low energy interface between matrix and precipitate[25]. In cases where intragranular precipitates are metastable the grain-boundary precipitate often becomes the more stable form, because the thermodynamic driving force for grain-boundary precipitate growth is greater than that for the matrix precipitate. Furthermore, the rapid supply of solute by grain-boundary diffusion promotes rapid growth[26] and may cause a vast deterioration in mechanical properties. Embrittlement of this type is likely in cast reformer steels where massive grain-boundary carbides have already formed during the casting cycle. The possibility of preventing further grain-boundary diffusion and precipitate growth by "fouling" the boundary, may well be precluded by the casting process having already induced segregation of harmful solutes to the interface. Guidelines in choosing the correct additions to bring about

the required effects, are virtually non-existent, and thus alloy development in this field is reduced to a trial and error basis.

The need to examine the detailed boundary structure cannot be over-emphasized. It is important that the effects of the boundary on the kinetics of nucleation and the distribution of nucleation sites, be positively established. For example, studies of $M_{23}C_6$ precipitation in austenitic steels[27,28] have shown geometrically shaped plates of carbide precipitated at isolated sites in grain-boundaries. The particle shape and density varied from boundary to boundary. Detailed examination suggested that these plates grew along specific matrix directions[27], which lay in or close to the boundary plane. Such a conclusion is consistent with the presence of areas of "good fit" in grain-boundaries[29].

Accelerated grain-boundary precipitation is likely if the solute taking part in the precipitation has already segregated to this region during manufacture. Even if the segregating atoms take no part in the reaction they may none the less hinder it by a "blanket" mechanism. Possibly, the retardation effect of boron on many grain-boundary nucleated reactions, is an example of this, although the reasons why the nucleation sites are "poisoned" are not clear.

A.3.1.3. Segregation

As already indicated, segregation processes and their effects on interfaces, are of prime importance if those interfaces take part in any subsequent transformation or

seperation process.

The most obvious form of macro-segregation is the coring of cast structures produced by non-equilibrium freezing rates. Compositional anomalies of this type are responsive to the usual laws of thermodynamics, and thus have a tendency to anneal out, although service temperatures are rather low to make this much of a reality. Other types of segregation actually occur in service and are caused by processes such as solute-vacancy couples moving towards or away from interfaces and boundaries. This type of solute enrichment is frequently encountered and often quite disruptive in its practical effects. It is likely to be of importance in reformer operation because temperature gradients are present, and continual precipitation-ageing processes are taking place during service.

This problem of interfacial or grain-boundary brittleness has at least two aspects. First, why do impurities segregate to these boundaries? Second, once at the boundary, why do these impurities promote fracture along it? It is the purpose of this section of the review to discuss these questions.

Segregation in service takes place because many interfaces possess a high surface-energy component in the free-energy term. Thus it is to be expected that any solute which decreases this term will concentrate in the region of the interface or boundary, providing that the corresponding change in strain-energy does not increase the total free-energy. Thus those solutes raising the interfacial-energy will be displaced from the interface, whilst those

lowering the energy will locate preferentially on that surface. Hence the segregated state may represent an equilibrium state, with a lower free-energy than that of the unsegregated state, and in this sense is permanent, with the equilibrium subject only to the usual constraints of time and temperature. Presumably, the more imperfect a boundary region is, the greater will by the degree of solute segregation. It remains an unfortunate fact that solutes reducing the surface-energy of any interface frequently lower its cohesive strength as well. Furthermore, there is no universal means of predicting the effects of various solutes on interfacial-energy from known atomic parameters, although maximum solid-solubility does give some guide[30].

It is tempting to treat wrought and cast stainless-steel reformer tube materials, in terms of this "imperfect boundary or interface" theory by speculating that boundaries in the cast steels contain more imperfections than their wrought counterparts, other effects being equal. Thus the degree of persistent segregation would be greater, and its influence on subsequent behaviour more profound. In practice it is impossible to ignore these other effects. Complications may arise from a variety of sources, for example, competitive segregation; the probability of the segregating solute affecting matrix solubility for other solutes; the formation of segregating solute complexes; solute effect on reaction kinetics, or problems of compensating solute segregation where a small and large atom segregating simultaneously might compensate for each other[31].

Bubble raft experiments[32] suggest that a grain-boundary contains "holes" of many sizes in which solute atoms may locate (segregate) if their size factors are right. Thus the interfacial-energy could be lowered if grain-boundary interstices were more completely filled, by having several solutes present of varying atomic size factor. Such a process could operate (in the absence of solute interactions), by expelling mechanically harmful segregating elements, and replacing them with elements which plug the boundary interstices more effectively. The action of lithium in bismuth embrittled copper has been cited as a possible example[33].

The tendency for solutes to be expelled from a lattice as measured by their maximum solid-solubilities in binary solutions, correlates inversely with interfacial activity for a number of systems[30], thus adding credibility to the above model. As a result, low solid-solubility may be a useful pointer to increased interfacial activity and possible embrittlement and, by analogy with ferritic systems, the action of oxygen, sulphur, phosphorus, bismuth, lead and tin would be deserving of attention in this respect. The inverse relation further suggests that a motivation for equilibrium segregation could be the relief of lattice strain-energy. These comments apply of course to interfaces between chemically similar phases. However, interfaces are always found between chemically dissimilar phases which are of particular interest here especially in cast steels, where the incidence of that type of phase boundary in interdendritic regions is high.

The segregation problem is difficult to analyse unequivocally because of the abrupt change in composition at the interface. Hence a considerable volume of work has been reported on particle ripening processes studied as a function of precipitate-matrix coherency; but the case of massive precipitate ripening processes of the type found in cast austenitics in the absence of coherency, has received but little attention. This is not really surprising as the effort required to resolve fully this kind of problem, is out of all proportion to the practical benefits to be gained, and it is simpler (and cheaper) to deal with problems as they arise, largely on an empirical or trial and error basis.

Considering the problem as a whole, precipitates are preferentially located in grain-boundary regions in concentrations and dispersions widely at variance with the conditional equilibrium values (whatever they may be); with chemical interactions occurring continuously on the surface producing stable compounds and precipitate growth. The driving force for these processes is initially, radically affected by the degree of chemical inhomogeneity caused by non-equilibrium freezing, and this, together with the grain-size, sets the level required for interdiffusion of solute atoms. Geometrical locking effects, the relative shear strengths of the interface and its components, and the temperature dependence of the interfacial-energy are also relevant to service behaviour. A qualitative indication of the significance of these effects within the sphere of the present research, has been attemp-

ted by a study of the interface after seperation using fractographic techniques. Further discussion of these aspects is given later when work relating fracture appearance to component history is presented.

A.3.1.4. Vacancies

Vacancies are an important feature of a large number of high temperature enrichment processes. The initial non-equilibrium vacancy concentration within the alloy may be produced by mechanical deformation, irradiation, precipitation and temperature changes. Typically, vacancy-solute couples can form and move to and from interfaces under a temperature gradient and alter the mobility of an interface. Hence indirectly vacancy flow and interface mobility may be considered to constitute a form of segregation by means of the so called "solute-drag" effect(34), particularly in more concentrated solid-solutions. The magnitude of this kind of effect is influenced by solute partitioning between the matrix and the boundary, whilst the diffusion coefficient of the solute controls the kinetics, and is important with respect to the rate at which the interface is moving. Elements with a strong tendency to segregate at a boundary or interface have the greatest effect on the mobility of that interface. Thus solutes with low diffusion coefficients strongly affect slow moving interfaces, whilst more rapidly moving interfaces are interfered with most, if solute diffusivity is high.

Solute-vacancy transfer processes require sources and sinks in order to function. As these are readily available at high activity interfaces, it is quite usual

to find gradients in such defects developing at interfaces. Thus interfaces and boundaries are sites for direct or indirect solute segregation by vacancy transport mechanisms, which continue to operate until the total concentration of vacancies reaches some new equilibrium value for the conditions imposed.

A.4. SUMMARY

Microstructurally, cast and wrought stainless-steels contain a variety of interfaces or boundaries composed of regions between chemically and structurally similar phases e g austenite to austenite· regions between chemically similar but structurally dissimilar phases e.g. austenite to delta-ferrite; and regions between chemically dissimilar solids e.g. austenite to metal carbide or non-metallic inclusion. The number and distribution of these phases is dependent upon the method of manufacture. However, all these interfaces, like many other defects or discontinuities in crystalline materials, invariably behave as sinks for impurities or secondary components. The movement of secondary components may produce new phases or change the proportion of existing ones. Equally, enriched zones of certain characteristics and influence may also develop, whose practical significance is manifest in their effects on the magnitude of the forces binding the interface, and thus on the stresses required to seperate them.

Any interface within a crystalline solid may be thermodynamically represented by its free-energy, a quantity reflecting the degree of atomic mismatch or disorder at that point. The magnitude of this free-energy is adjusted by

temperature changes, interface orientation and local segregation. Local segregation varies continuously, with solute atoms diffusing from the matrix towards highly defect regions in the interface A given manufacturing process establishes the segregation pattern by producing characteristic types of interface. These are continuously modified in service by mechanisms seeking to bring the interfacial free-energy to a minimum. Interfacial interactions and constraints which affect the system as a whole also occur, and may combine to inhibit the attainment of an absolute minumum value of free-energy. Instead, a series of provisional minima are substituted for each of the constituent interfaces, which are subject to the usual kinetic restraints of temperature and time at temperature. Thus the interfacial zones exist in a metastable equilibrium determined largely by the history of the component of which they are a part.

SECTION B

INTERFACIAL SEPERATION AND CRITERIA FOR FRACTURE

B.1. GENERAL

During the useful life of a high temperature component, the integrity of the microstructural interfaces is continually threatened. Eventually a stage is reached where it is no longer possible to maintain cohesion between the features constituting the interface, and the formation of free surfaces is energetically favoured. The definition of a useful life is necessarily arbitrary because it depends on the particular application as well as the design criteria. This study considers the formation and propagation of stable

cracks as a function of microstructure for rising load conditions. Thus interfacial seperation mechanisms are reviewed primarily for these conditions, with a view to establishing suitable criteria of toughness and ductility, to which correlations with the propagation controlling microstructural features can be made.

B.2. INTERFACIAL SEPERATION

Two criteria must be satisfied before interfacial seperation takes place. First, the energy balance must favour the creation of free surfaces; and second, an atomic mechanism must be possible whereby the seperation process can operate. These criteria reflect the influence of external factors such as temperature, level of stress, strain-rate and strain in the metal, which interact with microstructural features and modify both the nature and extent of the local deformation that either preceeds, or occurs in conjunction with fracture. Thus the fracture process and the events leading up to it, are highly heterogeneous. Because of this marked heterogeneity, it is imprudent to assign specific critical conditions and features identified as fracture-controlling events in one system to another different, though related system. An exercise of this nature is fruitless unless incorporated with practical experience of the system involved, and may be more usefully discussed after current results have been given.

This section is confined to an outline of some possible mechanisms of interfacial seperation and fracture which are likely to be important, together with a brief consideration of how chemical segregation may affect them.

B.2.1. Equicohesive Temperature Range

The most important external variable to the fracture process is temperature, because it exerts a large influence on the grain to grain-boundary strength ratio. This ratio has a value of unity at the equicohesive temperature. Below this temperature, seperation processes are essentially transgranular, whilst above it, the intergranular mode predominates. The spread of the equicohesive temperature range is affected by such factors as strain-rate and grain boundary area.

An interesting situation arises with centrifugally-cast stainless-steels because failure paths are reported[3,6] to be intergranular, or rather interdendritic at all temperatures. At first sight this observation appears to make nonsense of the concept of an equicohesive temperature as just described. However, it must be remembered that equicohesivity is not a fundamental property, particularly in heterogeneous alloys and thus is not attained at a unique temperature. It occurs over a fairly wide range of temperature and in this sense may be considered analogous to a recrystallization temperature and therefore dependent upon the initial microstructure. Thus the diversity of solidification and decomposition products within the dendrite interstices of castings, covers a large enough interfacial area so as to dominate the apparent macro-crack appearance and cause it to pass off as "intergranular fracture", although interfacial fracture is a more accurate description. It is probably more correct then to talk not of an equicohesive temperature for an alloy as a whole, but

of an equicohesive temperature for each constituent interface. Thus once the equicohesive temperature of the relatively 'clean' boundaries of the wrought steels is exceeded, the influence of the type, number and morphology of the grain boundary region interfaces in cast alloys may be most usefully contrasted with their wrought counterparts. Below this temperature, the comparison is of course between two predominantly differing fracture modes, and the usefulness of any such comparison is limited.

A final general point invokes the influence of local segregation patterns at microstructural interfaces, on the extent of the equicohesive temperature range. These patterns are likely to differ widely between manufacturing processes and complicate the direct comparison suggested earlier.

B.2.2. Fracture Mechanisms

A fracture mechanism is composed of the interactions between a number of processes or stages in the seperation sequence, each of which may differ in its relative importance from one material configuration to another. As an illustration of such a sequence, pores or micro-cracks in ductile fracture may be nucleated by a number of processes; for example by dislocation interactions, by inclusion fracture or by decohesion of second phases from the matrix. Subsequent pore growth may then be by plastic flow or local fracture along grain-boundaries, and if deformation becomes localized, due for example to a mechanical instability, then growth is accelerated and cracks are formed. The pores or holes may elongate and rotate and tend to overlap, and

depending upon the strain-rate sensitivity of the alloy, subsequent crack growth may be stable or catastrophic.

An increase in test-temperature could well alter specific effects such as work-hardening response or matrix-interface cohesive strength and produce a quite different set of interactions. Clearly, a variety of criteria are required to characterize each stage, and where a number of these processes occur simultaneously along a crack front, some combined form of fracture criterion is needed.

Below the equicohesive region, the ductility of a metal in tension is largely controlled by the presence of second phase particles; for a random dispersion of spherical particles it is frequently stated[35] that it is the particle volume fraction rather than the particle type and its mechanical properties, which ultimately limits the ductility. Irrespective of their distribution, some of these second phase particles provide sites for void formation. These voids ultimately coalesce to form dimples, with the initiating particle frequently observable at the base of the dimple on the final fracture surface. Coalescence in ductile fracture may be made somewhat easier by a low strain-hardening capacity[36,37], whilst the strain-hardening capacity itself is sensitive to the size and distribution of the second phase particles i.e. whether dislocations are able to climb around particles or whether it is necessary for them to cut through. The hardening response may be further complicated by the ability of second phase particles and inclusions to act as sites for the generation of dislocations[38,39].

The role of second phase particles as ductility-limiting microstructural features may, very crudely, be considered in terms of the particle-matrix interface, as it is the interfacial activity that determines both the strength of an interface and the degree of embrittlement in the component as a whole. Consequently, where particles are highly segregated and preferentially located in boundaries, as they are in coarse grained cast steels, then they frequently have a greater disruptive effect on deformation and relaxation processes, simply because the boundary provides an interconnecting path between precipitate-associated cracks.

At and above the equicohesive region, there are other possibilities to consider in addition to pore development and the role of particles just outlined. These depend upon the temperature and the level of stress, and are responsible for the appearance of cracks in grain-boundaries, although the mechanisms by which grain-boundary cracks nucleate and grow at elevated temperatures are not well understood[40-44]. Higher temperatures and lower stresses are usually associated with the formation of rounded cavities on grain-boundary surfaces, which grow and merge to form cracks[42-44]. Conversely, at higher stresses and lower temperatures, wedge-shaped cracks appear and seem to emanate from triple-points[41]. However, both these phenomena become more pronounced over extended periods of time and a detailed consideration is thus outside the scope of this study.

Additional sites for void formation may be provided

by non-metallic inclusions where poor interfacial cohesion leads to easy decohesion under the action of tensile stresses. Similar processes may also occur with a wide range of second phase particles other than the conventional non-metallic inclusions. Indeed, intergranular ductile fracture by carbide decohesion can be induced around the boundaries of austenite grains following suitable heat-treatments[45].

For good creep resistance, precipitates must therefore resist shear forces and possess a low energy particle-matrix interface to promote thermal stability[46]. Accordingly, efforts in cast alloy development for high temperature applications, must be directed at isolating those elements which segregate to interfaces and, by raising the interfacial activity, reduce creep-ductility.

B.2.3. Effect of Segregation on Interfacial Seperation

Generally, systems that display a low interfacial activity are ductile, whilst a high interfacial activity is synonymous with intergranular or, in cast alloys, interdendritic embrittlement e.g. iron-phosphorus and iron-nitrogen alloys are typical. There is reasonable agreement in the literature that elements provoking interfacial decohesion are also those most prone to segregate. The quantitative connection however, between intergranular weakness and grain-boundary segregation, has proved more difficult to establish; and recent evidence[47] suggests that the value of the interfacial-energy may be rather less important than previously thought. Nevertheless, impurities whether as trace additions or residuals, greatly modify the value of the interfacial-energy, either by the

formation of interfacial films, or by the nucleation of fine precipitates which provide stress-concentrations for the subsequent nucleation of cracks[48,49].

An interesting follow up[30] to the segregation question, is the action of certain elements which may replace harmful solutes at grain-boundaries and other interfaces and enhance ductility, possibly by allowing slip transfer across boundaries during deformation. An illustration of this may well be the action of molybdenum in mitigating temper-brittleness. In any complex alloy, the experimental difficulties in isolating such an effect are enormous. Thus whilst no references to such an effect citing examples in stainless-steels have been found, this is not taken as an indication that harmful solute replacement at boundaries in these alloys is non-existant.

B.3. FRACTURE CRITERIA

The final and most pertinent area to this research which must be considered before presenting and analysing fresh experimental data, is the selection and interpretation of suitable criteria of toughness and ductility. These must be capable of correlation with fracture-controlling microstructural features and further extension to include service conditions.

The influence of microstructure on mechanical behaviour is of course quite crucial, because complex interactions are known to occur between certain microstructural features and plastic flow mechanisms, both in manufacture and during service. An arbitrary classification of these microstructural aspects may be made according to their effects, although

features listed as having an effect in one class could equally well have an influence in the second. Thus the first group of features are those which control the seperation mechanisms, and the second comprises those that influence the rates at which embrittling processes can occur. The action of both groups is reflected externally by a reduction in the measured value of the final fracture strain. This fracture strain has an important influence on the toughness of the alloy.

The term toughness reflects the capacity of the material to deform locally in the vicinity of a crack-tip, and is really a measure of the ability of the alloy to resist fracture.

Although the qualitative association between toughness and fracture strain is well established, there is nevertheless an important distinction to make between uniform-elongation as measured in a tensile test, and the toughness previously defined. The former parameter is essentially a reflection of a material's capacity for strain-hardening under uniaxial load conditions. This may be expected to bear little direct relation to the fracture-toughness, because the latter is more closely connected with the work required to create free surfaces, which in ductile fracture is affected largely by the local stress-state.

Important objectives of this study are to determine and isolate the microstructural unit or units over which fracture takes place, and to distinguish the contributions to flow and fracture of the individual constituents within

the alloy. Ideally, these objectives are best realized by incorporation into a single fracture criterion. However, it is unlikely that a universal criterion will apply because of the complexity and range of microstructures studied. An additional requirement for the criterion is that it must be capable of interpretation and extension into the field of high temperature behaviour.

* * *

Many approaches to the fracture problem, particularly in ductile metals, rely heavily on the theories of continuum mechanics. They offer little enlightenment as to how materials fail microscopically, and provide virtually no guidance in selecting microstructural modifications to improve resistance to fracture. This difficulty is to some extent circumvented by the application of certain ideas of continuum mechanics and continuous dislocation theory to the vicinity of the crack itself, where the microstructural constituents rather than the stress-state, control fracture nucleation and growth. Of particular significance is the opening mode crack-tip displacement concept, describing ductile fracture in terms of a series of micro-tensile specimens fracturing at the crack-tip[50-52], and the shear mode ductile fracture concept developed in terms of a theory of hole or void coalescence[53,54].

B.3.1. Crack-tip Displacement

The usual definition of crack-tip displacement[55], relates to the plasticity controlled seperation experienced at a crack-tip upon application of a load. The displacement is considered to have attained a specific value at

the moment of crack initiation. Crack-growth then takes place by the fracturing of successive micro-tensile specimens at the crack-tip. The immediate problem posed by this sequence of events is to locate precisely the point on the load-displacement curve where the crack initiates, and to record the crack-tip displacement at this point. In ductile metals, crack initiation at the root of a notch occurs well before the attainment of maximum load[56].

A theoretical estimate of displacement prior to general-yielding, may be obtained by assigning a gauge-length to the micro-tensile specimen at the notch root equal to approximately twice the crack-tip radius[57]. The micro-specimen width is determined by the microstructural parameters governing ductility, e.g. the interparticle spacing between manganese sulphide inclusions[56]. Hence the crack-tip displacement may be given by[57]

$$\delta = 2\rho\epsilon \qquad (1)$$

where ϵ is the strain adjacent to the crack front, and ρ is the crack-tip radius.

At some point, the strain ϵ reaches the fracture ductility and the critical crack-tip displacement is then given by

$$\delta_c = 2\rho\epsilon_c \qquad (2)$$

Clearly, the larger the crack-tip displacement the larger is the fracture strain that can be sustained prior to fracture. Hence, as long as the fracture is intrinsically related closely with the plastic strain concentration at the crack-tip, the crack-tip displacement criterion is plausible, because it apparently represents roughly the

integrated value of plastic strain in the crack-tip plastic zone, despite the lack of any precise physical meaning for the parameter.

The foregoing treatment, suggests that the crack-tip displacement as a material property for the expression of the resistance of a material to crack initiation, has much in common with a limiting root strain. However, it has one important advantage in that it possesses dimensions of length and can thus encompass a size effect, whereas a limiting root strain of course reguires an initial arbitrary gauge length for its expression.

Theoretical predictions[58] of crack-tip displacement values are available to describe the non-linear relationships between applied stresses and displacements below general-yield. However, as a simplifying measure these analyses neglect strain-hardening thereby limiting predictive powers to displacements obtained below general-yield. Beyond general-yield they have only superficial value. Plastic slip-line field theory has also been applied to the problem with more succes, and this permits the extension of the overall crack-tip displacement relationships into the plastic region. Unfortunately, the method generally gives over-estimates for theoretical displacement values because of difficulties in predicting the effects of triaxial stress and work-hardening, particularly with respect to those microstructural constituents which finally limit the pre-fracture ductility of the alloy. As a result, such analyses are best applied to thin specimens of low work-hardening capacity to minimize the effect of changes

in section thickness which alter the pattern of yielding at the notch root by the intervention of a tensile stress through the thickness.

More recent research[59,60] indicates that strain-hardening is responsible for more rounded crack-openings, and this will lead to ambiguity in the definition of crack-opening displacement. This last point is considered fully in the discussion.

Ultimately, interpretation depends on whether measured crack-opening displacement (C.O.D.) reflects the specimen geometry and macro-stress state, or whether the value obtained is determined largely by microstructural features. Where ductile fracture occurs by stable crack growth under increasing load into previously strained material, there is no 'final' fracture event, but an instability in the growth process associated with a definite amount of slow or stable crack growth. Such C.O.D's are obtained by taking the C.O.D. value at maximum load as the fracture criterion.

It is a prime objective of this research to show that the C.O.D. value at maximum load is sufficiently discriminating towards different microstructures.

B.3.2. Microstructural Effects

The outstanding problem remains to incorporate well defined microstructural parameters into the analysis of the C.O.D. concept. in order to objectively analyse microstructural types and to provide answers to such problems as assessing the relative contributions of large particles with say good ductility, to those of small particles with poor ductility on cracking behaviour. There is an additional

factor to consider in the less well defined and non-uniform cast microstructures. Here identical crack-tip displacements could, according to equation (2) be composed of a large strain and a small microstructural size factor, or a small strain and a large microstructural size factor, suggesting a critical fracture strain rather than a displacement as the more relevant criterion.

The stress requirement for crack extension in the ductile mode does not remain the simple function of crack-tip displacement and crack-length that it is in the so called 'brittle' fractures. Indeed, the mechanical history of the specimen as a whole, has a marked influence on the propagation stress. This is because crack growth beyond general-yield requires propagation into material continually strain-hardened ahead of the crack, making the spread of yield-zones at later stages of growth progressively more difficult. Thus the growth of cracks occurs under an increasing applied stress, although a drop in the applied load may well be recorded since the fractures normally occur after necking has begun. The effect produces two halves of fracture surface which are heavily deformed. Microstructural constituents will disrupt this process. Thus randomly distributed particles may radically alter the energy requirements for fracture without necessarily altering the basic fracture mechanism. On the other hand preferentially located particles (for example at grain boundaries), may cause the fractures to become unstable and begin propagating when the applied stress produces a critical displacement at the crack-tip. Physically, such a

condition materializes when void formation at the crack-tip is excessive, and the material between the voids has necked down. In addition, confining the deformation to a particular path e.g. a grain-boundary generally leads to a reduction in fracture-toughness, an effect accentuated when a high density of brittle particles in these regions can be induced to either crack or decohere at the particle-matrix interface.

On the macroscopic scale however, the effect may be quite different because particles may for example, reduce the triaxial stress-state around a notch. This would happen when the shear strength of the particle-matrix interface was low, thereby promoting more homogeneous deformation patterns within the vicinity of the notch. The resultant increase in displacement would then be an increase in C.O.D.

B.3.3. Extension to Elevated Temperatures

Unified testing procedures, consistent where possible with fracture-mechanics concepts, have yet to be extended universally into high temperature regions, although extension to high temperature creep rupture has been reported[61]. Here one is really concerned with the fringe or twilight areas of fracture-mechanics, and particularly the development of a treatment for fracture preceeded by widespread recoverable yielding. The theoretical analyses for such conditions are not available and are unlikely to be so for some time. Thus inevitably answers have to be sought in empiricism and experimentation.

This research seeks to apply the C.O.D. concept to

fully plastic fracture and extend the treatment to elevated temperatures.

CHAPTER 3

EXPERIMENTAL PROCEDURE

3.1. MATERIALS

Two stainless-steels were studied a duplex steel referred to as steel A, and an austenitic steel referred to as steel B. The manufacturers' analyses are given in table 1.

The steels, supplied as commercially cast centrispun tubing, were received in 50 cm lengths of 15 cm external diameter and 2.5cms wall thickness. Sections were cut from each tube to produce blanks for either hot-working or heat-treatment.

3.2. HOT-WORKING

3.2.1. HOT-ROLLING

Longitudinal slabs, 30cms long, 6.5cms wide and 2.3cms thick were cut from each tube and placed in a furnace at 900°C, heated to 1100°C in 45minutes and soaked at this temperature for 15minutes prior to rolling. Reduction to a thickness of 1.1cms required four roll-passes, after which the material was reheated to 1100°C, flattened and allowed to air-cool.

3.2.2. HOT-FORGING

Ring sections 6.5cms long were cut from each tube and parted longitudinally to produce forging blanks 6.5cms long and 2.5cms square. Each blank was soaked at 1250°C for 1hour and reduced to a cross-section about 1.1cms square in a total of 10-12 forging sequences on an open die drop forge. A sequence consisted of six-hammer blows followed by a further 15minute soak at 1250°C before further reduction. During reduction the temperature did not fall below 1050°C. After the final reduction each blank

was given a further ½hour soak at 1250°C and allowed to air-cool. The forging operation required roughly 6hours at temperature.

3.3. HEAT-TREATMENT

All heat-treatments were performed on un-machined test blanks. Two basic heat-treatments were used; a solution treatment and/or an ageing treatment.

3.3.1. SOLUTION TREATMENT

A partial solution treatment at 1100°C for 1hour followed by air-cooling was given to a series of cast specimens. A further batch of cast steels were given a prolonged solution treatment of 3hours at 1250°C and either air-cooled or water quenched.

Rolled and forged specimens were not solution treated.

3.3.2 AGEING TREATMENT

The basic ageing treatment comprised a soak at 725°C for periods of 50,250,1000 and 2000hours. (A few specimens were also aged for these times at either 625°C or 825°C). Temperature control during ageing was ±5°C. No check was made for temperature control during solution treatment.

3.4. PREPARATION OF MECHANICAL TEST-PIECES

Two types of mechanical test-piece were used for this study: a notched bend test-piece of essentially Charpy dimensions required to maintain geometrical consistency for a slow-bend versus impact comparison (figure 1), and a No. 13 Hounsfield tensile test-piece (figure 2). This test-piece was the largest which could be extracted tangentially to the axis of the tube and yet remain within the capacity of the loading frame. Some preliminary work

required a multiple-notched tensile specimen (figure 3).

3.4.1. TEST-PIECE LOCATION

Cast Steels:- 11mm thick ring sections were cut from the tubes, and five or six bend and tensile specimen pairs extracted tangentially to the tube bore. An allowance of 2mms from the bore wall was made to avoid bore porosity. The majority of bend specimens were extracted close to the bore wall, and notched on the bore wall face. The tensile specimens were cut from regions adjacent to the bend samples. In addition, one 6.0cms thick ring section from each tube provided specimens cut longitudinally to the tube axis.

The location of the cast specimens is shown in figure 4.

Hot-rolled Steels:- Bend and tensile specimens were cut both parallel and perpendicular to the rolling direction (figure 5).

Hot-forged Steels:- Bend specimens were extracted from the ends of each forged bar and one tensile specimen cut from the centre.

3.4.2. TEST-PIECE DIMENSIONS

Bend Test-piece:- Each bend test-piece contained a notch starter. In the majority of cases this was a 2mm deep parallel sided slit, cut with a 0.15mm thick rubber-bonded slitting wheel. The width of the slit was 0.15mms at the tip and contained a slight radius. Some test-pieces were made with 4mm deep compound slits; the first 2mms were relieved to accommadate the cutter. Sixteen samples were prepared with 2mm deep and 1mm root radius Charpy U-notches. A further series of test-pieces were drilled and tapped either side of the notch starter so that knife edges could

be attached to accommodate a conventional fracture-toughness clip gauge.

Tensile Test-piece:- All tensile test-pieces were "shouldered" and contained a 16mm gauge length.

Multiple Notch Tensile Specimens:- A few multiple notch tensile test-pieces were cut tangentially from 3mm thick ring sections of tube B. The notches were 1.5mms deep and 12mms apart.

3.5. MECHANICAL TEST PROGRAMME

The mechanical test programme was divided into two stages.

3.5.1. Stage I :- Assessment of notch bend test.

3.5.2. Stage II:- Alloy study using bend and tensile tests.

3.5.1. STAGE I

The object of this stage of the programme was to select a suitable notch specimen and method of measurement of C.O.D. Similar work with ferritic steels has been widely reported but no information was available on its applicability and measurement in austenitic steels.

Test Procedure (Bend Specimens):- All testing was carried out at room temperature with specimen surfaces polished prior to loading to facilitate optical examination. Straining was achieved by three-point bending in a semi-stiff loading frame driven at a constant cross-head speed of 1.14mms/min. Specimens were contained in a specially constructed loading jig of specimen width-to-loading span ratio of 1:4. This loading geometry is identical to that operating in the Charpy impact test. Traces of load versus

cross-head travel were recorded. During loading the notch root was inspected visually for the first appearance of surface cracks. Notch profile displacement measurements were calculated from simultaneous on-load photographic records, recorded at various increments of load up to the maximum load. On some specimens a series of microhardness impressions as markers were made either side of the notch profile, so that displacements could be measured at a number of locations along the length of the slit. A further series of tests were performed with conventional general-yield fracture-toughness clip gauge instrumentation to provide continuous records of load versus displacement across the surface of the notch. Finally, a few tests were interrupted before the attainment of instability and the specimens sectioned at mid-thickness and examined for crack growth.

It was realized at an early stage that crosshead displacement values could provide the simplest measure of displacement but that they could be affected by indentation effects at the loading pins. Accordingly, a series of specimens were pre-indented at zero bending moment before testing to assess the significance of the effect.

Test Procedure (Notch Tensiles):- Tests were conducted at room temperarture, 625°C, 725°C and 900°C. Straining was performed at a constant cross-head speed of 1.14mms/min and carried through to final fracture. Slit widths were measured optically and with feeler gauges before and after straining to provide an estimate of the 'off-load' C.O.D. at instability.

3.5.2. STAGE II

Notch Testing:- The use of the multiple notch tensile test technique was discontinued. Crack-tip displacements were measured optically at room temperature and inferred at elevated temperatures by previous correlation with cross-head travel. A common cross-head speed of 1.14mms/min was used throughout. The bend test specimens had 2mm deep parallel-sided slits. The behaviour of cast, wrought and aged materials over a range of temperatures up to 800°C was studied. Prior to straining specimens were held at the test temperature for half an hour. The test temperature could be controlled to ±3°C or better. From load-displacement curves, the following parameters were recorded:- yield load, maximum load, offset displacement at maximum load, energy absorbed to maximum load, total energy absorbed. The last two parameters were obtained by counting squares under the load-displacement curve. Notch-root contractions on fractured test pieces were measured with a travelling microscope at a magnification of x6.

A series of Charpy type impact tests were performed on cast and wrought steels containing either a 2mm deep slit or a U-notch. Tests were made at room temperature and 725°C. Energy absorption and notch-root contraction were recorded.

Tensile Testing:- Tensile specimens were strained at a constant cross-head speed of 1.14mms/min, equivalent to an initial strain rate within the specimen of 0.071 per minute. Tests were conducted at 25°C and in the temperature range 400-800°C. Prior to straining specimens were held at the

test temperature for half an hour. The test temperature could be controlled to ±5°C or better. A few tests were discontinued immediately prior to final fracture. The testing frame was sufficiently stiff at the loads used for cross-head displacement to provide an accurate measure of the flow characteristics of the materials. This was checked by measuring displacements between gauge marks on the surface of a specimen at steadily increasing loads. From load versus cross-head travel curves, values of 0.2% proof stress, tensile strength uniform, necking and total elongation were obtained. Reduction of area was measured on the fractured test-piece. True stress-true strain values were calculated and plotted on log-log co-ordinates to give an indication of strain hardening behaviour. Work hardening rates were evaluated from the differential form of an equation relating true stress to true strain.

3.6. METALLOGRAPHY

Samples were prepared for optical microscopy by conventional metallographic techniques. Edge protection of fracture surface profiles was achieved by a single stage mounting operation in araldite. Results were comparable to those obtained by nickel plating the surface and required only a fraction of the time to produce. Oxidized fracture surfaces were afforded similar protection by the single stage araldite method, and although silvering followed by nickel plating gave a slightly better result, this was not justified by the time required to produce it. For high magnification microscopy, a final polish with gamma-alumina gave an acceptable finish.

A major problem in the examination of cracks and pores adjacent to the fracture profile was staining caused by seepage of etchant and moisture from these locations. This difficulty was largely eliminated by a prolonged soaking in absolute methyl alcohol before drying.

The following general, and phase staining etchants were used.

General Etch:-
- Hydrochloric acid - 15mls.
- Nitric acid - 5mls.
- Water - 100mls.

Phase Staining Etch:- (used hot.)
- Potassium ferricyanide - 20gms.
- Potassium hydroxide - 20gms.
- Water - 100mls.

* * *

- Copper chloride - 10gms.
- Hydrochloric acid - 10mls.
- Water - 200mls.

Surfaces were examined in the optical microscope under bright field, dark field and Normarski interference microscopy.

Macrostructures of the as-cast tubes were revealed by swabbing in a solution containing 15gms copper chloride, 30mls hydrochloric acid and 100mls water.

3.7. FRACTURE SURFACE EXAMINATION

3.7.1. INDIRECT METHOD (USING TWO STAGE CARBON REPLICA)

This technique was used during the initial stages of the investigation but discontinued when a scanning electron microscope became available. Although it is realized that the high resolution afforded by such replicas can provide certain additional information not obtainable by other

means, the overall interpretation is difficult owing to the complexities of the alloys investigated. Furthermore, the technique was not suitable for magnifications below about x1000, and difficulty was experienced in stripping replicas from the rough fracture surfaces.

3.7.2. DIRECT METHOD

Fracture surfaces were cut from broken bend test-pieces and mounted on aluminium stages for observation in the scanning electron microscope Specimens were tilted 45° to the direction of the incident beam and examined at an accelerating voltage of 20-30Kv.

3.8. X-RAY ANALSIS

Precipitates were extracted from weighed samples by dissolving the matrix in a continuously stirred solution containing 15ccs HCl, 5cc HNO_3 and 100ccs H_2O maintained at a temperature of 35-40°C to prevent the formation of brown precipitates of presumably ferric hydroxide. Some extractions were made electrolytically in a 5% solution of hydrochloric acid. Following dissolution, precipitates were centrifuged out, washed in distilled water, then analar acetone, oven dried and finally re-weighed. After x-ray analysis, weighed amounts of the residues were re-warmed in the dilute aqua regia for 24hours, washed, dried and re-weighed. Any weight-loss was negligible, and subsequent x-ray analysis gave no changes in the diffraction patterns.

Filings were also examined by x-ray powder techniques following stress relief at 600°C in evacuated silica-glass capsules. Despite these precautions, a fair amount of line

broadening persisted.

Powder diffraction photographs were obtained following irradiation of extracted residues with either nickel filtered copper K_α radiation or iron filtered cobalt radiation. The Evans-Straumanis technique for film mounting was employed obviating the need for film shrinkage corrections.

3.9. MAGNETIC MEASUREMENTS

The magnetic response of the gauge-lengths of tensile specimens manufactured from alloy A, increased during straining. Accordingly, a simple technique was developed to give some indication of the magnitude of these changes. A sample was placed on the span of an Archimede's bridge straddling one pan of a beam balance. A 6mm diameter bar magnet was suspended from the arm of the balance above and allowed to rest on the polished surface of the sample. The load on the opposite arm of the balance was steadily increased until the load required to just detach the magnet, could be recorded. Initial trials showed that the response was sensitive to the dimensions of the specimen. Accordingly, calibrations relating the changes in magnetic response to changes in specimen height for a fixed radius, and changes in specimen radius for a fixed height, were made. For a fixed length of specimen gauge-length, changes in magnetic response with differing ageing times, both before and after straining, were recorded.

C H A P T E R 4

R E S U L T S A N D D I S C U S S I O N

4.1. METALLOGRAPHY

4.1.1. AS-RECEIVED STRUCTURES

The as-cast alloys showed long columnar grains (figure 6) extending for almost the full thickness of the tube wall. A fine zone of equiaxed grains were present on both the inner and outer surfaces. The duplex steel had a finer and more unidirectional structure, whilst bore porosity was a feature common to both alloys.

The microstructure of steel B displayed a discontinuous network of massive niobium carbides (figure 7), along the dendrite secondary and tertiary arms. Steel A had less carbide and isolated islands of delta-ferrite (figure 8) comprising perhaps 10% volume fraction. This ferrite tended to follow dendrite boundaries and was divorced from the carbide which had a "script-like" morphology.

Wrought materials were obtained by hot-rolling or forging cast blanks at 1100°C and 1250°C respectively. The low hot-rolling temperature was insufficient to dissolve the massive carbides, but the working cycle did impart some directionality to the finished sheet. Both the carbide and the delta-ferrite had tendencies to align themselves parallel to the rolled surface (figure 9).

There was strong evidence for some recrystallization of the deformed matrix but this was rather obscured by the deformed columnar grain pattern which still persisted. Steel B was easier to hot-roll than steel A where edge cracking was a persistent problem. From metallographic observations it appeared that the volume fraction of delta-ferrite was largely unaffected by the rolling process.

The hot-rolling reduction was insufficient to produce a fully hot-worked structure and was more akin to a warm-working process.

Forging at 1250°C eliminated the cast dendritic structure and substituted a fully recrystallized matrix (figure 10). The number of massive carbides were reduced by dissolution, and the remainder broken up and redistributed throughout the matrix. The delta-ferrite content of alloy A was reduced to about 2% volume fraction and appeared as isolated spheroids dispersed throughout the matrix. Alloy B was only slightly easier to forge than alloy A.

4.1.2. SOLUTION TREATED STRUCTURES

Cast samples were solution treated at 1100°C and 1250°C. These temperatures were identical to those used in hot-working. Neither temperature removed the massive interdendritic carbides. In the duplex alloy a slight reduction in the amount of delta-ferrite took place at the lower solution treatment temperature. However, solution treating at 1250°C decreased the ferrite content from 10% to about 5-6% and produced a strong tendency for this phase to spheroidize (figure 11). The delta-ferrite remained divorced from the carbide after both solution treatments.

A more complete solution treatment of these steels was achieved by solution treating at 1350°C[2], although it was uncertain whether all the niobium carbide had dissolved.

The most important effect of the low temperature solution treatment was an acceleration of the rate of decomposition of delta-ferrite during subsequent ageing.

4.1.3. AGED STRUCTURES

An ageing treatment at 725°C produced little precipitation within the grains of the cast steels but was responsible for major microstructural changes at the dendrite interfaces. In steel B for example (figure 12), the dendrite boundaries contained a virtually continuous network of carbides, subsequently identified by x-ray diffraction as niobium carbide and $Cr_{23}C_6$. Some of the carbides were acicular and penetrated the grains at right-angles to the boundaries. In steel A, the delta-ferrite largely decomposed, and a sigma-phase formed in addition to the carbides. Sigma occurred in massive form and was distinguishable from the degenerate delta-ferrite by a blue colouration following an etch in the potassium ferricyanide solution.

Ageing produced a marked increase in the amount of precipitation in forged steels (figures 13 and 14). Precipitation took place at grain-boundaries and, to a lesser extent within the grains. A number of massive carbides appeared in isolated regions (figure 13), particularly in steel B, although these could have been a remnant of the cast structure. Using the ferricyanide etch it was possible to distinguish carbides (heavily attacked), sigma phase (stained blue) and degenerate ferrite (stained brownish-yellow). Thus the large elongated phase in figure 15 is massive sigma.

4.1.4. DEFORMED AND CRACKED STRUCTURES

The magnetic response of steel A increased after straining at room temperature. The effect was enhanced

by prior ageing and was greatest in hot-worked alloys. Following an ageing treatment at 725°C for 1000hours, the forged version (figure 16) was about 90% martensitic after straining at room temperature. The martensite had a fine acicular type structure in all cases.

Interdendritic carbides provided effective points for stress concentration and acted as barriers to plastic deformation. This is demonstrated in figure 17, where slip-lines on one side of the dendrite-carbide interface have nucleated very few slip-lines in the adjacent dendrite arm.

When slow crack growth occurred in the slow bend test, it did so in a variety of ways depending upon the initial microstructure. In fully aged cast alloys the prefered mode was by carbide cracking (figure 18), whilst an un-aged forged alloy with a random dispersion of second phases, exhibited crack propagation by the seperation of particles from the matrix (figure 19) to form dimples. Figures 18 and 19 represent behavioural extremes and it was more usual for the crack to propagate by a combination of these two mechanisms (figure 20).

4.2. X-RAY ANALYSIS

4.2.1. RESULTS

The results of the X-ray diffraction analysis using the A.S.T.M. powder index file to identify phases, are given in table 2, together with values of the lattice parameters. NbC was easily identifiable in all extracts. $Cr_{23}C_6$ could be detected in all grades only after a prolonged ageing time at 725°C, whilst the occurrence

of a sigma phase was confined to the duplex versions, and was first detected in specimens which had been aged for 50hours at 725°C. Lavés phases of the type Fe_2Nb were not found.

Marked changes in the intensity and width of the NbC lines were observed. These variations are recorded in table 3. Generally, forged grades had more intense NbC lines than their cast counterparts. However, it should be noted that an electrolytic extraction in 5% HCl of precipitates from the cast alloy B, gave an identical result to its wrought equivalent for NbC line intensities. The electrolytic extraction did not however remove all traces of the austenite matrix, and it was for this reason that the chemical extraction was preferred.

Dissolution of the matrix by warming in the dilute mixed acids took twice as long for steel A (duplex) than steel B. Dissolution time had no measurable effect on the amount and type of particles extracted, because weighed amounts of extract from each steel produced negligible weight loss after re-warming in the acid solvent for 48hours. Diffraction patterns were also unaltered. Thus the mixed acids gave a consistent though not necessarily complete extraction, since there remained the possibility that very fine precipitates could have dissolved on immediate exposure to the mixed acids.

An additional feature of the cast duplex extract from both as-received and aged material, was the persistent magnetic response displayed by a portion of the residue. The weight per-cent of these samples remaining as extract

markedly increased with ageing time (table 2), whilst that of the other grades remained virtually static. A possible explanation for the magnetic response was the presence of incompletely dissolved delta-ferrite. However, no lines appeared on the powder pattern consistent with those of that phase. This was confirmed by idexing the delta-ferrite lines obtained from stress-relieved filings of the duplex steel. The most prominent reflections (111), (200) and (311) from this pattern were absent in the chemically extracted samples.

4.2.2. DISCUSSION

A steady reduction in lattice parameter for niobium carbide occurs with increased ageing time (table 2). Despite the error band ($\pm\frac{1}{2}\%$) encompassing part of this reduction, the trend is nevertheless consistent for both grades. A reduction in the lattice parameter of this carbide has been shown to accompany deviations from stoichometry[62]. These deviations may be large, with a maximum value reported equivalent to a formula of $NbC_{0.7}$[63]. The reported concurrent decrease in lattice parameter is slightly less than 1.0%, [63] and similar to the decrease recorded in table 2. Thus assigning formulae to niobium carbide of NbC and $NbC_{0.7}$, the weight per-cent of niobium required to combine all the carbon in each steel is as follows:-

	%Niobium (Analysed)	%Niobium required to combine all carbon as NbC	%Niobium required to combine all carbon as $NbC_{0.7}$
Alloy A	0.8	0.46	0.73
Alloy B	1.25	0.695	1.00

Hence if the non-stoichometric formula is correct, it is unlikely that there is sufficient niobium in the steels to remove all available carbon as niobium carbide. Thus additional carbides may form. These were identified as $Cr_{23}C_6$ in aged steels but could not be detected in un-aged alloys. There may be two explanations for this. First, the precipitates may have been so fine that they were dissolved by the mixed acids and not extracted. Second (and more likely), the presence of excess niobium could have decarburized chromium carbide as soon as it formed. Ageing would remove this excess niobium by the formation of non-stoichometric niobium carbide and thus chromium carbide would be free to form from any excess carbon.

An explanation for the increasing non-stoichometry of niobium carbide is obscure. A possible mechanism may be based on the fact that the diffusion rate of carbon is much greater than that of niobium. Thus prolonged ageing allows sufficient time for free niobium atoms from carbon depleted areas, to diffuse towards a niobium carbide precipitate and eventually dissolve in that precipitate. This proposal is consistent with reports that non-stoichometric niobium carbide contains an excess of niobium as a result of anion vacancies[64].

Changes in the lattice parameter of niobium carbide could also be caused by the substitution of other elements. Nitrogen is a possibility although the decrease in lattice parameter recorded in table 2 is too large to be adequately explained on the basis of nitrogen substitution alone[63].

The variation of per-cent extract by weight with

ageing time for steel A, is considered to be unreliable because of the magnetic response exhibited by a portion of the extract. Sigma phase is non-magnetic[65], thus this magnetic response is presumably caused by delta-ferrite despite the lack of any distinguishing lines on powder films. No reasons to account for this anomalous behaviour can be offered. In steel B, the per-cent extracts by weight for cast and forged steels after prolonged ageing are remarkably similar. Thus it is concluded that particle shape, size and distribution is responsible for the marked embrittlement displayed by the cast alloy.

From table 3, prolonged ageing of forged grades produces an increase in the niobium carbide line width. Line broadening in powder diffraction patterns in the absence of non-uniform strain results from a decrease in diffracting crystal thickness. Thus it is likely that the ageing product is a fine niobium carbide, a conclusion strengthened by the observation that centrifuging of the extract was more difficult in the forged grades in general and the aged forged grades in particular.

Line broadening is not a characteristic of cast alloys with the notable exception of the cast duplex steel which had been aged for 50hours. This may have been a result of floresence due to the presence of iron in the precipitate.

4.3. MAGNETIC TESTING

4.3.1. RESULTS

The magnetic response of the duplex alloy was found to vary with manufacturing process, heat-treatment and

degree of straining. The load required to detach the magnet was sensitive to the dimensions of the specimen but, by taking specimens of constant length and variable radii, a linear relationship between specimen volume to surface area ratio and magnetic response was obtained. It was possible to reproduce the load required to detach the magnet to ±0.05grams irrespective of the magnetic response and the load range. A change of ±5% in the radius of a specimen produced a change in magnetic response equivalent to ±3% of the load required to detach the magnet. Test-piece radii were always well within the 5% tolerance, thus error bands may be drawn in figures 21 and 22 to represent ±3% of the load reported. These bands have been omitted in the interests of clarity. At values of load less than about 3grams, the reproducibility (±0.05grams) becomes a significant error and must be included, although at higher loads it may be neglected.

Figure 21 illustrates the change in magnetic response induced by ageing at 725°C for cast, cast and solution treated at 1100°C, hot-rolled and forged alloys. Ageing produced a marked reduction in magnetic response and, by inference a reduction in the delta-ferrite content. This was confirmed metallographically. Hot-rolling the cast steel in the temperature range 950-1100°C with a finish rolling temperature of 1100°C, had no effect on the delta-ferrite content, but solution treating the cast alloy at this temperature did give a small reduction from about 10% to 8% estimated metallographically.

The as-forged steels contained only about 2% delta-

ferrite, which decreased slightly on ageing. The major reduction in the ferrite content of the rolled steel occurred after only 50hours at 725°C (10% to 2-3%), and approached that of the forged condition after 1000hours. The reduction in ferrite content in the cast steel occurred at a reduced rate, but the solution treatment produced the accelerated rate found in the rolled steel. Ferrite contents after 1000hours were comparable in all versions (2-3%).

The increase in magnetic response recorded by the gauge-lengths of strained tensile specimens was most marked (figure 22). The values quoted were obtained from sections cut from the uniformly strained part of the gauge-length. The contribution to magnetic response due to delta-ferrite (figure 21), has been subtracted from the load values, and thus figure 22 represents the increase in magnetic response due solely to the result of a strain-induced transformation. The extent of the transformation was greatest in the worked steels and least in the cast steels, and increased with prior ageing time at 725°C.

An additional feature of strain-induced transformations in many semi-stable austenitic steels [66,67], is the formation of a paramagnetic[68] transitional ϵ-phase with a hexagonal structure. A simple post-straining heat-treatment may serve to convert this phase to the ferromagnetic α-form. Thus samples were heated at 450°C for 4hours in evacuated silica glass capsules after straining, and re-tested for magnetic response. The results are shown by the dashed lines in figure 22. The most striking feature of this

heat-treatment was the production of an almost identical magnetic response in the hot-worked grades, particularly after longer ageing times. The solution treated and cast steels also displayed comparable responses for the entire aging range.

4.3.2. DISCUSSION

The most important factor obscuring an interpretation of these results, is the difficultly of seperating the relative contributions of matrix compositional changes and the degree of strain, on the amount of martensite formed. The problem arises because a shortage of specimens necessitated the determination of martensite contents in specimens strained to instability. Thus the larger instability strains recorded by hot-worked versions, may be expected to produce more martensite than the lower instability strains attained by cast grades (figure 22).

The Ageing Process:- The amount of martensite formed after straining to instability increases with increased ageing time at 725°C prior to straining, although the instability strain itself actually decreases. Thus changes in matrix composition during progessive ageing are responsible for a large increase in the susceptibility to martensite formation. If it had been possible to assess martensite contents at the same strain for each specimen, it seems highly probable that the rate of increase of martensite formation with prior ageing time would be greater than that shown in figure 22.

The most significant feature of the ageing process is reflected by the results of the 450°C post-straining

heat-treatment. Unaged alloys, irrespective of manufacturing process or solution treatment gave no increase in magnetic response as a result of this heat-treatment. All versions of alloy A required ageing at 725°C prior to straining before such an effect was observed. Thus a feature of the ageing process is an apparently increased susceptibility to the formation of a transitional ϵ-martensite.

The activation-energy for the formation of such a transitional phase, is much less than that required to form an α-martensite, because the hexagonal structure of the transitional phase is similar to the structural characteristics of a stacking-fault. Presumably then a low stacking-fault energy is synonymous with an increased susceptibility to ϵ-martensite formation[69]. If this is the case then the inference from figure 22 is that a decrease in stacking-fault energy takes place during ageing.

In the absence of additional experimental data, it is difficult to give an explanation for this behaviour. However, progressive ageing would seem to decrease the chromium content of the matrix, both by the formation of an iron-chromium sigma phase and a chromium carbide (table 2). In addition niobium is removed from the matrix, both by dissolution in existing niobium carbide and by the formation of new precipititates. Chromium is variously reported as increasing[70] and decreasing[71] the stacking-fault energy, whilst niobium may have little effect[72] or alternatively produce an increase[70]. However, these results appear to be highly dependent upon even small variations in the initial base composition[73]. Thus present work

suggests that for steel A, the net effect of matrix depletion in chromium, niobium and carbon is a lowering of stacking-fault energy. This is consistent with the findings of Dulieu and Putting[70] who determined stacking-fault energies by measuring the radius of extended dislocation nodes. Unfortunately, thin foil electron-microscopy to confirm these findings was outside the scope of this thesis, although it is under consideration elsewhere[2].

4.4. STAGE I. ASSESSMENT OF NOTCH TEST

4.4.1. EVALUATION OF MULTIPLE NOTCH TEST

The multiple notch technique was investigated using notch tensile specimens cut from the cast austenitic tube. The results of the investigation are given in table 4.

It proved very difficult to measure the residual crack-tip displacement, since the notch-tip was obscured by oxide layers and surface deformation, and without actually photographing the notch and extrapolating its linear sides, consistent results could not be obtained. This procedure would of course have removed the speed advantage of the multiple notch technique, and so an alternative means of measurement was tried with feeler gauges. The results depended very much upon the operator making the measurement as well as the state of the notch. Reproducibility was no better than ±30%.

Examination of failed test-pieces showed that the notches had been cut sufficiently far apart to prevent the plastic zone associated with each, from interfering with one another. The major problem seemed to be the irregular amount of tearing and crack extension at each of the un-

fractured notches, i.e. one notch frequently had a large tear whilst the other still retained the rounded tip profile typical of the early stages of loading. Slight variations in the original depth of the notch (as little as 3%) produced large changes in the residual crack-tip displacement. An additional problem was the change in root radius from notch to notch caused by the wearing away of the slitting cutter: this gave problems in measuring slit widths with the feeler gauges.

The final and perhaps most severe limitation encountered was the observation that the attainment of instability at one notch did not necessarily mean that deformation had ceased at the others. Indeed, removal of the load from a specimen shortly before instability was reached and then reloading, led to further deformation and final fracture without the previous load ever being reached. Thus it is possible for crack extension to occur at one notch after the attainment of instability at another. For this reason, and because of the difficulties in producing accurate measurements reported earlier, residual crack-tip displacement measurement by the multiple notch technique was abandoned.

4.4.2. EVALUATION OF BEND TEST (2mm DEEP NOTCH STARTERS)

4.4.2.1. Load-deflection Diagrams

The principal features of the load-deflection diagram are shown in figure 23. The initial load rose steeply to point A, and was directly proportional to the deflection. The strains were essentially elastic although a small plastic zone formed at the tip of the notch before point A

was reached. Beyond the linear portion of the curve the slope decreased, gradually at first but more rapidly as the deflection increased, and eventually became zero at the point of maximum load. The maximum load was associated with a mechanical instability and related in some way to the amount of crack-growth at that point.

There was no consistent pattern to the formation and development of cracks within the plane of the notch root, although fine cracks sometimes formed soon after point A was reached. Crack initiation was an obscure and imprecise event, and difficult to distinguish from the heavy plastic deformation concentrated in the root of the notch. Its visual detection was sensitive also to the machined finish in the notch root, and thus it became exceedingly difficult to pin-point the exact value of deflection associated with the initiation of the crack.

There was no consistent pattern as to the location of the first crack within the root of the notch, although in forged steels the trend was for it to form at the centre, whereas in cast steels it was not uncommon for the crack to initiate on the surface and grow inwards. The inference from this observation is that crack initiation in cast steels was more sensitive to microstructure than stress state. An added complication was for the more ductile samples to display multiple crack nucleation, an effect common in as-cast steels but observed only twice on a limited scale in aged forged steels. These fine cracks either joined up by lateral growth to form the major crack-front, or remained as non-propagating micro-cracks along the

machined notch root, (see figure 68 later). Growth of the major crack front occurred both laterally and longitudinally as the load increased to the maximum load, and finally adopted a roughly crescent shape irrespective of its original nucleation site.

The shape of the crack and amount of stable crack-growth, was easily revealed by heating specimens at 600°C for 5minutes after straining to maximum load, and finally fracturing in impact. Crack-growth, as revealed by the oxidized surface was irregular. The maximum load instability did not consistently coincide with the full lateral growth of a crack. Unaged steels, whether cast, rolled or forged frequently had cracks extending several tenths of one millimetre down the free surface of the specimen, before instability occurred. In aged steels full lateral growth coincided with the attainment of the maximum load. There was no difference in the cracking behaviour from parallel slits and U-notches.

After the maximum load had been reached, the crack deepened while extending down the sides of the specimen. The deflection mechanism at this stage differed from that before maximum load. Prior to instability, deflection was associated with the bending strain contained in a relatively large volume of metal. This extended up to about the ligament length of the specimen either side of the notch. After instability, the deflection was achieved through a tearing-like mechanism which produced an intensification of the strain in the metal immediately adjacent to the fracture. The final tail portion of the curve was associated

with the interference of the centre loading pin with the propagating crack. This was significant in unaged steels due to the large bend angles achieved in these alloys.

4.4.2.2. Notch Behaviour in Loading

As loading proceeded, the profile of the parallel-sided slit did not retain its linear sides to the notch-tip. Strain-hardening and rotation effects caused by bending produced a constraint at the tip (figure 24). The profile of the notch in this region was obscured by heavy surface distortion and there was considerable uncertainty in measuring the tip displacement with any accuracy or reproducibility. The problem was more acute at large displacements, but was circumvented by photographing the notch and extrapolating the linear sides to the original root location. Thus the crack-tip displacement was the effective displacement of the notch faces measured at the original root location.

The usefulness of this measurement was confirmed on a number of control specimens by extrapolating to the notch-tip the linear portions of a series of micro-hardness impressions placed adjacent to the sides of the notch. These impressions were made originally on undeformed specimens to provide markers. The values obtained were equal to those obtained from a straight forward extrapolation of the notch sides.

As a result of this observation, there appeared a strong likelihood, that measurement of the displacement of the sides of the notch at the free surface (δ_s), could provide a convenient method of inferring crack-tip values (δ_t),

if it were possible to relate the two by means of a simple scaling factor[74]. Optical measurements of the tip and surface displacements expressed as the variation of δ_s with δ_s/δ_t (figure 25), showed that a simple scaling factor was obtainable, but only for values of δ_t greater than 0.3mms. Figure 25 includes points for a wide range of heat-treatments, and if a scaling factor of 1.8 ±0.3 is taken, crack-tip displacement values greater than 0.3mms may be read to an accuracy of ±16%. The greatest amount of scatter in the results in figure 25, were provided by points included for values of δ_t close to the yield load of steels which ultimately gave high values of δ_t at maximum load. This could have been because a greater amount of strain-hardening was required to achieve a constant hinge point in the ligament in these more ductile steels. Thus a plot of the scaling factor at maximum load against the crack-tip displacement at maximum load δ_m (figure 26), yields a reduction in the scatter and an increased range over which δ_t may be usefully inferred. Maintaining the original accuracy of ±16%, δ_m may be usefully inferred for values as low as 0.15mms. Similar trends were obtained using clip gauge instrumentation although the scaling factor was of course much larger.

An alternative method of inferring δ_t, was to investigate the relationship between δ_t and the offset displacement ϵ_{off} (figure 27). The latter parameter is readily obtained from the load-deflection diagram (figure 6). The following relationship was found:-

$$\epsilon_{off} = 2.8\delta_t - 0.07 \qquad (3)$$

The scatter in results was less than with the δ_s correlation, and δ_t may be inferred to an accuracy of $\pm 7\%$. Points 'a' and 'b' in figure 27, are for as-cast alloys where cracks were observed on the notched face of the specimen. Thus an increased value of ϵ_{off} was produced for a given value of δ_t. The accuracy of the correlation was not improved by including only values of ϵ_{off} recorded at the maximum load, as it was with the δ_s correlation above. A partial explanation for this could be that the measured value of δ_s included the elastic component of strain, whereas ϵ_{off} did not.

No consistent variation was observed in values of ϵ_{off} obtained from similar specimens pre-indented at zero bending moment before testing, and those which had not.

U-notches, in addition to slits were used for the determination of surface and offset displacement versus δ_t relationships. U-notches as expected, gave higher values of ϵ_{off} and δ_s at the maximum load point, than did slits of the same depth in identical specimens. By including points for U-notches, the ϵ_{off} versus δ_{ML} and δ_s vs δ_{ML} relationships could be extended to much higher values (figures 28 and 29). The existing relationship was fairly well maintained in the case of the offset displacement correlation, but a distinct change in slope occurred at $\delta_{ML} = 0.8$ mm with the δ_s correlation. A possible explanation for this, is that crack extension has now reached the stage where δ_t values measured at the original notch-tip, no longer reflect the events at the crack-tip. Thus the measurement recorded at these high δ_t values is simply the

ratio of δ_s/δ_t for unconstrained material. The result is a decrease in slope.

The maintainance of the offset-displacement correlation in the presence of increased crack-growth, is more difficult to analyse, because of the complicating feature of surface crack formation. These cracks formed on the surface of the notched face in cast steels at large bend angles. Possibly the two effects were mutually corrective.

4.4.2.3. Energy Absorption in the Slow Bend Test

Despite the appearance of cracks well before the instability load was reached, there existed a consistent relationship in the bend test, between the post-yield displacement 'd' and the corresponding value of load 'L' normalized by dividing the load by the yield load 'L_y'. The post-yield displacement was taken to be the total displacement to maximum load minus the displacement at which the yield force was measured. The yield load was the force at a point 0.1mm offset from the initial linear portion of the load-displacement curve. The relationship took the form:-

$$\frac{L}{L_Y} = 1 + h\sqrt{d} \qquad (4)$$

with 'h' a constant entirely dependent upon material and notch geometry.

Equation (4) may be expanded to give the energy absorption prior to the maximum load instability (E_{ml}), by integrating and adding on the 'elastic' energy that was absorbed prior to general-yielding. Thus

$$E_{ML} = \tfrac{1}{2} C L_Y^2 + L_Y \int_0^{d_m} \left(\frac{L}{L_Y}\right) d(d) \qquad (5)$$

where 'C' is the elastic compliance of the specimen and d_{ml} is the post-yield displacement at maximum load. Substituting equation (4) into equation (5) and integrating:-

$$E_{ML} = \tfrac{1}{2} C L_Y^2 + d_{ML} L_Y \left(1 + \frac{2n\sqrt{d_m}}{3}\right) \qquad (6)$$

An experimentally determined value of 'C' for the cast alloys was 53.1mm N^{-1} (1.92×10^{-3}mm Kg^{-1}) and for the forged alloys 62.2mm N^{-1} (1.64×10^{-3}mm Kg^{-1}). The type of notch had only a small effect on the value of 'C' and was neglected. Values of 'n' for 'L_y' measured in kilograms and d_{ml} in millimetres were as follows:-

Cast Steels $n = 0.44$

Forged Steels $n = 0.34$

A small variation in the value of 'n' was found according to the notch starter used, but this variation could be neglected without significantly impairing accuracy.

Table 5 shows values of E_{ml} calculated from equation (6) above, and compares them with experimentally determined values obtained by counting squares under the load-deflection curve. The percentage difference between the two values does not exceed $\pm 2\frac{1}{2}\%$.

Forged steels tested at room temperature had values of d_{ml} much greater than those of their cast equivalents. However, by assigning to 'n' a value of 0.375 equation (6) may be expressed as:-

$$E_{ML} = \tfrac{1}{2} C L_Y^2 + d_{ML} L_Y \left(1 + \frac{\sqrt{d_m}}{4}\right) \qquad (7)$$

without too great a loss of accuracy. Equation (7) underestimates E_{ml} for cast steels and over-estimates it for forged steels, but has the advantage that it may be applied to either steel in any heat-treated or manufactured condi-

tion. Values of E_{ml} calculated from equation (7) are included in table 5. The percentage error is now increased to ±8%, but this reduces to ±5% if only parallel slits are considered.

The elastic component of the measured energy varied between 9 and 12% for the slit notch and 4 and 8½% for the U-notch.

It was possible to extend equation (7) to include the C.O.D. at maxium load as a function of the energy absorption to that point. The relationship between ϵ_{off} and δ_t has already been established (figure 27), and in addition a further empirical relation was found between ϵ_{off} and the post-yield displacement (d).

$$\epsilon_{off} = (0.75 \pm 0.05)d \qquad (8)$$

Thus the energy to maximum load may be related to the C.O.D. by combining equations (3), (7) and (8) to give:-

$$E_{ML} = \tfrac{1}{2} C L_y^2 + 3.75\, \delta_{ML} L_y (1 + 0.484 \sqrt{\delta_{ML}}) \qquad (9)$$

where δ_{ML} is C.O.D. at maximum load. Equation (9) is valid for Charpy-size specimens containing 2mm deep parallel-sided slits. The constant term and error band in equations (3) and (8) respectively, have been omitted from the derivation of equation (9). Values of E_{ml} calculated from equation (9) are given in table 5 and could be inferred from measurements of 'Ly' and δ_{ML} to an accuracy of ±7%.

4.4.2.4. Estimate of Plastic Zone Sizes

A semi-empirical relationship was found between the normalized value of load and the C.O.D. (δ) (figure 30), which takes account of the elastic component of displacement.

Cast Alloys $$\frac{L}{L_Y} = (0.8 + 1.14\sqrt{\delta}) \quad (10)$$

Forged Alloys $$\frac{L}{L_Y} = (0.8 + 0.93\sqrt{\delta}) \quad (11)$$

Integrating equations (10) and (11) to obtain a value of the energy absorption associated solely with the seperation of the faces of the crack-tip gives:-

Cast Alloys $$E_{\delta_t} = \delta_{m_L} L_Y (0.8 + 0.75\sqrt{\delta_{m_L}}) \quad (12)$$

Forged Alloys $$E_{\delta_t} = \delta_{m_L} L_Y (0.8 + 0.62/\delta_{m_L}) \quad (13)$$

A considerable proportion of the energy absorbed to maximum load (E_{ml}) in a bend test, is taken up by compressing metal in that part of the ligament remote from the notch, and from other factors not directly connected with the tensile stretching of that part of the ligament immediately adjacent to the notch-tip. E_{δ_t} calculated from equations (12) and (13) on the other hand is for material in the immediate vicinity of the notch which has been subjected to essentially tensile loading, except at the free surface where the 'through the thickness stress' causes a lateral contraction. In tension, the specific fracture energy (E_s), is calculated by dividing the fracture energy (obtained from the area under the load-extension curve) by the volume of the deforming specimen gauge length. Thus an estimate of the volume of metal subjected to tensile forces at the notch-tip may be obtained by dividing E_{δ_t} by E_s. Such estimates are given in table 6.

Two points are apparent from the data. First, an increase in fracture toughness, measured in terms of δ_m, results in an increased volume of strain-hardened material beneath the notch, i.e. more ductile specimens are able to

dissipate the effects of a notch more effectively and are thus less notch sensitive. Second, the ratio E_{α}/E_{γ} is the same for the as-cast alloys (0.17) but less than that for the as-forged steels (0.24), probably because the former are unable to realize the full strain-hardening potential of the grains before crack-growth removes the stress concentration from the vicinity.

4.4.3. EFFECT OF TEST-PIECE ORIENTATION ON MECHANICAL PROPERTIES

There was no consistent trend in mechanical properties as a function of test-piece orientation (table 7). Tangential specimens in cast alloy B were stronger and less ductile than those cut longitudinally. C.O.D. values at maximum load (δ_m) were largely unaffected, presumably because there was little change in local ductility (reduction of area at fracture). In the cast duplex alloy (alloy A), the strength was higher in the longitudinal direction whilst the ductility was little affected by test-piece orientation.

Hot-rolled steels were even less consistent in their response to test-piece orientation. The lower tensile strength of alloy A in the longitudinal direction would seem to account for the reduced uniform elongation, whilst the corresponding decrease in δ_m was offset to some extent by the increased local ductility. The transverse strength and ductility of alloy B was slightly greater than it was in the longitudinal direction. Inexplicably, δ_m showed a marked decrease.

4.4.4. INFLUENCE OF SOLUTION TREATMENT ON MECHANICAL PROPERTIES

The two temperatures used for solution treating were

those used for hot-rolling (1100°C) and forging (1250°C) respectively. Samples were water quenched from the solution treatment temperature and the mechanical properties measured (table 8). Both steels increased in strength at the expense of ductility following the low temperature solution treatment. A more prolonged treatment at the higher solution temperature, decreased the strength of alloy A, and markedly increased the uniform elongation. Local ductility was increased to a lesser extent, whilst δ_m remained unaffected. Conversely, an identical heat-treatment given to alloy B produced an increase in all properties measured relative to the as-cast state.

4.4.5. INFLUENCE OF AGEING TIME AND TEMPERATURE ON δ_m

In some preliminary work, a series of bend test-pieces containing 4mm deep notches were aged for various times at 625°C, 725°C and 825°C. The results are included as table 9 for completeness.

The accuracy of these results was low because the optical system employed in the initial trials failed to produce a clear image suitable for enlargement. Furthermore, the deeper notch employed appeared more sensitive to interaction with the yielding effects caused by the centre loading pin. Duplicate tests showed scatter and the accuracy of the results quoted is only about ±10%. Absolute values of δ_m reported elsewhere for 2mm deep slits could be measured to ±2%. Figures for inferred values have been given previously.

Returning to table 9, the results show a progressive decrease of δ_m with increased test temperature and time.

The austenitic alloy was more susceptible to this kind of ageing embrittlement.

4.5. STAGE II. ALLOY STUDY USING BEND AND TENSILE TESTS

4.5.1. EFFECT OF AGEING AT 725°C ON MECHANICAL PROPERTIES

Room Temperature:- Cast, cast and solution treated at 1100°C, rolled and forged samples of both steels were aged at 725°C for increasing periods of time up to 2000hours and tested in tension or slow bend at room temperature. The following parameters are recorded in figures 31-34 and plotted on a semi-log scale as a function of the ageing time; per-cent reduction of area at fracture, total elongation, tensile strength, 0.2% proof strength, work-hardening rate at a true strain of 0.15 and at instability, and the maximum load crack opening displacement. A number of trends were clearly discernible.

i) Proof and tensile strengths of hot-worked versions were largely unaffected by ageing. Increases in proof and tensile strengths were most marked in cast steels after shorter ageing periods (50hours). The effect was mitigated by solution treating at 1100°C, particularly for the duplex grade.

ii) Ageing progressively reduced the ductility and toughness. Cast steels were more susceptible to this ageing embrittlement, where major property degradations were recorded after only short ageing periods (50hours).

Again the effect was mitigated by a prior solution treatment

iii) Increased work-hardening rates relative to the as-cast grades, were for the most part responsible for the improved toughness and ductility recorded by the hot-worked grades. The rates decreased progressively with increased ageing time. Work-hardening rates in cast steels varied erratically with ageing time and reached a minimum after about 250hours and then sharply increased. (This may be a result of the inadequacy of the Ludwik relationship in describing the work-hardening behaviour at these low strains close to the limit of its validity - see section 5.3.1. later).

Elevated Temperature:- Cast and solution-treated samples were also tested in tension at 725°C after ageing at that temperature for increasing periods of time. The results appear as figure 35. Progressive ageing generally reduced the tensile strength and increased the proof strength. After 250hours the proof strength decreased. Reduction of area at fracture showed a progressive increase due almost entirely to a marked increase in the post-instability or necking strain, despite the appreciable fall in uniform strain which occurred throughout this period to partially offset it. A prior partial solution treatment of 1hour at 1100°C, served to increase the reduction of area after ageing by markedly increasing the post-instability strain.

4.5.2. INFLUENCE OF AGEING TIME AT 725°C ON BEND-TEST PROPERTIES MEASURED AT 725°C

Both alloys in the cast and forged conditions were aged for 50hours and 250hours at 725°C and tested at the ageing temperature at the slow strain rate. The results are given in figures 36 and 37 and the trends summarized as follows:-

i) Steel B, either cast or forged was stronger, tougher and more ductile than steel A.

ii) The toughness of each steel as reflected by the total-energy absorbed in fracture, increased with ageing time. The effect was more marked in steel B which had an energy absorption about twice that of the duplex alloy. No major difference existed between the cast and forged versions of each steel, although cast versions had a slight superiority at shorter ageing times.

iii) The major contribution to the increase in total-energy with ageing time, was an increase in the energy required to propagate the crack after instability.

iv) A halving of yield load after 50hours ageing registered by the forged steels was largely cancelled by an increase in ϵ_{off}. The increase in yield load after 50hours ageing exhibited by the cast steels was mitigated by the concurrent decrease in ϵ_{off}. Thus the value of E_{ml} in either case remained largely unchanged.

4.5.3. NOTE ON SELECTION OF TEST FOR MECHANICAL PROPERTY DETERMINATION AT ELEVATED TEMPERATURES

Mechanical properties determined for selected conditions from tensile and bend tests at 725°C, are reproduced in table 10. The results show that the tensile test fails to discriminate between the two manufactured conditions as convincingly as the bend test. In mitigation it must be pointed out, that although the same cross-head speed was used in each test, the strain-rate in the root of the notch is clearly much greater than that in the gauge-length of the tensile specimen. The most striking example of the greater discriminatory power of the bend test, is obtained by comparing bend and tensile parameters for the 250hour aged condition of the cast steels. In this example tensile properties are virtually identical although the bend test indicates a much reduced toughness and ductility for the duplex alloy. Thus the bend test is preferred in this investigation for elevated temperature work, because of its apparently increased sensitivity to microstructural changes, and was always used in cases of material shortage.

An additional factor influencing this choice was the probable temperature sensitivity of the constants 'k' and 'n' in the Ludwick relation (section 5.3.4. later). These could easily give misleading impressions of changes in work-hardening ability as a function of temperature, when used to calculate $d\sigma/d\epsilon$ from the differential form of the Ludwik relation (see later). Nevertheless, a number of tensile tests were carried out particularly at those temperatures where serrated or jerky flow occurred. The results

of these tests have been gathered together for the sake of completeness and presented as table 11. All results in table 11 are for tests carried out at a constant crosshead-speed equivalent to a strain-rate in the specimen of $0.071 min^{-1}$. An asterisk by a result indicates that serrated flow occurred.

4.5.4. INCIDENCE OF SERRATED FLOW

During tensile testing in the temperature range 400-600°C, all grades exhibited discontinuous yielding or serrated flow after a certain critical strain ϵ_c had been reached. Within this temperature range, the critical strain increased with decrease in temperature and increase in strain-rate. The characteristics of the serrations were sensitive to the manufacturing process of the alloy and the test temperature. Three types of serration were formed (figure 38) and their characteristics and incidence are described in detail in appendix I.

4.5.4.1. General Observations

Irrespective of manufacturing process, the critical strain to the onset of jerky flow was less for steel B. The critical strain was difficult to measure with any great precision and the degree of uncertainty is represented by wide error bars in figures 39 and 40. These figures are plots of the logarithm of the critical strain versus the reciprocal of the absolute temperature. There was no consistent trend in serration type and amplitude with manufacturing process between alloys nor with heat-treatment within a single grade. However, the 0.2% proof stress in forged steels was much greater than in cast

alloys (table 11) whereas the instability strain was much less Serrations in forged alloys generally had a larger amplitude than their cast counterparts.

4 5.4.2. Discussion

Serrated flow in alloys may be the result of a single mechanism or a number of mechanisms operating in concert. Possible explanations for the phenomena in this work include phase transformations [75], and the interaction of dislocations with precipitates [76,77] interstial atoms [78], substitutional atoms [79,80] and vacancy-interstial pairs [81].

Phase Transformations:- An examination of equilibrium diagrams for base compositions of steels similar to those of alloys A and B, indicates that the likelihood of phase transformations taking place on straining in the temperature range 400-600°C is remote. Martensite formation is most unlikely because the test temperatures employed are much greater than the M_s temperature. Ferrite formation in steel A cannot be entirely ruled out. It is possible that local areas become depleted in alloy elements by carbide precipitation and that these areas subsequently transform to delta-ferrite. The concurrent volume expansion would be responsible for the sharp load drop. There are three objections to this theory.

a) Delta-ferrite could not be detected metallographically in regions other than where it pre-existed: nor was there any increase in magnetic response after straining.

b) Carbide precipitation in the absence of strain at higher ageing temperatures (725°C), reduced

rather than increased the ferrite content (figure 21).

c) The more stable alloy B exhibited serrated flow at lower strains than the less stable alloy A.

On the basis of these observations delta-ferrite formation is discounted as a mechanism responsible for serrated flow

Precipitation of Carbides:- The evidence in support of a process of fine alloy-carbide precipitation as a mechanism causing dislocation multiplication and discontinuous flow, is inconclusive and may be summarized as follows:-

a) Test temperartures are rather low for extensive precipitation to occur although at 600°C this objection loses some of its validity.

b) When precipitation takes place from solid-solution it does so because the matrix is meta-stable at that temperature. Accordingly, an applied strain will assist the process, but it is not a necessary pre-condition. Thus given sufficient time, carbide precipitation will take place in the absence of strain. However, no difference was observed in the mechanical behaviour of forged steels soaked at a test temperature of 550°C for several hours prior to straining and those which were not.

c) High test temperatures promote general precipitation which could account for the absence of serretions at 650°C.

These observations suggest that fine alloy carbide precipitation could contribute to serrated flow, but that the contribution is probably of only secondary importance.

Dislocation-Solute Interactions - The final process contributing to serrated flow invokes the interaction of dislocations with some kind of solute atmosphere. In this type of process, the solute responsible possesses a diffusion-rate fast enough to interfere with, and inhibit the movement of dislocations by forming atmospheres around them. Crucial to this model[62], is the formation during straining of a sufficient quantity of vacancies to effectively increase the rate of self-diffusion or of diffusion of substitutional solutes. Sufficient vacancies will be produced when a certain critical strain ϵ_c has been reached. A simple kinetic relationship between the test temperature T and ϵ_c, provides a rough estimate of the energy requirements for the process[61,82]:

$$\epsilon_c = A e^{-Q/RT} \qquad (17)$$

where Q is an energy and A a factor independent of ϵ_c and T but a function of strain-rate . Thus at constant strain-rate, a plot of $\log \epsilon_c$ against T^{-1} will give a straight line of constant slope for a strain induced process, (figures 39 and 40). As the results available were limited in number, and included a wide variety of microstructural types, the slope of the broad scatter-band drawn in figures 39 and 40, is of necessity somewhat arbitrary. It should be noted that points for the lower test-temperatures fall well outside the scatter-bands, indicating that at these lower temperatures, other factors e.g. dislocation-interstial solute

interactions, may be more important.

Equation 17 fails to take account of the variation of dislocation density with strain[63], but nevertheless indicates a strain induced process for serrated yielding, associated with substitutional atoms. Thus the occurrence of serrations in forged steels at values of ϵ_c lower than their cast counterparts may be attributed to increased matrix supersaturation, or grain-size differences or both. The grain-size is considered important[84], because at a given temperature, the dislocation density for a fixed strain, is higher in fine grain (forged) materials. Hence serrations appear at smaller strains because the average dislocation velocity is lower.

A value of the activation energy Q, may be calculated from the model used to derive equation (17), by assuming that the excess vacancy concentration is given by $10^{-4}\epsilon$ [85] where ϵ is the strain. Thus equation (17) is re-written[85]

$$Q = RT \log_e \left(\frac{\epsilon_c}{\dot{\epsilon}} \times 10^{-4} \right) \qquad (18)$$

where $\dot{\epsilon}$ is the strain-rate, and Q is the energy for migration of a vacancy and is approximately $\frac{1}{3}$ of the activation energy for lattice diffusion of substitutional atoms[86]. Table 12 gives values of Q calculated from equation (18) for a wide range of pre-test heat-treatments and test temperatures for a constant strain-rate $0.071 sec^{-1}$. Also included are a few results for different strain-rates. Average values of Q are 82 ± 6 kJoules $mole^{-1}$ for the austenitic steel, and 89 ± 6 kJoules $mole^{-1}$ for the duplex alloy. An experimentally determined value of activation energy

for the diffusion of substitutional atoms in austenite is ~280 kJoules mole^{-1} [87], thus an expected value of Q would be 92 kJoules mole^{-1} if serrated flow results from dislocation locking and unlocking by substitutional atoms. In view of the wide range of microstructures examined and the difficulty in determining an accurate value for ϵ_c, the measured value of Q is in good agreement with this value.

Those substitutional atoms likely to have the greatest effect in locking dislocations are those with a large atomic misfit with the parent lattice. It has been suggested [88] that the strain field of each substitutional atom or cluster of atoms will be reduced by their association with dislocations. In an austenite matrix, iron, chromium and nickel have similar atomic radii, but niobium has a large misfit (13%) whilst molybdenum has only a slightly smaller one (11%). In both these steels, niobium is present in abundance, whilst molybdenum is present in alloy A, but in much reduced quantities. Thus it is probable that niobium (and to a much lesser extent molybdenum in the duplex alloy), is responsible for serrated flow in these alloys. Differences in Q between each steel, could be accounted for by the presence of molybdenum and/or delta-ferrite in the duplex alloy. The role of delta-ferrite in this alloy is obscure, because the forged alloy, although having the highest incidence of serrated flow in terms of serration amplitude and ϵ_c, nevertheless has a much reduced quantity of delta-ferrite in the microstructure. Thus there is the possibility that molybdenum is partitioned between delta-ferrite and austenite in the cast version and takes only

a minor part in the locking process, whilst in the forged steel in the virtual absence of partitioning, molybdenum is more active This may account for the alternating serrations (described in appendix I), which were observed at 500°C in steel A, as well as for the generally increased serration amplitude in the forged version of this alloy compared with forged alloy B.

Substitutional-Interstial Atom Pairs:- Interactions of combinations of substitutional and interstial atoms with dislocations have been proposed(89) as a further mechanism of serrated flow in these steels The two elements most likely to be effective by such a mechanism in this work, are niobium and carbon The two atoms could remain in solution but be associated, perhaps in pairs. The activation energy for diffusion of these pairs would be greater than that for a single niobium atom as lattice strain fields would be non-symmetrical and movement thus more difficult. Measured activation energies are rather low and do not support this hypthesis and are more consistent with values for single substitutional atom diffusion.

Interstial Solutes:- The diffusion rates of interstial solutes are largely unaffected by the presence of excess vacancies in austenitic steels, because the interstial sites in the FCC lattice are quite large. Thus the contribution of interstial elements to serrated flow in the austenitic alloy is considered to be negligible. There may be a contribution however from this source in the cast duplex alloy. The mechanism may provide a partial explanation for the anomalous result obtained for the low test temperature of

375°C, but in the absence of additional data at these lower temperatures, the point cannot be pursued further.

4.5.5. INFLUENCE OF HOT-WORKING ON TOUGHNESS AND DUCTILITY

4.5.5.1. Slow Bend Tests at 25°C

Figure 41 illustrates the influence of hot-working on the room temperature offset displacement, and the correlation with the energy absorbed to the point of instability in the slow-bend test. Points are included for both parallel slits and U-notches.

Forged steels display enhanced ductility and toughness, and there is a near linear correlation between toughness and ductility. The toughness of the duplex steel is greater than that of the austenitic steel in the equivalent condition. Also included in figure 41, are the values of the yield load to maximum load ratio recorded in the test. This ratio steadily decreases from 0.7 to 0.46 as the ductility of the cast steels increases. However, whilst the ductility of the forged steels increases, the ratio retains a constant value of about 0.55. Thus the diagram may be divided into two sections at an energy absorption of about 60 joules, with each section describing the behaviour of a range of conditions of either cast or forged steels. Unfortunately, no reliable data was available to include points for rolled steels, but such approximate figures as were available suggested that "rolled" behaviour was similar to that for cast steels. The reason may be associated with the fact that fracture remains predominantly intergranular in the "rolled" region whereas it is transgranular

in the forged region.

4.5.5.2. Slow Bend Tests at 725°C

Fracture was predominantly intergranular for all conditions tested at this temperature. Figure 42 shows the results of bend tests conducted at 725°C. The form of the results are quite different from those found at room temperature; the major difference is the superior ductilities of the cast steels. The toughness as measured by the energy to maximum load, of both forged grades and the cast duplex steel are comparable. However, the cast austenitic steel is superior in all respects, even to the point of the sharp notch properties having higher values than the U-notch properties of the cast duplex steel. Sharp notch properties of rolled steels are intermediate between those of the cast and forged alloys. The poor ductility of the forged steels is associated with the high yield load to maximum load ratio (0.7-0.8), whereas the corresponding values for cast steels (0.35-0.55), are much lower.

The effects of hot-working on high temperature strength and ductility are summarized in figure 43. Generally, forging increases hot strength and reduces ductility. The effect of hot-working on measured toughness is small in the duplex steel, but in the austenitic steel there is a marked reduction. The semi-wrought or rolled structure offers an improvement in strength, ductility and toughness over the cast structure in the duplex steel, whereas for the austenitic steel toughness is largely unaffected by the increase in strength and decrease in ductility caused by rolling.

4.5.5.3. Effect of Strain-rate

Dynamic (Charpy) loading had little effect on the total energy required to fracture a specimen at room temperature (figure 44), although the static Charpy energy was slightly greater than the dynamic value.

At 725°C, a very different result was obtained (figure 45). The room temperature impact values of forged steels were maintained at 725°C (and for U-notches there was a small increase), whilst the static values were reduced by a factor of 3-4 for steel B and 5-7 for steel A. The higher test temperature increased the dynamic fracture energy of cast alloy B by 200%, whilst the increase recorded by steel A was only 10%. The room temperature fracture energy of cast steel B under static-loading conditions was maintained at 725°C whilst cast steel A registered a three-fold decrease under the same conditions. Under static conditions at 725°C the toughness of the cast and derived wrought steels is equal; the austenitic alloy has a higher value than the duplex. Included in figure 45 are two points for sharply notched rolled steels. Both had a superior static toughness at 725°C, and gave a 25% increase in energy absorption in impact when the test temperature was increased from 25°C to 725°C. Decreasing the strain-rate produced a comparable reduction in the energy absorption at 725°C.

4.5.5.4. Contribution of E_{ml} to Etotal

The energy absorption to maximum load could only be measured under static-loading conditions. The ratio $E_{ml}/Etot$ was sensitive to the sharpness of the initial

notch, but the effect was by no means consistent. Changing from a parallel slit to a U-notch at 25°C, increased the ratio for forged alloys from 0.66 - 0.76 (alloy B) and 0.66 - 0.86 (alloy A). At 725°C the values were 0.38 - 0.37 (alloy B) and 0.39 - 0.52 (alloy A). The figures for cast steels at 25°C were increases from 0.55 - 0.82 (alloy A) and 0.64 - 0.66 (alloy B) and at 725°C the increases were 0.58 - 0.68 (alloy B) and 0.48 - 0.58 (alloy A).

Taking a mean value of the ratio for U-notches and slits, the principal effect of the increased test temperature is to decrease E_{ml}/E_{tot} from 0.71 to 0.3[illegible] in the forged austenitic steel, decrease from 0.75 to 0.45 in the forged duplex material, decrease from 0.71 to 0.63 in the cast austenitic and decrease from 0.65 to 0.53 in the cast duplex alloy. Thus the energy to maximum load as a fraction of the total energy to fracture, is markedly decreased by the rise in temperature for the forged steels, but the decrease observed for cast steels is much less. A consideration of figures 41 and 42 shows that an increased test temperature, causes an increase in the yield load to maximum load ratio for forged steels, but produces a small decrease in this ratio for cast steels. Concurrently, there is a large decrease in offset displacement in forged steels but a small increase in offset displacement for the cast grades. Thus the low ductility exhibited by forged steels is a major factor in producing low values of E_{ml} at 725°C.

It would be helpful if the measured energies could be split into the components associated with crack initiation

and crack propagation. Unfortunately, the energy associated with the maximum load instability is not the energy required to initiate a crack, as significant amounts of stable crack-growth are already present at this stage. The maximum load energy parameter is an instability criterion associated with the ability of the material at the test temperature to withstand a certain amount of stable crack-growth.

It has been suggested(90) that the slope of the "fairly" linear portion of the load displacement curve after instability, gives an indication of the ability of the material to prevent a crack from propagating. This measurement was difficult to make with any precision, whilst such figures as were obtained, produced no consistent trend.

4.5.5.5. Notch Root Contraction (NRC)

An additional indication of notch ductility was provided by the measurement of the notch root or lateral contraction. Presumably, the maximum value of this parameter is attained at the moment the crack initiates, since the very act of initiation relieves the triaxial stress causing the contraction. This measurement would appear to be a better indication of pre-crack initiation ductility than the offset displacement to maximum load. Regretably, heavy surface deformation together with the tearing nature of ductile crack propagation, distorted the fracture surface profile and rendered accurate measurement impossible, and made NRC determination highly dependent upon the experience of the operator making the measurement. Nevertheless, in

view of the established linear correlation between slow bend and impact energies, there should exist a similar relation between notch root contractions measured on statically and dynamically fractured test-piece surfaces. Figure 46 shows this relationship, and taking account of the reservations above, the amount of scatter is quite acceptable. More reliance can be placed on the lower values of NRC, as these are less likely to be distorted by the heavy surface deformation associated with the more ductile samples.

A comparison of notch root contractions formed in either slow bend or impact at 725°C (figure 47), was inconclusive. The contraction measured on either the cast or forged duplex steel in impact was considerably greater than in slow bend whereas the austenitic alloy showed only a small increase at the higher strain-rate. Both steels in the rolled condition had comparable values of NRC at 725°C and were unaffected by strain-rate. Nevertheless, the value of NRC recorded for the rolled duplex steel, represented a significant increase over the values measured for the cast or forged conditions. For the austenitic alloy however, hot-rolling produced a value intermediate between that of the cast and forged conditions.

Since measurements of NRC are subject to the reservations recorded earlier, it is unwise to place too much reliance on specific values. Thus the trend which emerges from figures 45 and 47, is that the greater toughness in impact at 725°C for the duplex steel is the result of increased ductility, whereas the contribution from this source

for the austenitic alloy, is small.

4.5.6. INFLUENCE OF TEST-TEMPERATURE ON BEND TEST PROPERTIES

Steels A and B in the cast and forged conditions were aged for 50hours at 725°C and tested in slow bend in the temperature range 400-800°C. The comparison was made following a 50hour age at 725°C, because figures 36 and 37 showed that the major changes which occurred on ageing, did so during the first 50hours. The results are presented as figures 48 and 49 and may be summarized as follows:-

1) Cast alloy B was tougher than cast alloy A, particularly at higher temperatures.
2) Toughness as measured by the total energy absorbed in fracturing a specimen, was sensitive to both test-temperature and manufacturing process. Cast steels were slightly superior above 700°C but markedly inferior at lower temperatures.
3) The shape of the energy absorption to maximum load, the post-instability energy absorption and the offset displacement versus test temperature curves, were remarkably similar to those for the total energy versus test temperature relations. An exception was the failure of the cast steel B to register the increase in maximum load energy absorption at temperatures greater than about 600°C.
4) Yield loads increased as the temperature decreased but remained virtually constant below about 650°C. Maximum load increased sharply

as the test-temperature decreased. The effect was more pronounced in the forged grades. This response was reflected by the yield load to maximum load ratio which did not vary a great deal for the cast alloys, but exhibited a sharp decrease for both forged steels.

5) Fractographic evidence suggested that toughness was much influenced by the propensity for interfacial seperation. This in turn determined whether the full strain-hardening capacity of the stcels could be realized before fracture. Thus at lower temperatures, forged grades had high yield load to maximum load ratios, i.e. much increased ductility and therefore greater toughness.

* * *

The influence of test-temperature on the slow bend properties of steels in the as-rolled and as-forged conditions, are shown in figure 50. In all cases the notch starter employed was the 2mm deep parallel slit. The most striking feature of the results was the relative insensitivity of the properties of the rolled steels to large changes in temperature, compared to the response shown by the forged grades. The only feature to possibly escape this trend, was the large decrease in the energy absorbed to maximum load registered by the rolled alloy A at 725°C, a response common to both forged grades. The effect was associated with a change over from a predominantly trans-

granular fracture mode to an intergranular one.

In the transgranular mode (400 to 650°C) the forged alloys were superior to the equivalent rolled versions, with steel B generally better than steel A.

4.5.7. CORRELATION BETWEEN δ_{ML} AND NRC

A good correlation existed between the maximum load C.O.D. and the notch root contraction (figure 51). Despite the errors inherent in the measurement of the latter parameter as described earlier, the correlation indicates that NRC may provide a simple quality-control type test for the assessment of fracture-toughness. Figure 51 includes points for both as-received and aged steels, thereby encompassing the complete range of δ_{ML} values measured.

An extension of the correlation to higher test temperatures produced a large amount of scatter (figure 52). This was not surprising in view of the many fracture mechanisms represented in the temperature range 400 - 800°C. Nevertheless a number of trends were evident:-

1) Alloy A (duplex) either cast or forged was associated with low values of NRC, although the range of δ_{ML} values exhibited by the forged version was large.
2) Both alloys in the rolled condition had high values of δ_{ML} and NRC.
3) Alloy B in the cast condition was superior to alloy A in this condition.

4.5.8. CORRELATION BETWEEN SLOW BEND AND TENSILE PROPERTIES

Correlations between slow bend and tensile properties were strictly only valid for test temperatures where strain-rate effects were negligible. Thus the difference in strain-rate between the gauge-length of a tensile specimen and the notch root of a bend specimen deformed at constant cross-head speed, precluded the establishment of meaningful correlations at all temperatures other than room temperature. In addition, those parameters most responsive to changes in metallurgical structure, were those which measured a displacement or strain of some kind. Accordingly, figures 53 and 54 show the reasonable correlations which existed between the maximum load C.O.D. and the reduction of area at fracture for the austenitic and duplex grades respectively. Reduction of area at fracture was taken as the most likely parameter to correlate with δ_{ML}, because the latter included in its measurement a certain amount of slow crack-growth, and like reduction of area at fracture, was a measure of local ductility. The correlation held for the full range of microstructures tested in the austenitic steel. In the duplex steel however, it was necessary to draw a seperate curve for the cast steel, which for a fixed value of δ_{ML}, gave lower values of reduction of area than the wrought grades.

4.6. FRACTOGRAPHY

4.6.1. INTRODUCTORY

All fractures examined in the scanning electron microscope were of the over-load type, i.e. they were produced

by subjecting a test-piece to a continuously increasing load until the ultimate strength was exceeded. Despite the fact that this loading cycle applied to each fracture examined, there was no common characteristic of either a macroscopic or microscopic nature present on the fracture surface which could be attributed to it. Indeed, for each particular metallurgical condition, the fracture surface showed a large diversity of fracture modes. Furthermore, strain-rate, test temperature and relative plasticity as determined by the proximity and locality of certain microstructural features, were found to have a significant influence on the appearance of the fracture surface. Thus the first (not unexpected), finding established by a cursory examination of scanning electron fractographs, was that fracture in these steels was an extremely heterogeneous event. It appeared to be controlled largely by microstructural features and local stress state, whilst such macroscopic considerations as overall stress state were of only secondary importance.

As a result of these observations, a detailed qualitative analysis of the fractographic response of each group of fractures is given, together with specific examples of the fracture modes as they reflect the major influence of the manufacturing method on the role of microstructural constituents in initiating and propagating cracks.

Definition of Terms:- The adjectives 'ductile' and 'brittle' are often used to describe not only the amount of plastic deformation which occurs before fracture, but also the

fracture mode itself. Thus, of two fractures propagated by identical 'brittle' modes, one could be preceded by a large amount of plasticity and the other occur before general-yield, and yet both may be described as 'brittle'. These two adjectives are confined in this work to describing fracture behaviour i.e. the amount of plasticity which precedes fracture. The fracture path or mode is described literally e.g. as transgranular or as interfacial decohesion. Thus 'behaviour' is a macroscopic term whilst 'fracture mode' is a microscopic one. However, intense deformation often occurs in small regions of the microstructure, and it is important to distinguish this local ductility from the overall macroscopic behaviour plasticity.

4.6.2. FRACTURES FORMED AT ROOM TEMPERATURE

4.6.2.1. Influence of Manufacturing Process

Cast Steels:- The original notch root region contained several non-propagating cracks distributed in random lengths over the entire length of the machined notch root. The demarcation between this root and the fracture surface was distinct, and there was no evidence of any stretch-zone formation in the transition region of the kind widely reported elsewhere[91,92]. Stretch-zones were not identified in any sample, although rigorous attempts were made to locate them.

Fracture surfaces were characterized by two distinctive features. The first consisted of groups of fine depressions or micro-voids (figure 55) located primarily on the upper slopes of tear-ridges. These tear-ridges rose to considerable heights above the floor of the fracture

and were regions of intense local plastic deformation. In alloy A, the arête was sometimes a micro-chisel point seperation (figure 55), although in alloy B the ridge was surmounted by the more common array of fine micro-voids. The second feature (figure 56), was associated with a marked reduction in the amount of local plasticity, and an increased incidence of irregularly-shaped platelets embedded in the slopes of matrix undulations. These platelets had large surface areas and were often cracked in well defined crystallographic directions (figure 57). In addition, the morphology of some platelets (figure 58), suggested that they might be the carbide component of the eutectic phase formed to complete solidification. It was usual for both distinctive features to be associated, particularly in steel B (figure 59).

Alloy B contained fewer tear-ridges and micro-voids and had a higher proportion of cracked carbides than alloy A. This observation is consistent with metallographic work described earlier (section 4.1.1.), where alloy A was found to contain interdendritic ferrite divorced from the carbide, whilst alloy B had a more established interdendritic carbide network. In addition, plastic deformation of delta-ferrite may mitigate local stress concentrations in steel A, and thereby reduce the incidence of carbide cracking. Finally, there existed the possibility of a difference between the two alloys in the segregation pattern of tramp elements in interdendritic regions. These elements could radically lower the cohesive strength of the carbide-matrix interface in one alloy, but not in the other, perhaps because of

increased solubility in the delta-ferrite. The idea of a low strength interface in alloy B, was reinforced by the remarkable lack in figure 58 of any broken carbide debris, or of plastic deformation and distortion on the fracture surface. In this figure, the interstices between what were the tertiary arms of a dendrite, appear to be faithfully reproduced by the morphology of the eutectic carbide. Figure 60 shows a crack on the polished surface of a specimen unloaded before final fracture. Once again a straight forward opening mode of plate-like carbide and austenite matrix decohesion is indicated as the principal mode of fracture.

Ageing:- Ageing for 50hours at 725°C, reduced the number of dimples associated with the peaks of tear-ridges, and caused their complete elimination after 250hours (figure 61). Instead, slopes became predominantly featureless and the flat areas were covered by numerous small feathery and needle-like growths Second phase (carbide) debris was a feature of the aged condition as distinct from the as-cast state where it was the exception rather than the rule. The incidence of localized plastic deformation decreased, and where it did occur, it was on a much reduced scale. On the macroscale, the prior austenite dendrites were clearly outlined (figure 62), producing a very "rough" fracture surface, with very little plastic deformation at the root of the notch.

It is perhaps significant to record that porosity was found at least 5mms below the surface of the bore of the tube. Figure 63 shows carbide networks quite clearly

delineated on the smooth walls of the cavities enclosing the pores. These carbides, judging from the rounded profile of the area enclosing them, are eutectic carbides rejected from the final liquid which froze before feeding was complete.

A detailed inspection of fracture surfaces in the vicinity of the notch revealed two types of fracture area (figure 64). In the first, located in the upper portion of figure 64 and shown at a higher magnification in figure 65, are the feathery type carbides deposited on the existing as-cast network. These carbides were wafer thin and appeared to have collapsed onto the floor of the fracture. They were quite literally drawn out from between the fine arms of dendrites, strained slightly apart by a tensile stress acting at right angles to the large surface area faces of the carbides. The platelets simply collapsed under their own weight as a result of local distortions caused by deformation in adjacent regions. Many of the original eutectic carbides contained a number of very fine cracks, parallel to one another in any one platelet.

The second feature shown in figure 64, is the row of ovular depressions containing fine debris at the base. This feature, although uncommon may be significant since its incidence was confined to aged alloys. The depressions may have been associated with non-metallic inclusions, and were not found in as-cast steels because the cohesive strength between matrix and inclusion was much greater than that between carbide and matrix, and thus seperation at the latter interface intervened before the inclusion could play a part.

Ageing could possibly reduce the inclusion-matrix cohesive strength by imposing a brittle carbide film around it. This may account for the debris at the base of the depressions in figure 64, and explain why plastic deformation in the region was extremely limited.

Hot-rolled Steels:- Hot-rolling markedly increased the number of dimples on the fracture surface, particularly in alloy A. The dimples tended to be small in size and more regularly spaced, either as large clusters on the slopes of tear-ridges or as individual arrays between regions of cracked carbide. The amount of cracked carbide was reduced, although small amounts of irregularly shaped, high volume to surface-area ratio debris was observed. This feature was absent in as-cast alloys. Thus hot-rolled alloys were characterized by an increase in micro-void coalescence, the presence of small amounts of surface debris and a marked reduction in carbide-matrix decohesion. Fracture regions were not so heterogeneous (figure 66) i.e. typical regions covered much wider areas of the fracture surface. Evidence of a dendritic structure still persisted (figure 67), particularly in alloy B, although the primary dendrite arms were well spread-out in the direction of rolling. Large fracture dimples caused by matrix decohesion from non-metallic inclusions were found on a limited scale.

There was a large incidence of non-propagating micro-cracks within the notch root, persisting in both steels up to and including a 50hour ageing treatment at 725°C (figure 68). These cracks were similar to those found in cast

alloys.

Prolonged ageing reduced the number of dimples formed in both alloys causing plastic flow to become highly localized (figure 69). Nevertheless, dimpling occurred on a greater scale in fully aged rolled alloys than in fully aged cast steels, and accounted for the former's greater toughness and ductility. Furthermore, ageing did not entirely eliminate the formation of tear-ridges. Figure 69 was typical of both alloys in the fully aged condition.

Hot-forged Steels:- Examination of the notch root following fracture in slow bend, revealed a heavily distorted surface with machining marks following a variety of contours. A few small pores were present, probably caused by the close proximity of a second phase particle to the surface. However, there was no evidence of multiple cracking of the kind observed in cast or rolled steels. The entire fracture surface consisted of dimples of varying sizes and shapes. These dimples were considerably larger than those which formed in cast or rolled steels. It was usual to find a large dimple or pore which was itself composed of a number of smaller dimples. Surface debris generally consisted of small, irregularly shaped particles frequently associated with a dimple.

The final important feature of the fracture was the tear-ridge, the peaks of which were often surmounted by small dimples. Figure 70 was typical of alloy A. The pore size of alloy B was more uniform than that of alloy A. Micro-pores or dimples in steel B were large, whilst the summits of the ridges between them were sharper and con-

tained fewer small dimples than alloy A. Tear regions on all fractures examined, showed long drawn out areas between dimples. These regions of intense localized necking produced a final seperation by plastic rupture on the micro scale, and contributed greatly to the increased energy absorption required for fracture. Close examination of dimpled regions, revealed the presence of fractured second phase debris (figure 71) at the base, whilst the walls of the dimples appeared irregular and uneven.

Ageing at 725°C markedly reduced the dimple size, promoted the formation of non-propagating subsidary cracks, and produced a flatter macro-fracture, although the micro-fracture (figure 72) was more heterogeneous. Figure 72 included most of the fractographic features associated with a long term (2000hours) ageing treatment in both steel since fractographically it was impossible to distinguish between the alloys in the fully aged condition. Fractures always contained regions associated with the presence of non-metallic inclusions e.g. manganese sulphide, and a typical example can be seen in the top left-hand corner of figure 72. Here, three particles in close proximity have each nucleated a dimple. These dimples have subsequently only partially coalesced. The remains of a tear-ridge between each dimple can still be seen. Across the whole fractograph, three or four major ridges traverse the structure and form boundaries to regions of great complexity. In these regions, dimples vary greatly in size and are smaller than those found in the as-forged state. Considerable quantities of fracture debris were accumulated on

the surface. Local deformation though more restricted than in the as-forged condition, is nevertheless greater than that found in either as-cast or rolled versions.

4.6.2.2. Effect of Strain-rate

Identical samples fractured in impact at room temperature gave no discernible differences in fracture appearance for cast, rolled or forged steels.

4.6.3. FRACTURES FORMED AT 725°C

4.6.3.1. Influence of Manufacturing Process and Strain-rate

Fracture surfaces discussed below were obtained from bend specimens tested at 725°C in impact and slow bend.

Cast Steels:- Fracture surfaces produced by impact loading showed no differences between the grades tested. However, under slow bend conditions, each grade produced its own distinctive fracture, which was also different from that obtained at the high strain-rate.

At high strain-rates plastic deformation was a general feature of the fracture surface (figure 73). A variety of dimple sizes were present, the larger ones masking the dendritic characteristics of the alloy so apparent in the room-temperature fractures (figure 59). A fair amount of fracture debris was scattered about the surface of the fracture, and in figure 73 a non-metallic inclusion is present, which has not only initiated a dimple but has itself been fractured in the process. The extent of local plastic deformation was most marked (figure 74), with tear-ridges an important feature of the seperation process. The extent of the fracture-path between dendrite arms seemed to be less than at room temperature (figure 74).

The path appeared to run close to the interdendritic zone where seperation was by a form of boundary shearing (figure 73), whilst in others there was strong evidence of carbide-matrix decohesion (figure 74).

Under slow bend loading conditions, the fracture appearance of each alloy was quite different. Evidence of plastic deformation prominent under impact loading, was markedly reduced. Alloy A at low magnification showed a series of steps with well defined treads, which at higher magnifications (figure 75) were found to contain fine shallow "dimples" of a kind not previously observed. These dimples had a ghost-like appearance and formed a honeycomb film on certain areas of the fracture. The peaks of the steps were drawn out, suggesting a shearing or sliding process of seperation rather than the internal necking associated with the formation of a tear-ridge. Elsewhere, the fracture surface was made up of regions where direct interfacial seperation had occurred (figure 76), although there was evidence of a feathery-appearance to the exposed phase, but this could be a result of the oxide film present on the specimen. A few large dimples were present clearly nucleated by non-metallic inclusions.

The austenitic alloy under slow bend conditions had a fracture surface completely covered by debris of a second phase. This debris was quite smooth, and from its shape was most probably the eutectic carbide. Considerable amounts of energy were absorbed by the formation of a number of non-propagating cracks (figure 77) formed at right angles to the main crack front. Evidence of localized

plastic deformation was slight.

Forged Steels:- Both steels produced similar fractures under conditions of impact loading. These had a fair resemblance to those formed at room temperature. The major difference was in the characteristics of the dimples. Here they were either deep and narrow or oval and shallow (figure 78), whereas at room temperature the tendency was for a much larger dimple, both in depth and area, and associated with numerous tear-ridges. There was more second phase debris associated with fracture in steel A. The whole of the fracture surface in both alloys was drawn out in the direction of the macroscopic crack front, a feature probably responsible for the high fracture energy absorption in these alloys.

At low strain-rates the fracture changed from a predominantly transgranular to an intergranular mode (figure 79), whilst the associated general plastic deformation was reduced. The change was more obvious in the duplex alloy (figure 80) where a marked increase in embrittlement took place. In alloy B, there was an increased incidence of localized plastic flow and a decrease in the shear component of failure (figure 81). A few, fine ghost-like dimples were observable in both alloys at higher magnifications, whilst dimples in general were quite shallow and would seem to have formed late in the fracture process. The fracture surface of the duplex alloy was remarkable for the high incidence of "loosened" grains (figures 79 and 80) i.e. grains which were seperated from their neighbours by large cracks.

4.6.3.2. Influence of Prior Ageing at 725°C

An increased ageing time produced an increase in the amount of debris on the fracture surface. In addition, the fracture mode was predominantly intergranular. The increase in fracture debris was most marked in steel B after ageing for 50hours, whilst much longer times (250hours) were required for the duplex alloys. This latter alloy had a more heterogeneous fracture surface. Figure 82 was typical of the cast alloy B where the remains of a degenerate eutectic carbide phase were clearly visible beneath the feathery adornments of the ageing product debris. A few areas of featureless sliding type fracture, were still present on the fracture surface.

In the forged condition, the austenitic alloy fracture path was intergranular after 50hours ageing whilst after 250hours, the ageing product masked the fracture appearance so effectively as to cause some doubt as to whether or not a change in fracture mode had occurred in some regions. The main impression was however, that the increased volume of ageing product within the fracture path contributed greatly to the increased energy absorption required for fracture. The forged duplex alloy had a greater proportion of the fracture area covered by smooth featureless regions (figure 83) which may have been regions of grain-boundary sliding or shear. Further ageing increased the incidence of debris on these featureless areas and presumably contributed to the increase in energy recorded to fracture the test-piece after 250hours at 725°C. Ageing caused a marked reduction in the notched bar yield

stress and a large increase in the offset displacement. These findings were consistent with the increase in grain-boundary shear or sliding observed after short ageing times (particularly in steel A), as well as the reduction in localized plastic deformation which accompanied ageing. However, it is always dangerous to try and relate pre-fracture properties e.g. yield, to the post-deformation fracture event, unless there is strong evidence to suggest that the two are connected. No evidence of this connection was established.

Prolonged ageing of cast alloy A increased the incidence of fine shallow dimples over that of the as-cast state, to a point where their equiaxed form covered significant areas of the fracture surface (figure 84). Inclusions were also able to nucleate shallow dimples, e.g. figure 85 shows an inclusion-nucleated dimple seperating a shallow dimpled region from an area where plastic deformation was absent.

CHAPTER 5

GENERAL DISCUSSION

5.1. INTRODUCTORY

The principal objective of this work has been to develop a suitable mechanical test to study stable crack-growth in high temperature service stainless-steels manufactured by either casting or hot-working processes. The significance of the test in its engineering context is discussed later, and it is proposed here to comment upon those features peculiar to notch-bar testing at elevated temperatures. In addition, an analysis of some of the results of high temperature tests previously reported is presented, with particular emphasis placed on fractographic features and the possible role of segregation.

The complexity of commercial materials makes it difficult in a study of this kind to isolate unequivocally, those rate controlling metallurgical processes which limit the service life. These processes are being studied elsewhere[2] but nevertheless, current work does provide a number of useful pointers to those processes likely to be worthy of fuller study.

5.2. ELEVATED TEMPERATURE NOTCH-BAR TESTING

There are a number of features of notch-bar testing at elevated temperatures which are of little or no importance at low temperatures. The first is the increasing significance of stress relaxation processes at the notch-tip that occurs with increased test temperatures. At low temperatures, the triaxial stresses developed in the region of the notch are relieved by plastic yielding, but at elevated temperatures relaxation may occur, both on-loading and during subsequent creep. As the effect is strain-rate

sensitive, a fairly fast strain-rate has been used in this work to reduce creep processes to a minimum. In addition to this, there exists the possibility of a warm-working process taking place in the vicinity of the notch during loading which could produce a notch-strengthening effect. Precipitation processes in these steels are markedly enhanced by warm-working[93], and the degree of matrix supersaturation would have a profound effect in this respect. Thus the higher yield stresses of the forged grades compared to the cast alloys, could be because a higher matrix supersaturation in the former leads to a greater degree of warm-working. Slow precipitation rates would have little effect in the yielded regions at the strain-rate employed, but fast precipitation rates would promote excessive grain-hardening and may lead to severe intergranular cracking. Metallographic evidence for notch root precipitation could not be obtained by optical microscopy.

It is interesting to note that the rolling-cycle used produced an approximately warm-worked structure, and it was this structure which displayed the least temperature sensitivity for fracture-toughness (figure 50).

Perhaps the most important aspect of an increasing test temperature (at constant strain-rate), is that the grain to grain-boundary strength ratio approaches unity so that the grain-boundary regions become the preferred fracture path in this equicohesive range. At 725°C both the cast and wrought alloys display predominantly intergranular fracture in slow bend (figures 75 and 79), and a high incidence of grain-boundary sliding in unaged

structures (figure 79). Fracture-toughness at these temperatures is markedly improved by the presence of grain-boundary precipitates. However, under conditions of constant load the reverse may be the case and grain-boundary precipitates and particles could act as sites of stress concentration for the initiation of cracks. Thus, the role of the boundary precipitate must be clearly established for both the initiation and propagation of cracks under service loading conditions.

In cast alloys, crack propagation is intergranular or interdendritic at all temperatures, and this produces a number of interesting fractographic features as a result of the different temperature sensitivities of the cohesive strengths of the various constituent interfaces. These are illustrated by a series of fractographs (figures 86 to 93) for cast alloys, aged 50hours at 725°C prior to testing in slow bend at different temperatures. (Corresponding bend test properties were given previously in figures 48 and 49). At the lower test temperatures (375-550°C) an extraordinary range of exposed second phase morphologies are produced. These are worth discussing in detail because the decohesion process leaves the underlying hard phase relatively intact and thus gives a fairly undistorted picture of its morphology.

Alloy A:- A good example of the decohesion mechanism with relatively little cleavage of the underlying carbide is provided by figure 86, where small amounts of plastic deformation are associated with the periphery of the region. The effect is not confined to the carbide phase (figure 87)

as non-metallic inclusions may nucleate a shallow depression. Figure 87 is included because it demonstrates unequivocally, that the shape of the initiating particle determines the shape of the dimple. A further point of interest in this figure is the smooth appearance of the dimple sides compared with those formed at room temperature (figure 55). A low magnification fractograph of this surface (figure 88), shows that the bulk of the fracture is composed of low energy surfaces characterized by featureless depressions, which on closer inspection are found to contain regions typical of figure 86.

Thus the distinguishing features of these fractures compared with those formed at room temperature, are their relative flatness and marked absence of any intense plastic deformation. Thses effects are more pronounced in cast alloy A and a possible reason for this may be associated with the presence of low melting-point trace elements which have segregated to carbide-matrix interfaces. A probable candidate is lead because its concentration in alloy A is about four times that in alloy B (table 1), whilst its melting-point (327°C) is close to the test temperature (375°C) where the energy absorption for fracture was least. The presence of a segregated element immiscible with the final liquid to freeze e.g. lead or possibly tin and bismuth, would promote zones of weakness around the dendrite arms, which would be sensitive to the test temperature. Hot-working would be expected to distribute this segregate throughout the matrix, and it is notable that forged alloys fractured at these lower temperatures

display a predominantly transgranular crack path. Thus the fracture surface of a hot-worked alloy (figure 92), whilst displaying a certain degree of 'flatness' is characterized by large amounts of plastic deformation, with no evidence for the direct decohesion process which typifies cast alloys at these lower test-temperatures.

An increase in the test-temperature from 375°C to 670°C increases the amount of surface deformation although dimple sizes remain small. There is a marked reduction in the amount of carbide debris and decohesion (figure 89), although the stepped nature of the surface persists. At 725°C, the fracture surface is littered with debris and characterized by many fine dimples and tear-ridges, even in the unaged condition (figure 77).

Alloy B:- The austenitic alloy, like the duplex grade has a higher incidence of particle-matrix decohesion at test-temperatures below about 600°C than above. However, the difference is not so marked. In addition large areas of carbide are cracked, distorted and pulled apart, by flow of the underlying matrix (figure 90). Increased plastic deformation characterized by larger dimples is also a feature. Figure 91 shows presumably as NbC platelet from which the surrounding matrix has been pulled away. A number of fine cracks traverse the platelet indicating that the energy required to cause decohesion was exceeded and absorbed by platelet cracking. At this test-temperature (550°C), a few fine dimples are present along the tops of fine tear-ridges and scattered about on the slopes. It is unlikely that the formation of these dimples contributes

much to the fracture energy absorption, not only because of their fineness but also because they appear to form late in the seperation process. Decreasing the test-temperature to 500°C produces an increase in the number of these fine dimples. Figure 93 although not typical of the fracture surface as a whole at this temperature, supports the argument that the dimples contribute little to the fracture energy. The large void in the centre of this fractograph contains a number of fine dimples of approximately the same diameter as those on the faces of the ridge. These however are not elongated, probably because they are shielded from the macro crack front. Thus elongated dimples here are not necessarily indicative of increased fracture toughness, but could be the result of post-cracking deformation.

An increased test-temperature (600°C) produces large amounts of fracture debris (figure 82), which greatly increases the energy requirements for the propagation of a crack.

5.3. TENSILE DATA

5.3.1. ROOM TEMPERATURE RESULTS

It was possible to relate the true stress σ, to the true strain ϵ, in uniaxial tension by a simple power law relation:

$$\sigma = k\epsilon^n \qquad (14)$$

where 'k' and 'n' are constants. The equation was valid for true strains greater than about 0.1. At lower strains an identical power law but with reduced values for 'k' and 'n', gave a reasonable fit to the data. Similar results have been widely recorded in the literature and referred

to as 'double n' behaviour[94,95].

The engineering stress-strain curves of forged and aged steels exhibit a necking strain after the instability point has been reached. The cast duplex steel has a small necking strain but this is eliminated on ageing. The cast austenitic steel displays zero necking strain and requires a prolonged solution treatment at 1250°C before necking strain is observed. Characteristically, mechanical instability and the onset of necking, are associated with the point on the stress-strain curve, where the increase in flow-stress caused by strain-hardening, is insufficient to offset the increased applied stress caused by the decreasing cross-section area of the test-piece[96]. The work-hardening rate at a particular value of stress and strain is obtained by differentiating equation (14).

$$\frac{d\sigma}{d\epsilon} = \frac{n\sigma}{\epsilon} \qquad (15)$$

It has been shown[96] that materials obeying the power law reach a mechanical instability when the true strain in the material becomes equal to the strain-hardening exponent 'n'. However, the instability or maximum load true strain ϵ_I, and 'n' are not always equal in these steels (figure 94), and it is possible to categorize the discrepancies according to the manufacturing process of the alloy. Forged steels, either as-worked or aged, have strain-hardening coefficients equal to the instability strain. The semi-wrought or rolled structure displays similar behaviour, but prolonged ageing causes ϵ_I to become less than 'n'.
In cast steels there is a large discrepancy between 'n' and

ϵ_I. This discrepancy may be reduced by solution-treating or markedly increased by ageing at 725°C. Duplex steels generally have higher work-hardening coefficients and instability strains than austenitic steels. For those manufacturing processes and heat-treatments where $n \neq \epsilon_I$, the maximum load instability is largely the result of second phase particle - matrix decohesion rather than a mechanical instability. This explanation is supported by fractographic evidence (figure 58 for example), and the observation that a prolonged solution treatment of the cast alloys reduces the discrepancy between 'n' and ϵ_I by increasing ϵ_I at a greater rate than 'n'.

The use of 'n' as a measure of the work-hardening characteristics of an alloy can be misleading, particularly for comparative purposes[97]. It is possible for two materials with the same value of 'n', to have different work-hardening rates when the flow-stress of one material at constant strain is greater than that of the other. Thus the work-hardening rate $d\sigma/d\epsilon$ is preferred to 'n'. The latter merely reflects the average strain-hardening behaviour, correlating well for these particular alloys with the yield to tensile ratio in tension (figure 95).

Figures 96 and 97, show the variation of flow-stress with work-hardening rate for each steel, measured at a true strain of 0.15 and at the maximum load instability. The points are for a variety of heat-treatments including solution and ageing treatments. Where the maximum load instability is a true mechanical instability then $n = \epsilon_I$, and thus the work-hardening rate is equal to the maximum

value of true stress. This equality is shown by the dashed lines in figures 28 and 29. Considering the instability behaviour and the results for $\epsilon = 0.15$, it is possible to draw scatter-bands encompassing points for each manufacturing process for the complete range of strains to instability. For clarity only the values at $\epsilon = 0.15$ and $\epsilon = \epsilon_T$ have been included. For any particular strain, the work-hardening rate is greatest in forged alloys and least in cast steels, although the range of work-hardening rates is greatest for cast alloys and least for forged alloys. As the strain increases, the range of $d\sigma/d\epsilon$ decreases.

At instability the work-hardening rate is approximately the same irrespective of manufacturing process with the exception of the fully aged (1000hours 725°C) cast alloys. (Point I in figures 96 and 97). The range of flow-stresses at instability is very large and is a maximum for forged grades. It is impossible to categorize rolled and forged duplex alloys in this way as their behaviour is similar, possibly as a result of the strain induced transformation. For a given value of flow-stress, wrought steels have higher work-hardening rates than the equivalent cast grades, despite the much wider range of 'n' values displayed by the latter (0.18 to 0.5) compared to forged steels (0.35 to 0.5). A final feature of figures 96 and 97, is the similar slopes of $d\sigma/d\epsilon$ vs σ_T for both alloys. A value for this slope is -2.85 although its significance is not understood.

5.3.2. EFFECT OF SECOND PHASE PARTICLES

It is important that considerable care is taken in

interpreting the effects of second phases on strength, ductility and toughness. Direct comparisons between the cast and hot-worked states must take account of unavoidable differences in other microstructural variables. In particular, dislocation density and distribution as well as the extent of solid solution hardening, may produce unquantifiable interactions which could effectively mask other changes. However, figures 96 and 97 suggest that despite wide variations in heat-treatment, the work-hardening characteristics of each alloy still retain the influence of the manufacturing process. Thus it is assumed for this discussion that changes in microstructural variables other than those associated with the size, morphology and distribution of second phase particles are of only secondary importance.

Second phases, whether as hard particles like carbides or soft phases such as delta-ferrite, have a most pronounced influence on the fracture mode and pre-fracture ductility of these alloys. Scanning electron microscopy of the fracture surface revealed that the most important factors were the location of these particles within the microstructure, and their ability to dissipate local stress concentrations. This can occur by localized plastic deformation (figure 55) before the particle either fractures (figure 57), or decoheres from the surrounding matrix (figure 58) or both (figure 66). This ability to dissipate local stress concentrations is controlled by the particles size (figure 72), morphology (figure 59) and distribution (figure 67). The major difference in the room temperature fracture toughness

of cast and forged alloys is thus a reflection of the ability of the latter version to withstand large amounts of localized plastic flow before the creation of free surfaces. This is a direct consequence of the more uniform distribution of the second phases throughout the matrix, and their low surface area to volume ratio in forged alloys. In cast alloys, the reduced fracture-toughness is a direct result of particles with high surface area to volume ratios being preferentially located in interdendritic regions.

The yield strengths of wrought materials are little different from their cast counter-parts at room temperature, whilst the tensile strength generally shows an increase of about 20% (figures 31 - 34). However, the fracture-toughness as measured by an energy criterion (e.g. E_{ml}), for wrought steels is at least three times that of the cast equivalent (table 5). Thus the ease of ductile crack propagation as measured by δ_{ml}, is more likely to be described by the basic strain and work-hardening characteristics of the alloys rather than by strength parameters. This suggestion gains further credence from the observation of notch strengthening in the bend test i.e. the yield-stress in notch bend is more sensitive to microstructure than the 0.2% proof-stress in tension, e.g. yield-stress in bending for forged alloys is approximately twice that for cast alloys. Thus ductile crack propagation is more difficult in forged steels, because the increased work-hardening rate (figures 31 - 34) increases the plastic zone size (table 6), thereby promoting crack stabilization.

In the ordinary tensile test the two commonly accepted indices of ductility which may have an influence on fracture-toughness, are uniform elongation prior to necking and reduction of area at fracture. The relation between the uniform elongation and the strain-hardening capacity 'n' has already been described. This relation predicts that large strain-hardening capacities will promote extensive uniform elongation providing some form of interfacial decohesion does not intervene. Tensile reduction of area at fracture is an indication of "local" ductility. This measurement is an indication of the strain at fracture of a bulk sample, and is reduced by the presence of weakly bonded inclusions and second phase particles which can act as centres for the nucleation of micro-cracks and cavities. Thus pure metals if completely free of second phase particles, can exhibit 100% reduction of area. The relevance of local ductility is its possible correlation with ductile cracking resistance or fracture-toughness . The correlation was established as figures 53 and 54 and showed that large changes in local ductility produced only small change in fracture-toughness at lower levels of local ductility. This is the region where interfacial decohesion is the preferred mode for fracture. Thus high fracture-toughness is associated with increased local ductility.

5.3.3. 'DOUBLE - n' BEHAVIOUR

Earlier it was reported that two equations of the form $\sigma = k\epsilon^n$ could be fitted to the true stress - ture strain data for both alloys. The changeover point occurred in the range of strains ϵ = 0.11 to 0.07, with the changeover

taking place at the lower end of the strain-range as ageing progressed. Heavily embrittled cast steels displayed only 'single - n' behaviour. The value of the strain-hardening exponent at low strains (n_1) was less than the value (n_2) at higher strains. Similar behaviour in austenitic stainless-steels has been reported elsewhere[94] and associated with the formation of a strain-induced martensite. This would seem to provide only a partial explanation for the transition, because martensite formation could not be detected either magnetically or metallographically in steel B.

Hot-working markedly increased n_2 but had no effect on n_1. Subsequent ageing slightly increases n_1 (from 0.22 to 0.26) across all grades whilst n_2 registered a more pronounced decrease, e.g. from 0.38 to 0.26 for cast alloys and from 0.46 to 0.38 for forged alloys. Thus it seems probable that a basic change in the work-hardening process is responsible for the 'double - n' behaviour when a certain degree of strain-hardening is achieved. The insensitivity of n_1 to hot-working further indicates that the initial strain-hardening process is largely unaffected by considerations of particle size and distribution, so that particle boundary conditions are only important at higher strains. Such an hypothesis may account for the roughly linear correlations observed between k_2 and n_2 for each manufacturing process (figure 98) irrespective of subsequent heat-treatment. Thus the final strength k_2 (at ϵ = 1.0), is a function of the strain-hardening capacity as determined by the manufacturing process.

Finally, the 'double - n' behaviour offers an explanation for an apparent anomaly in figures 32 and 34. These figures show that constant or falling work-hardening rates are produced by ageing hot-worked alloys. Since the tensile strength is largely unaffected, a falling work-hardening rate may be expected to increase and not decrease the instability strain as indicated[98]. However, progressive ageing causes the change from n_1 to n_2 behaviour to take place at lower strains whilst the value of n_1 itself increases. These changes are indicated schematically in figure 99, and show that for a constant or slowly decreasing work-hardening rate, the instability strain will also decrease.

5.3.4. ELEVATED TEMPERATURE RESULTS

The simple power law (equation 14), described the relationship between σ and ϵ for test-temperatures in the range 400-800°C. 'Double - n' behaviour was observed but the value of strain for the changeover was erratic. The limitations of 'k' and 'n' for describing the strain-hardening characteristics have already been discussed, and $d\sigma/d\epsilon$ has shown to be a more useful parameter. Equation (14) is even less satisfactory for investigationg the temperature dependence of work-hardening behaviour, because it fails to differentiate between the temperature dependence of flow-stress and work-hardening. The difficulty may be resolved by seperating the two effects in an equation of the form:

$$\sigma = \sigma_0 + k_t \epsilon^{n_t} \qquad (16)$$

where σ_0 is the flow-stress at zero plastic strain. The

temperature dependence of flow-stress is reflected by changes in σ_o, whilst K_t and n_t are determined solely by the work-hardening behaviour at each temperature. The difficulty in applying equation 16, is assigning values for K_t, n_t and σ_o, although an existing method[97] has been extended and is described in appendix II. Equation 16 was valid for low strains only ($\epsilon \sim 0.1$) and showed a progressive positive increase in slope at higher strains. Further attempts to fit equations to high temperature stress-strain data were abandoned.

5.4. THE RELEVANCE OF THE MAXIMUM LOAD C.O.D.

In ductile alloys, the importance of the maximum load C.O.D., or its equivalent ϵ-offset, lies in its possible extension to describing crack behaviour in real structures. Ductile fracture processes irrespective of formation in laboratory test-pieces or structures, are always associated with three somewhat overlapping events. First, the initiation of a ductile tear at a certain crack-tip displacement δ_i, (in the cast steels considered here this is taken to be equivalent to a fixed amount of interfacial decohesion). Secondly, the incidence of a certain amount of stable crack-growth 'x', which leads to a third event, a maximum load instability associated with a crack-tip displacement δ_m measured at the original notch-tip location. The C.O.D. test in these and similar alloys may therefore in theory provide two measures of ductile fracture resistance. In the first, the C.O.D. at the instant of crack initiation (δ_i) is measured, whilst in the second the C.O.D. corresponding to the maximum load instability on the

load-deflection diagram (δ_m) is recorded. This at once raises the question of a definition of the practical as well as the experimental significance of the C.O.D. concept, because it is now necessary to draw a distinction between δ_m and δ_i and rationalize the contribution of stable crack-growth 'x' to the measured crack-tip displacement at maximum load. More specifically, δ_m could have the same value in two different steels, but be composed of a high value of δ_i with a small amount of crack extension in one alloy, and a low δ_i coupled with an increased crack extension in the other. Which of these conditions is preferable would depend upon the particular application envisaged as well as the design criteria. The simplest answer to the problem, is to adopt the most rigid design criteria possible i.e. consider that the first initiation of a crack constitutes failure and thus measure only δ_i. This solution is unrealistic because it is uneconomic in terms of material and poses the additional experimental problem of measuring δ_i quickly and reliably. In addition, no information on crack propagation characteristics is obtained from a measurement of δ_i. This was one of the disadvantages of the tensile test which prompted the current investigation.

The measurement of δ_i is difficult experimentally, because the distinction between small amounts of microcrack extension which occur soon after general yield, and the macroscopic seperation of the faces of the notch which defines the measured C.O.D., is a very subtle one. In addition, δ_i does not adequately reflect changes over the

whole crack front during the early stages of the plastic loading process, since crack fronts are seldom uniform and may contain non-propagating micro-cracks (figure 68). These additional cracks are in themselves an indication of toughness, and indeed the first crack to form may not be the one which ultimately propagates to final fracture. Measurement of δ_i would ignore these features.

Knott[99] has described a technique for measuring δ_i in structural steels, whereby a series of specimens are unloaded from various levels below the maximum load and then fractured in impact. The length of fibrous thumbnail on the fracture surface is recorded and plotted against the measured C.O.D. Extrapolation of the curve to zero crack length provides a value for δ_i. It was further shown that this value of δ_i varied according to the width of the initial slot. However, a consistent fracture strain of 80% was obtained by dividing δ_i by the initial slot width, suggesting that the fracture criterion for the material was one of constant strain. The value of δ_i for a fatigue-crack starter was also determined using the extrapolation procedure, and the resultant value of δ_i when divided by the 80% fracture strain, gave an effective gauge-length for the fatigue crack equal to the inter-particle spacing between the MnS inclusions in the steels which Knott examined.

In the current work, fatigue pre-cracked specimens were not available and there were insufficient test-pieces to repeat this experiment. However, it is unlikely that a similar result would be obtained, at least for the cast

steels, because the fracture mechanism is quite different and not necessarily controlled by particle spacings. In addition it is unlikely that the concept as described could be extended to elevated temperatures where boundary sliding processes are important forms of cracking.

The relevance of δ_i to design in these steels is also limited because of the infrequency of catastrophic failures reported in service[3], immediately following the initiation of a crack. More usually an extended period of slow crack-growth is required before growth becomes unstable. Thus it is essential to have some indication, no matter how restricted, of the ability of the alloy to tolerate extensive slow crack-growth without the structure becoming unstable. Indeed, this property is probably indicative of a greater toughness than that typified by a high value of δ_i followed by immediate fast fracture. Experimentally, δ_{ML} is a great deal simpler to measure, both by direct optical methods or indirectly via the correlation with ϵ offset. A further desirable feature is the fair correlation of δ_{ML} with notch root contraction (figure 51) which provides a possible quality control type test which is both economic and straightforward to conduct. Thus the instability point and its associated C.O.D. (δ_m) or displacement (ϵ_{off}), is considered to adequately describe the toughness of the material in terms of its ability to tolerate slow crack-growth without becoming unstable. Its usefulness, particularly in design would be further enhanced[100] if the results from small scale laboratory test-pieces could be related to crack-growth in real

structures.

5.5. RELATIONSHIP BETWEEN MECHANICAL PROPERTIES AND FRACTURE

Ductile fracture properties are much influenced by the local stress state, and this imposes a severe limitation on the tensile test because ductile fracture occurs in the neck of the specimen where the degree of macro-triaxiality is highest. In addition, information about the resistance of the material to propagating cracks is severely curtailed by the instability which occurs at the onset of necking. Against this, the test does provide easily recorded measurements related to tensile instability and fracture, and gives accurate indications of work-hardening response useful for comparative purposes.

In contrast to this, the crack-tip displacement bend test does permit an approximate differentiation between crack initiation and propagation resistance, although the location of the initiation point on the load-deflection diagram is difficult to determine. The test offers other advantages:-

1) It takes account of large strains.
2) It may be used to study intermittent crack-growth.
3) It takes account of three-dimensional effects without having to resort to complex mathematical analyses.
4) It may be used as a scaling factor for translation from small laboratory test-pieces to service structures.
5) In a corrosive environment, the crack-tip

displacement controls the rate of approach of the environment to the crack-tip.

The major disadvantages of the test, particularly as a screening or quality-control test are its cost and the time taken to conduct it. The failure of the multiple notch technique reported earlier as an easy measure of C.O.D. is unfortunate, but the notch root contraction correlation is perhaps more hopeful.

5.5.1. EFFECT OF MICROSTRUCTURE ON NOTCH-TIP DEFORMATION

The interdendritic networks of carbides are the principal features of the cast-steels. Fractographs (figures 57 and 58) show large plates of high surface area to volume ratio. These plates interweave between dendrite arms to produce what is almost a continuous network. In forged alloys the situation is quite different. Here, the carbides are present more as discrete particles (figure 70) randomly distributed throughout the matrix, with no apparent preference for either a grain-boundary or intragranular precipitation site. The rolled steels share features common to both cast and forged steels, although there is a marked dominance of those features more closely associated with the cast grades. Thus these steels will be considered for this discussion as behaving as "cast".

The deformation and fracture response at the tip of a narrow slit situated in each microstructure, is very different. The possibility of an interaction between the finite width of the slit (0.15mm) and the columnar grain width in cast steels, cannot be excluded. Fractographic evidence (figure 62) suggests that the fracture path tends

to favour the region between columnar grains in cast steels, and this tendency is enhanced by ageing. In contrast to this, the tip of the notch does not remain enclosed by a precipitate free columnar grain for the full thickness of the specimen, but contains regions of dendritic carbide as well. Thus the measured C.O.D. reflects rather the integrated value of strain along the notch root and should not reflect the interaction of the finite width of the slit. If notch starters of infinite root radius e.g. fatigue cracks were employed then the interaction may be highly significant in both versions, because the slit width is now less than that of the microstructural components. In forged steels, the width of the machined slit is always far greater than any microstructural feature so no interaction should be recorded.

A further point connected with the finite root radius interaction, is the problem of stable crack-growth. Since cracks initiate very early in the test cycle ($\delta_i \ll \delta_{ML}$), the bulk of the contribution of displacement to δ_{ML} is made up of the stable growth of a crack with a sharp tip radius. Thus a maximum load C.O.D. is unlikely to be affected significantly by the finite root radius interaction. The initiation C.O.D. δ_i on the other hand, would be very sensitive to this effect. Thus δ_{ML} is assumed to be independent of the microstructural root radius interaction.

The large displacements recorded by all but the most brittle samples, suggests that the effects of macro stress-state along the plane of the root of the notch, may be safely ignored, and that a state of virtual plane stress

exists. The credibility of this assumption is further enhanced by the observation recorded earlier, that the crack does not necessarily initiate at the mid-section thickness, where the maximum degree of restraint may be reasonably expected to exist. The conclusion drawn from this, is that fracture is controlled by events on a local or micro-scale rather than by the macro-stress state. The presence of continued slow crack-growth after the geometrical instability in the bend test is further evidence for this. Thus the fracture process is concerned with the effects of microstructural constituents on the mechanisms of stress and strain concentration, which produce a local instability and a further increment of crack-growth. Each microstructural constituent, will make a discrete contribution to the measured crack-tip displacement, by an amount dependent upon its size, shape and orientation to the crack front and upon its position within the plastic zone. The integrated sum of all these contributions will be the measured crack-opening displacement, and thus the C.O.D. reflects a kind of integrated value of strain.

An increased bending moment during the early stages of the C.O.D. test, produces an increased stress concentration at the slot tip. Eventually, at some point below general-yield, the local-yield stress of the matrix at a few places along the plane of the notch will be exceeded, and small amounts of plastic flow will take place. The exact location and number of these points, will depend very closely on the distribution of local stress concentra-

ting microstructural features at the root. In a situation where a uniform dispersion of particles is present (forged), there will be a tendency for the point of initial local fracture to be influenced by the point of maximum constraint. This point is generally close to the centre of the notch root. Thus restricted plastic flow precedes fracture at the centre of notch root whilst an increased amount of deformation can occur before fracture at the surface. Subsequent loading to the point where cracks become visible confirms this, although there were a few cases where initiation seemed to take place close to the surface. This can only be ascribed to inadequate notch preparation. Forged samples, aged at 725°C prior to testing always initiated cracks close to the mid point of the notch root.

Conversely, a non-uniform dispersion of irregularly shaped particles (cast), gives an entirely different response. A high proportion of carbide plates with an orientation such that the maximum surface area of the plate is exposed perpendicular to the tensile stress at the notch root, will provide a preferred site for crack initiation. This arises because local matrix flow in the root of the notch, is forestalled by decohesion at the plate-matrix interface or by the carbide plate itself cracking. This process may describe events over a certain portion of the total notch width. Elsewhere, small plastic zones develop, until the concentration of strain is such that the strength of particle-matrix interfaces is exceeded and decohesion or plate fracture occurs as before. Thus initiation of a visible crack within the notch root occurs over a range of

strains, and the incidence of non-propagating micro-cracks (figure 68) is high. Examination of fracture surfaces shows large amounts of carbide debris to be present, but it is impossible to be sure whether this is a consequence of plastic deformation inducing plate cracking ahead of the main crack, or whether it is a result of post-fracture surface deformation caused by the non-uniform crack front.

Scanning electron microscopy shows many cracks in the machined notch root of cast and rolled specimens after fracture. Some of these cracks have propagated only a few microns, but others as much as 0.5mms. Subsequent ageing reduces the incidence of these cracks, and prolonged ageing (250hours at 725°C) eliminates them altogether. There are two explanations for this behaviour. In the first, the grains themselves are strengthened by the ageing process, which means that higher stresses are required to cause equivalent amounts of plastic flow, so that the matrix-carbide interfacial strength is exceeded at lower strains (displacements). The second explanation proposes an increase in carbide-matrix interfacial area together with a possible segregation of trace elements, which promote a weakening of the interface. Thus reduced strains and displacements are required before the matrix-carbide interfacial strength is exceeded.

Available evidence suggests that an interdendritic boundary weakening process is the more likely cause, for a number of reasons. First, grain strengthening although likely to reduce the incidence of multiple cracking along the root of the notch, will not eliminate it. Secondly,

no evidence of grain strengthening could be detected by micro-hardness methods. Thirdly, the increase in yield-strength in tension after 50hours ageing at 725°C, is insufficient to account for the large decrease observed in δ_m. Finally, a test temperature of 375°C after ageing produced a fracture surface (figure 86) characterized by large areas of carbide-matrix decohesion, suggesting segregation of a low melting point element, presumably lead. Additional fractographic evidence (figure 61), demonstrates that a large increase in carbide-matrix decohesion occurs during ageing, almost to the complete exclusion of ductile tear-ridges and dimples. These observations are consistent with the second explanation and with the absence of non-propagating cracks within the notch root.

Multiple notch root cracking is not a feature of forged alloys, because precipitates are more uniformly distributed throughout the matrix, and thus only one type of fracture mechanism is operative.

Finally, the suggestion that local displacement varies considerably along the root of the notch is given substance by the observation that parallel scratches along the notch root imparted by the notch cutting process, meander considerably after straining. This suggests quite forceably, that events leading up to the initiation of a crack, are very much a function of the microstructural constituents within the immediate vicinity of the crack, and that the macro-stress state is of only secondary importance.

CHAPTER 6

CONCLUSIONS AND IMPLICATIONS

6.1. CONCLUSIONS

1. The measurement of a maximum load C.O.D. (or its equivalent) in these steels, constitutes a realistic measure of fracture-toughness because it takes account of stable crack-growth.

2. The alloy manufacturing process has a marked effect on fracture-toughness because it determines the location, number and morphology of second phase particles. These in turn control the incidence of plastic deformation and thus the energy requirements for intermittent crack propagation.

3. The test-temperature has a significant effect on the fracture-toughness because the intermittent nature of slow crack-growth in these alloys, is affected by the differing temperature sensitivities of the bond strengths of the microstructural interfaces.

4. The relief of local stress concentrations has a marked effect on the incidence of cracking. Thus the height of the tear-ridges and the depth of the dimples on the fracture surface have the greatest influence on the measured C.O.D.

5. Measurement of notch root contraction provides a simple guide to fracture-toughness.

6. The fracture-toughness of alloy A at 25°C was superior to that of alloy B in an equivalent condition.

7. Above the equicohesive temperature, the fracture-toughness of alloy B was superior to that of alloy A irrespective of manufacturing process.

8. Alloy A in the cast form was more prone to embrittlement

in the temperature range 375-600°C than alloy B. This may have been due to the segregation of lead to the dendrite interfaces.

6.2. IMPLICATIONS

This research has been primarily concerned with the development and extension of the C.O.D. concept as a measure of fracture-toughness to two austenitic steels. In particular, the fracture-toughness has been assessed for a few selected microstructures and test conditions. Certain practical implications are apparent in the limited number of results obtained, from which a few suggestions for possible alloy development and further work can be made. In outline these include:-

1. Optimum Structure:- This would seem to be based on a warm working process which in this work approximated to the rolled structure. This structure combined the superior fracture-toughness exhibited by fully hot-worked structures at temperatures below equicohesivity, with the increased toughness of cast alloys displayed above the equicohesive temperature i.e. the variation of fracture-toughness with the temperature (figure 50) was low. Thus a detailed examination by transmission electron microscopy of the microstructure of cast, warm-worked and hot-worked alloys, is required to establish the type and nature of the second phase particles most effective in improving the resistance to slow crack-growth.
2. Role of Delta-Ferrite:- This was difficult to establish because its influence in steel A could not be seperated from the effects of trace element segregation. In

addition the base compositions of steels A and B were too dissimilar for a meaningful comparison to be made. Accordingly, a third steel will be examined where it is hoped that these objections will be absent.

3. Suitable Test for Alloy Comparison:- Current work indicates that the slow bend test is adequate for this purpose and provides measures of strength, fracture-toughness and ductility. However, the use of an impact test is discouraged on two counts. First, it yields only a single test parameter, i.e. the total fracture energy; and secondly the high strain-rate tends to produce equi-cohesivity at higher temperatures than those found in service, and may thus discriminate in favour of hot-worked alloys because their fracture-toughness is superior in the transgranular mode.

REFERENCES

1. "Materials for Steam Reformer Furnaces", A research programme proposed by Battelle Memorial Institute, Columbus Ohio, 1968.

2. D.E.Relf, Brunel University, Research in Progress.

3. Materials Technology in Steam Reforming Processes (ed. C.Edeleanu), Pergamon Press, 1966.

4. R.G.Baker, J.I.Mercer, Gas Council Research Communication, GL 129, 1966.

5. R.T.White, PhD. Thesis, University of Leeds, 1970.

6. H.S.Avery, Welding Council Res. Bull. 143, 1969.

7. G.S.Cole, Met. Trans. 2, 357, 1971.

8. C.Edeleanu, B.Estruch, I.S.I. Spec. Rep. 86, 220, 1964.

9. G.F.Bolling, W.Tiller, J.Appl.Phys. 32, 2587, 1961.

10. J.J.Kramer, etal, Trans. A.I.M.E., 227, 374, 1963.

11. A.Kohn, Rev. Met., 67, 23, 1970.

12. J.H.Decroix, etal, I.S.I. Pub. 108, 135, 1968.

13. J.M.Silcock, J.I.S.I. 201, 409, 1963.

14. J.Van Aswegen, etal, Acta Met. 12, 1, 1964.

15. M.C.Chaturvedi, etal, J.I.S.I. 206, 1146, 1968.

16. D.W.Borland, R.W.Honeycombe, Met.Sci.J. 4, 14, 1970.

17. J.Irani, R.Weiner, J.I.S.I. 203, 913, 1965.

18. J.M.Silcock, Acta Met. 14, 687, 1966.

19. J.W.Cahn, Acta Met. 15, 168, 1967.

20. F.B.Pickering, "The Relation between the Structure and Properties of Metals", P.397, H.M.S.O. London, 1963.

21. J.Van Aswegen, R.W.Honeycombe, Acta Met. 10, 262, 1962.

22. J.M.Silcock, W.T.Tunstal, Phil. Mag., 10, 361, 1964.

23. P. S.Kotval, Trans. A.I.M.E. 242, 1651, 1968.

24. J.M.Silcock, A.W.Denham, "The Mechanism of Phase Transformations in Crystalline Solids", P.59, Inst. Metals, London, 1969.

25. J.W.Cahn, Acta Met. 4, 449, 1956.

26. H.B.Aaron, H.I.Aaronson, Acta Met. 16, 789, 1968.

27. U.E.Wolff, Trans. A.I.M.E. 236, 19, 1966.

28. L.K.Singhal, J.W.Martin, Trans. A.I.M.E. 242, 814, 1968.

29. H.Gleiter, Acta Met. 17, 565, 1969.

30. E.D.Hondros, "Interfaces", P.77, (ed. R.R.Gifkins), Australian Institute of Metals, Melbourne, Butterworths, London, 1969.

31 J.H.Westbrook, Met. Revs., 9, 415, 1965.

32. P.Davies, "Grain Control", P.1. Institution of Metallurgists Course, Sussex University, 1969.

33. E.Voce, A.P.Hallowes, J.I.M. 73, 323, 1947.

34. R.E.Howard, A.B.Liddiard, Phil. Mag., 12, 1179, 1965.

35. B.J.Edelson, W.M.Baldwin, Trans. A.S.M., 55, 230, 1962.

36. B.A.Bilby, etal, Proc.Roy.Soc. A272, 304, 1963.

37. J.M.Krafft, App.Mat.Res., 3, 88, 1968.

38. J.T.Barnby, etal, Acta Met. 12, 1253, 1964.

39. J.Gurland, Trans. A.S.M., 56, 442, 1963.

40. C.Zener, "Elasticity and Anelasticity of Metals", P.158, Chicago Univ. Press, 1948.

41. D.McClean, J.I.M., 85, 468, 1956-7.

42. R.C.Gifkins, Acta Met., 4, 98, 1956.

43. D.Hull, D.E.Rimmer, Phil. Mag., 4, 673, 1959.

44. A.H.Cottrell, I.S.I., Spec.Rep. 70, P.1, 1961.

45. J.Plateau, I.S.I., Spec.Rep. 64, 157, 1959.

46. J.Plateau, I.S.I. Spec.Rep. 64, 147, 1959.

47. I.G.Palmer, etal, "Physical Basis of Yield and Fracture", P.53, Inst. of Physics Conf.Proc.1, 1966.

48. A.R.Rosenfield, Met.Revs. 13, 29, 1968.

49. I.L.Mogford, Met.Revs., 12, 49, 1967.

50. A.H.Cottrell, "The Tewkesbury Symposium on Fracture", P.1, (ed. C.J.Osborn), Brown Prior and Anderson, 1965.

51. A.A.Wells, Brit.Weld.J., 10, 563, 1965.

52. A.S.Tetelman, A.J.McEvily, "Fracture of Structural Materials", John Wiley, 1967.

53. F.A.McClintock, Proc.Roy.Soc., 285, 58, 1965.

54. F.A.McClintock, etal, Int.J.Frac.Mech., 2, 614, 1966.

55. F.M.Burdekin, "Practical Fracture Mechanics for Structural Steel", P.C1, Chapman Hall, 1969.

56. D.Elliott, etal, B.I.S.R.A. Open Report MG/S/7/71, 1971.

57. A.S.Tetelman, "Weld Imperfections", P.249, A.S.M., 1969.

58. D.S.Dugdale, J.Mech.Physics Solids, 8, 100, 1960.

59. J.L.Williams, etal, 1st Int.Conf.Fracture, Sendai, Japan, Paper A - 16, 1965.

60. J.R.Dixon, Int.J.Frac.Mech., 1, 224, 1965.

61. A.A.Wells, F.H.McBride, Canadian Met.Quart., 6, 347, 1967.

62. G.Brauer, R.Lesser, Z.Metallk, 50, 8, 1959.

63. N.E.Hannerz, etal, J.I.S.I., 206, 68, 1968.

64. H.J.Goldschmidt, Interstial Alloys, P.52, Butterworths, 1967.

65. E.G.Bain, W.E.Griffith, Trans. A.I.M.E., 75, 166, 1927.

66. J.A.Venables, Phil. Mag., 7, 35, 1965.

67. C.J.Gunter, R.P.Read, Trans. A.S.L., 55, 399, 1962.

68. L.Weil, Rev.Met., 61, 63, 1964.

69. I.Tamura, etal, 2nd Int.Conf. on Strength of Metals and Alloys, Paper 13 - 7, A.S.M., 1970.

70. D.Dulieu, J.Nutting, I.S.I., Spec.Rep., 86, 140, 1964.

71. D.T.Llewellyn, J.D.Murray, ibid, P.197.

72. M.Chaturvedi, ibid, P.153 (in discussion).

73. J.Nutting, ibid, P.160 (in discussion).

74. D.Elliott, M.J.May, B.I.S.R.A. Open Rept. MG/C/86/68, 1968.

75. J.F.Watson, J.L.Christian, Trans. A.I.M.E., 224, 998, 1962.

76. J.T.Barnby, J.I.S.I., 203, 342, 1965.

77. G.Thomas, etal, 2nd Int.Symp. "High Strength Materials", P.251, John Wiley, 1965.

78. J.S.Blakemore, E.O.hall, J.I.S.I., 204, 817, 1966.

79. E.Russell, Phil Mag., 8, 615, 1963.

80. B.J.Brindley, P.J.Worthington, Met.Rev. 145, 1970.

81. K.S.Rose, S.G.Glover, Acta Met., 14, 1505, 1966.

82. A.H.Cottrell, Phil. Mag., 44, 829, 1953.

83. R.K.Ham, D.Jaffrey, Phil. Mag., 15, 247, 1967.

84. W.Charnock, Phil Mag., 18, 89, 1968.

85. A.H.Cottrell, "Creep and Fracture of Metals", P.141, N.P.L. Symposium, H.M.S.O., London, 1956.

86. A.Westwood, T.Broom, Acta Met., 5, 249, 1957.

87. D.Sprake, etal, J.I.S.I., 203, 152, 1965.

88. R.Summerling, J.Nutting, J.I.S.I., 203, 398, 1965.

89. J.D.Baird, A.Jamieson, J.I.S.I., 204, 793, 1966.

90. R.Raring, Paper presented at 55th Annual Meeting of A.S.T.M., 1952.

91. D.Elliott, H.Stuart, Proc.3rd Annual Scanning Electon Microscope Symposium, P.305, Chicago, 1970.

92. W.A.Spitzig, etal, "Electron Fractography", P.17, A.S.T.M. - S.T.P. 436, 1968.

93. G.P.Sanderson, D.T.Llewellyn, J.I.S.I., 207, 1129, 1969.

94. J.Lefevre, C.D.S. Circ. (3), p.805, B.I.S.I. Translation 8411, 1970.

95. H.J.Kleemola, J.I.S.I., 208, 1025, 1970.

96. G.Deiter, Proceedings of A.S.M. Seminar 'Ductility', P.5, 1968.

97. S.V.Ramani, P.Rodriguez, Scripta Met, 4, 755, 1970.

98. C.Bodsworth, Private Communication.

99. J.F.Knott, R.F.Smith, "Practical Applications of Fracture Mechanics to Pressure Vessel Technology", P.65, Inst.Mech.Engrs., 1971.

100. G.D.Fearnehough, B.Watkins, Int.J.Frac.Mechs., 4, 233, 1968.

APPENDIX I

FORM OF SERRATIONS
(strain rate = 0.071 sec^{-1})

AS-FORGED STEELS

At the lower end of the temperature range (450°C), alloy A exhibited a gentle fluctuation in the load at a strain close to the instability strain. An increase in the test temperature to 500°C produced a more distinct type of serration (figure 38a) in steel B. As the strain increased, each serration required a progressively larger strain range for its completion, but close to the instability point they disappeared completely. After instability, there was a very pronounced oscillation of the load around the mean value on the falling-load portion of the curve.

In addition, steel A exhibited a second type of serration (figure 38b) which alternated with that just described. The new serration appeared first, and required about half the strain range of the former to complete a cycle. In all, three serrations of this type (figure 38b) were formed and two of the former (figure 38a). Following instability, the load-extension curve remained quite smooth. ϵ_c in steel A was much greater than ϵ_c in steel B.

An increase in test-temperature to 600°C produced a third type of serration (figure 38c) common to both alloys. Each serration required only a small increment of strain for its completion. The amplitude of the serrations increased steadily with strain up to instability and decreased thereafter. Serration amplitude in steel A was approximately two thirds that in steel B, although the instability

strain of the latter was about two thirds of the former.

CAST STEELS

In the temperature range 500-600°C one basic type of serration was observed (figure 38a), which became more irregular as the strain increased. Solution treating at 1250°C before testing increased the instability strain and the amplitude of the serrations. Serrations were more profuse and irregular in steel B, whilst in steel A a number of small fluctuations in the load occurred on the rising load portion of each serration. The effect was more pronounced in alloys which had been air-cooled rather than water-quenched from the solution treatment temperature. Post-instability oscillations were recorded in steel B, but these disappeared at the lower test-temperatures (500°C). A decreased test-temperature, an increased strain rate or an ageing treatment at 725°C prior to testing, all increased ϵ_c and the strain range required to complete a serration.

At high test-temperatures (600°C), the serrations decreased both in amplitude and the strain required to complete a cycle, to a point where they were not resolved by the sensitivity of the recording apparatus. These serrations (figure 38a) were completely different from those found in wrought steels tested at this temperature (figure 38c).

TEST TEMPERATURES BELOW 400°C

A series of gentle fluctuations were observed in the flow curves of both forged steels tested at 375°C. The effect was greatest in steel B. The critical strains

required to produce the effect were less than those recorded at 450°C. However, the type of load fluctuation observed at 375°C barely constituted a serration and it is likely that such fluctuations were produced by a totally different mechanism to that operating at the higher temperatures.

APPENDIX II

DETERMINATION OF σ_0, k_t & n_t FOR $\sigma = \sigma_0 + k_t \epsilon^{n_t}$

Integrating equation (16) for finite increases in stress and corresponding increases in strain gives[97]

$$\frac{A}{\epsilon_2 - \epsilon_1} = \left(\frac{n_t}{n_t+1}\right)\sigma_0 + \frac{1}{n_t+1}\left(\frac{\sigma_2\epsilon_2 - \sigma_1\epsilon_1}{\epsilon_2 - \epsilon_1}\right) \qquad (A1)$$

where 'A' is the area under the true stress-strain curve between ϵ_1 & ϵ_2. Each increment of area may be approximated to the area of a trapezium without impairing accuracy significantly i.e.

$$A = \tfrac{1}{2}(\sigma_2 + \sigma_1)(\epsilon_2 - \epsilon_1) \qquad (A2)$$

Substituting equation (A2) into equation (A1), gives

$$\tfrac{1}{2}(\sigma_2 + \sigma_1) = \left(\frac{n_t}{n_t+1}\right)\sigma_0 + \frac{1}{n_t+1}\left(\frac{\sigma_2\epsilon_2 - \sigma_1\epsilon_1}{\epsilon_2 - \epsilon_1}\right) \qquad (A3)$$

Taking fixed values of σ_1 & ϵ_1 and calculating the cumulative area for increasing values of σ_2 & ϵ_2, errors in area measurement are progressively decreased. Thus a plot of $\frac{1}{2}(\sigma_2+\sigma_1)$ against $\left(\frac{\sigma_2\epsilon_2 - \sigma_1\epsilon_1}{\epsilon_2 - \epsilon_1}\right)$ will yield a straight line of slope $\left(\frac{1}{n_t+1}\right)$ and intercept $\left(\frac{n_t}{n_t+1}\right)\sigma_0$, if equation (16) is valid for all values of true stress and strain.

	ALLOY	C	Si	Mn	Ni	Cr	S	P	Nb	Mo	Pb
A	DUPLEX	0.06	0.52	0.62	9.3	19.2	0.018	0.028	0.8	0.53	0.003
B	AUSTENITIC	0.09	0.85	1.89	14.1	20.1	0.017	0.018	1.25	-	0.002

TABLE 1 Chemical Composition (weight per cent).

ALLOY	HEAT TREATMENT (HOURS AT 725°C)	LATTICE PARAMETERS OF PHASES				% EXTRACT BY WEIGHT
		IDENTIFIED Å ±½%				
		NbC a	'SIGMA' a_o	'SIGMA' c_o	$Cr_{23}C_6$ a	
A Cast	-	4.45	-	-	-	1.43
"	50	4.42	trace		-	2.98
"	250	4.42	8.75	4.59	10.61	3.54
"	1000	4.41	8.75	4.58	10.61	3.15
A Forged	-	4.43	-	-	-	1.19
"	1000	4.41	8.75	4.58	10.63	1.56
B Cast	-	4.44	-	-	-	1.89
"	50	4.44	-	-	-	1.50
"	250	4.43	-	-	trace	1.77
"	1000	4.43	-	-	10.61	1.66
B Forged	-	4.45	-	-	-	1.57
"	1000	4.43	-	-	10.61	1.70

		Å±1%			
A Cast	Filings	Austenite	3.52	delta-ferrite	2.81
B Cast	Filings	Austenite	3.51		

TABLE 2 X-ray Diffraction Analysis.

ALLOY	HEAT TREATMENT (HOURS AT 725°C)	INTENSITY	SHARPNESS	REMARKS
A Cast	-	average-	sharp	part of residue v.slighfly magnetic
"	50	average	diffuse	part of residue slightly magnetic
"	250	weak	sharp	" " " "
"	1000	weak+	"	part of residue v.slightly magnetic
B Cast	-	average-	"	
"	50	"	"	slight increase in
"	250	"	"	intensity on ageing
"	1000	average	"	
A Forged	-	average+	"	
"	1000	average-	sharp-	increase in fluorescence
B Forged	-	v.strong	"	
"	1000	"	diffuse	
B Cast	-	"	sharp-	electrolytic extraction

Intensity Scale:- feint, weak, average, strong, v.strong.

TABLE 3 Appearance of NbC Diffraction Lines following Chemical Extraction.

Treatment	Test Temp.	Residual C.O.D. (mms).			
		Microscope		Feeler-Gauge	
As Cast	25°C	0.31	0.33	0.3	0.25
" "	25°C	0.30	0.40	0.2	0.35
" "	625°C	0.19	0.26	0.20	0.25
" "	625°C	0.15	0.30	0.30	0.40
" "	800°C	0.16	0.38	0.10	0.35
" "	800°C	0.31	0.36	0.30	0.35
" "+250hrs./725°C	725°C	0.07	0.05	0.0	0.0
" " " " "	725°C	0.16	0.19	0.15	0.20

TABLE 4 Effect of Test-Temperature and Method of Measurement on Residual Crack-Tip Displacement (Alloy B).

ALLOY	NOTCH	ENERGY TO MAXIMUM LOAD (JOULES) CALCULATED FROM Eq.6	Eq.7	Eq.9	EXPERIMENTAL VALUE	% ERROR ON Eq.7	ELASTIC ENERGY / TOTAL ENERGY %
A Cast	Slit	30.9	30.0	29.4	31.5	-5	12
B "	"	18.7	18.0	17.2	18.4	-2	12
A Forged	"	89.8	91.0	96.6	90.3	+2	8
B "	"	97.3	99.5	97.4	96.8	+3	9.5
A Cast	'U'	54.1	50.4	-	55.1	-8	7
B "	"	39.7	37.4	-	38.8	-3.5	8.5
A Forged	"	171.9	182.6	-	174.9	+4	4.5
B "	"	114.6	120.4	-	112.5	+7	7.5

TABLE 5 Calculation of E_{ml} from Bend Test Parameters.

ALLOY	$E_{\delta t}$ (J)	E_{ml} (J)	E_s (Jmm^{-3})	$E_{\delta t}/E_{ml}$	$E_{\delta t}/E_s$ (mm^3)
CAST A	5.2	31.5	.225	.165	23.0
CAST B	3.2	18.4	.178	.172	17.9
FORGED A	22.2	90.3	.489	.246	45.4
FORGED B	24.0	96.8	.398	.248	60.4

TABLE 6 Estimate of Plastic Zone Size for Bend Specimens Containing Parellel Slits.

ALLOY	SPECIMEN ORIENTATION	0.2% P.S. MNm^{-2}	T.S. MNm^{-2}	UN.EL. %	TOT.EL. %	R of A (FRAC.) %	C.O.D. mms.
B Cast	tangential	224.7	491.8	30.6	31.6	25/42	.45
B "	longitudinal	208.3	475.4	40.2	40.6	22/40	.47
A Cast	tangential	254.4	530.6	41.0	44.1	32/64	.67
A "	longitudinal	261.6	544.0	40.0	43.4	40/60	.67+
B Rolled	transverse	279.5	511.7	45.9	50.0	40/48	.53
B "	longitudinal	260.9	560.9	44.9	48.2	45/53	.78
A Rolled	transverse	326.6	649.2	46.7	59.8	62/65	.86
A "	longitudinal	326.9	611.9	39.0	52.9	64/76	.74

TABLE 7 Influence of Test-Piece Orientation on Mechanical Properties.

ALLOY	SOL^{N} TREATMENT TEMP. ^{o}C	0.2% P.S. MNm^{-2}	T.S. MNm^{-2}	UN.EL. %	TOT.EL. %	R of A (FRAC.) %	C.O.D. mms
A	-	254.4	530.6	41.0	44.1	32/64	.67
A	1100°C 1hr.	284.7	559.7	38.1	41.2	45/52	.53
A	1250°C 3hrs.	230.8	525.1	62.9	68.8	44/66	.59
B	-	224.8	491.8	30.6	31.6	25/42	.45
B	1100°C 1hr.	266.0	487.0	27.5	28.3	30	.42
B	1250°C 3hrs.	247.7	500.2	37.1	38.3	35/43	.49

TABLE 8 Influence of Solution Treatment on Mechanical Properties of Cast Alloys.

ALLOY A CAST			ALLOY B CAST		
AGEING TEMP. °C	AGEING TIME (HOURS)	C.O.D. (mms±10%)	AGEING TEMP. °C	AGEING TIME (HOURS)	C.O.D. (mms±10%)
-	-	0.55	-	-	0.42
625	50	0.40	625	50	0.27
725	50	0.25	725	50	0.26
825	50	0.17	825	50	0.08
625	250	0.31	625	250	0.30
725	250	0.15	725	250	0.03
825	250	0.14	825	250	0.06
625	1000	0.34	625	1000	0.29
725	1000	0.17	725	1000	0.02
825	1000	-	825	1000	-

TABLE 9 Influence of Ageing Time and Temperature on Maximum Load C.O.D. using a 4mm. Slit.

ALLOY	HEAT TREATMENT SOLUTION TREATMENT	HEAT TREATMENT HOURS AT 725°C	TENSION 0.2% P.S. MNm^{-2}	TENSION T.S. MNm^{-2}	TENSION ELONG. % UNIF.	TENSION ELONG. % NECK	TENSION R of A (FRAC.) %	BENDING mms	BENDING YIELD MNm^{-2}	BENDING E_{ml} J	BENDING E_{tot} J
A Cast	-	-	134.4	278.5	19.3	1.8	21.5	1.32	40.6	10.3	21.2
A Forged	-	-	139.3	337.4	17.4	4.9	20.0	0.52	80.1	9.4	23.9
A Cast	-	250	194.2	266.7	10.9	15.3	30.5	1.87	58.0	17.1	41.2
A "	-	2000	151.0	254.0	11.7	15.1	46.5	-	-	-	-
A "	1100°C/30mins.	250	177.5	223.6	14.8	21.9	40.0	-	-	-	-
B Cast	-	-	127.3	304.0	21.9	7.8	33.0	2.92	40.5	22.1	38.2
B "	1100°C/30mins.	-	154.9	290.3	19.5	4.7	31.5	-	-	-	-
B Forged	-	-	133.4	308.9	20.9	8.6	26.5	0.75	83.4	12.3	32.1
B Cast	-	50	181.4	254.0	13.9	17.3	40	-	-	-	-
B "	-	250	192.2	266.7	12.9	15.6	34.5	2.88	55.4	22.2	67.7
B "	-	2000	154.9	249.1	11.3	23.5	43	-	-	-	-
B "	1100°C/30mins.	250	191.2	244.2	9.8	22.4	49	-	-	-	-

TABLE 10 Effect of Heat Treatment on the Mechanical Properties of Cast and Forged Alloys Tested in Tension and Slow Bend at 725°C

ALLOY + HEAT TREATMENT	TEST TEMP. °C	0.2% P.S. MNm^{-2}	T.S. MNm^{-2}	ELONGATION UNIFORM %	ELONGATION NECKING %	R of A (FRAC.) %
B Forged	800	275.6	279.5	0.7	28.6	48/51
"	725	133.0	309.2	20.9	8.6	25/28
"	670	250.0	377.6	21.7	13.5	42/45
"	600*	355.0	470.7	19.5	10.6	52/55
"	500*	356.0	487.4	21.7	10.3	55/60
"	380*	358.9	497.2	19.5	8.4	43/47
A Forged	800	133.4	207.9	9.4	3.9	12/15
"	725	139.0	337.3	17.4	4.9	20
"	600*	228.2	408.0	27.7	13.0	54/58
"	500*	341.3	492.3	20.1	10.2	55/58
"	450*	283.4	479.5	27.8	11.1	52/58
"	375*	315.8	492.3	26.2	10.1	50/55
"	300	388.3	515.8	16.4	13.3	50/55
B Cast + 50hrs./725°C	800	146.7	179.7	10.9	23.3	40/47
"	725	181.6	253.8	13.9	17.3	37/43
"	670	190.3	304.5	15.6	7.9	25/34
"	550*	196.9	358.7	18.4	5.0	24/31
"	500*	205.7	371.7	16.8	4.7	32/38

* Signifies Serrated Flow Occured.

TABLE 11 Influence of Test-Temperature on Tensile Properties.

ALLOY	TEST TEMP. °C	STRAIN-RATE min^{-1}.	CRITICAL STRAIN %	ACTIVATION ENERGY from Eq.18 (KJ $mole^{-1}$ ±6)
A Forged	375	0.071	15.8	78
A "	450	"	26.0	91
A "	500	"	5.6	87
A "	600	"	0.78	84
A Cast +S.T.1250°C	550	"	5.4	92
A " "	550	"	4.3	91
A Cast	500	"	12.9	93
A Cast	500	0.036	6.1	92
B Forged	380	0.071	3.1	70
B "	500	"	2.2	81
B "	600	"	0.4	79
B Cast +S.T.1250°C	550	"	1.6	84
B " "	550	"	1.5	84
B Cast	500	"	3.1	83
B "	600	"	0.4	79
B Cast +50hrs./725°C	550	"	2.3	84
B " "	500	"	3.5	84
B Cast	600	0.036	0.5	86
B Cast +50hrs./725°C	550	0.036	1.2	87
B " "	550	0.72	2.4	71

TABLE 12 Activation Energy for Serrated Flow. Calculated from Critical Strain Measurements.

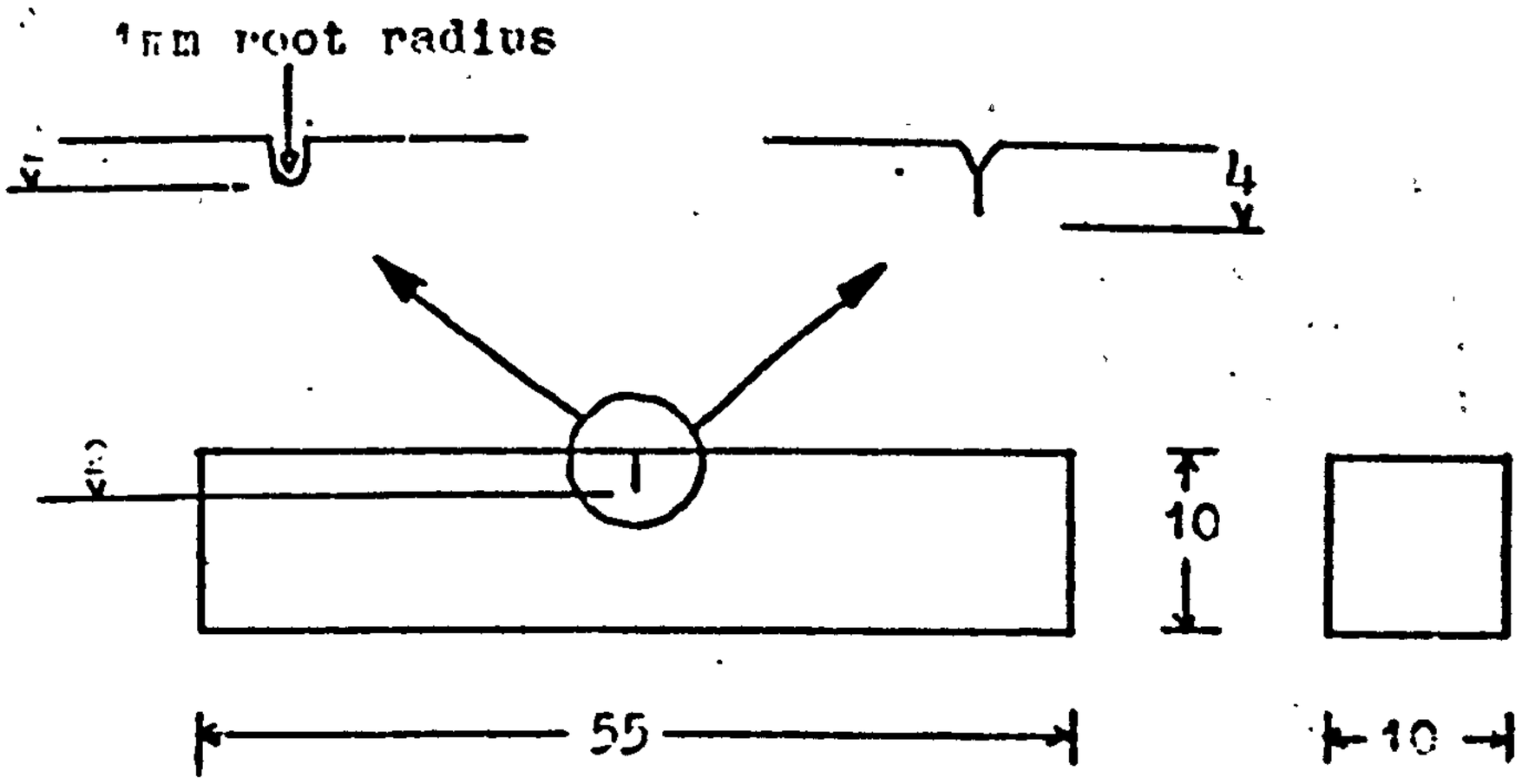

Fig 1. C.O.D. (Bend) Specimen Dimensions. x1½, scale

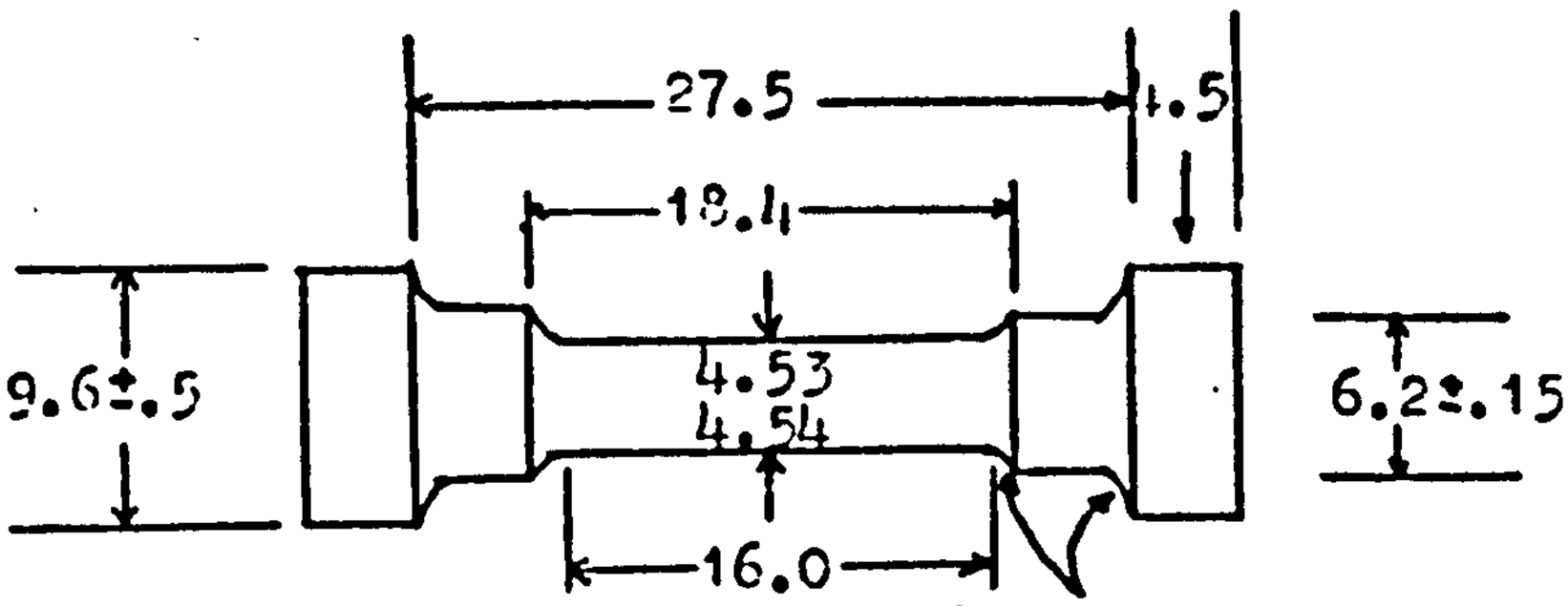

Fig 2. Tensile Specimen Dimensions. x2, scale

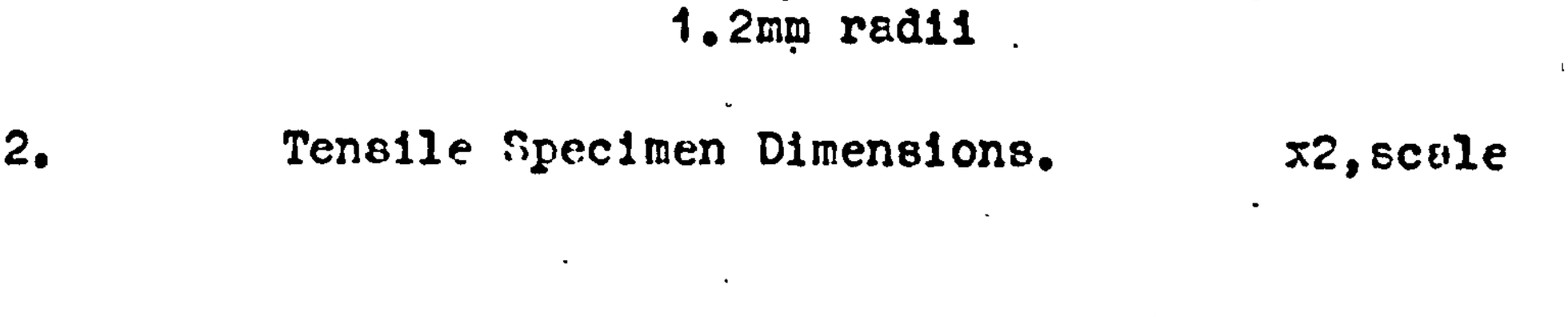

Fig 3. Multiple Notch Tensile Specimen. x1½, scale

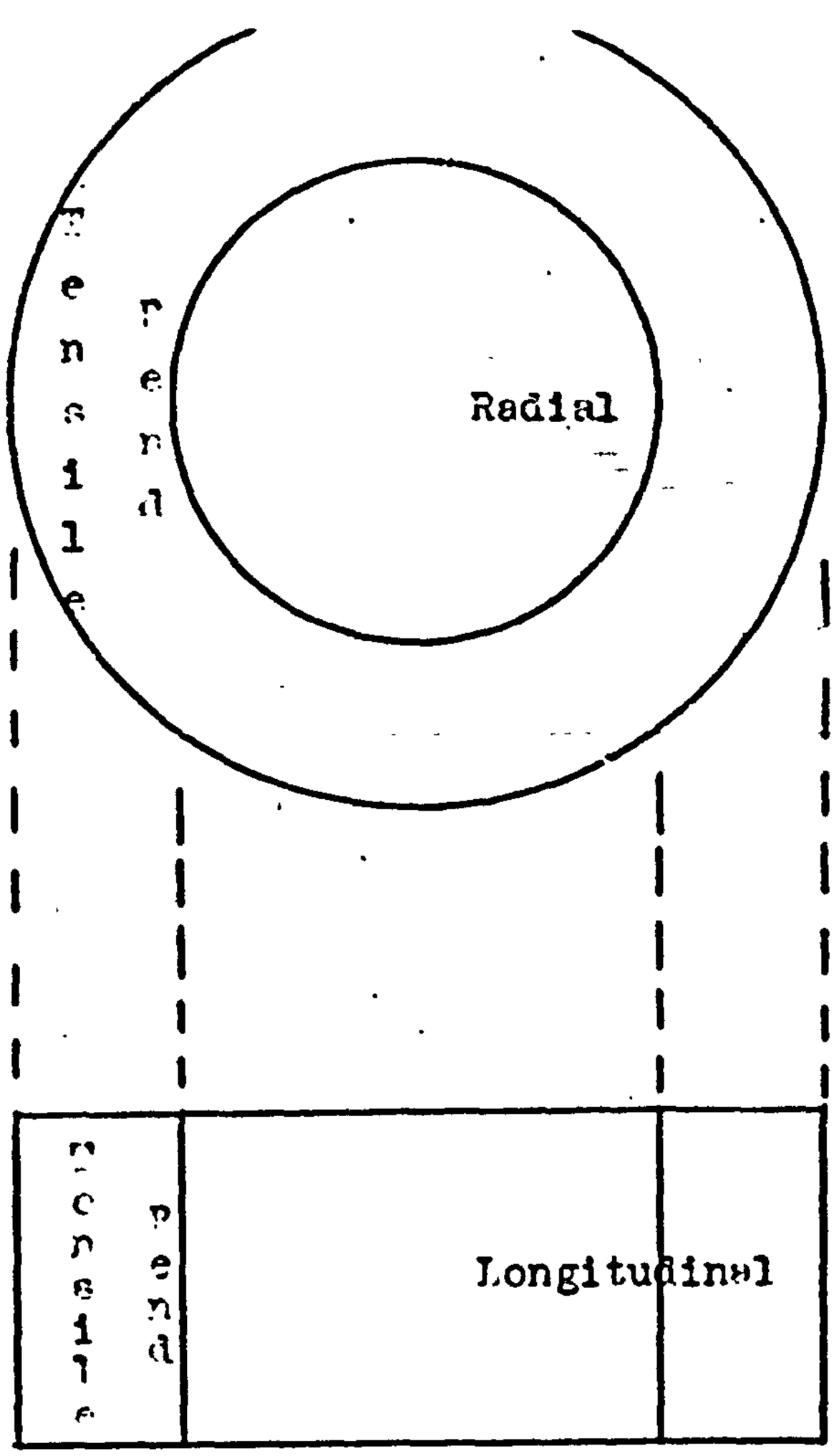

Fig 4. Location of Mechanical Test Pieces in Cast Steels.

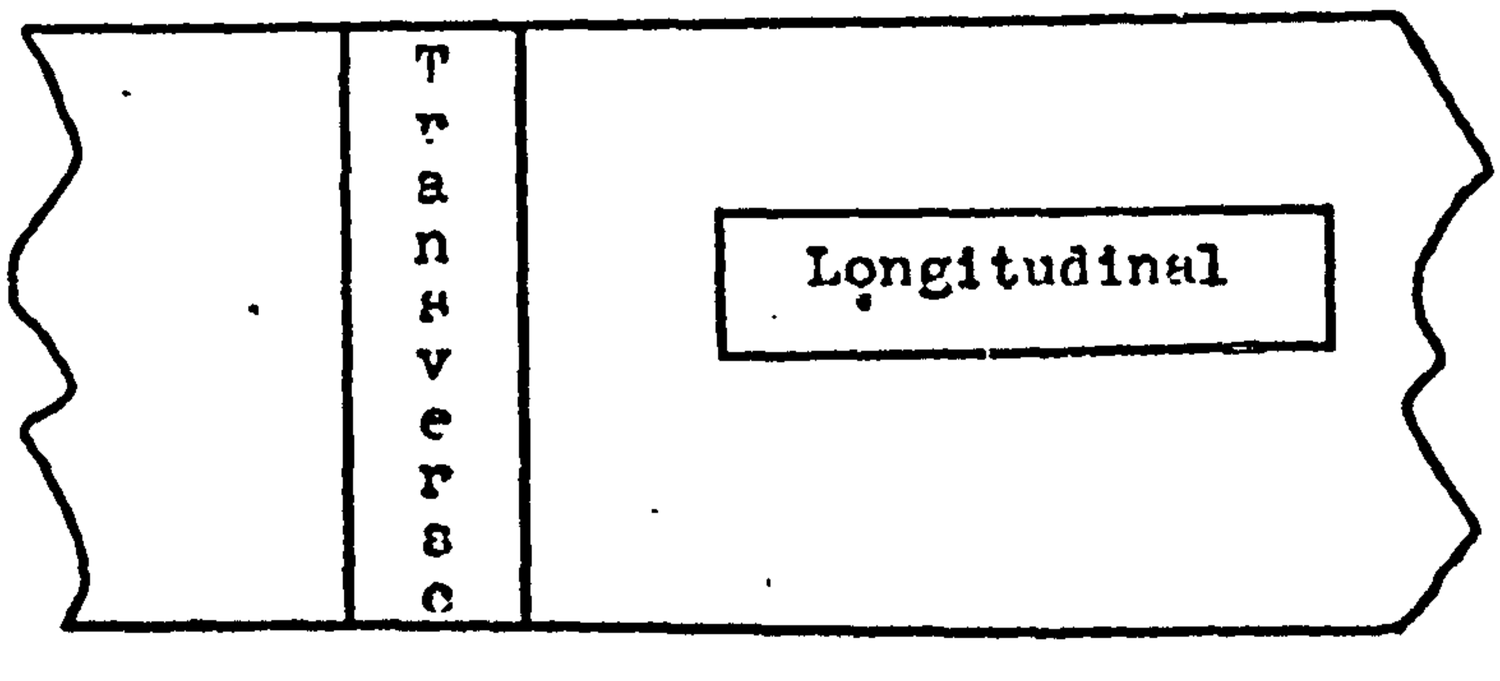

Fig 5. Location of Mechanical Test Pieces in Rolled Alloys.

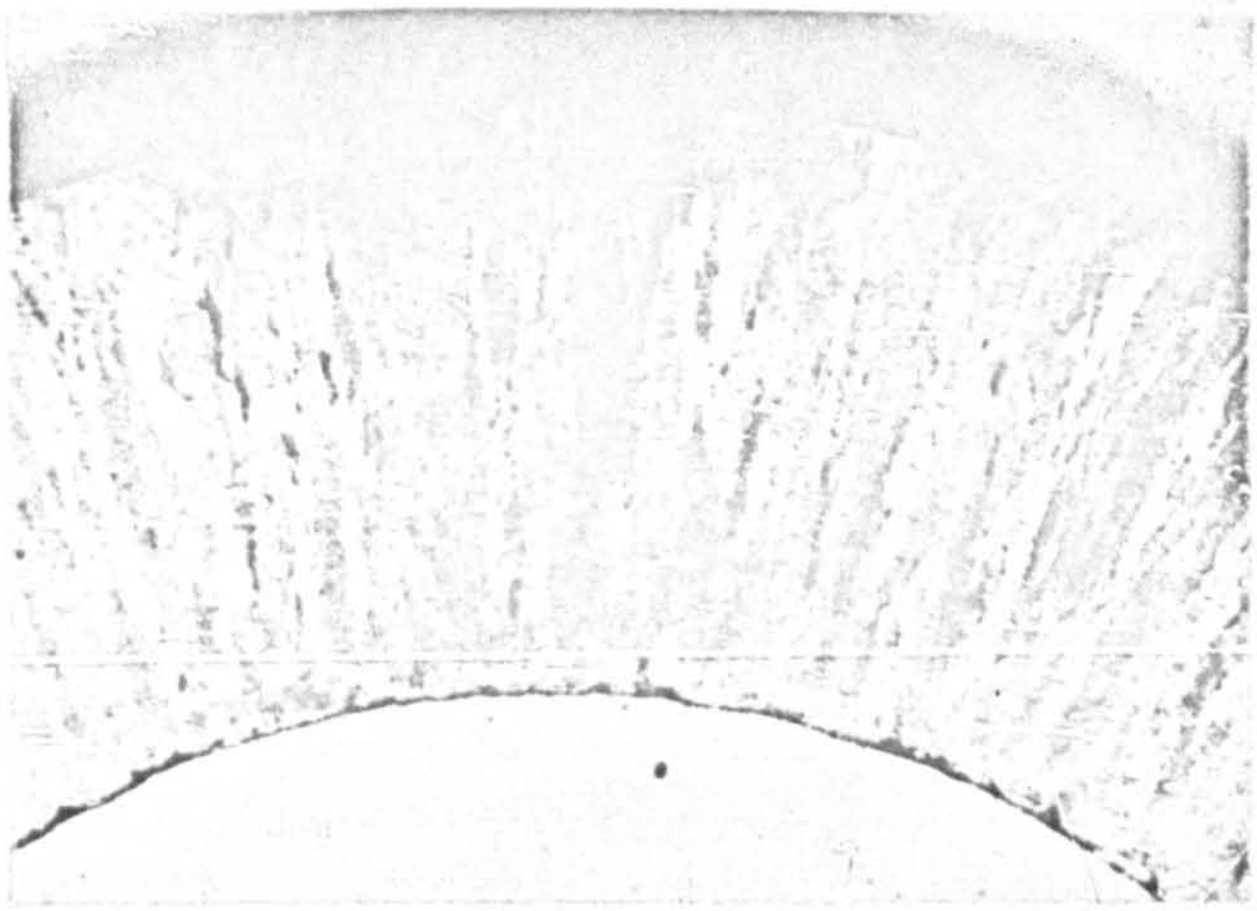

Fig.6. Alloy A As-Cast x1¾

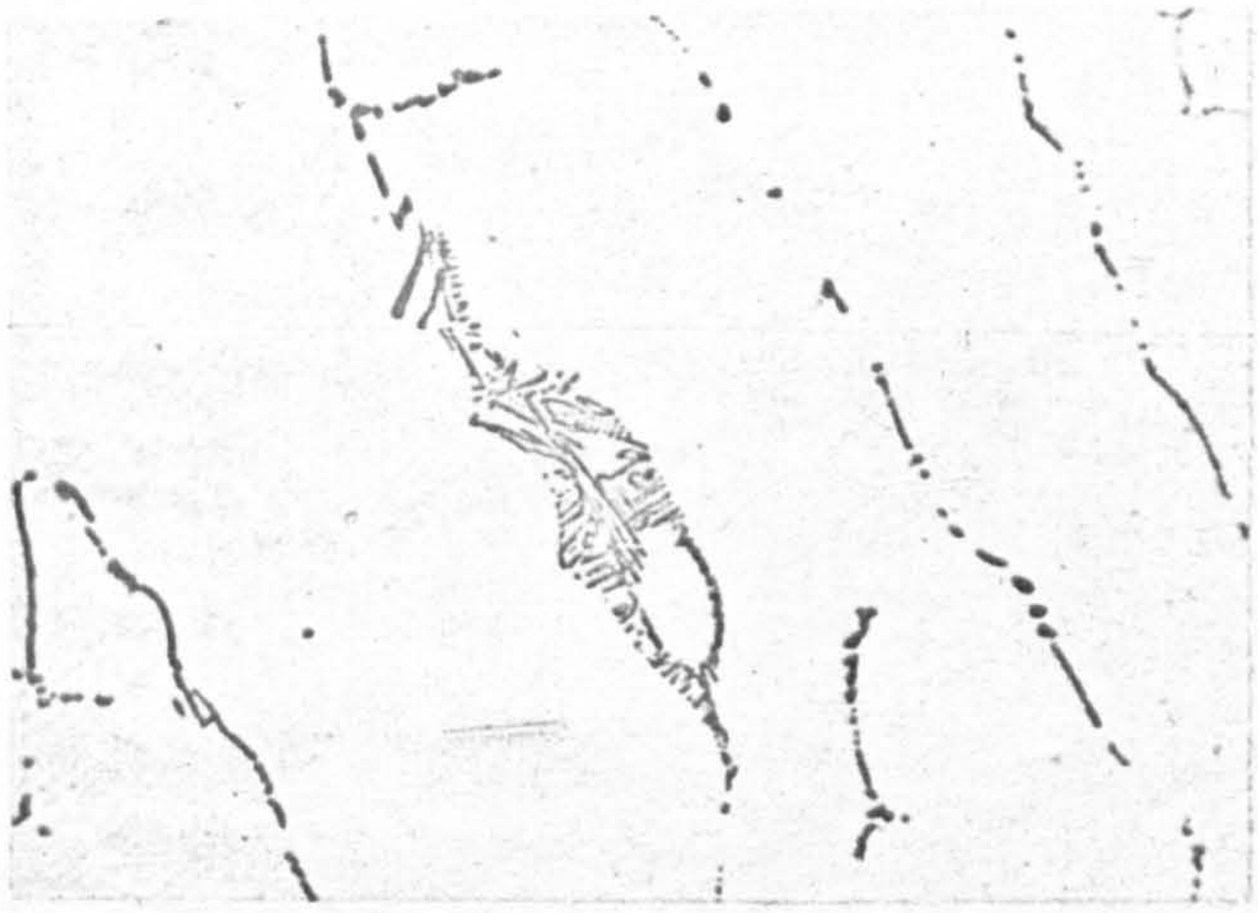

Fig.7. Alloy B As-Cast x400

Fig.8. Alloy A As-Cast x900

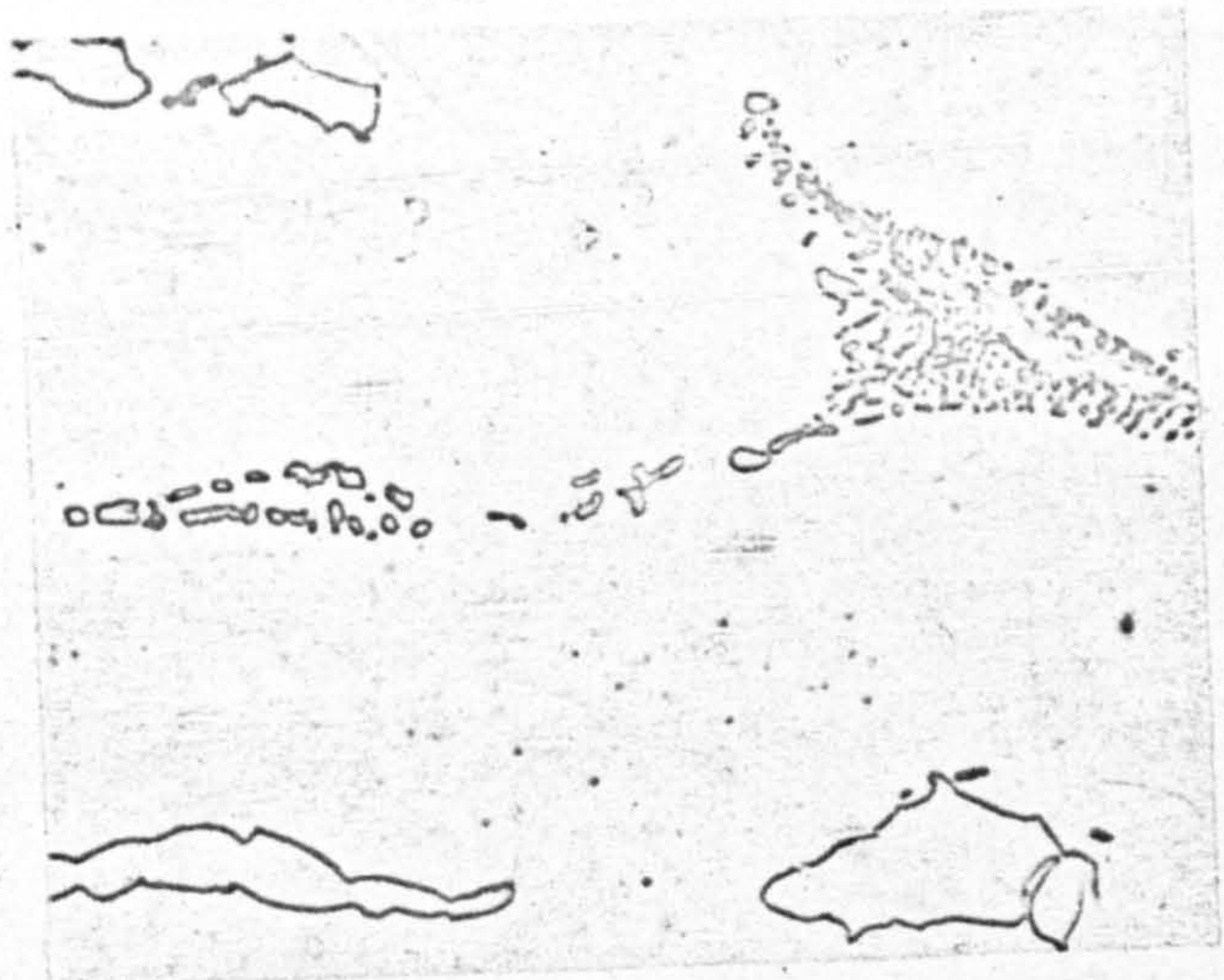

Fig.9. Alloy A As-Rolled x900

Fig.10. Alloy B As-Forged x200

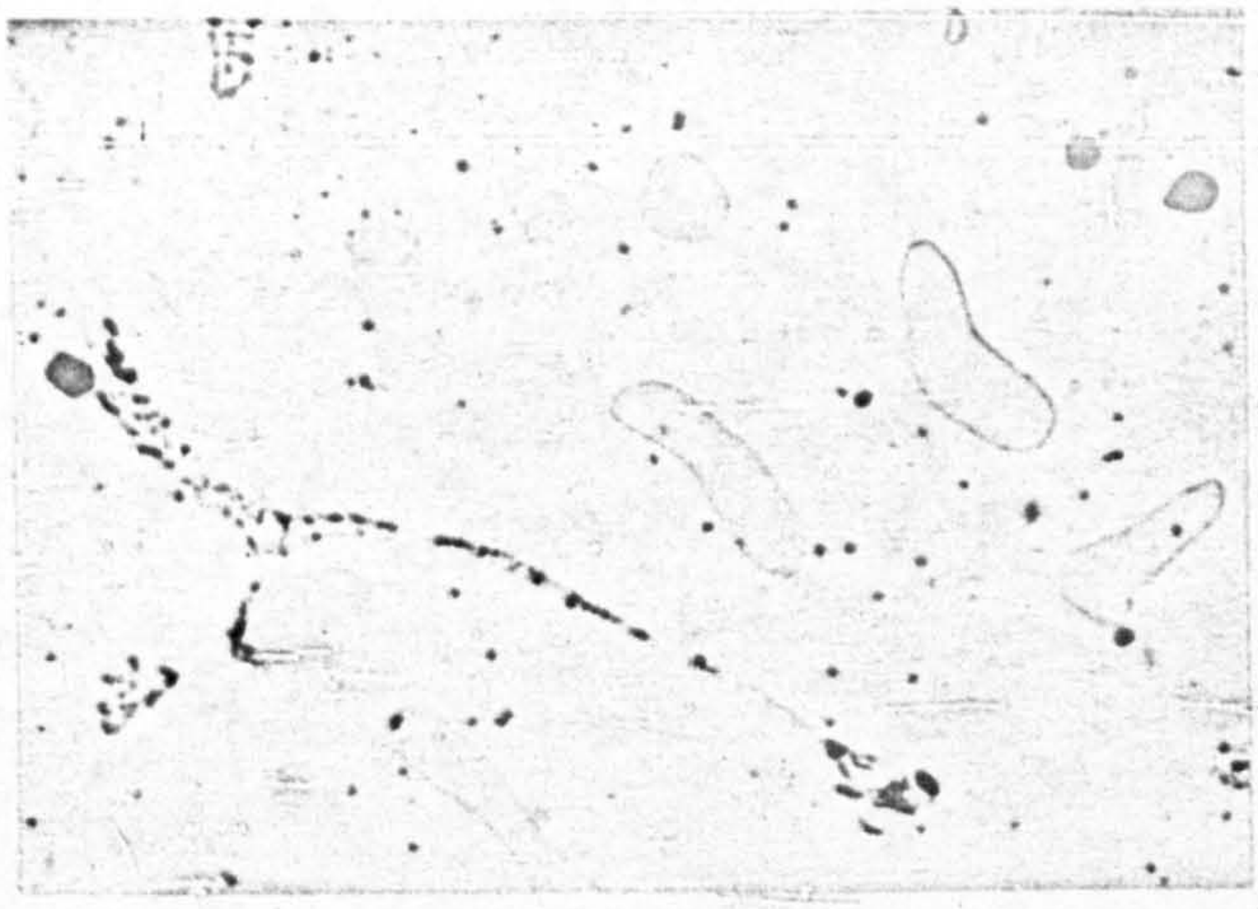

Fig.11. Alloy A Cast+S.T.1250°C x900

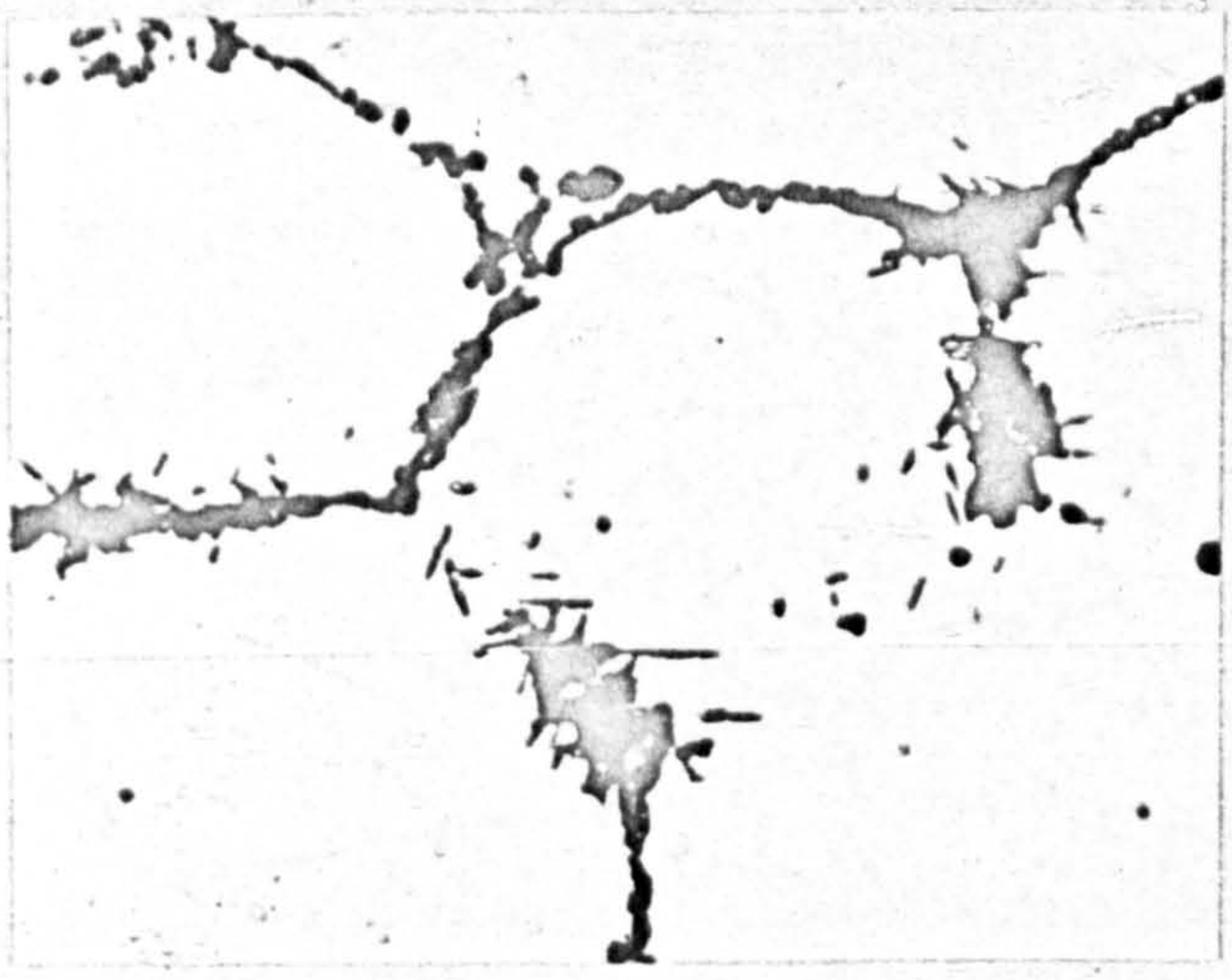

Fig.12. Alloy B Cast+1000hrs./725°C x900

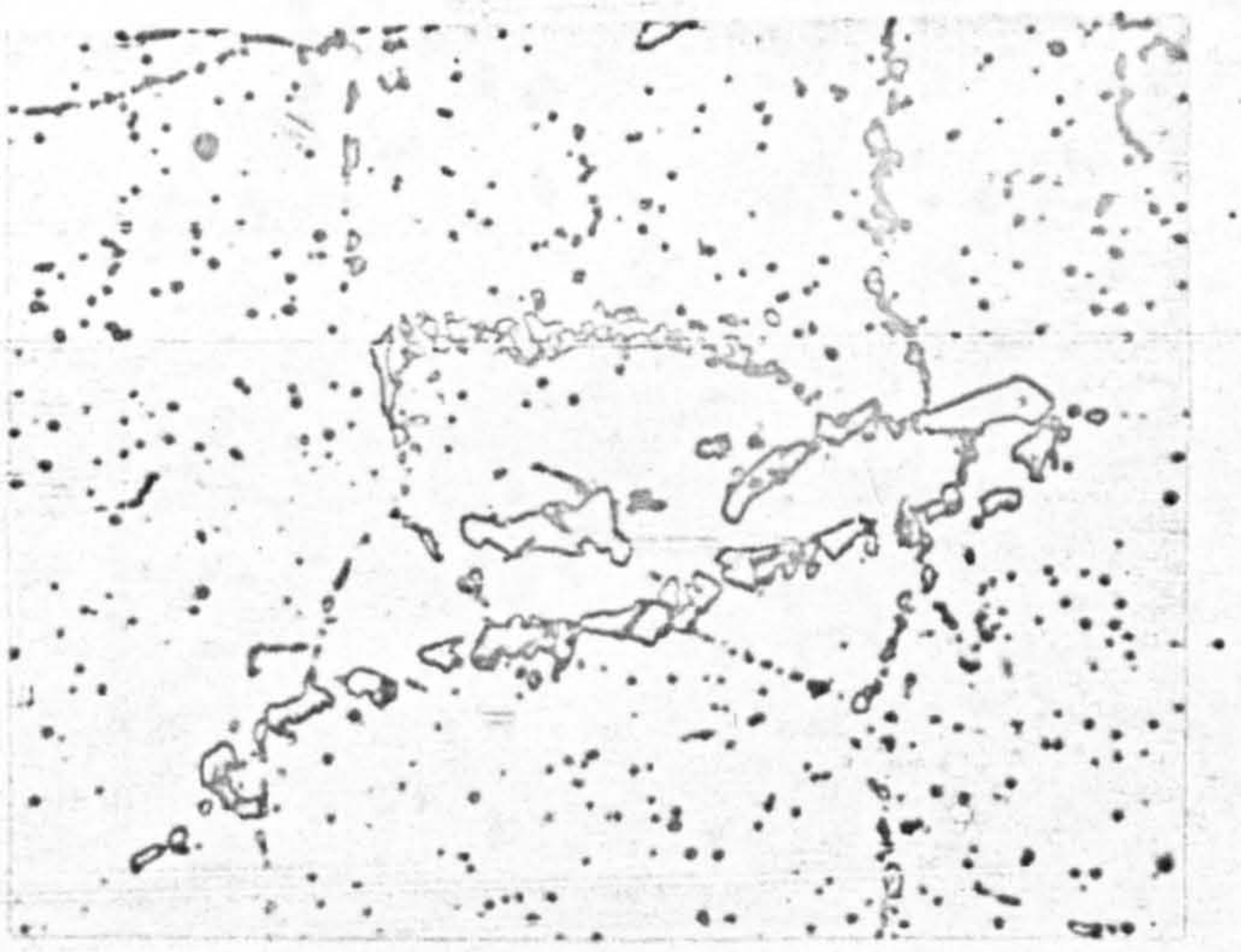

Fig.13. Alloy B Forged+1000hrs./725°C x900

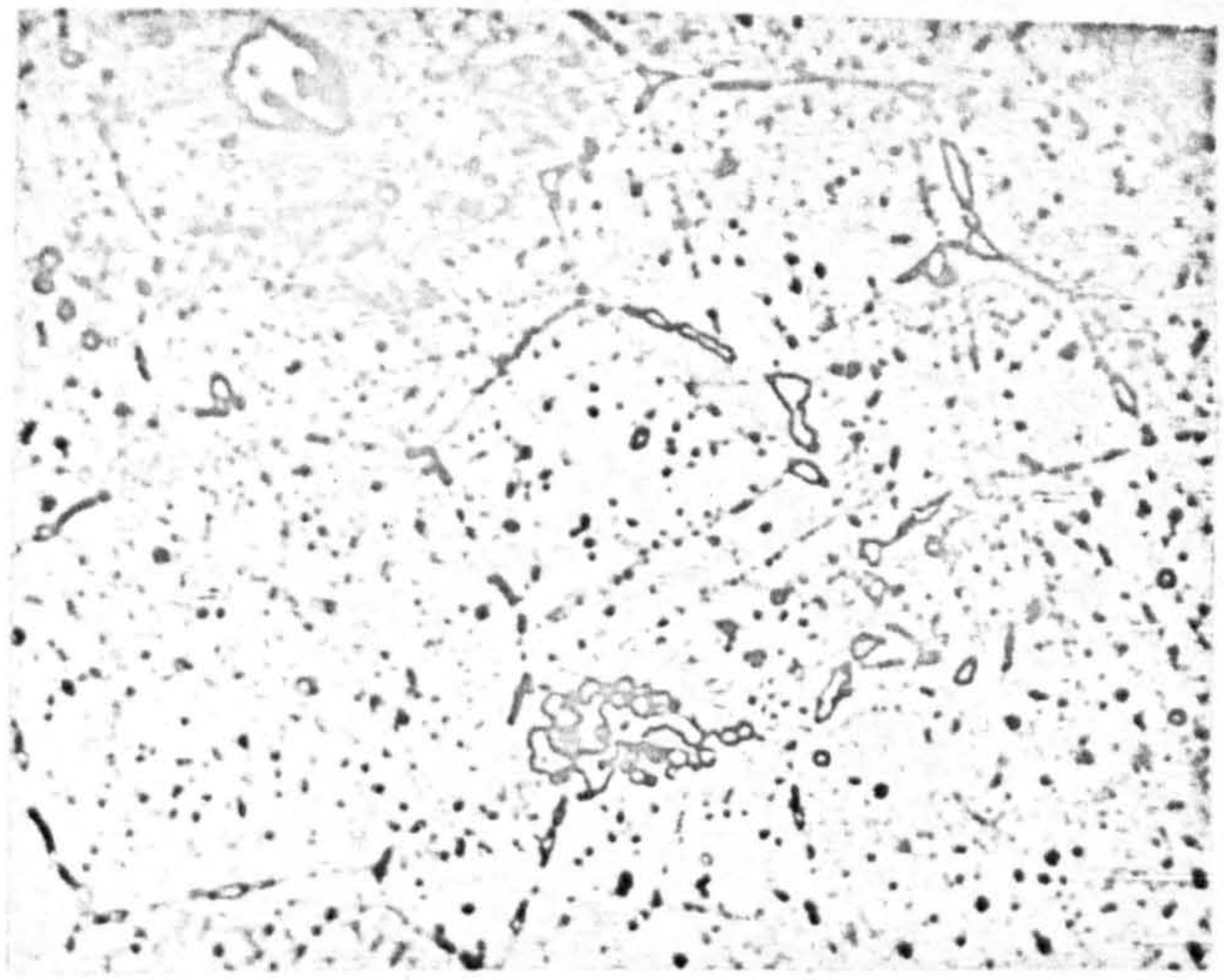

Fig.14. Alloy A Forged+1000hrs./725°C x900

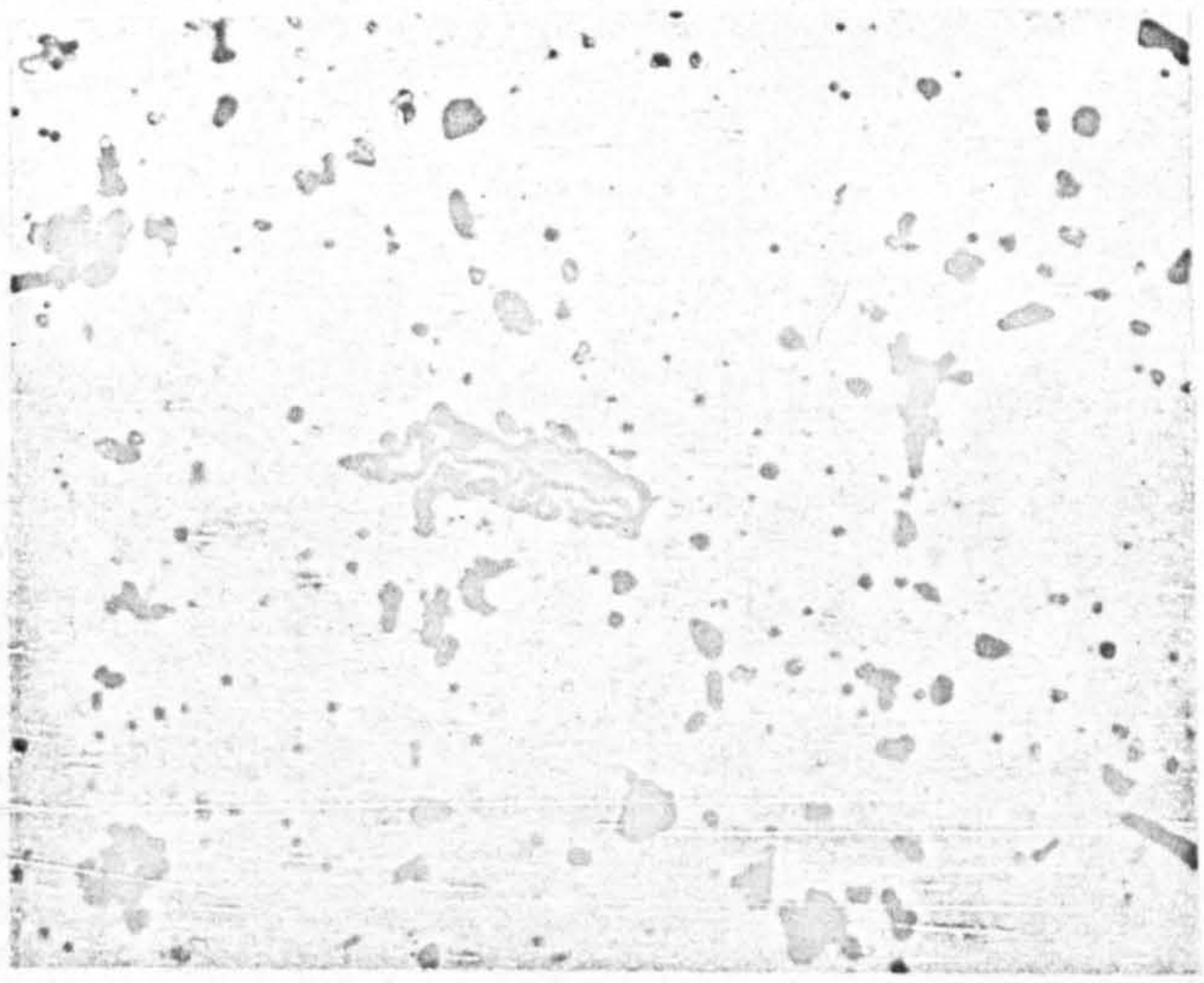

Fig.15. Alloy A Forged+1000hrs./725°C x900

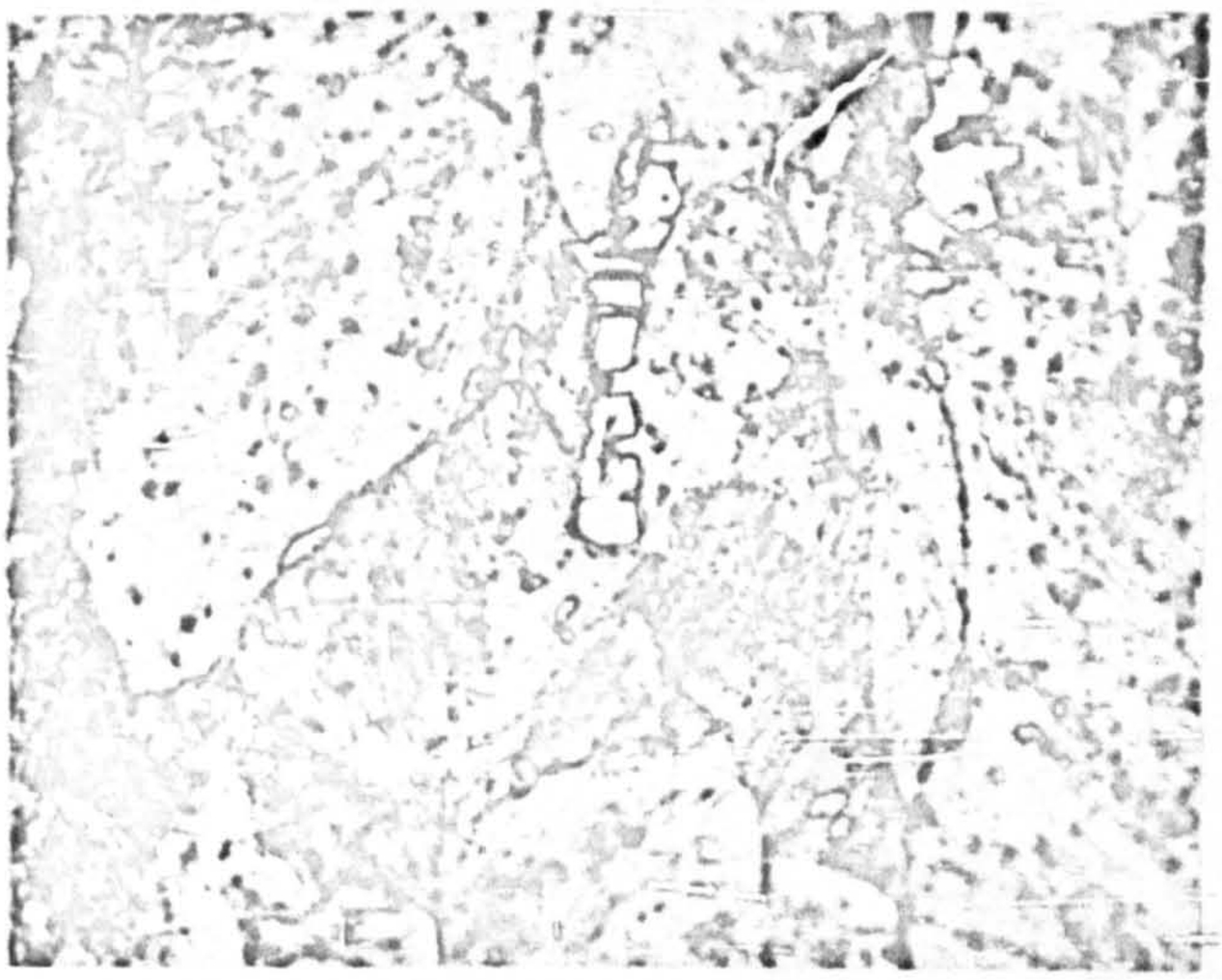

(deformed gauge length)
Fig.16. Alloy A Forged+1000hrs./725°C x900

(Normarski Interference Contrast)
Fig.17. Alloy B As-Cast x900

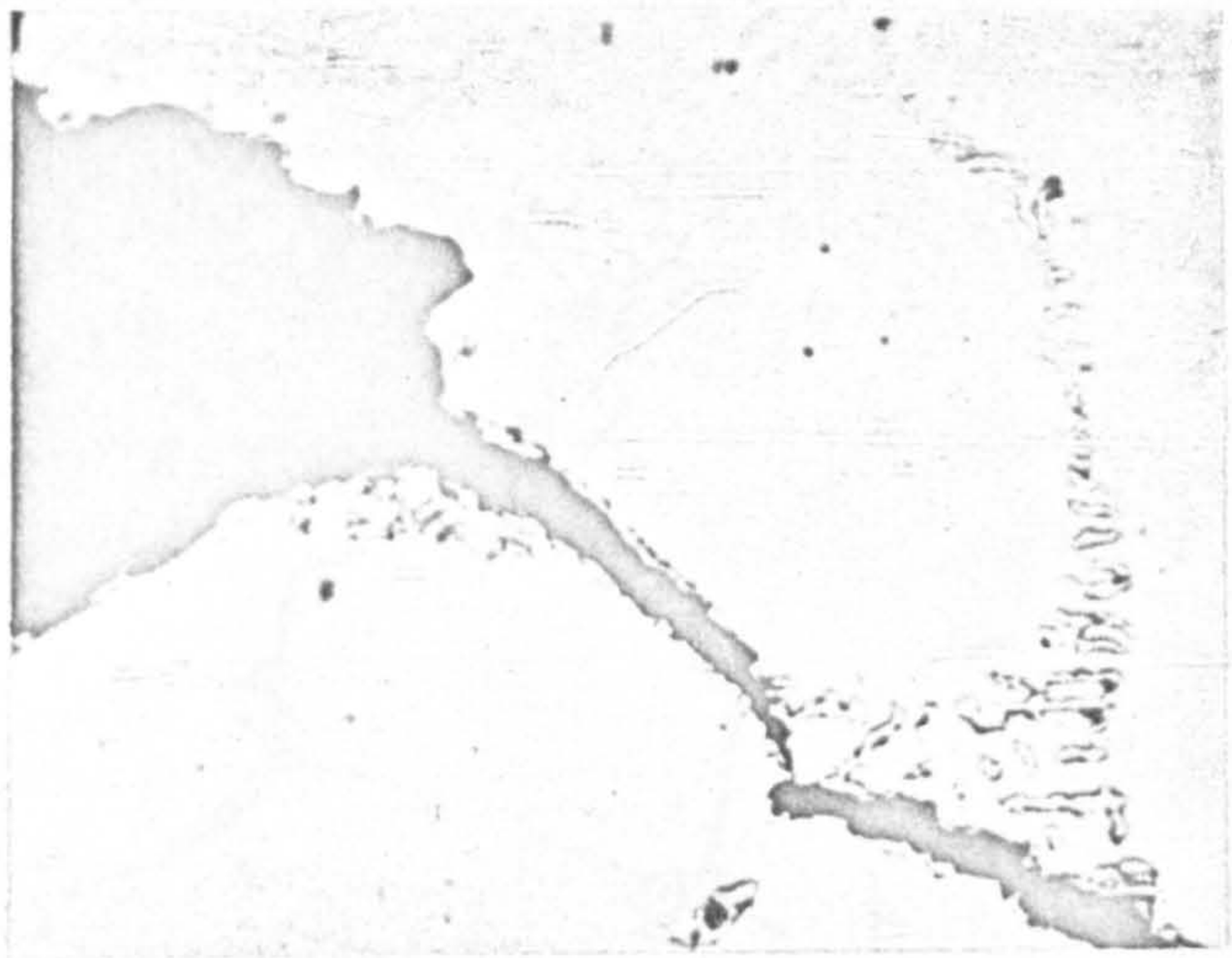

Fig.18. Alloy B Cast+1000hrs./725°C x675

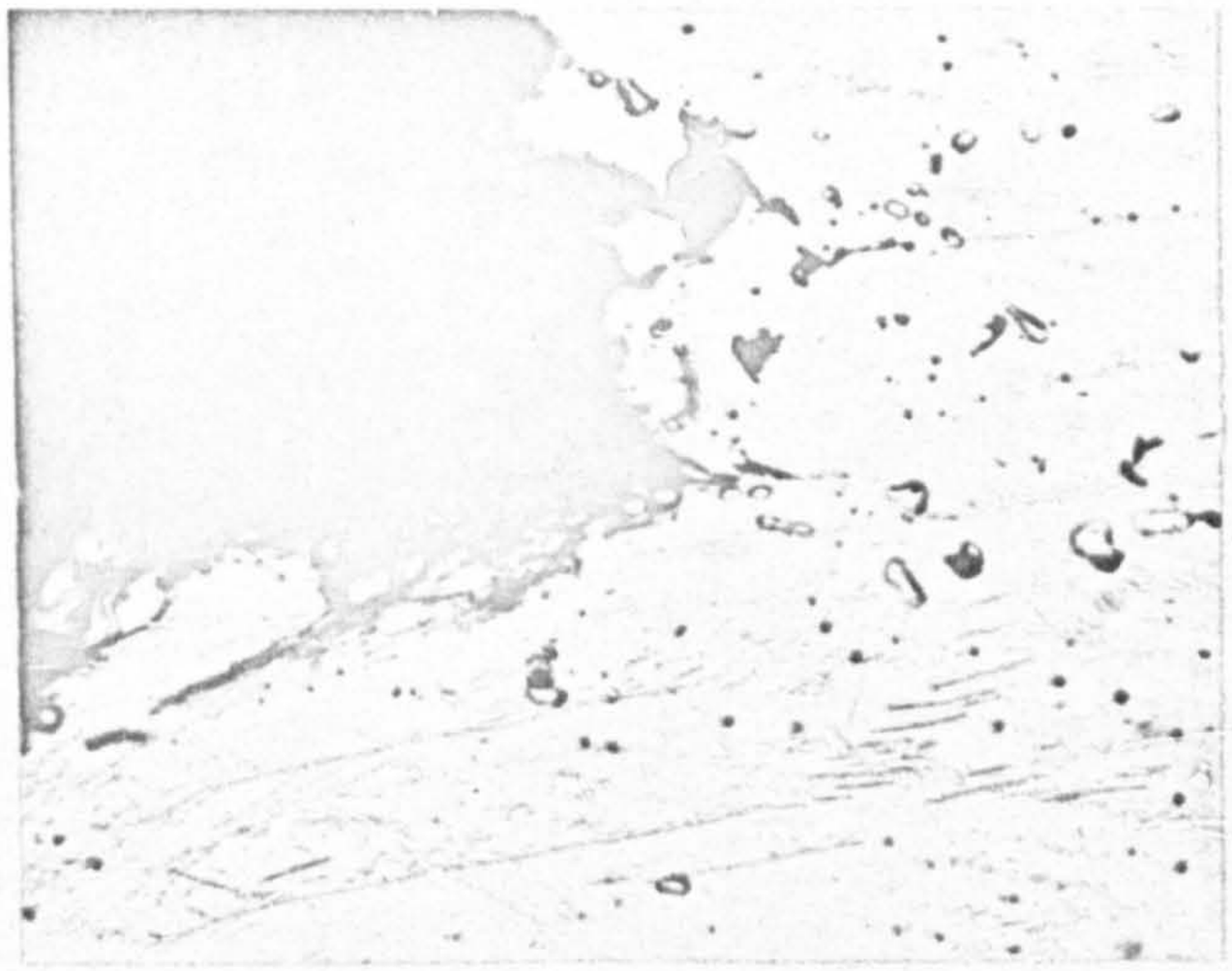

Fig.19. Alloy B As-Forged x675

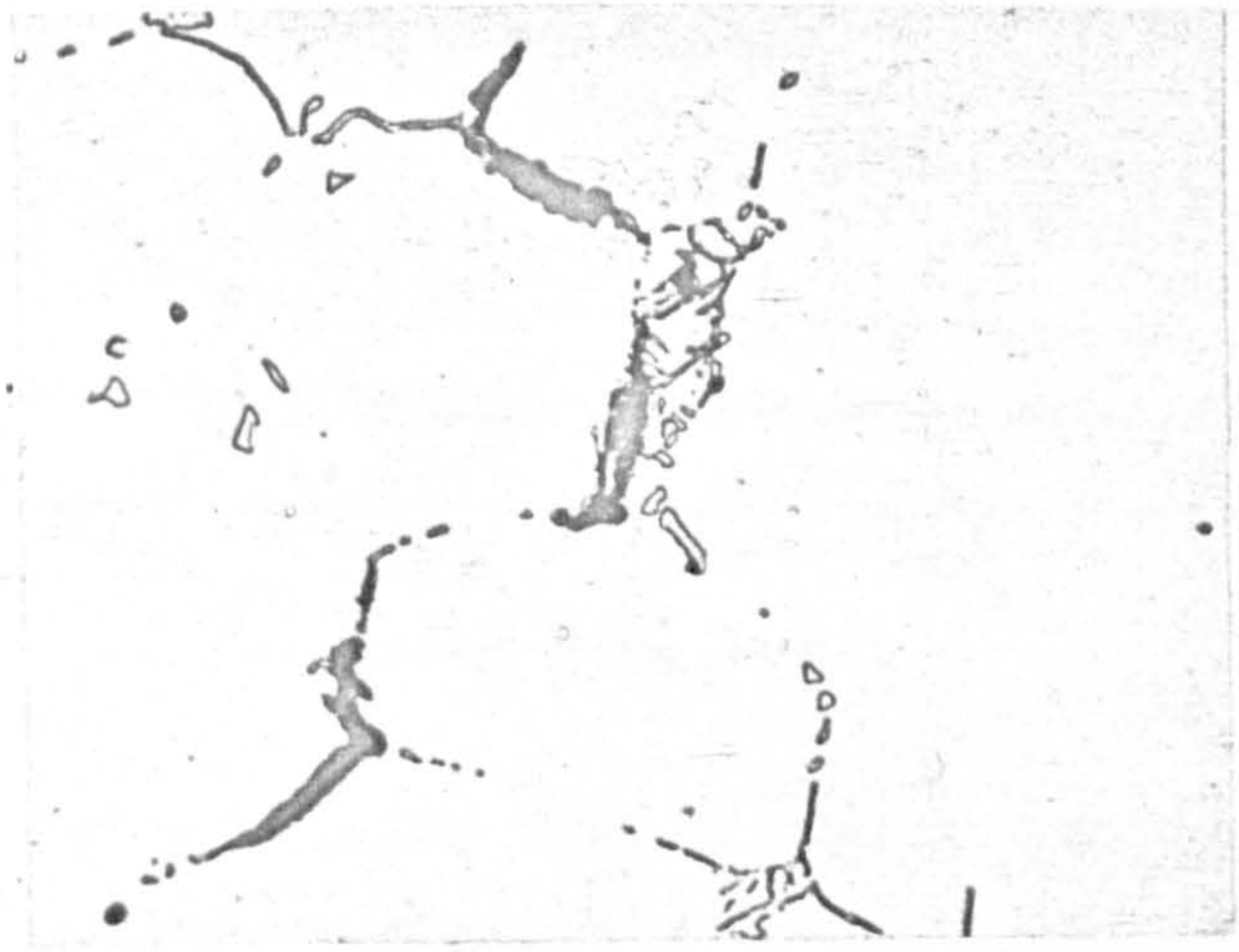

Fig.20. Alloy B As-Cast x675

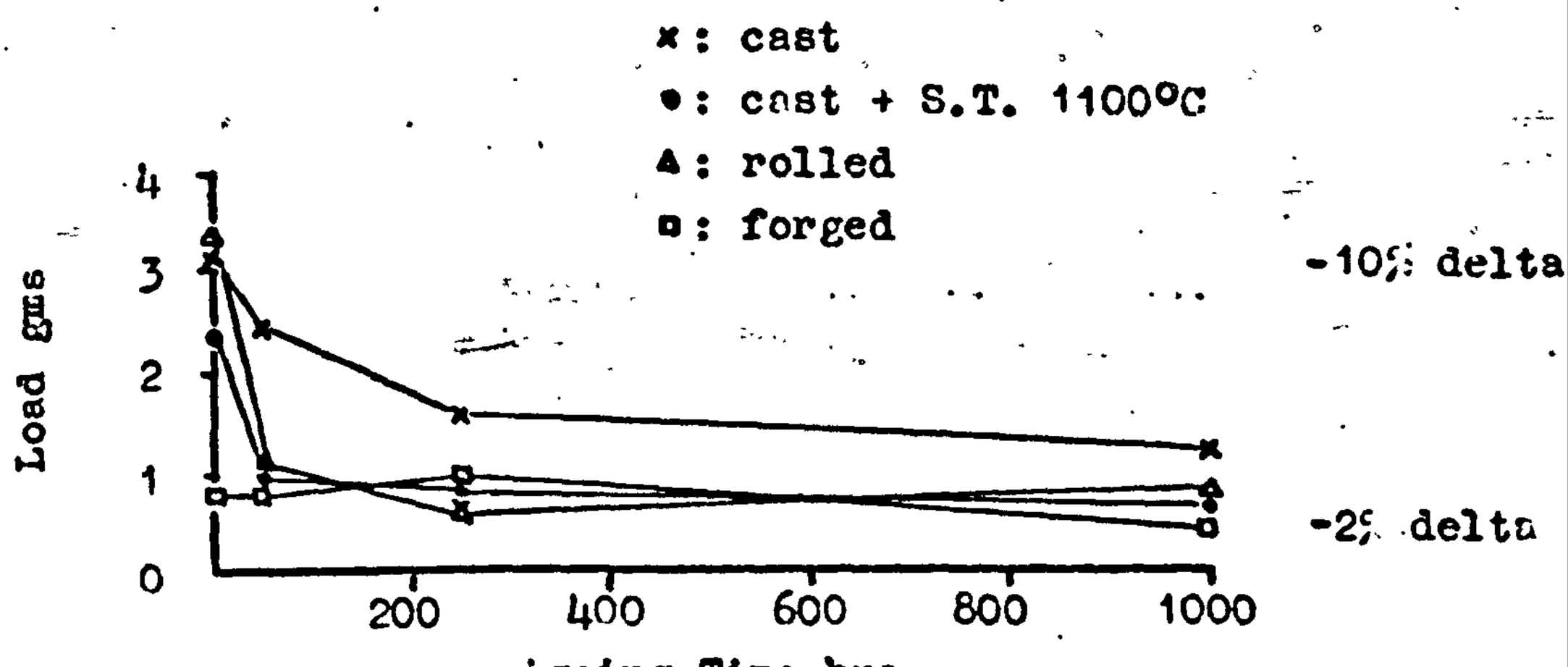

Fig 21. Effect of Ageing Time on Delta Ferrite Content of Steel A.

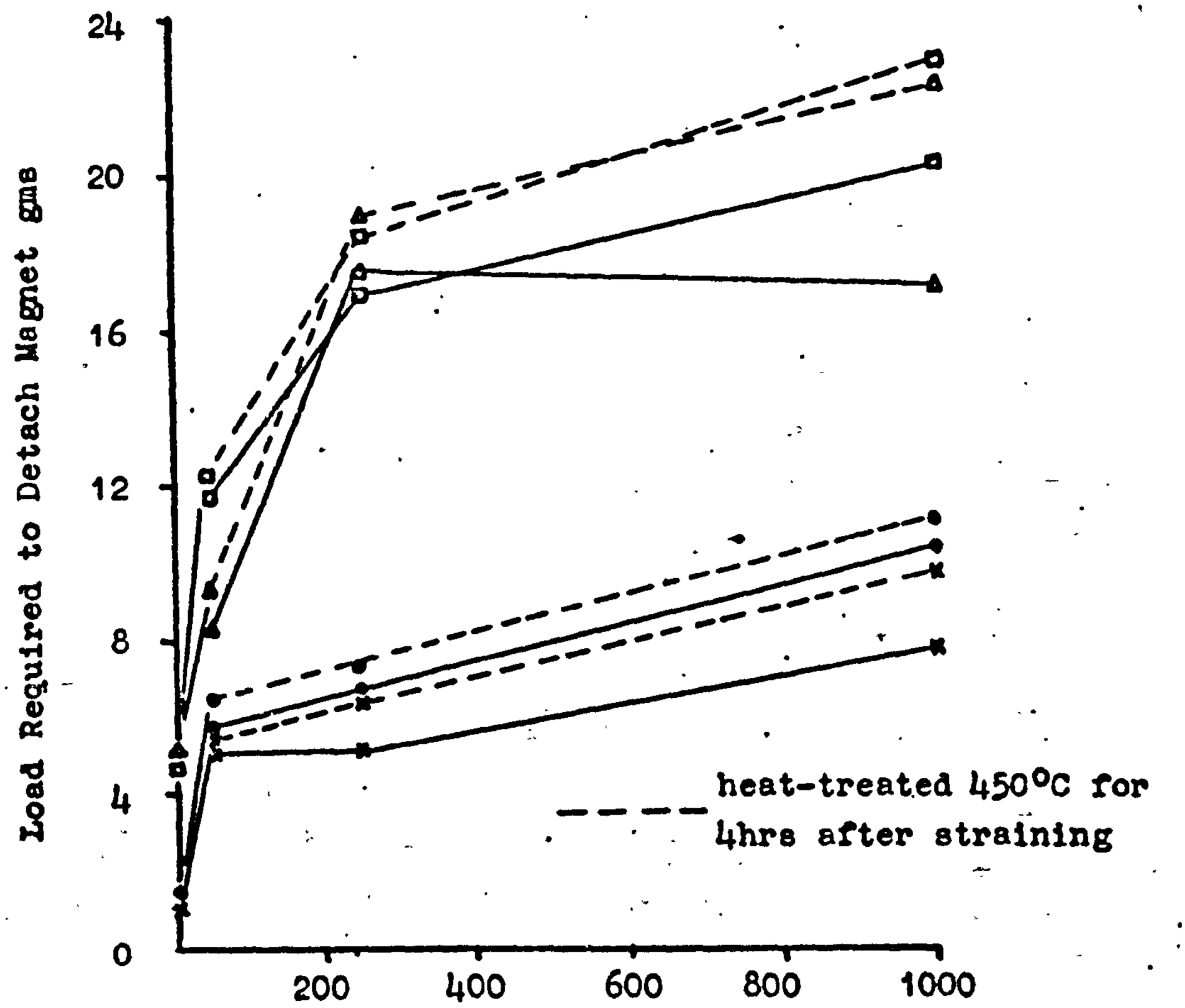

Fig 22. Effect of Prior Ageing Time at 725°C on the Formation of Strain Induced Martensite in Alloy A.

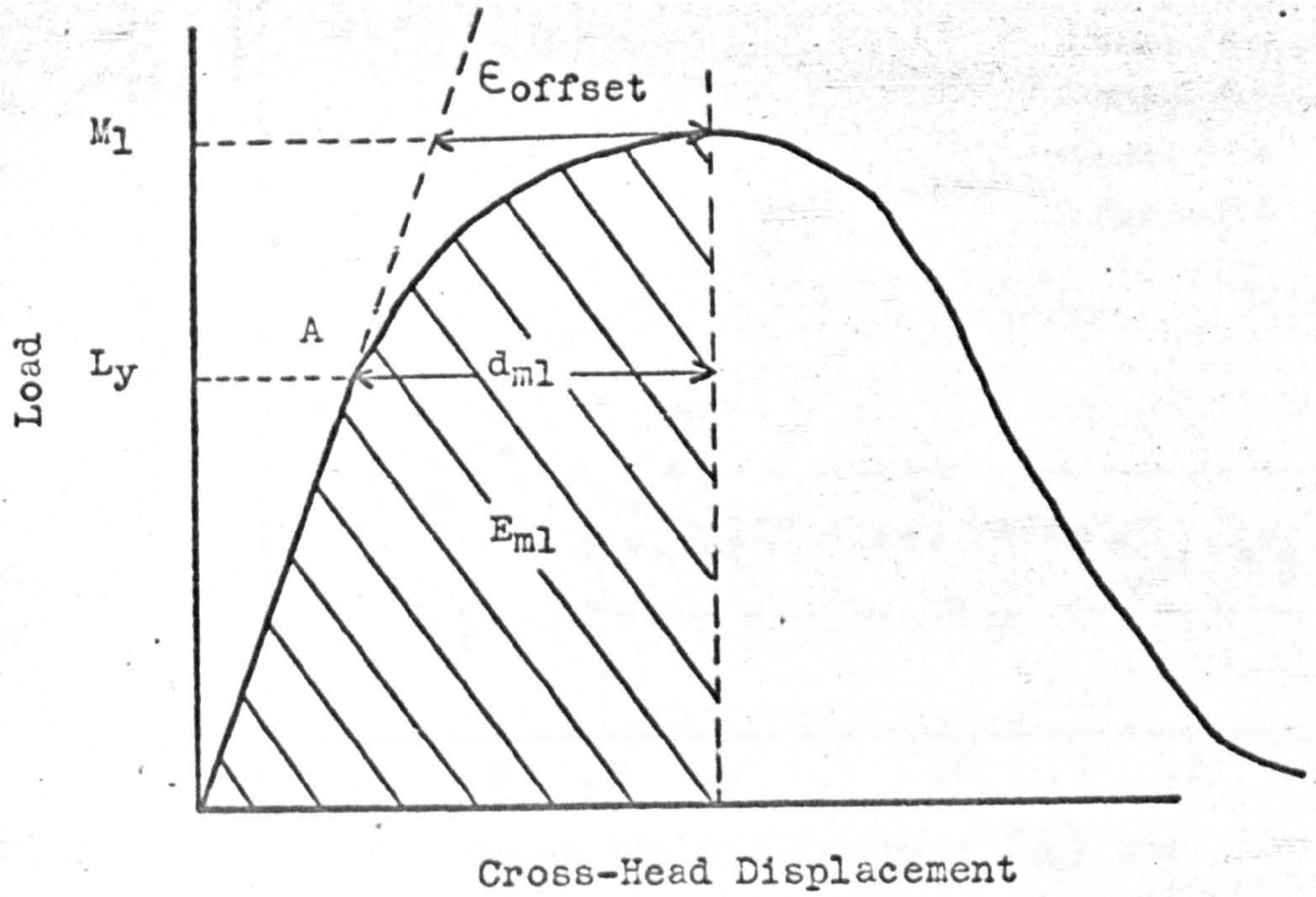

Fig 23. Schematic Load-Deflection Diagram.

Fig 24. Profile of Notch Tip During Loading. x15

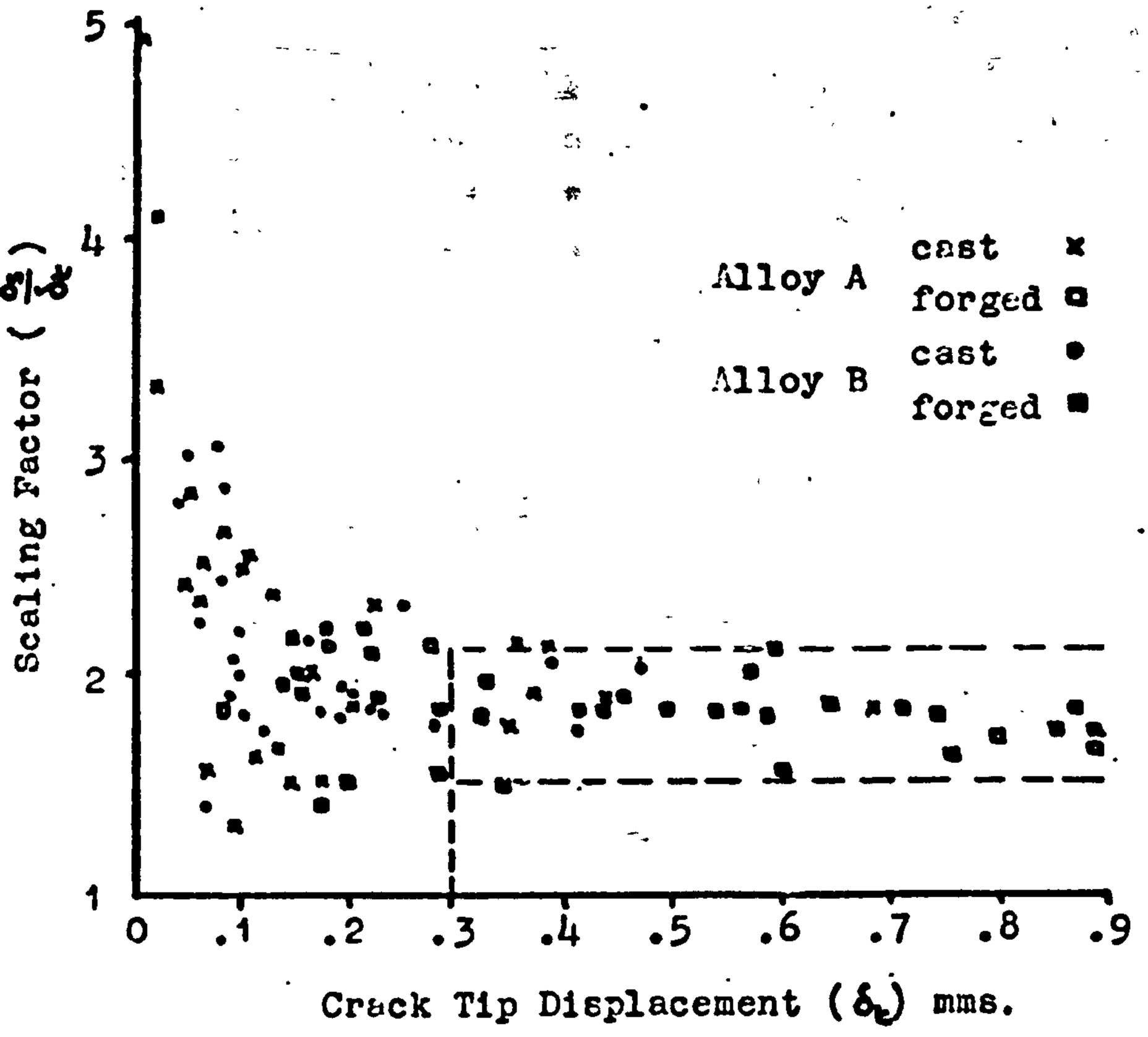

Fig 25. Variation of Scaling Factor with Crack Tip Displacement.

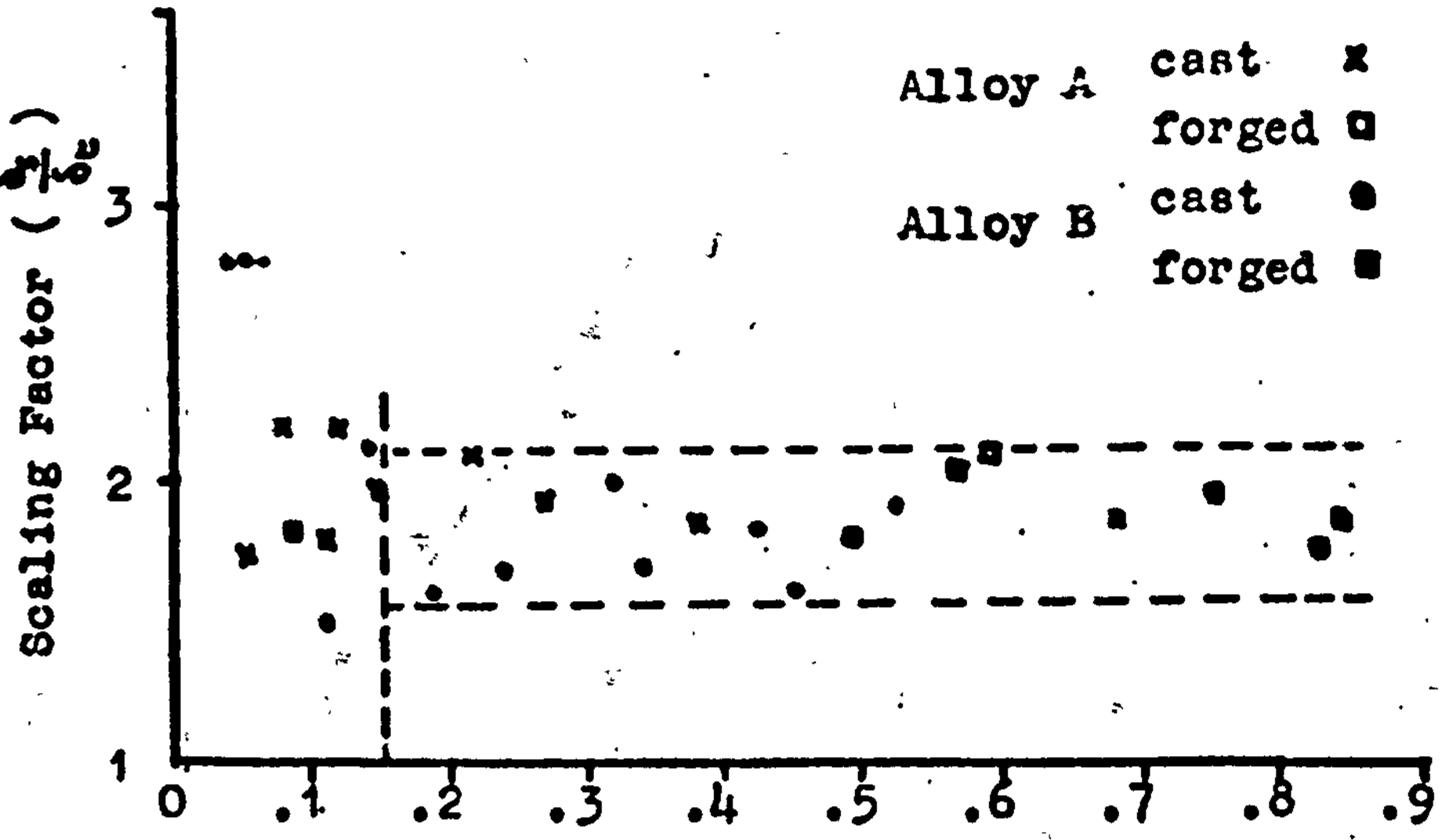

Fig 26. Variation of Scaling Factor with Maximum Load Crack Tip Displacement.

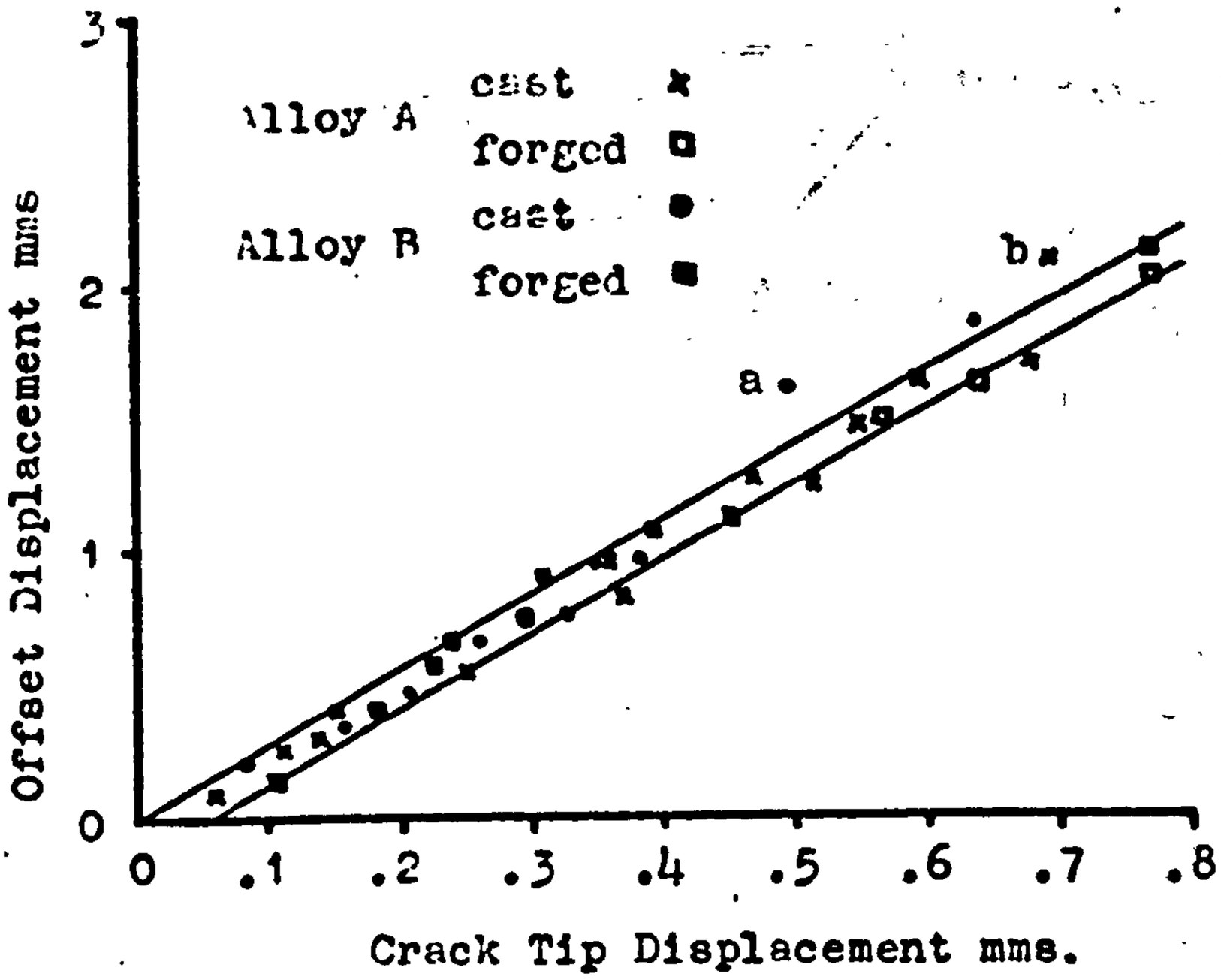

Fig 27. Relationship Between Offset and Crack Tip Displacements.

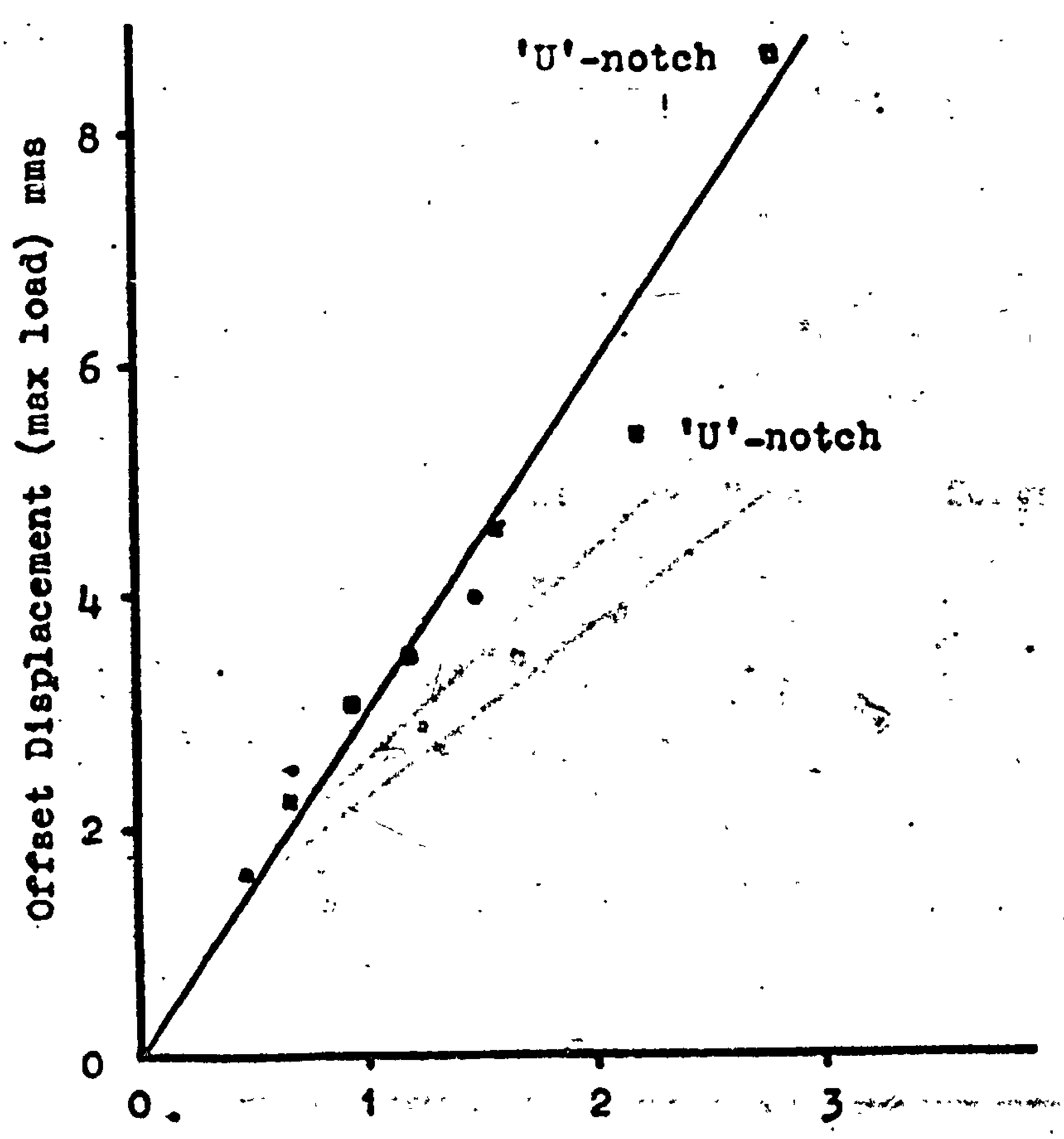

Fig 28. Relationship Between C.O.D. and Offset Displacement at Maximum Load.

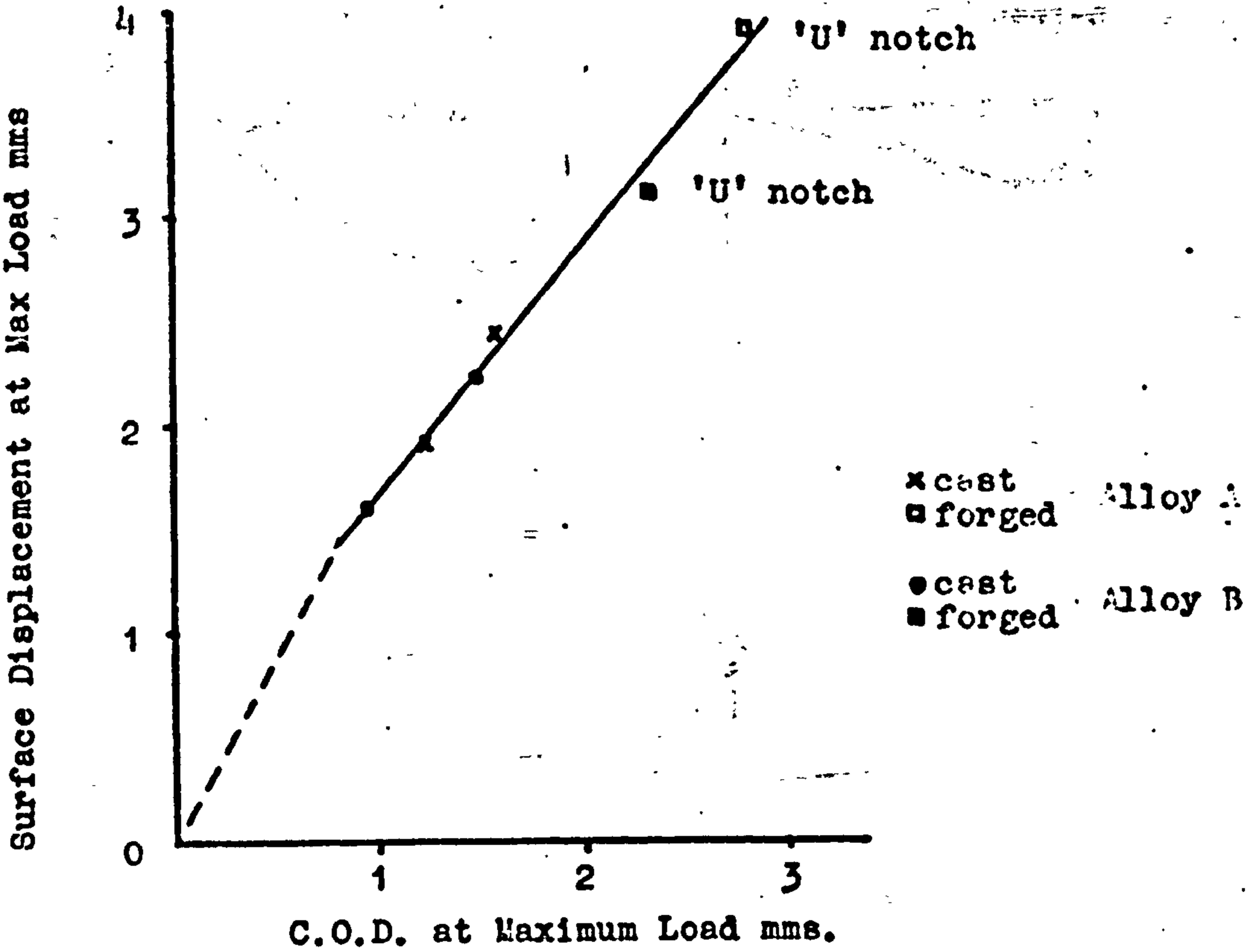

Fig 29. Relationship Between C.O.D. and Surface Displacement at the Maximum Load.

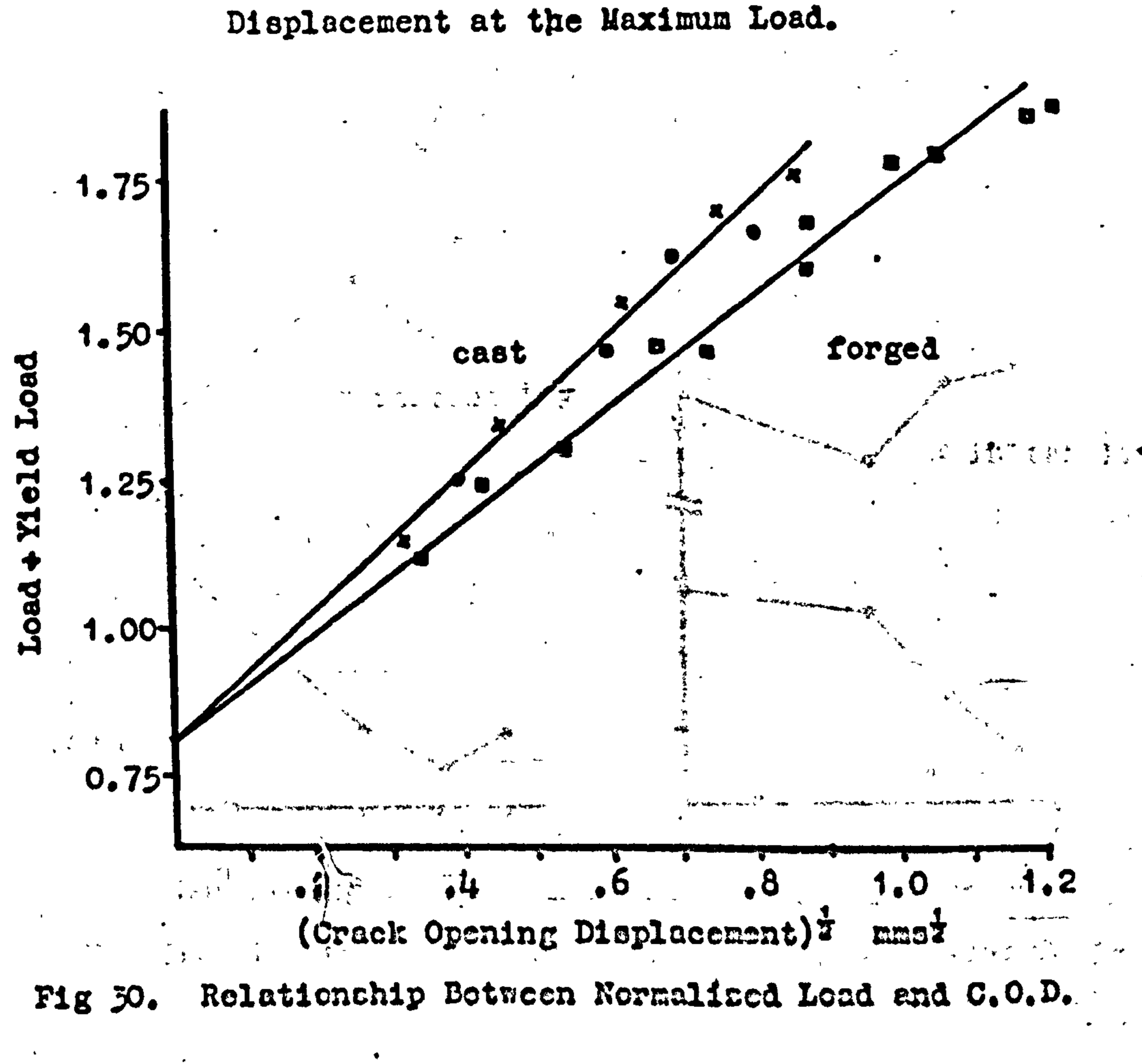

Fig 30. Relationchip Between Normalised Load and C.O.D.

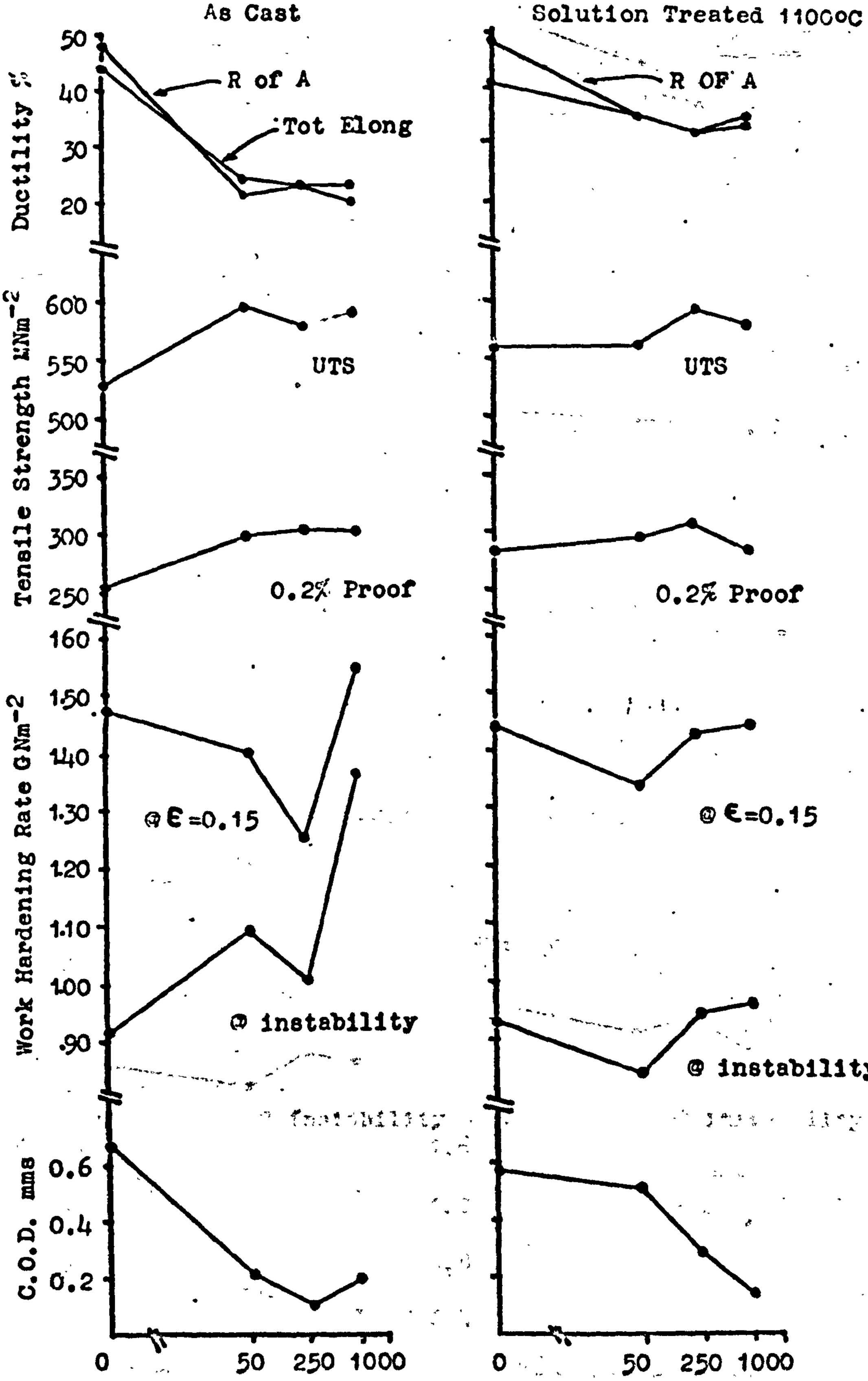

Fig 31. Influence of Ageing Time at 725°C on Room Temperature Mechanical Properties of the Cast Duplex Allo

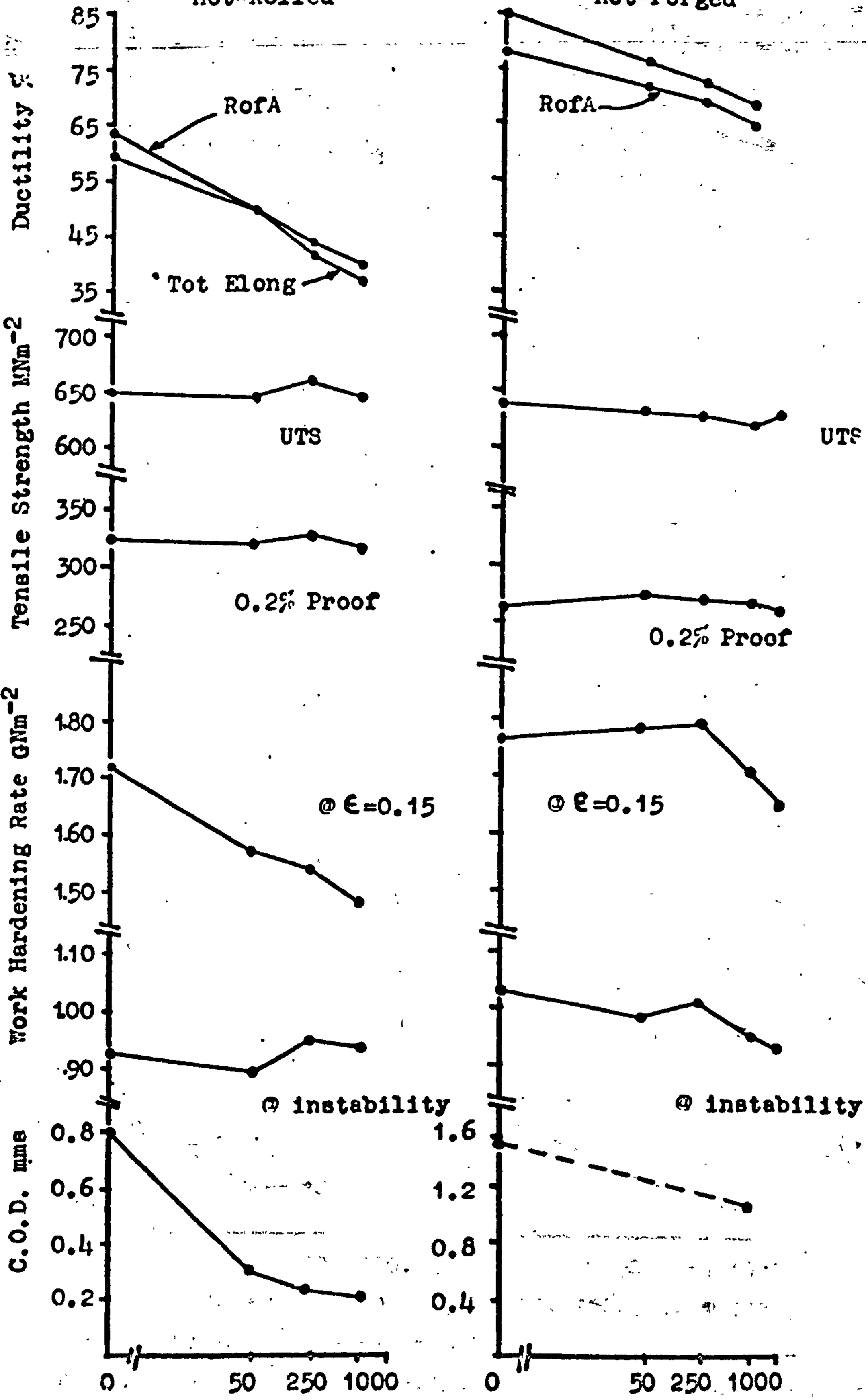

Fig 32. Influence of Ageing Time at 725°C on Room Temperature Mechanical Properties of the Hot-Worked Duplex Alloys.

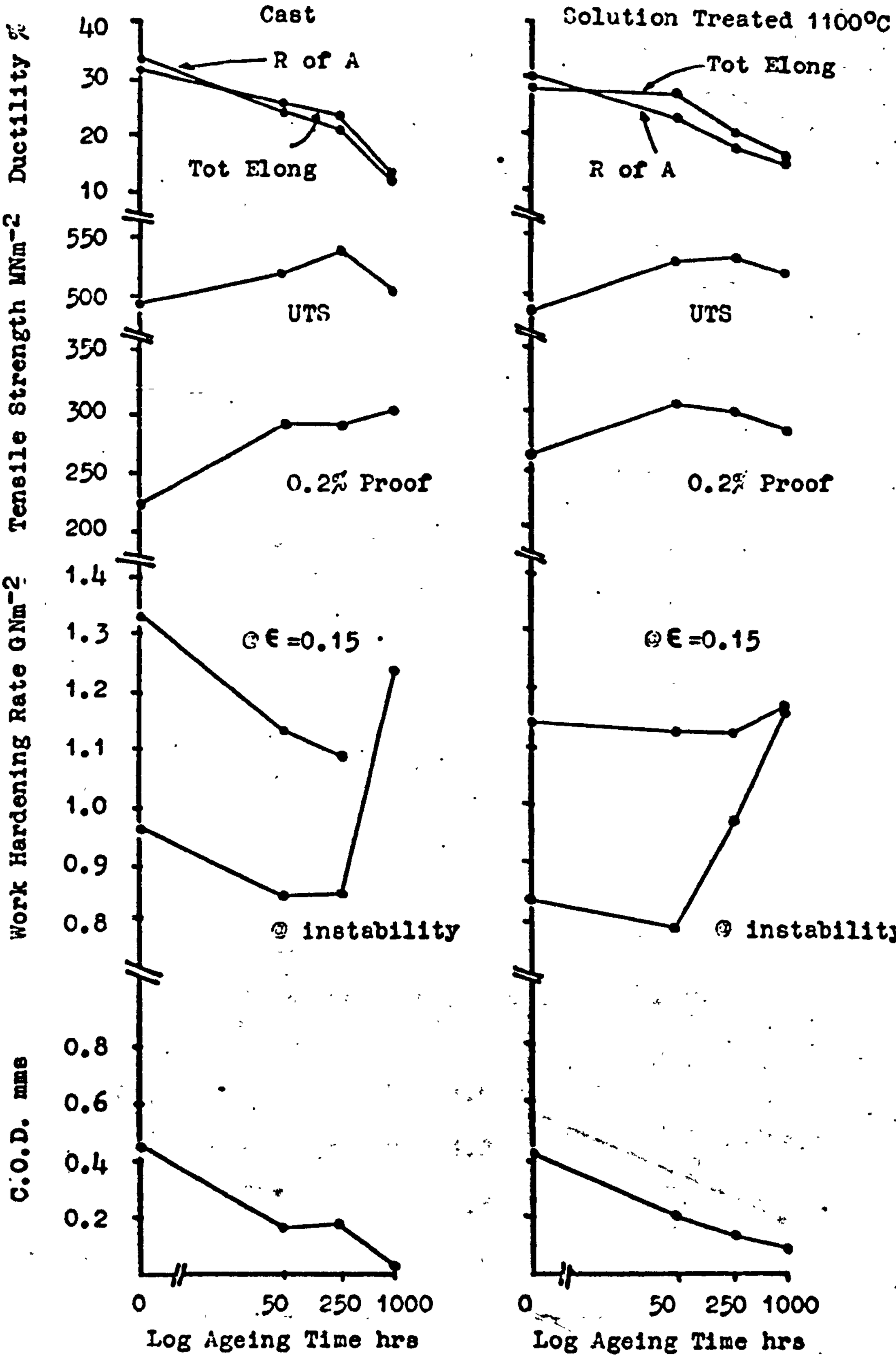

Fig 33. Influence of Ageing Time at 725°C on Room Temperature Mechanical Properties of the Cast Austenitic Alloy.

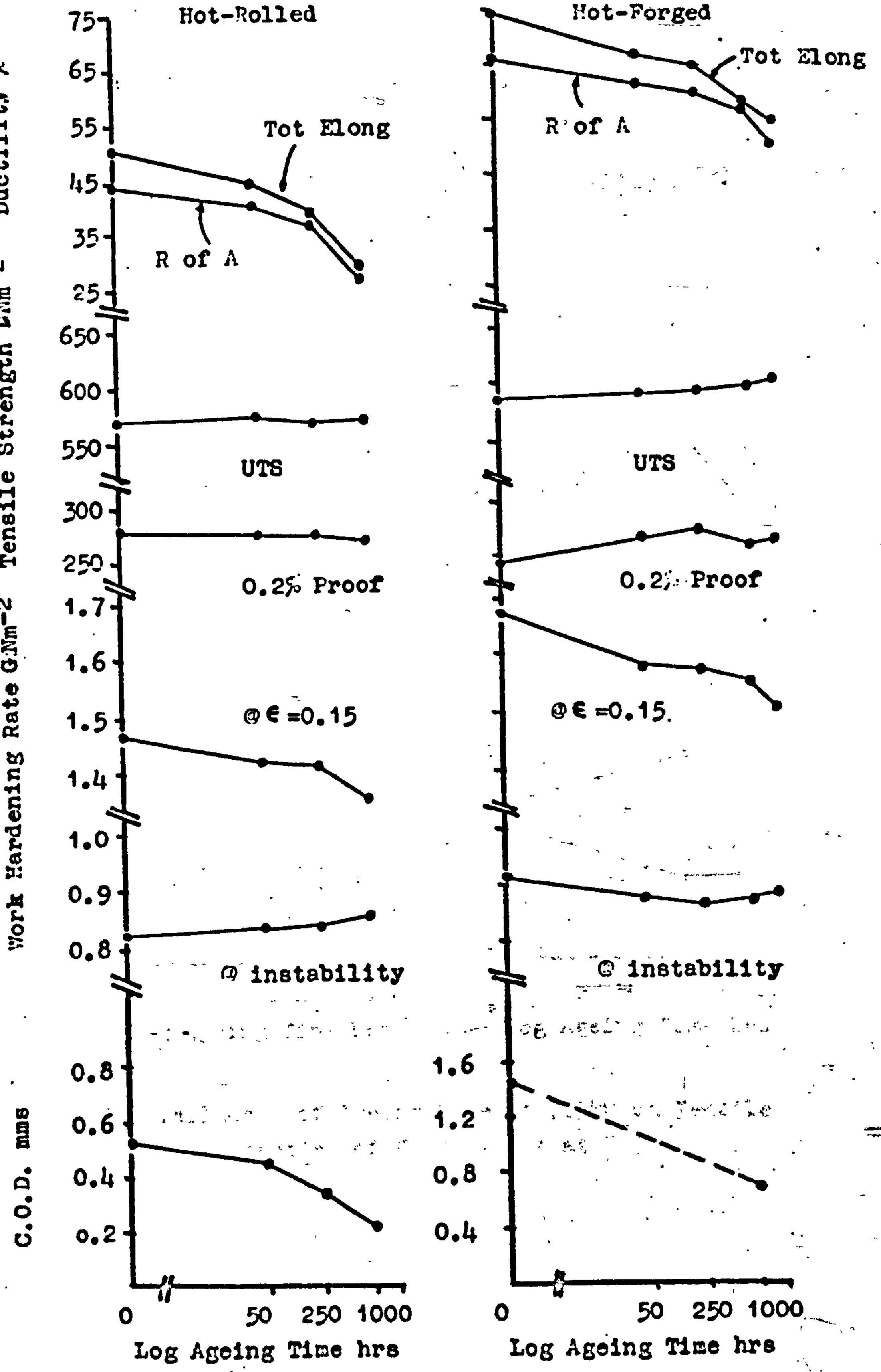

Fig 34. Influence of Ageing Time At 725°C on Room Temperature Mechanical Properties of the Hot-Worked Austenitic Alloy.

x Solution Treated 1100°C prior to ageing.

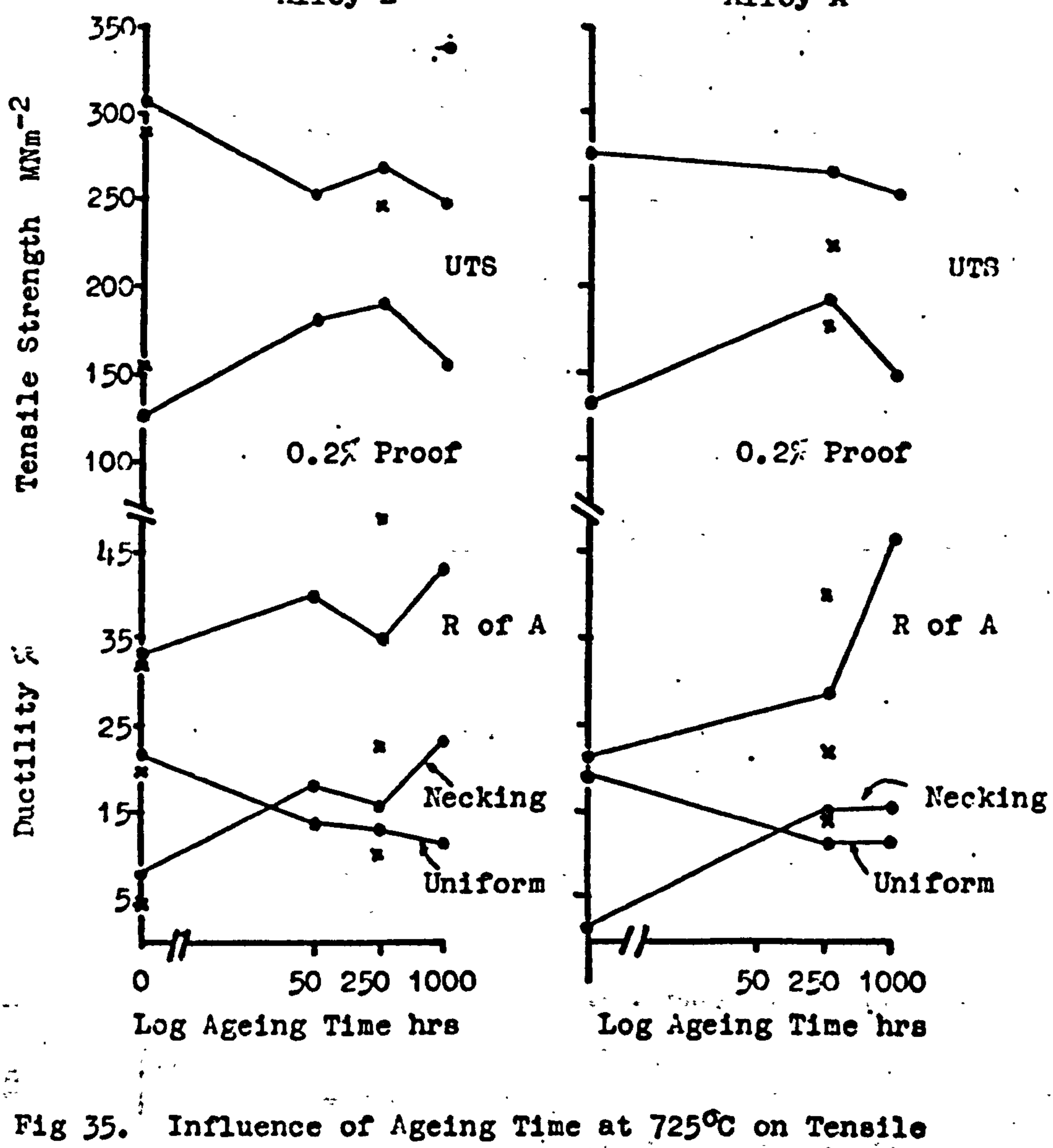

Fig 35. Influence of Ageing Time at 725°C on Tensile Properties of Cast Alloys at 725°C.

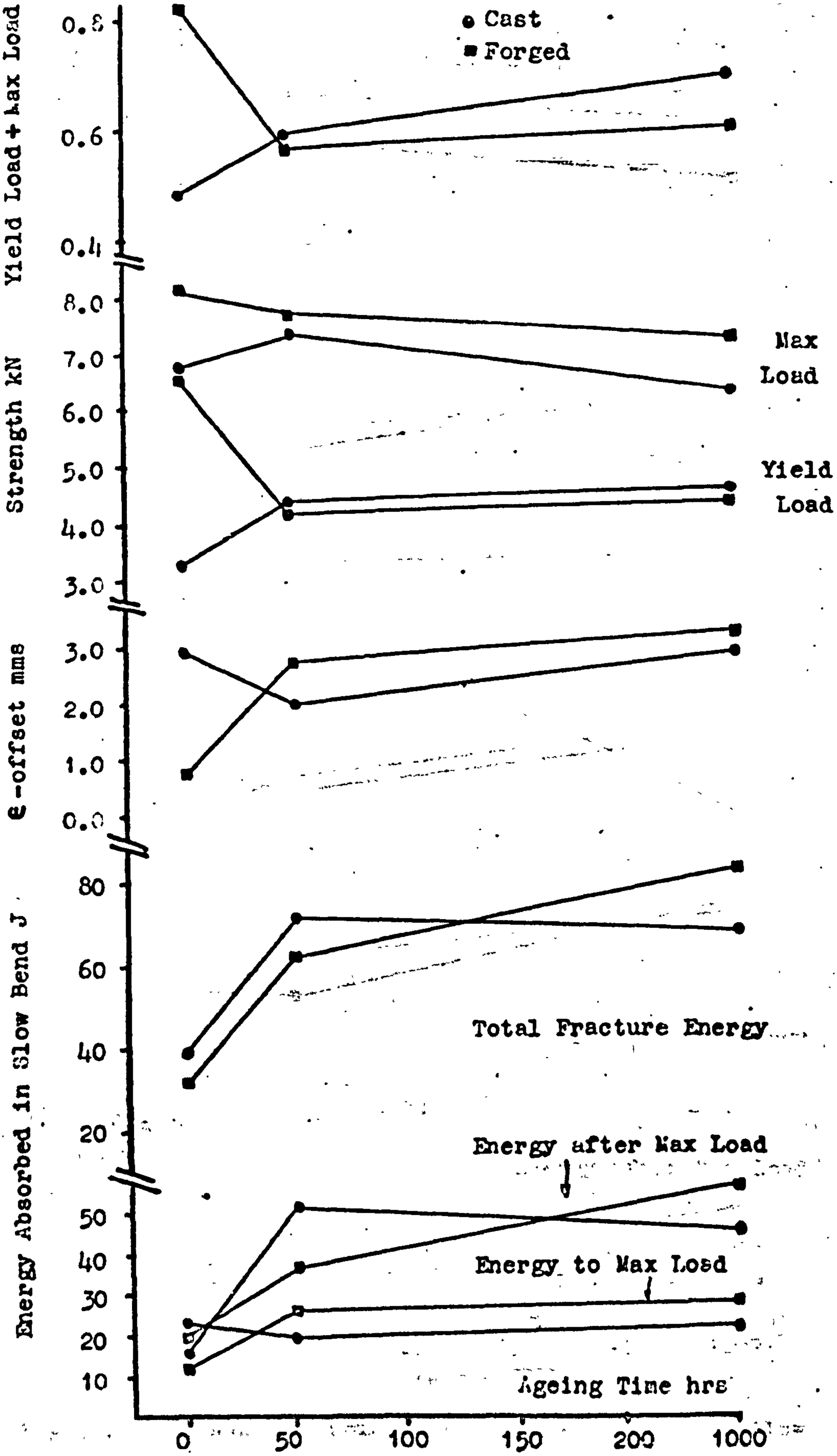

Fig 36. Influence of Prior Ageing Time at 725°C on Slow Bend Properties of Alloy B at 725°C.

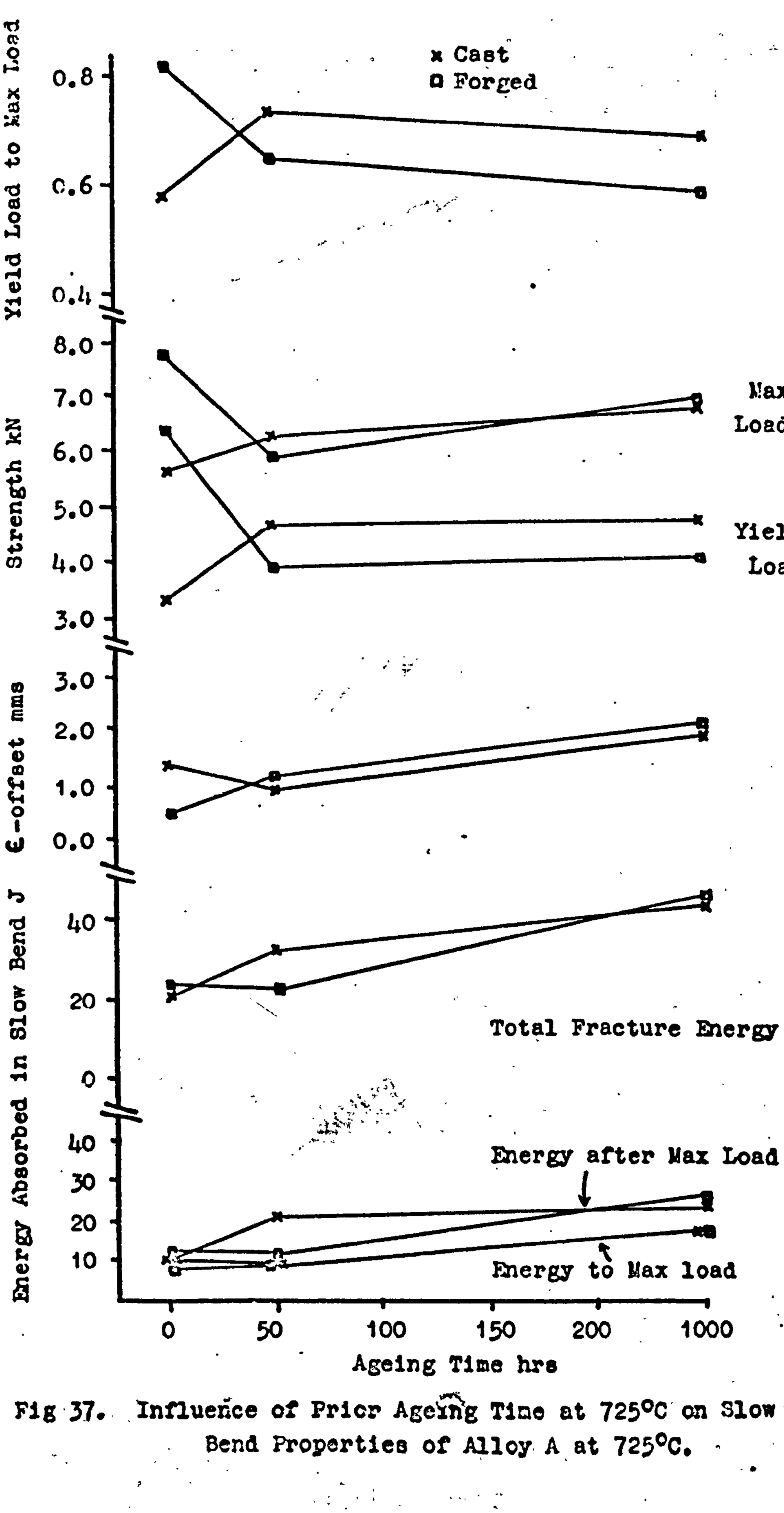

Fig 37. Influence of Prior Ageing Time at 725°C on Slow Bend Properties of Alloy A at 725°C.

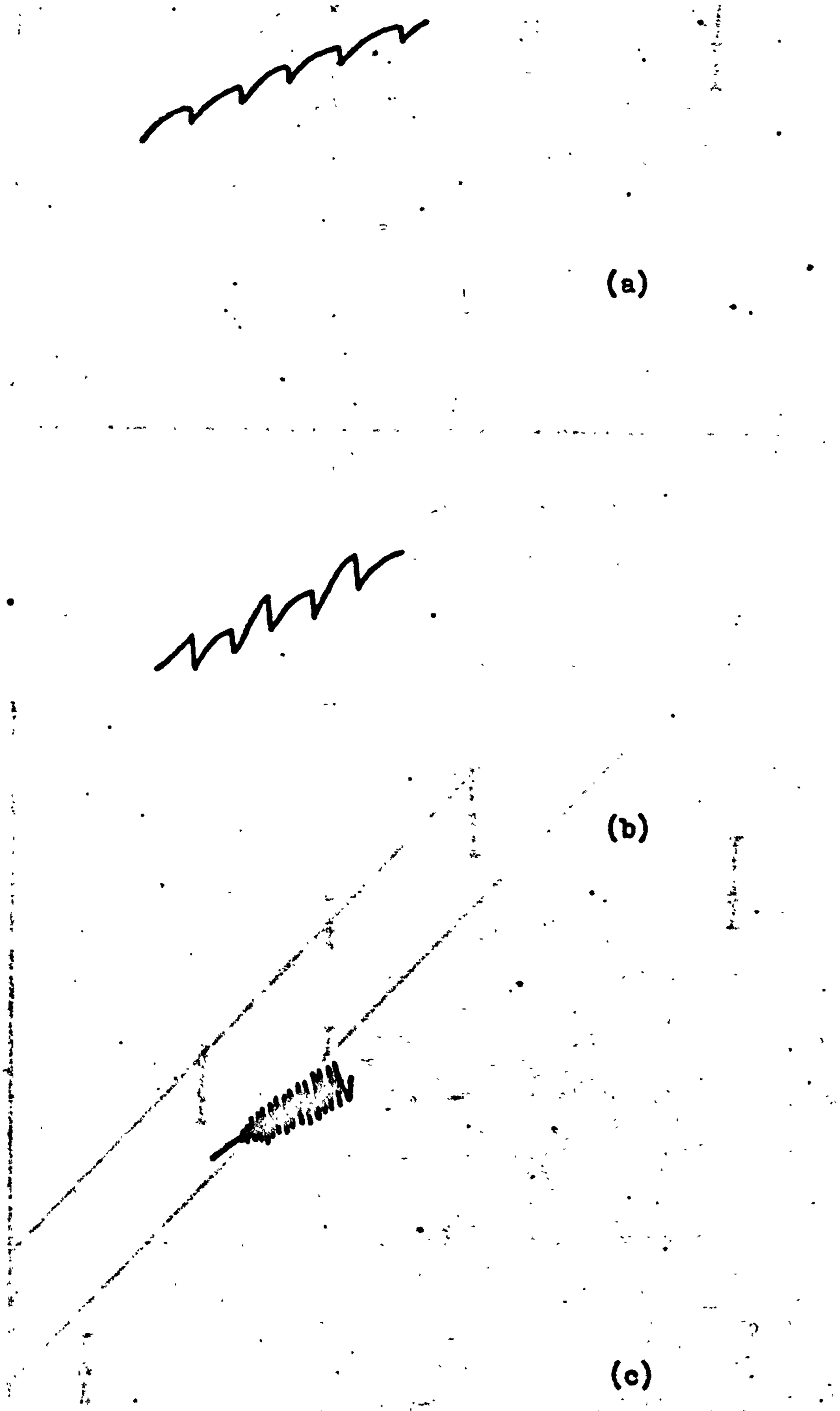

Fig 38. Form of Serrations Exhibited by Tensile Stress-Strain Curves in the Temperature Range 400-600°C

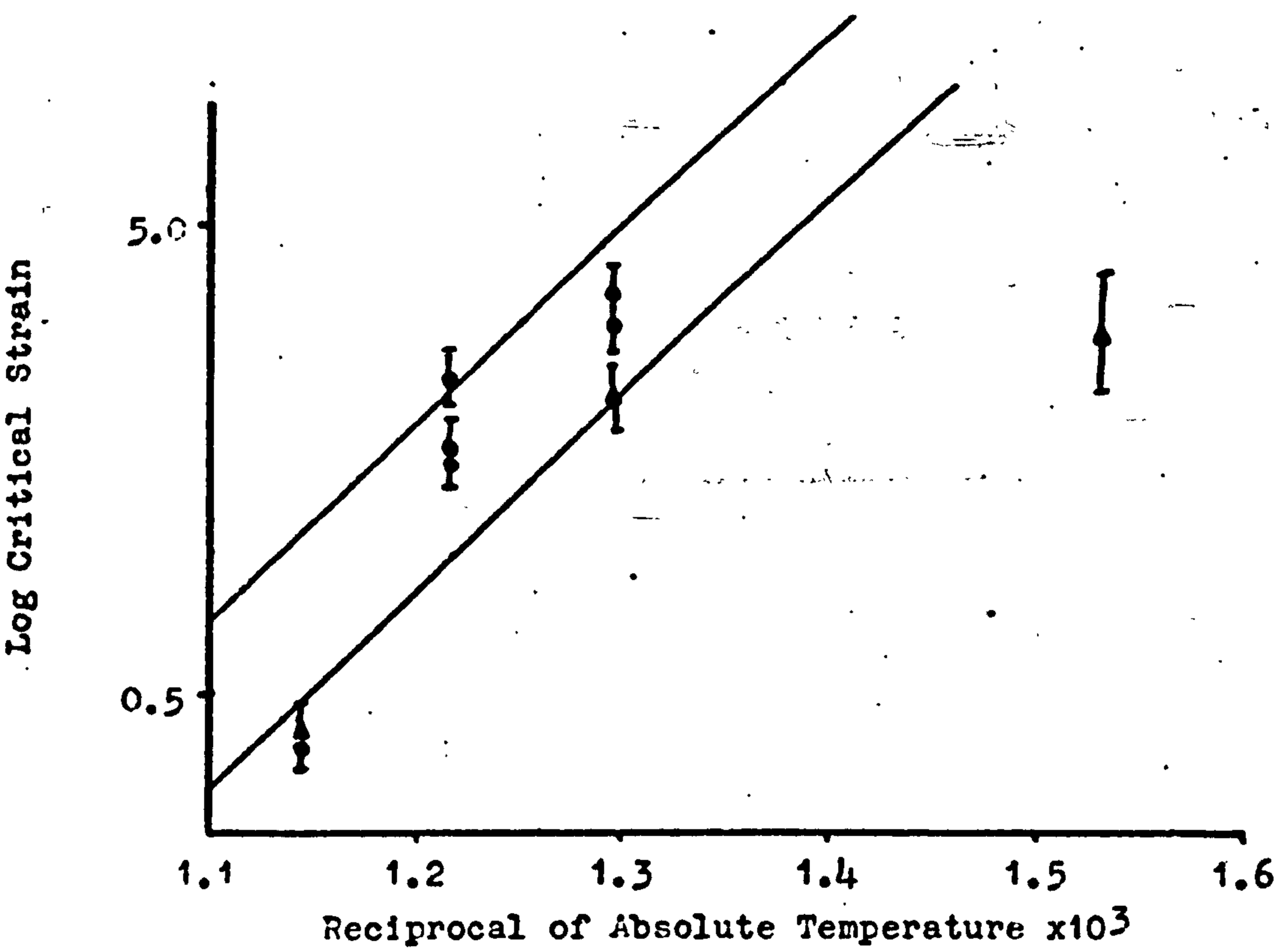

Fig 39. Temperature Dependency of Critical Strain in Alloy B.

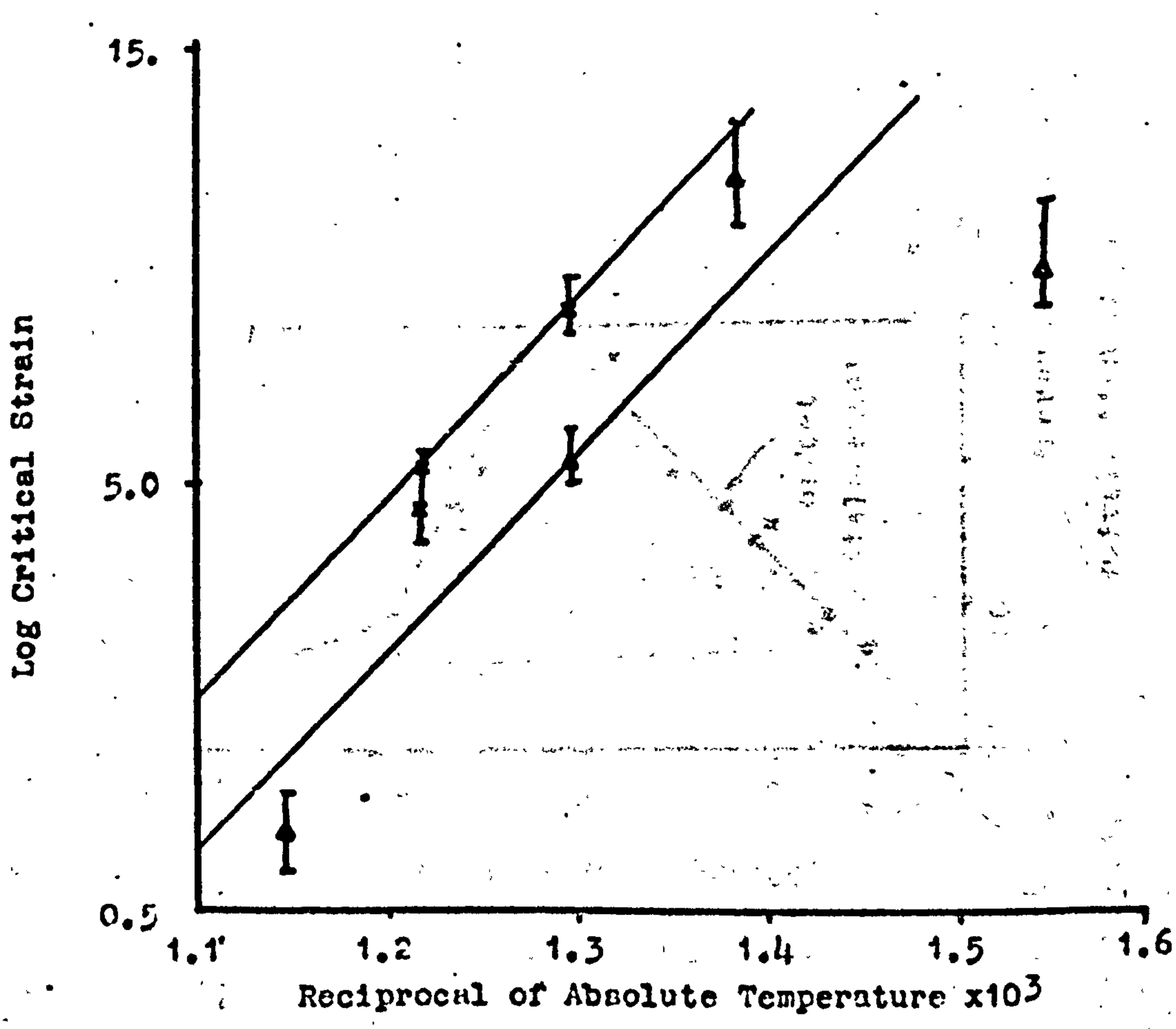

Fig 40. Temperature Dependency of Critical Strain in Alloy A.

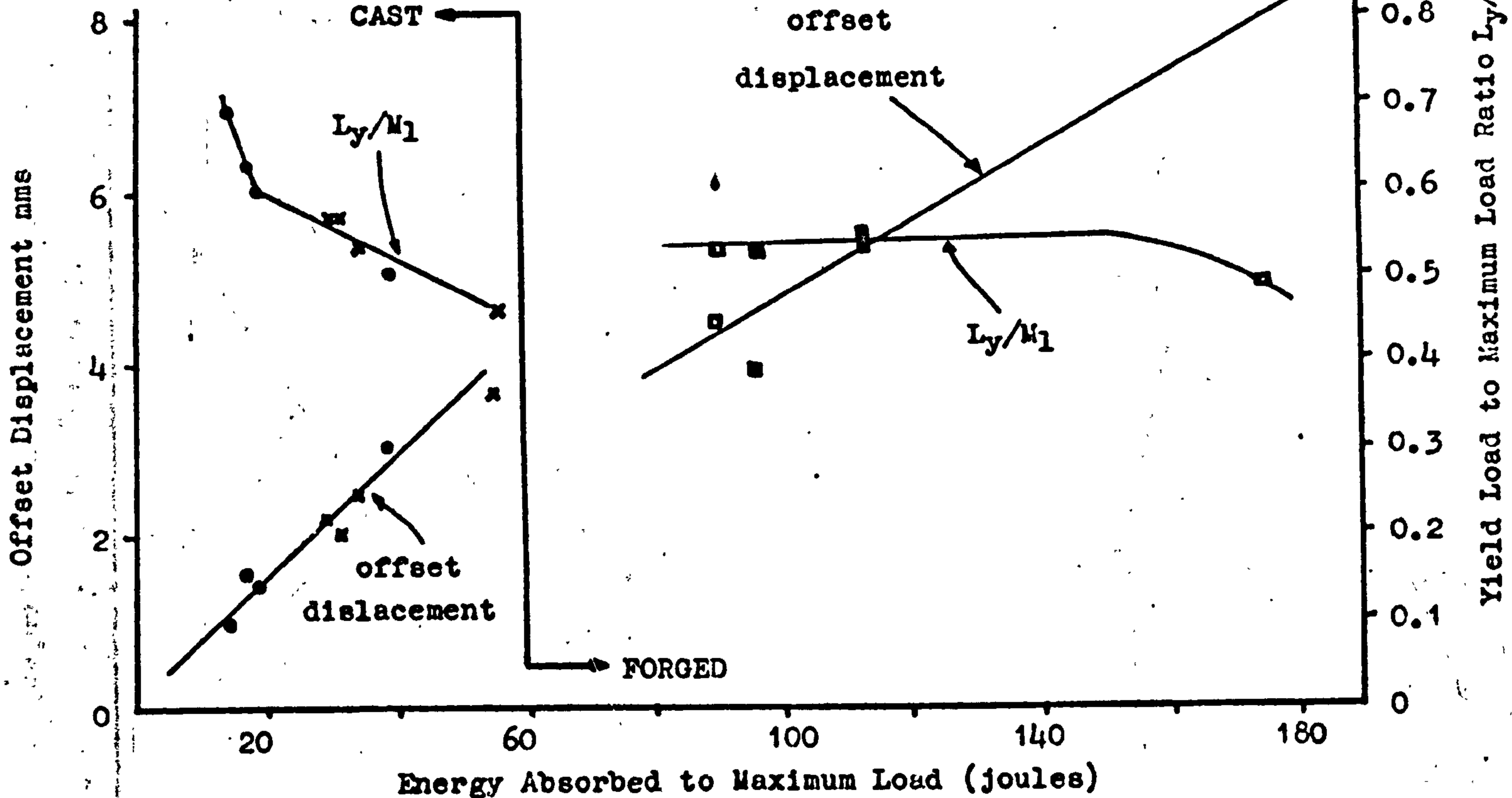

Fig 41. An Evaluation of Slow Bend Test at 25°C by Microstructure.

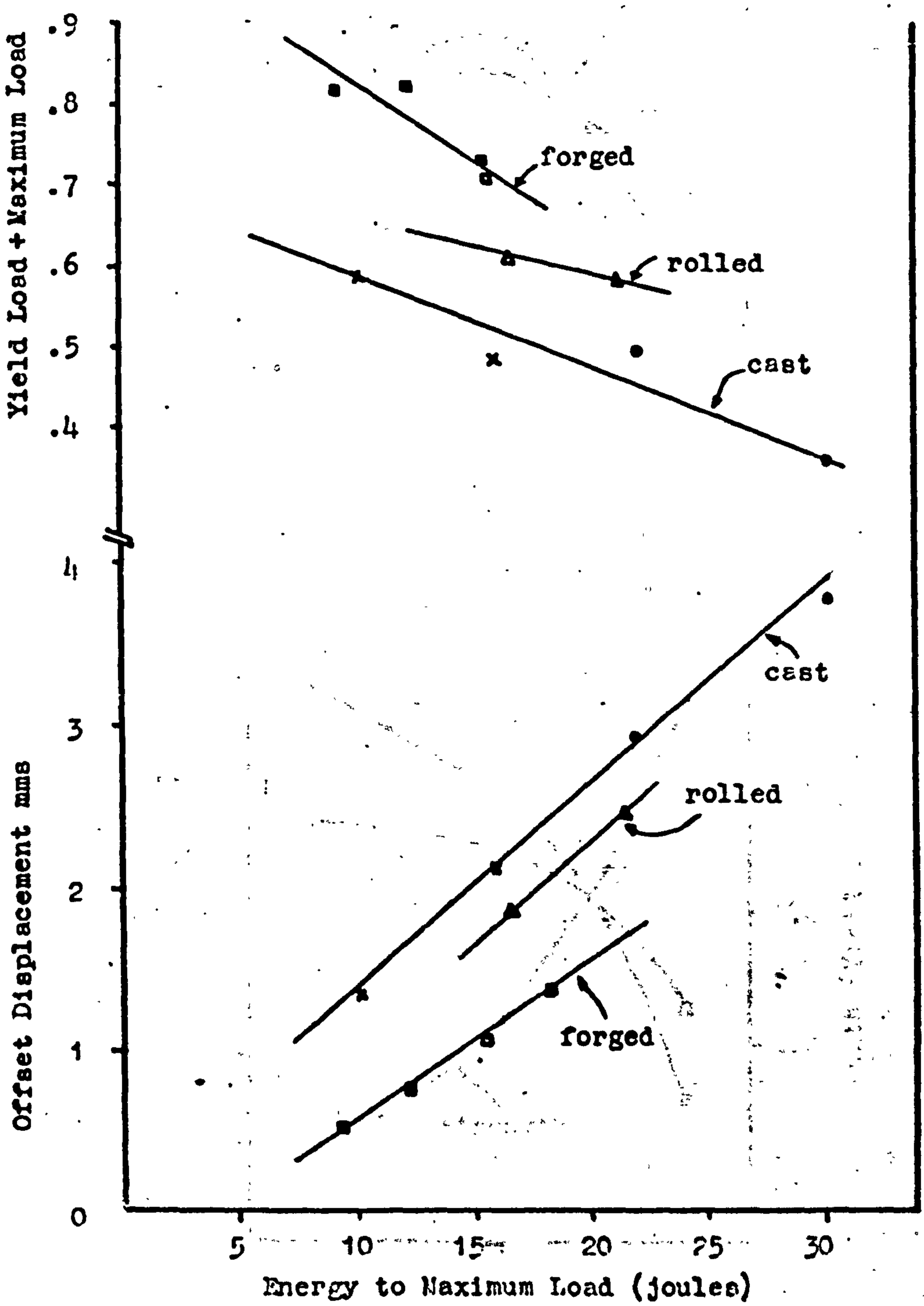

Fig 42. Evaluation of Slow Bend Test at 725°C by Microstructure.

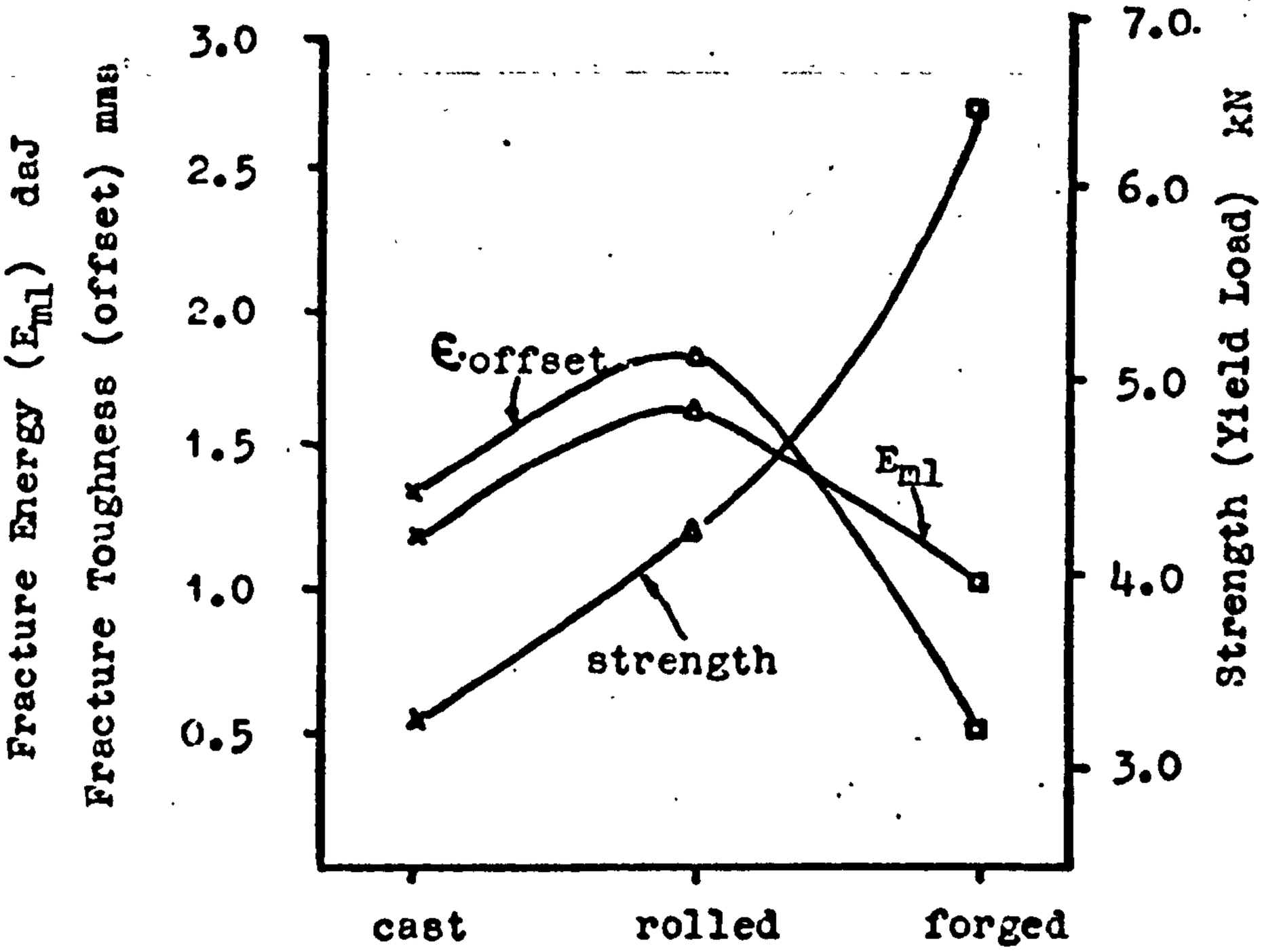

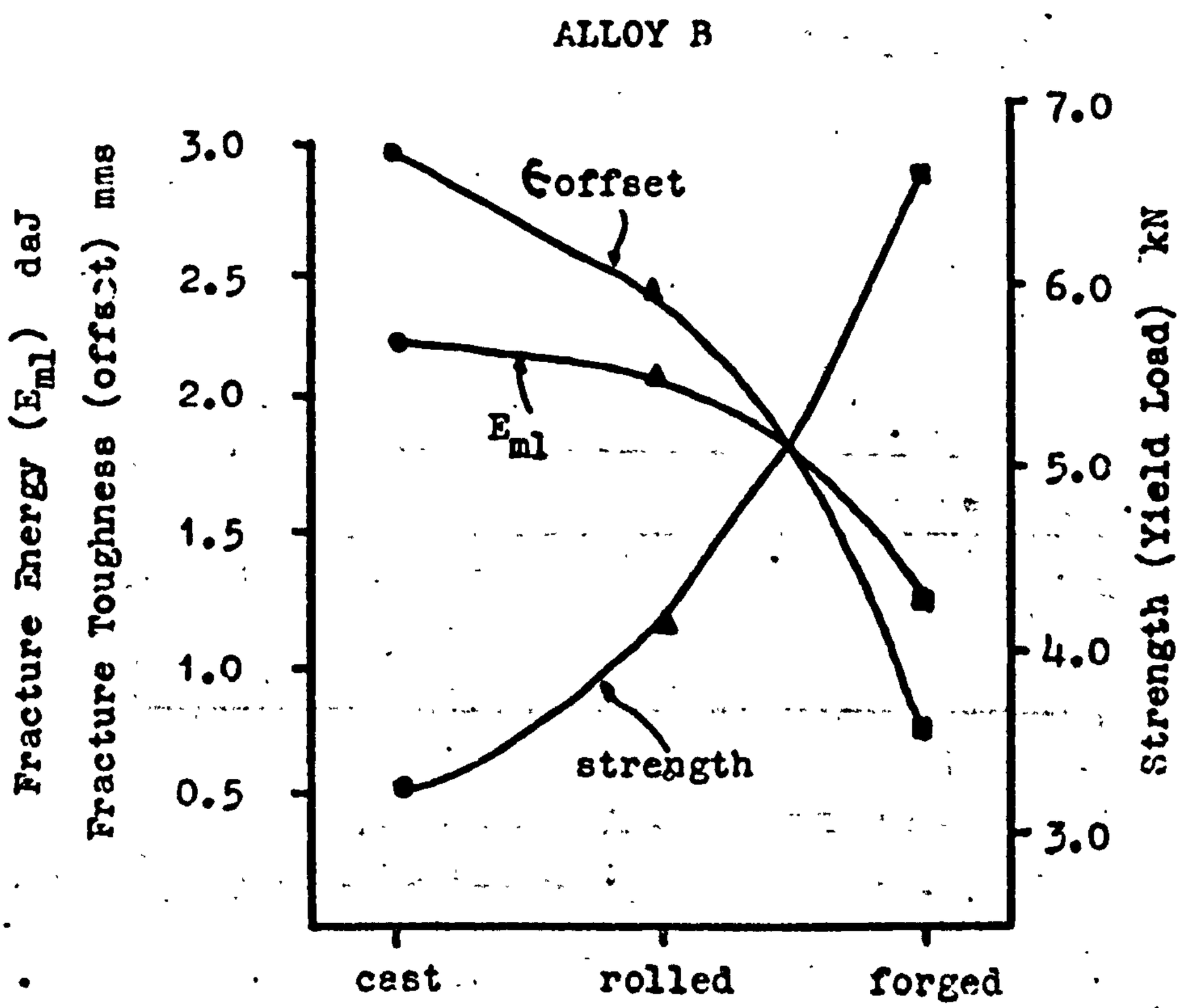

Fig 43. Influence of Manufacturing Process on Strength and Fracture Toughness in Slow Bend at 725°C.

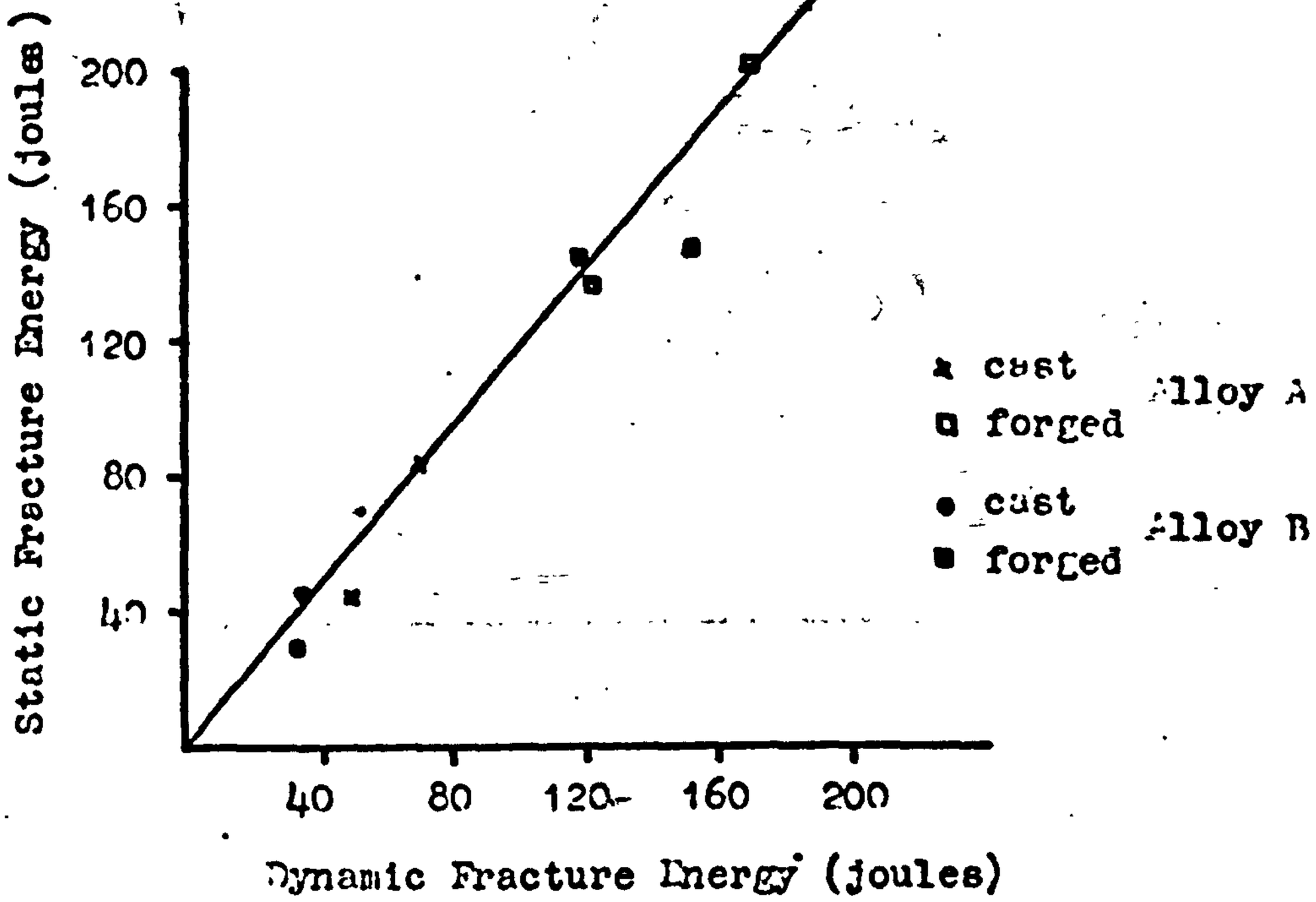

Fig 44. Effect of Strain-Rate on Total Fracture Energy at Room Temperature.

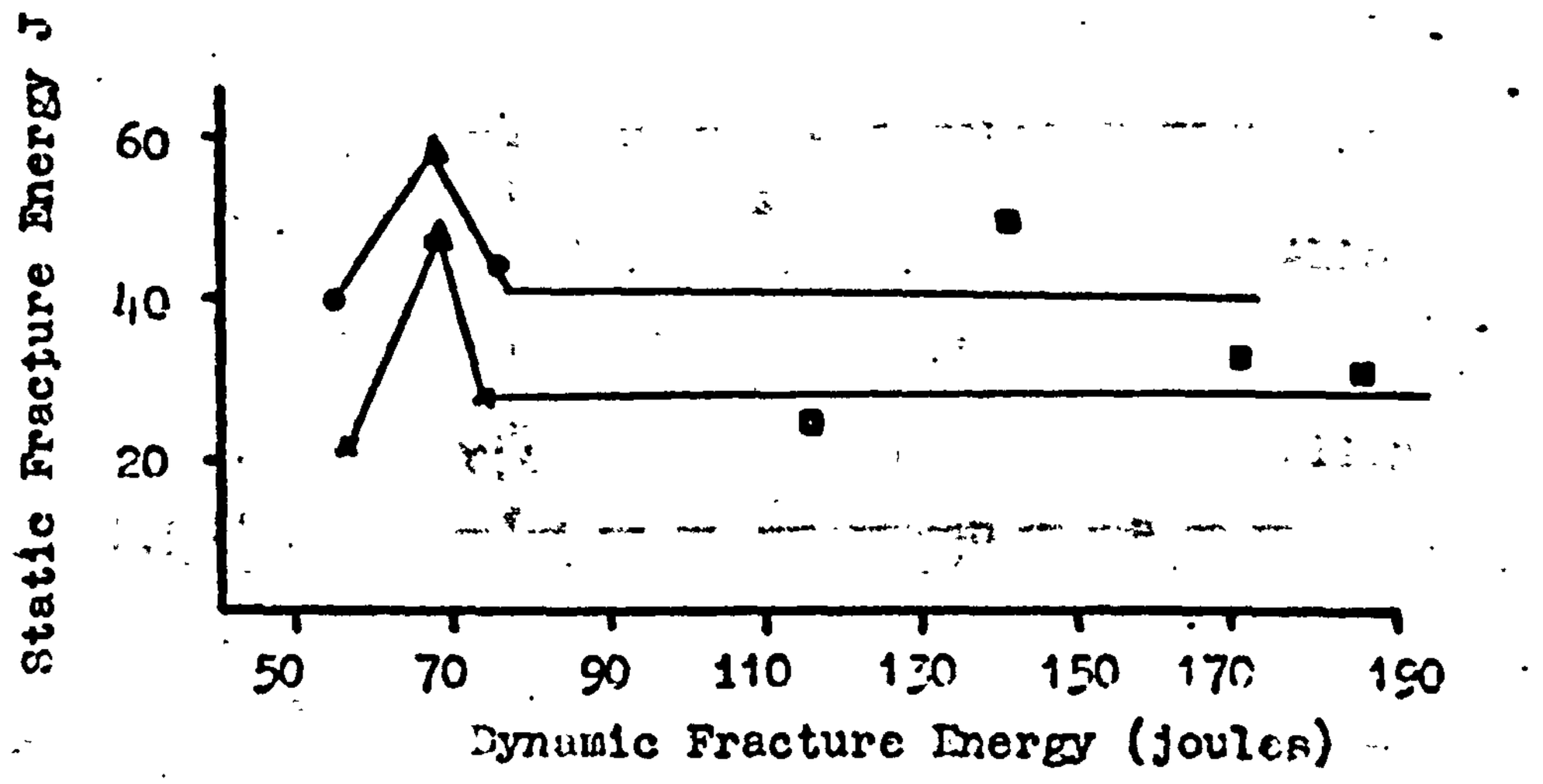

Fig 45. Effect of Strain-Rate on Total Fracture Energy at 725°C.

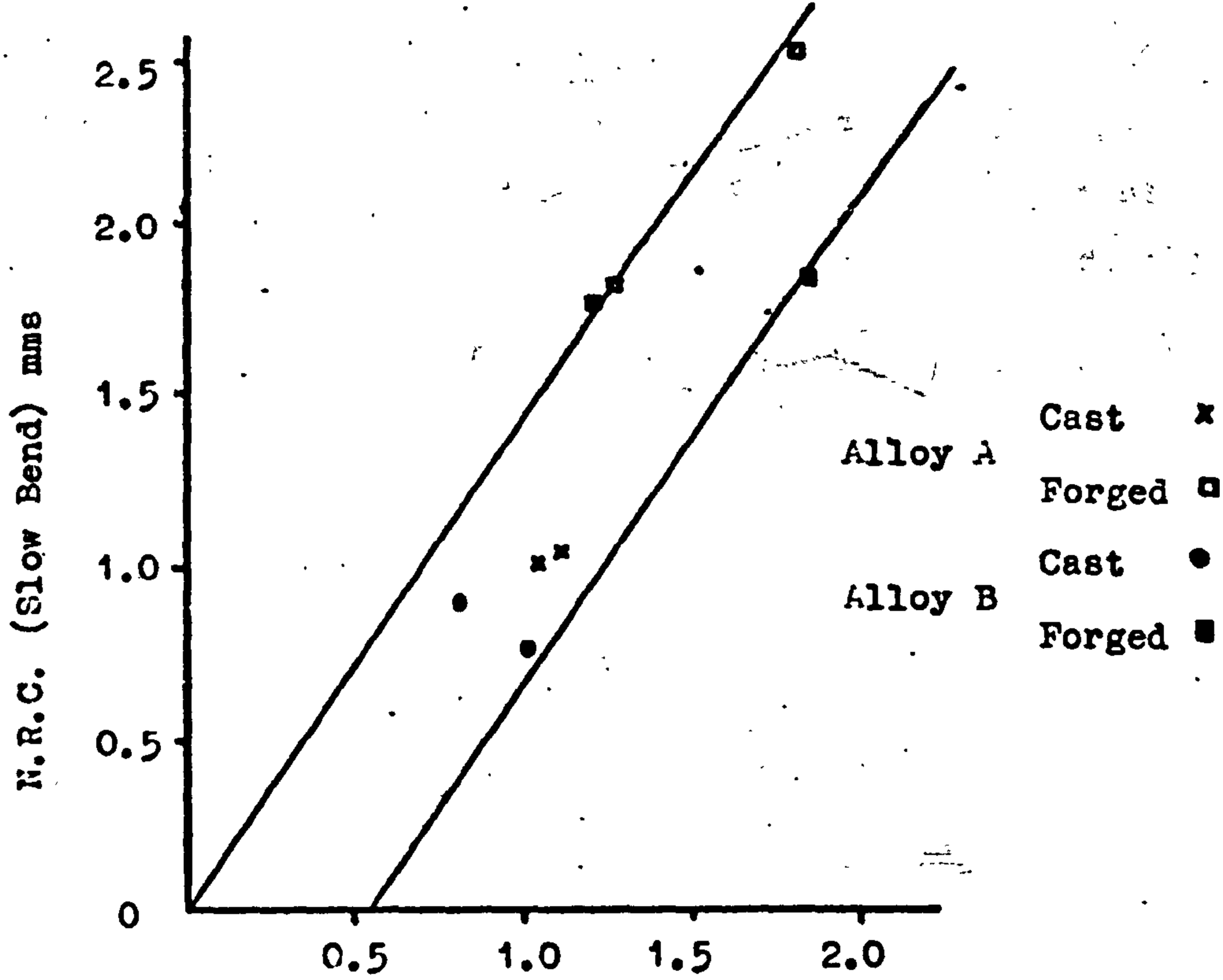

Fig 46. Correlation Between Notch Root Contraction in Impact and Slow Bend at Room Temperature.

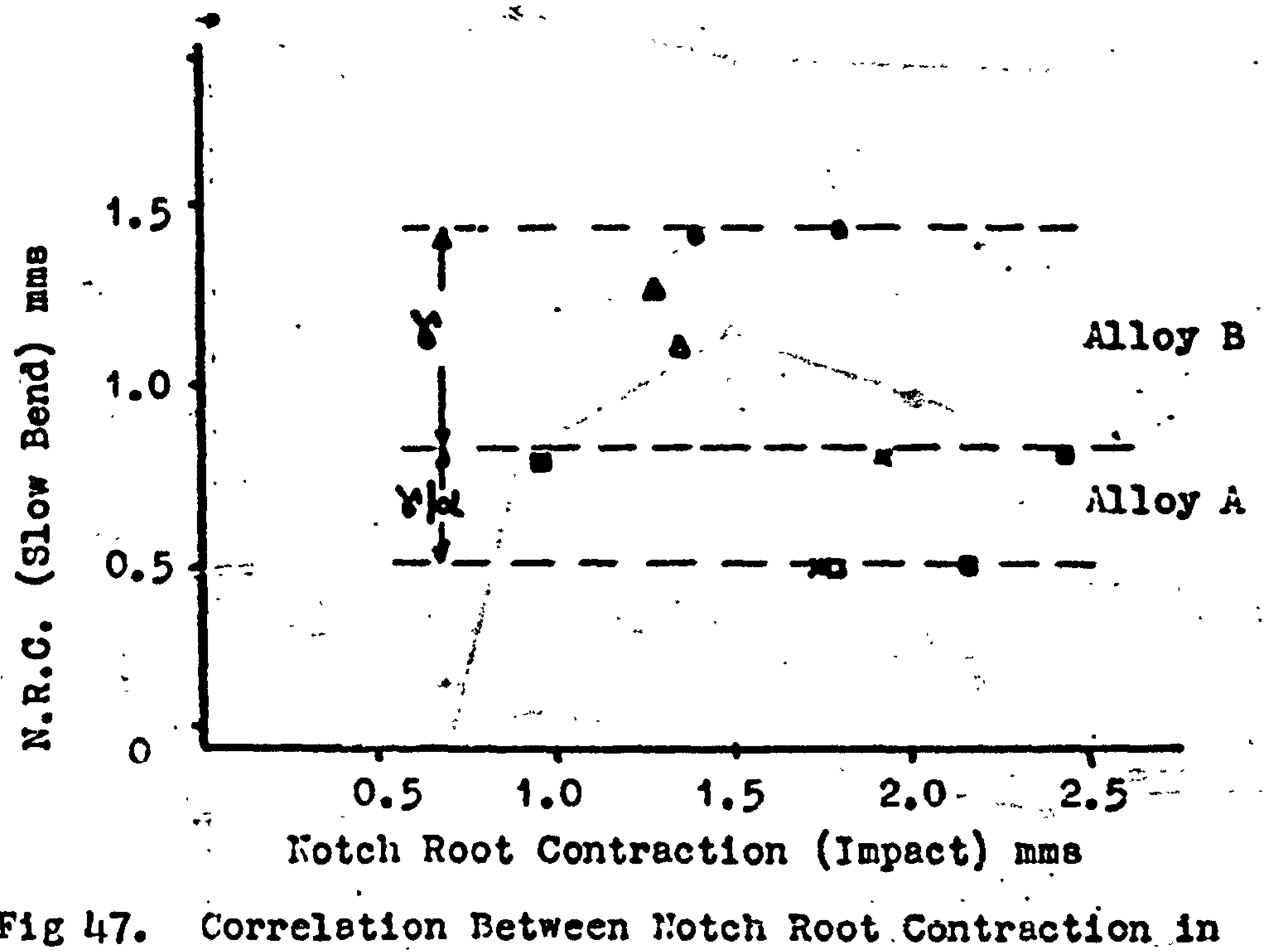

Fig 47. Correlation Between Notch Root Contraction in Impact and Slow Bend at 725°C.

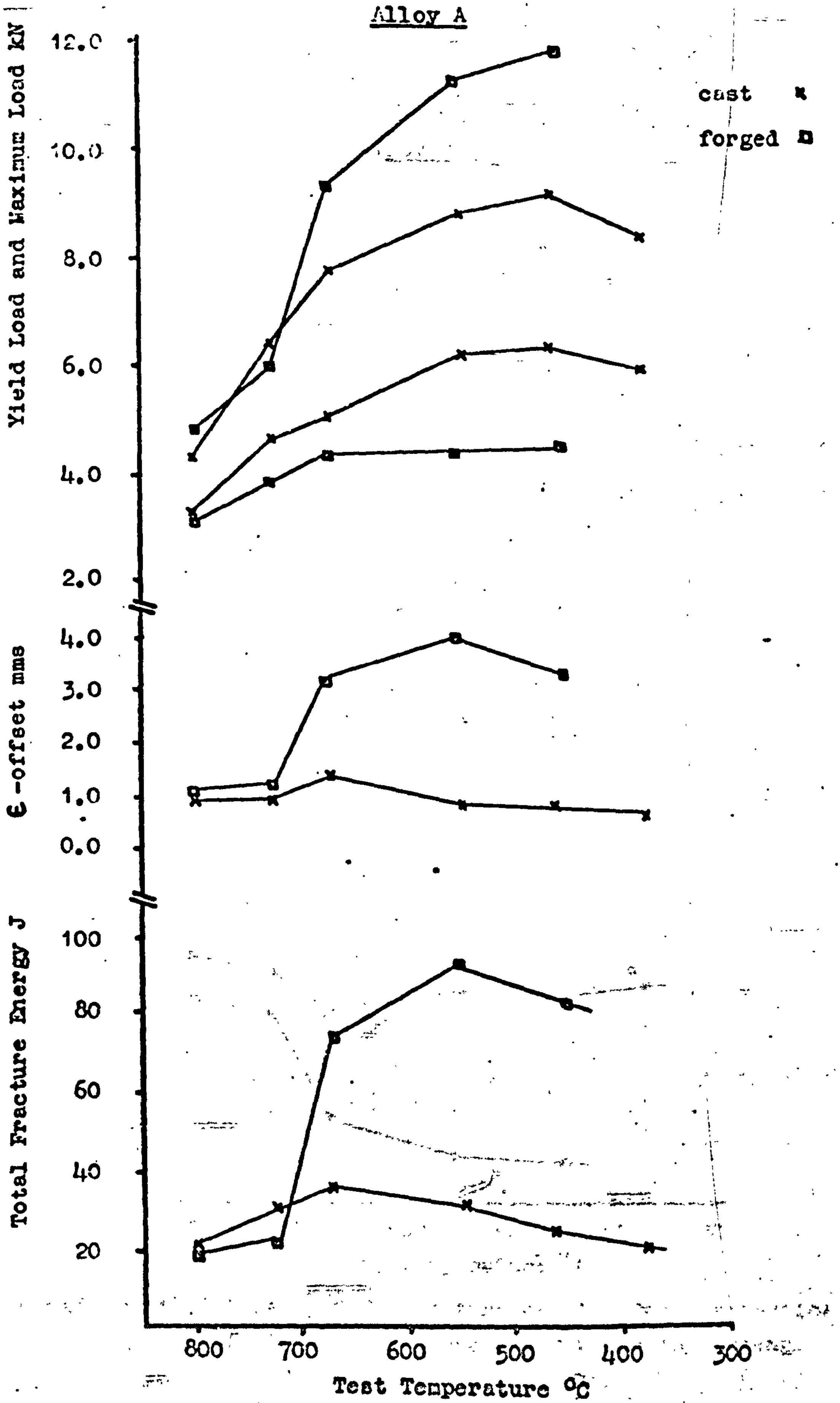

Fig 48. Effect of Test Temperature on Slow Bend Properties of Alloys Aged 50hrs/725°C Prior to Testing.

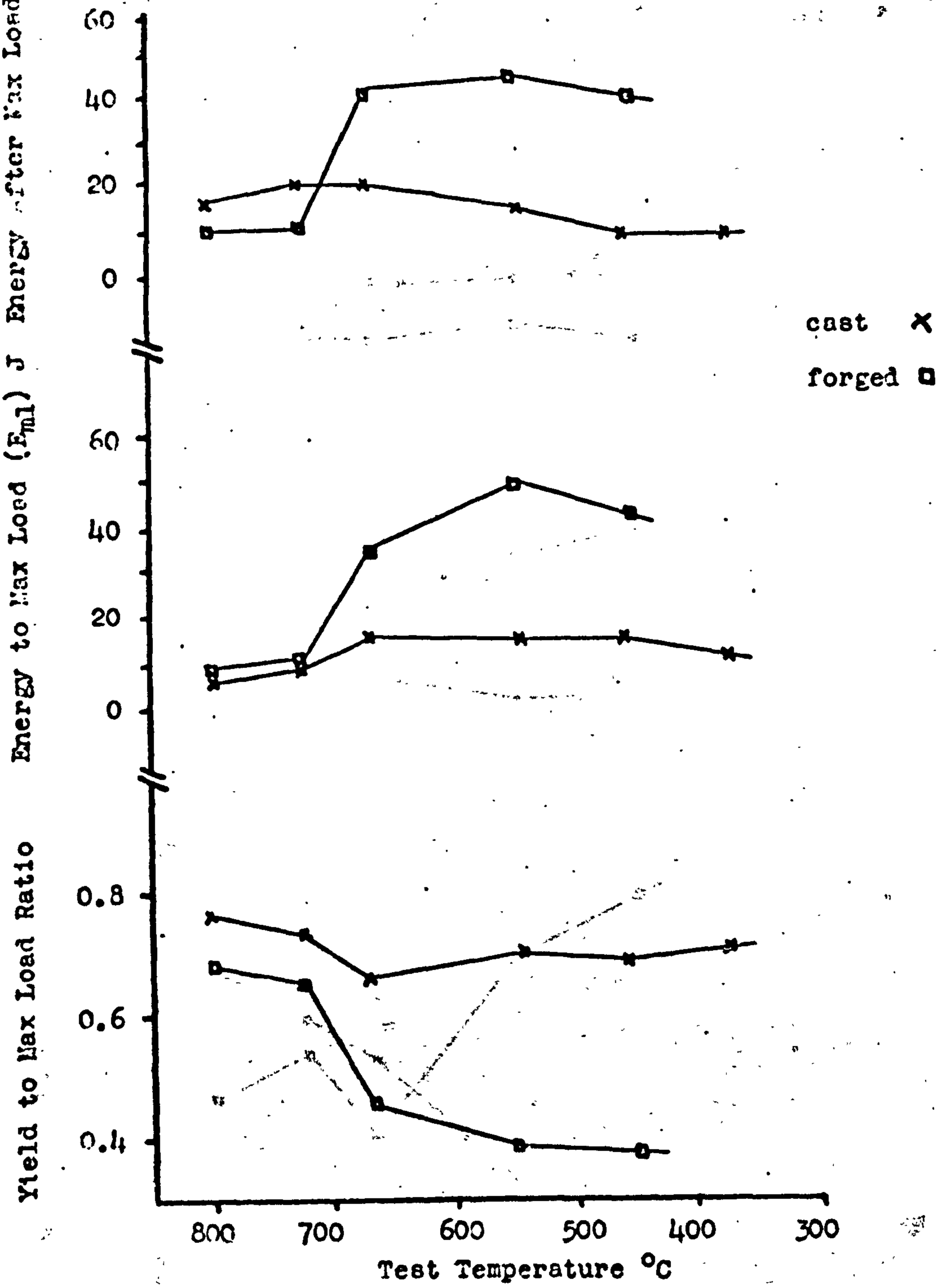

Fig 48 (cont). Effect of Temperature on Slow Bend Properties of Alloys Aged 50hrs/725°C Prior to Testing.

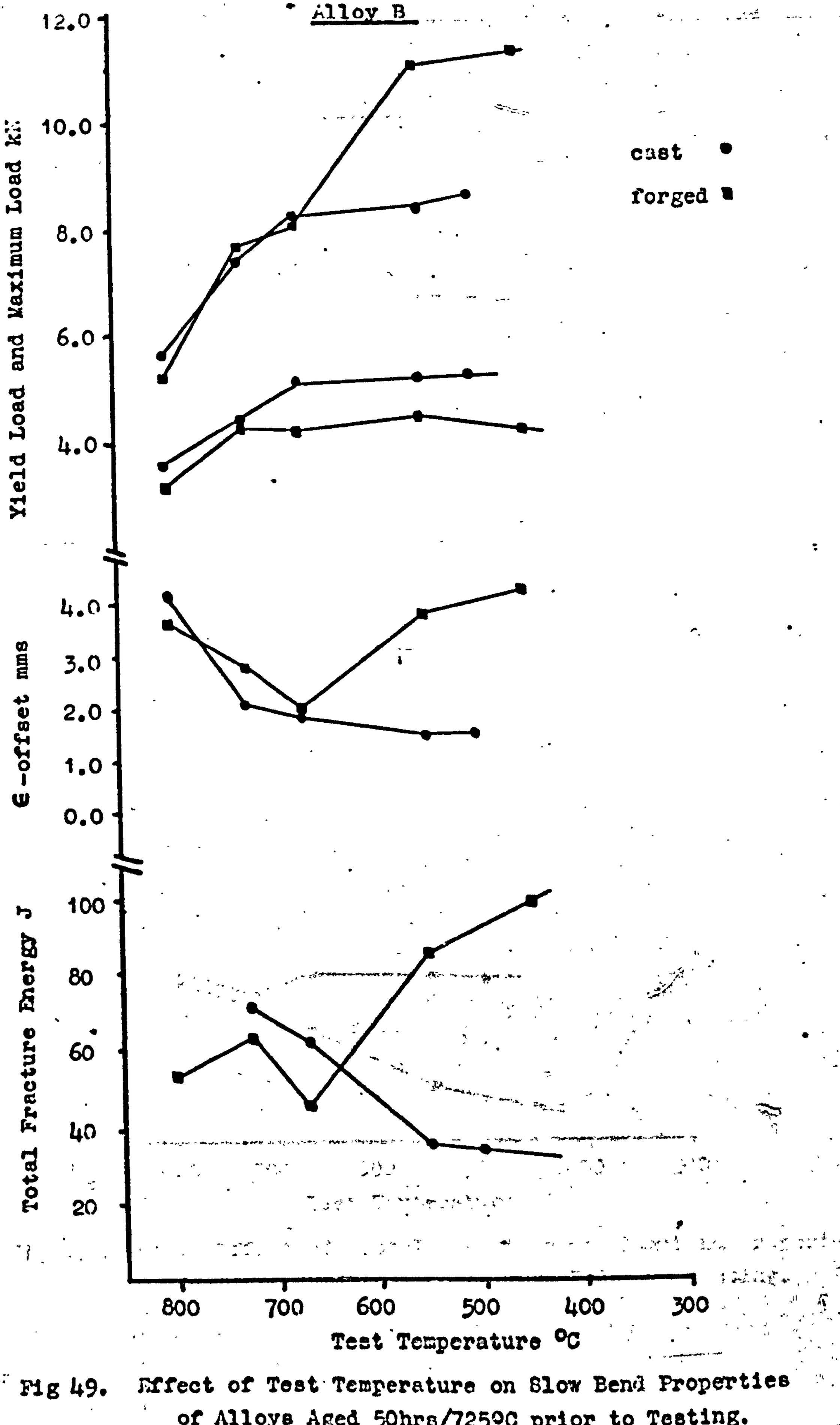

Fig 49. Effect of Test Temperature on Slow Bend Properties of Alloys Aged 50hrs/725°C prior to Testing.

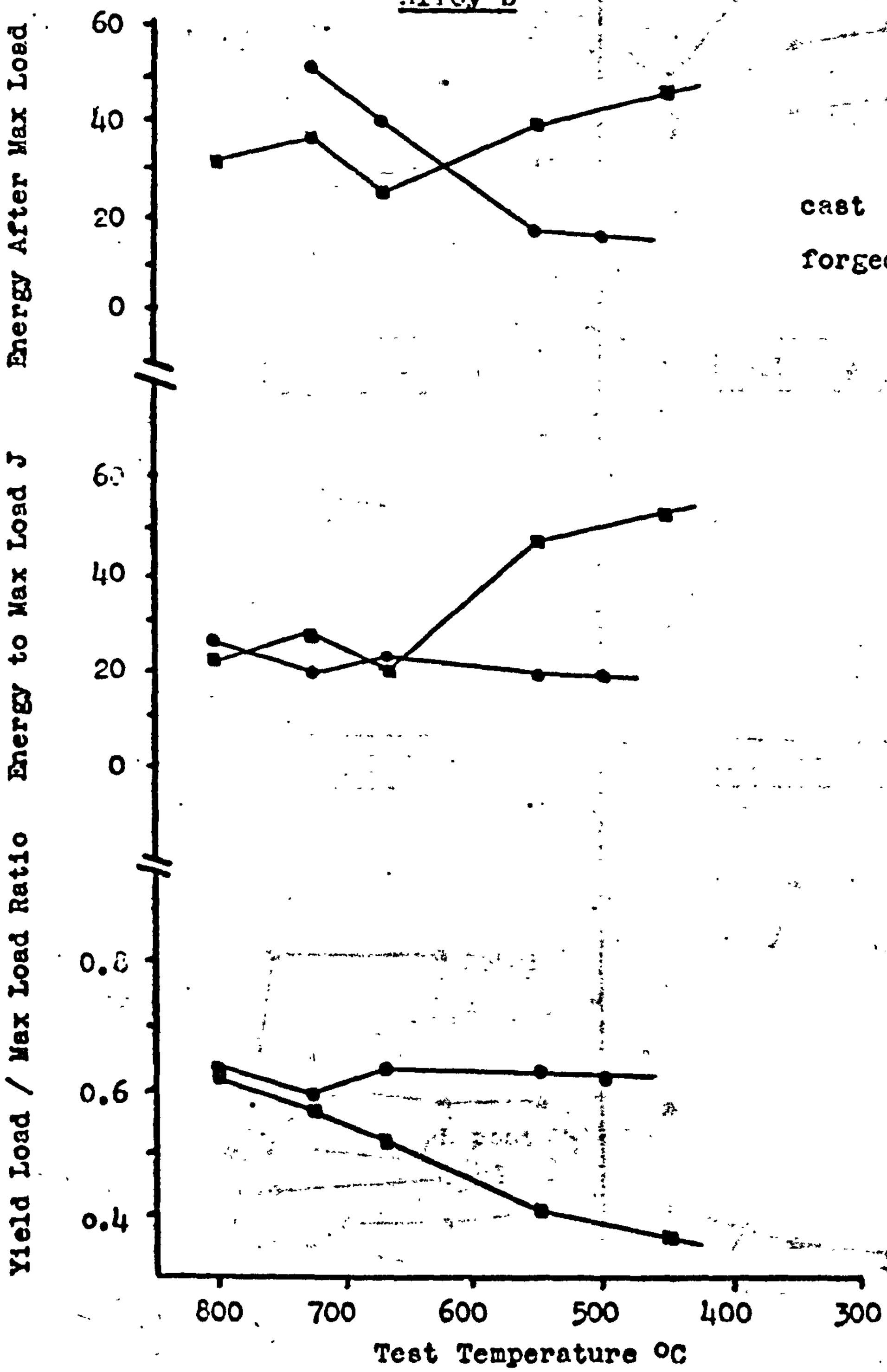

Fig 49 (cont). Effect of Test Temperature on Slow Bend Properties of Alloys Aged 50hrs/725°C Prior to Testing.

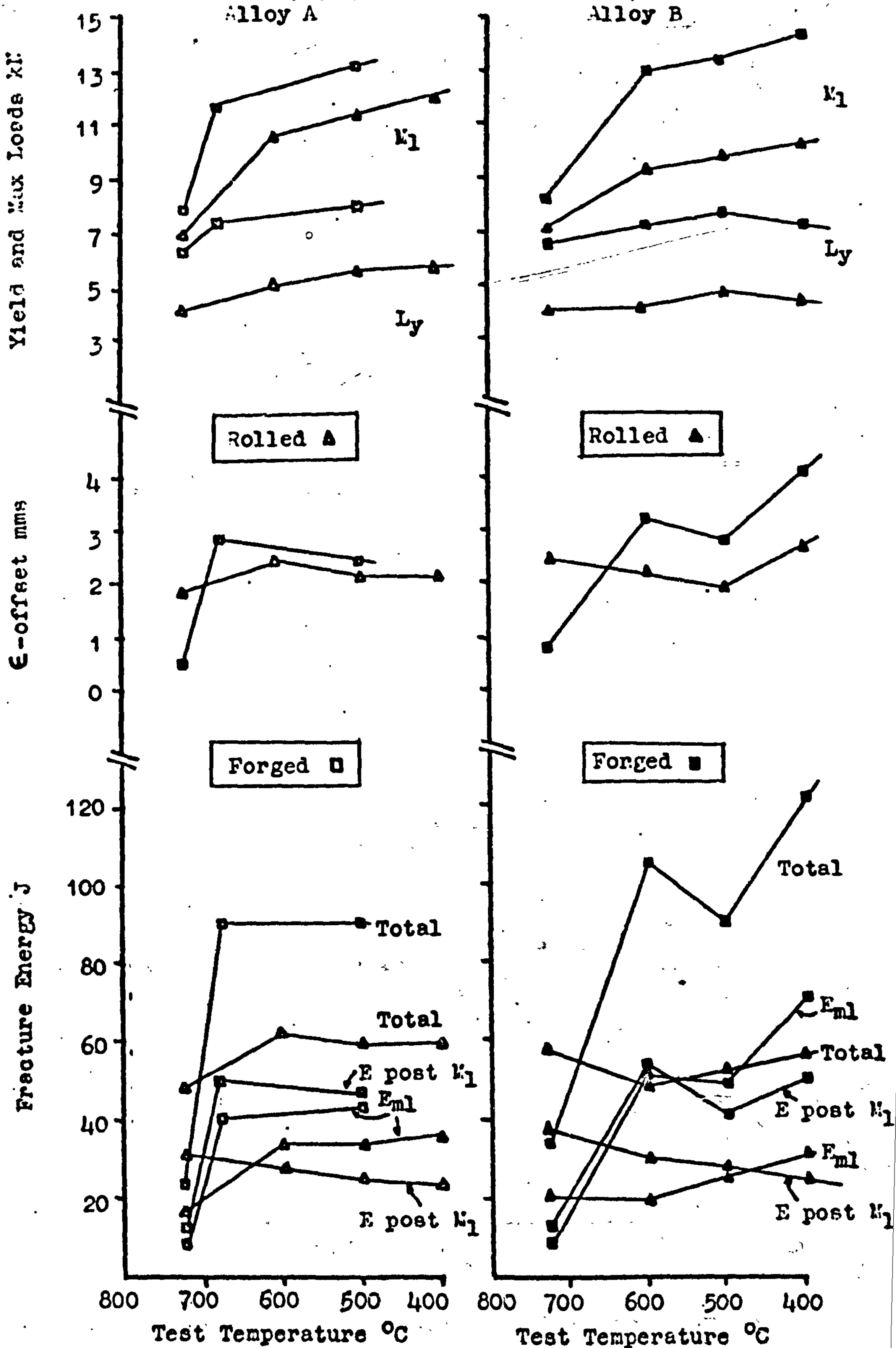

Fig 50. Effect of Test Temperature on Slow Bend Properties of As Rolled and As Forged Alloys.

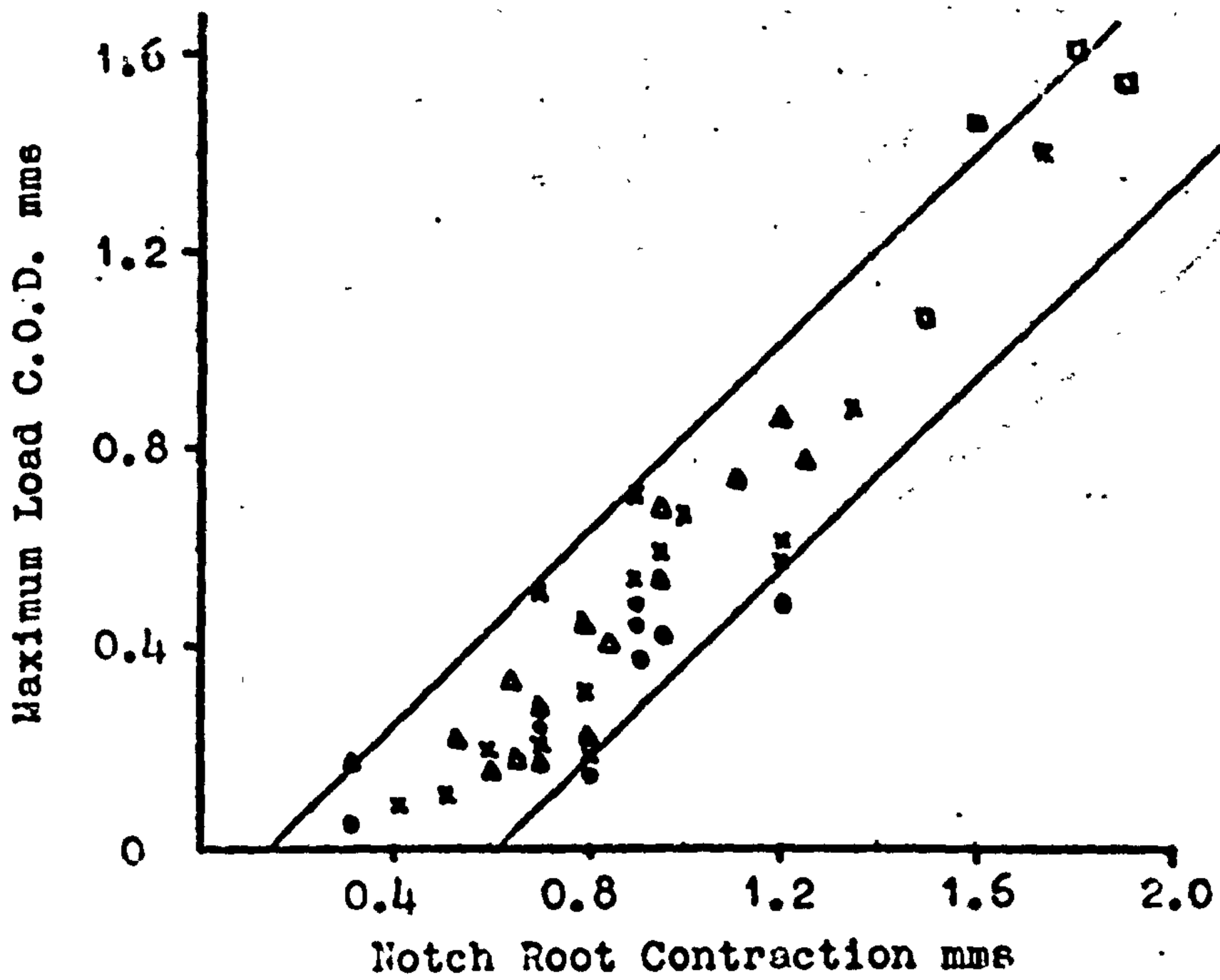

Fig 51. Correlation Between N.R.C. and Maximum Load C.O.D. (25°C)

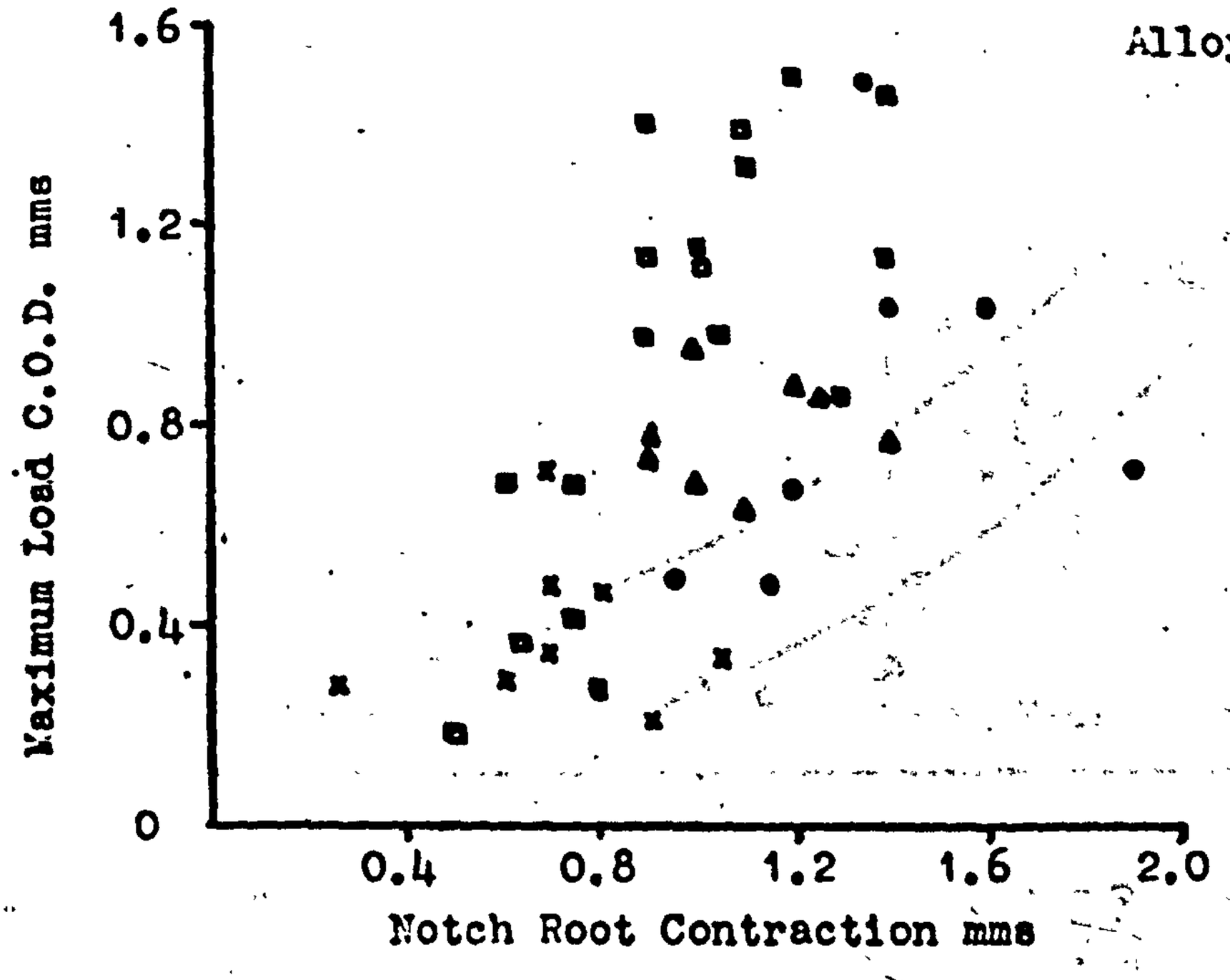

Fig 52. Correlation Between N.R.C. and Maximum Load C.O.D. in the Temperature Range 400-800°C.

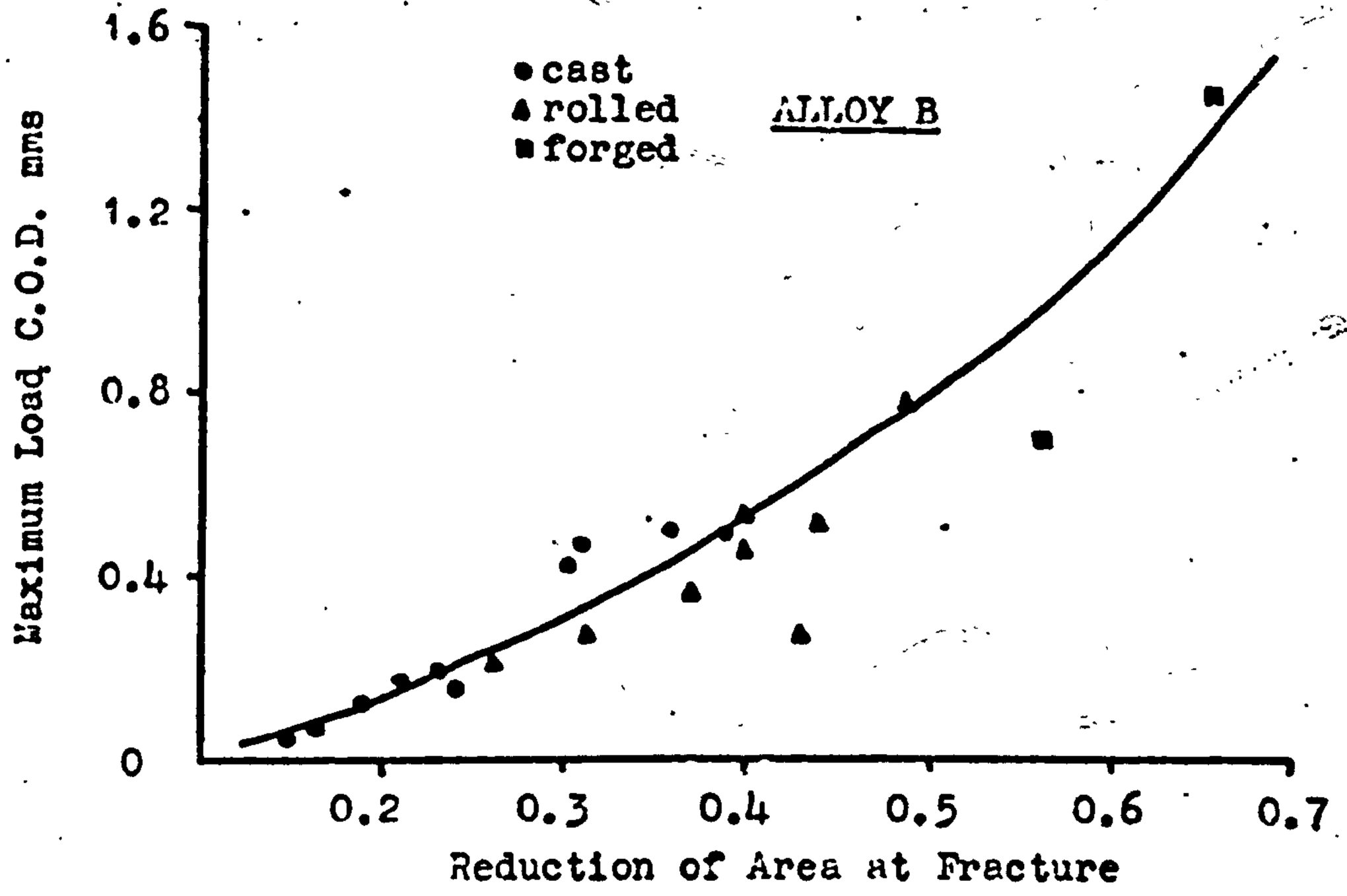

Fig 53. Correlation Between Maximum Load C.O.D. and Reduction of Area at Fracture.

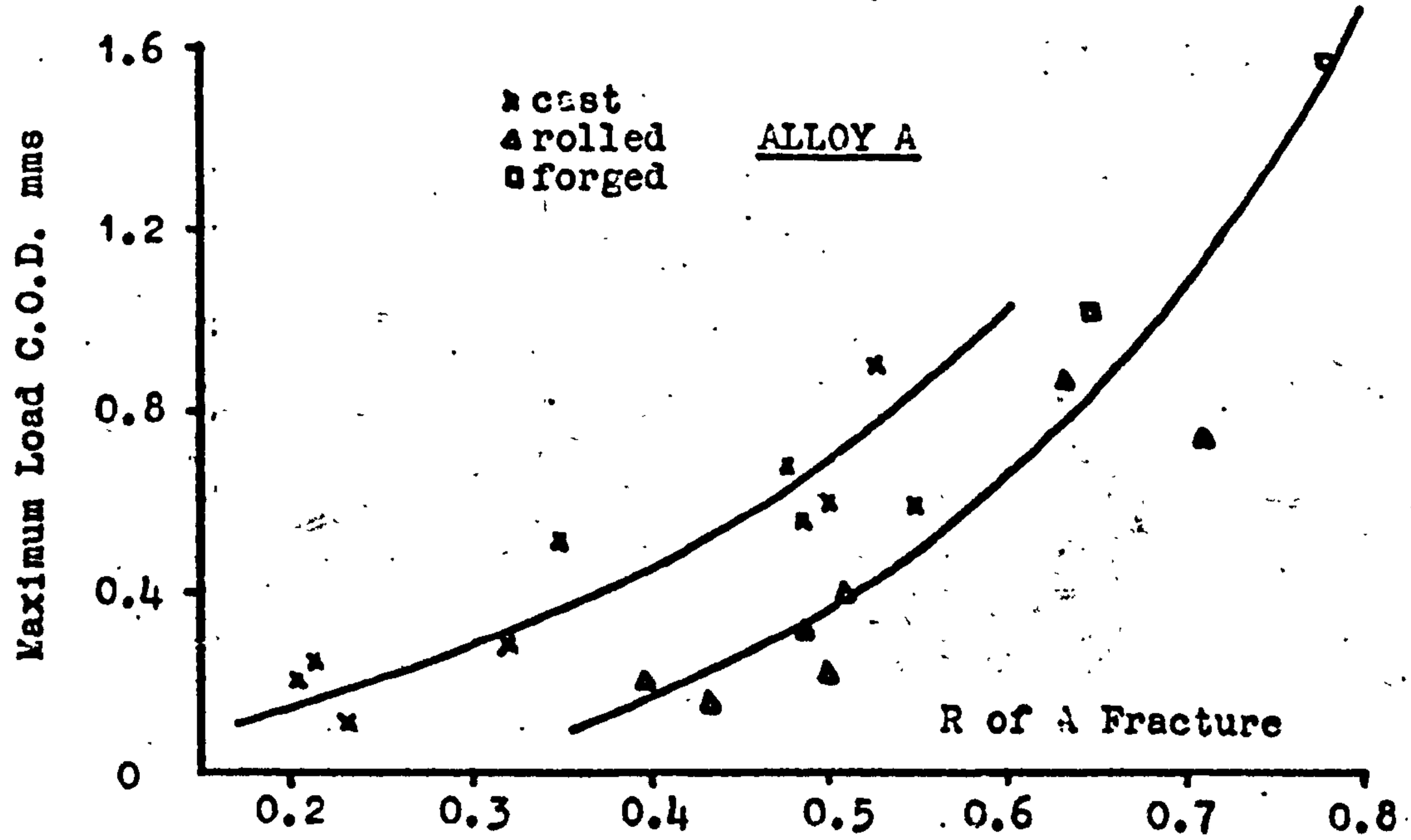

Fig 54. Correlation Between Maximum Load C.O.D. and Reduction of Area at Fracture.

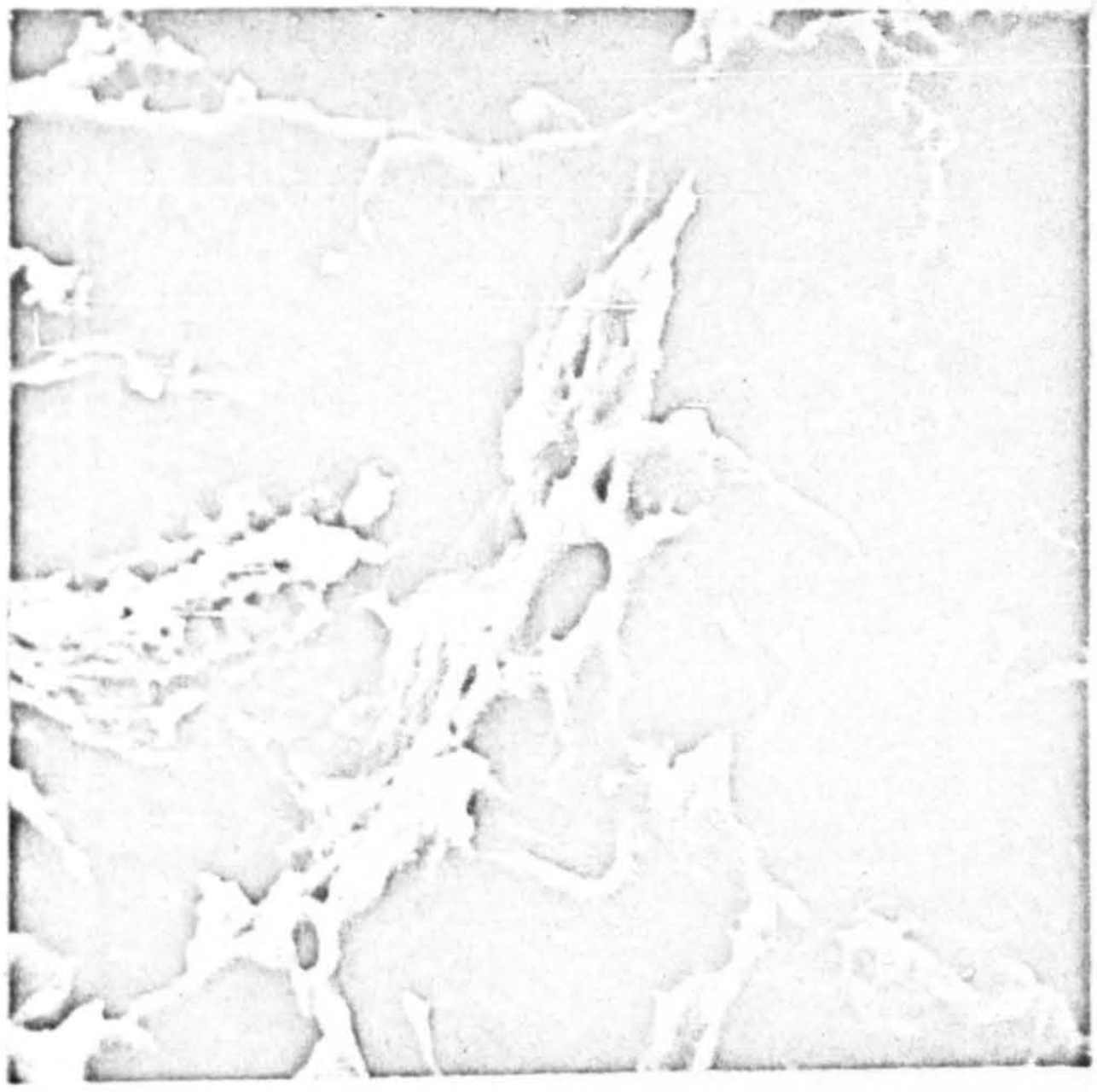

Fig.55. Alloy A As-Cast Fractured 25°C x2200

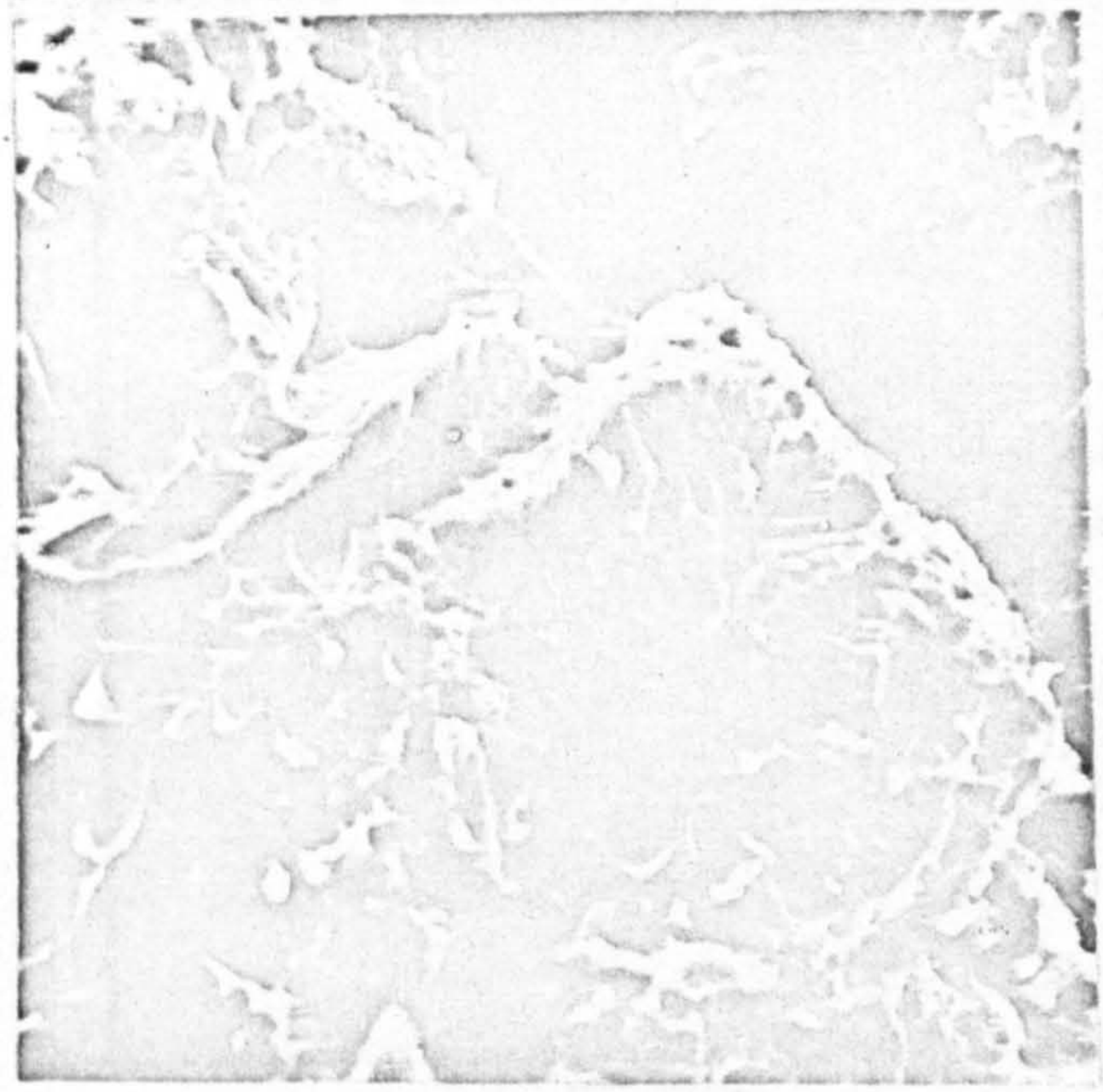

Fig.56. Alloy A As-Cast Fractured 25°C x1300

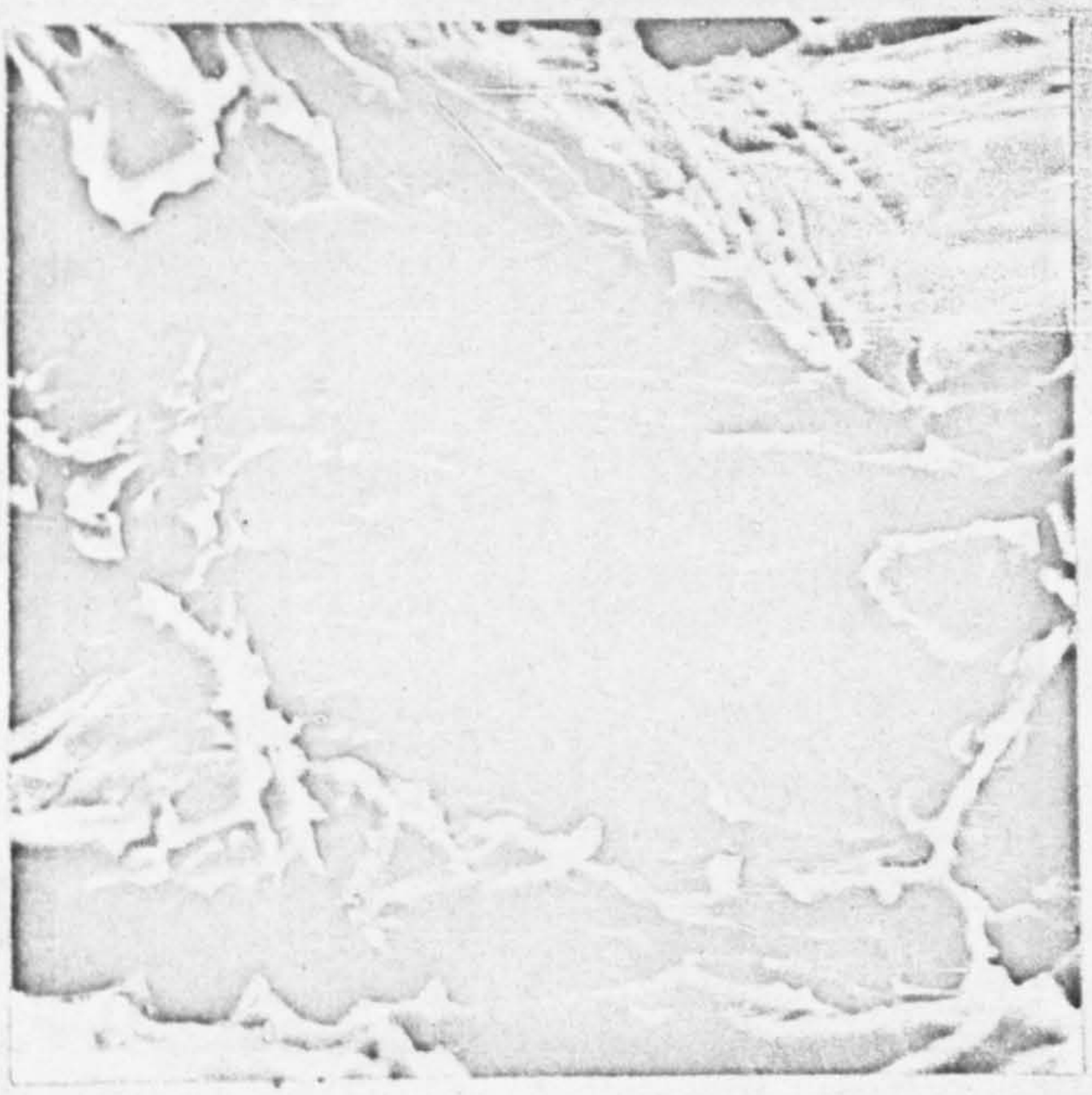

Fig.57. Alloy B As-Cast Fractured 25°C x1300

Fig.58. Alloy B As-Cast Fractured 25°C x2200

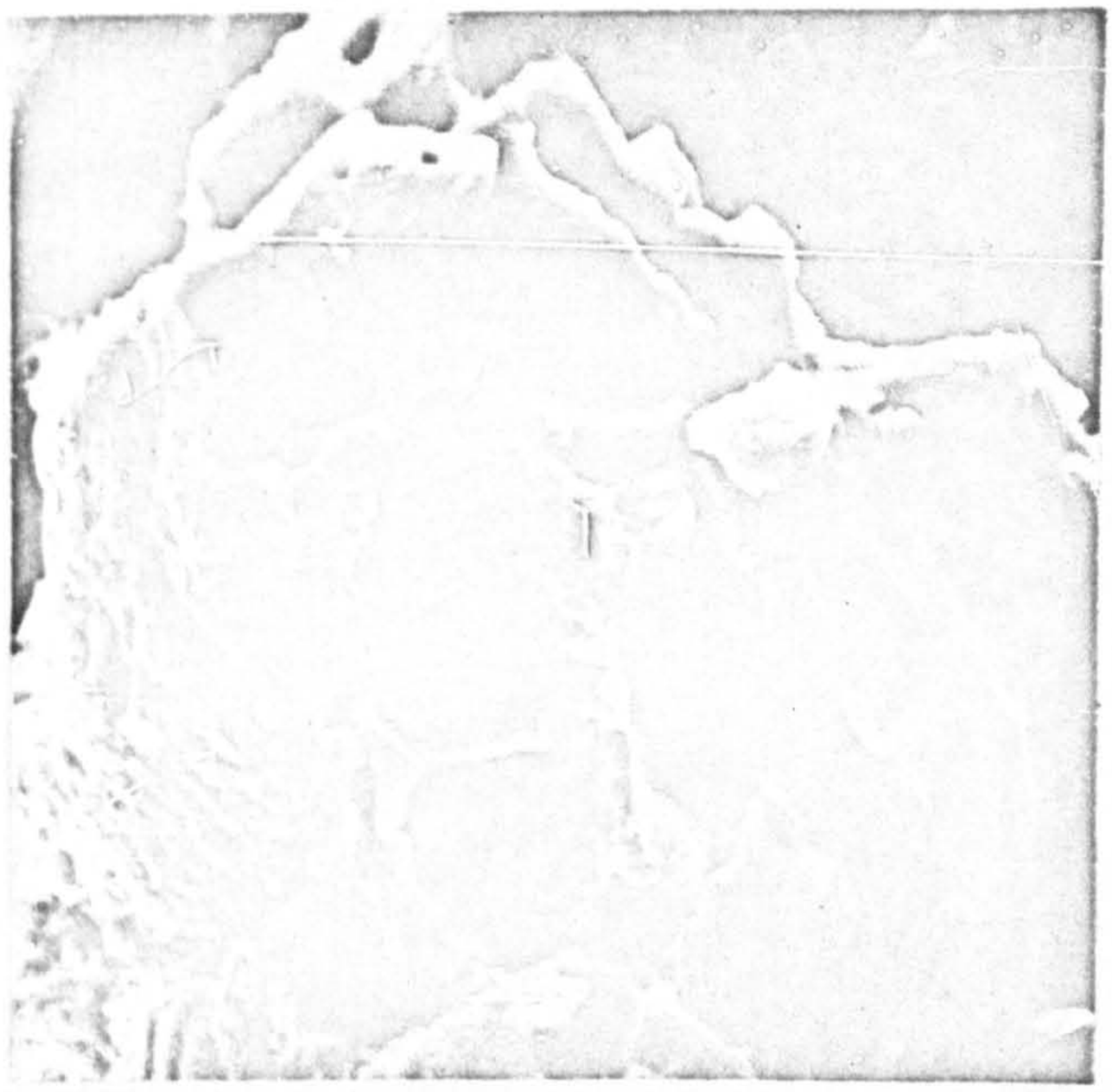

Fig.59. Alloy B As-Cast Fractured 25°C x2200

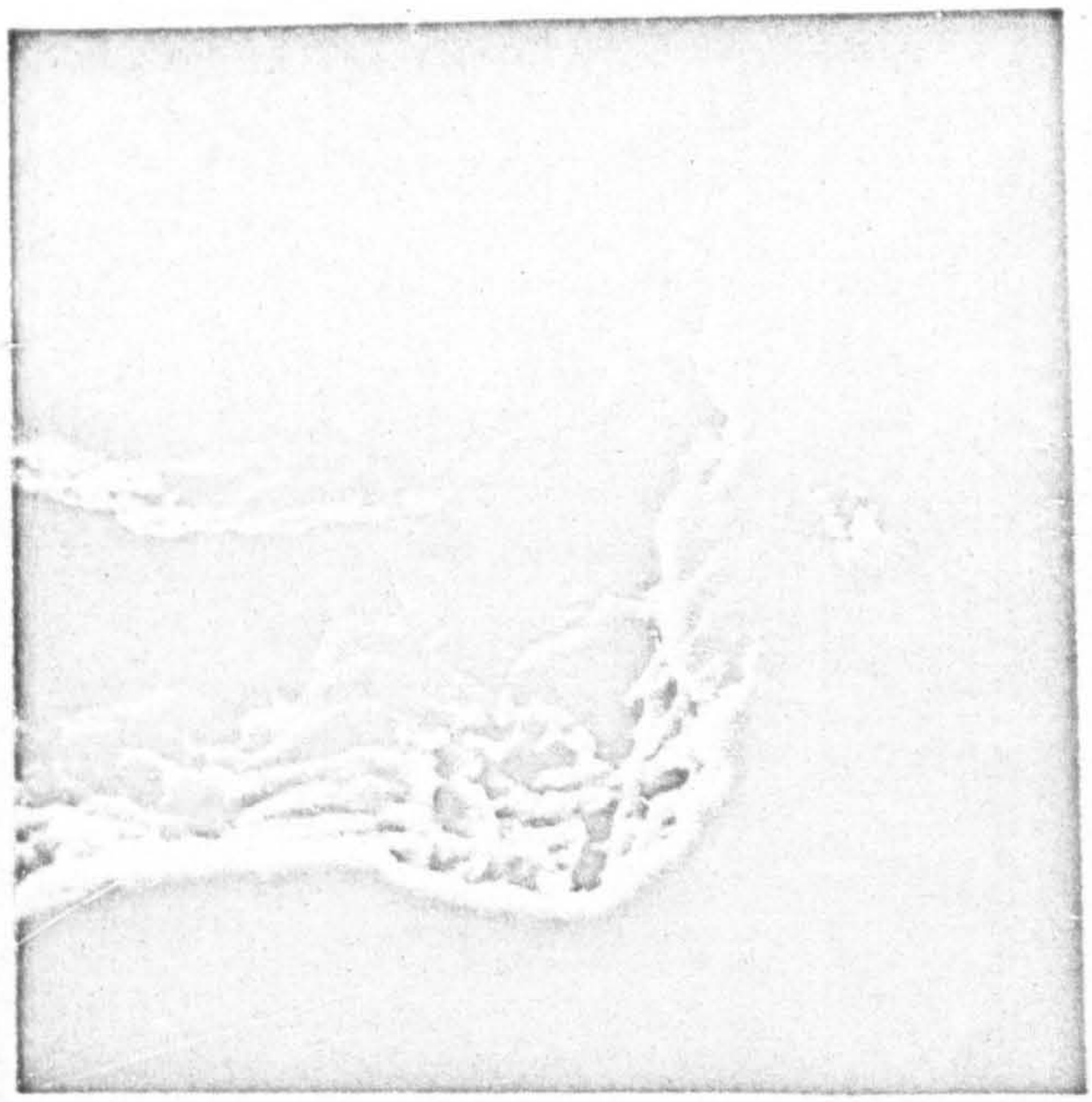

Fig.60. Alloy B As-Cast Fractured 25°C x1500

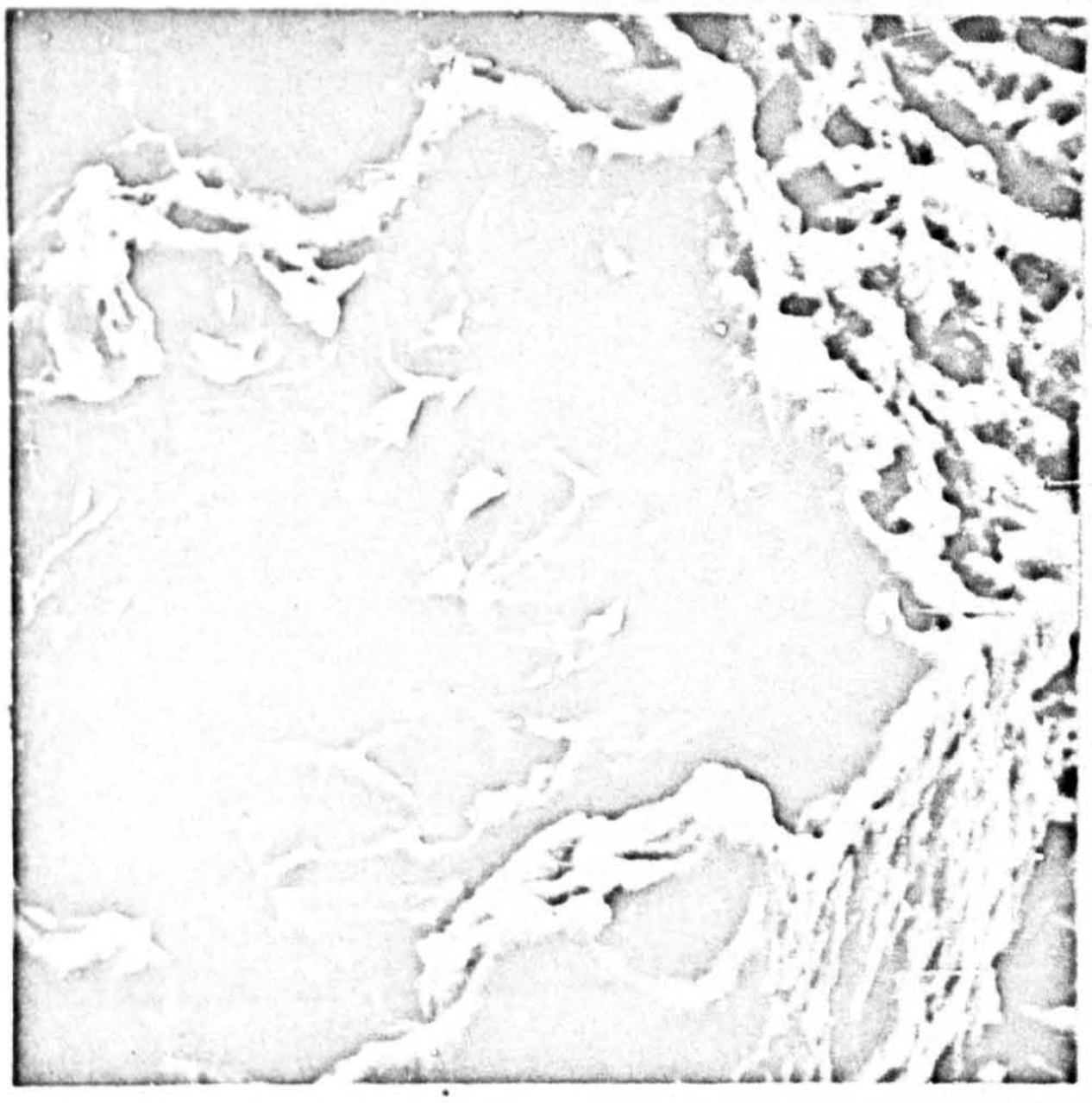

Fig.61. Alloy A Cast+250hrs./725°C Fractured 25°C x2100

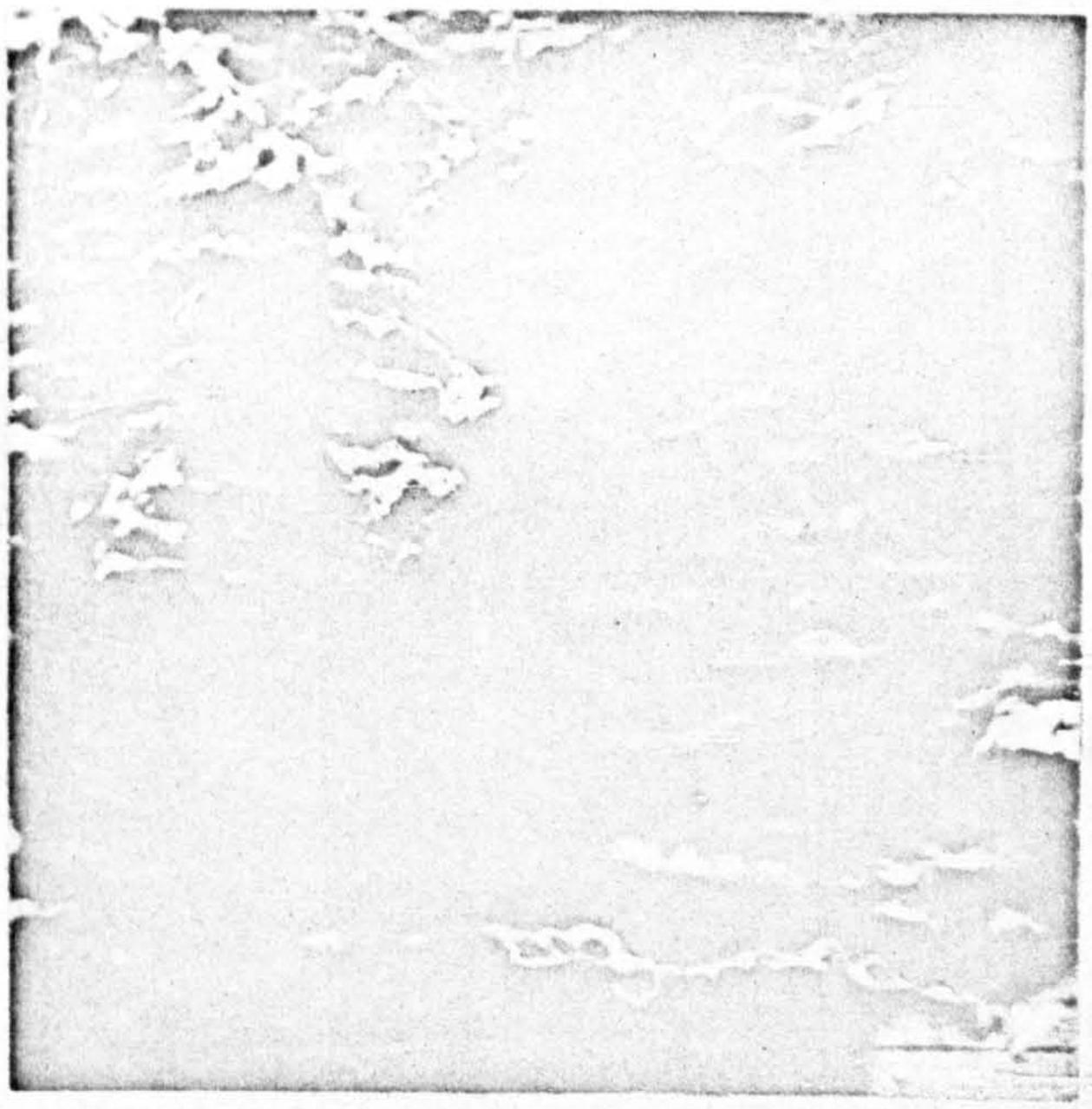

Fig.62. Alloy B Cast+250hrs./725°C Fractured 25°C x50

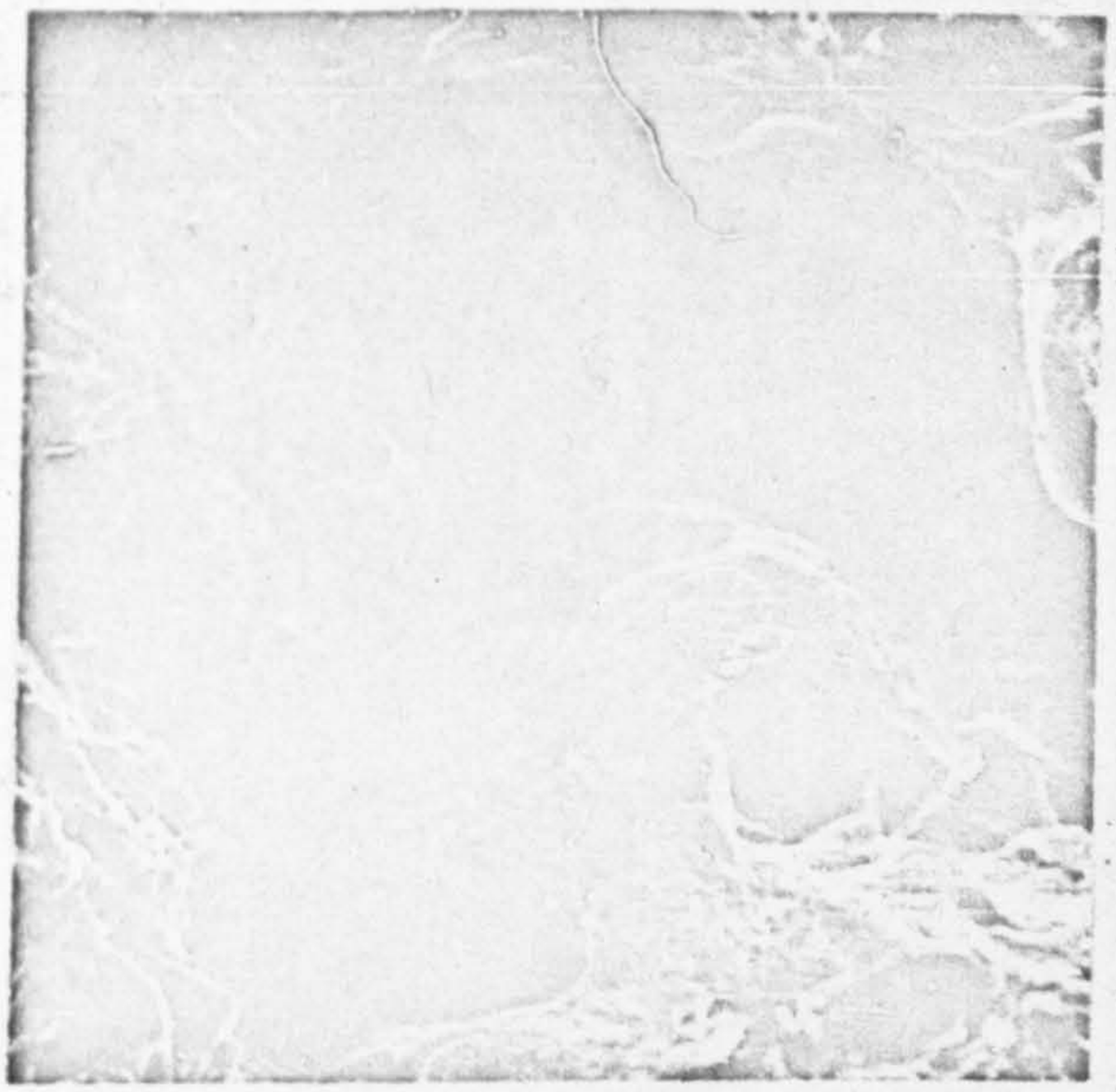

Fig.63. Alloy B Cast+250hrs./725°C Fractured 25°C x550

Fig.64. Alloy B Cast+250hrs./725°C Fractured 25°C x1100

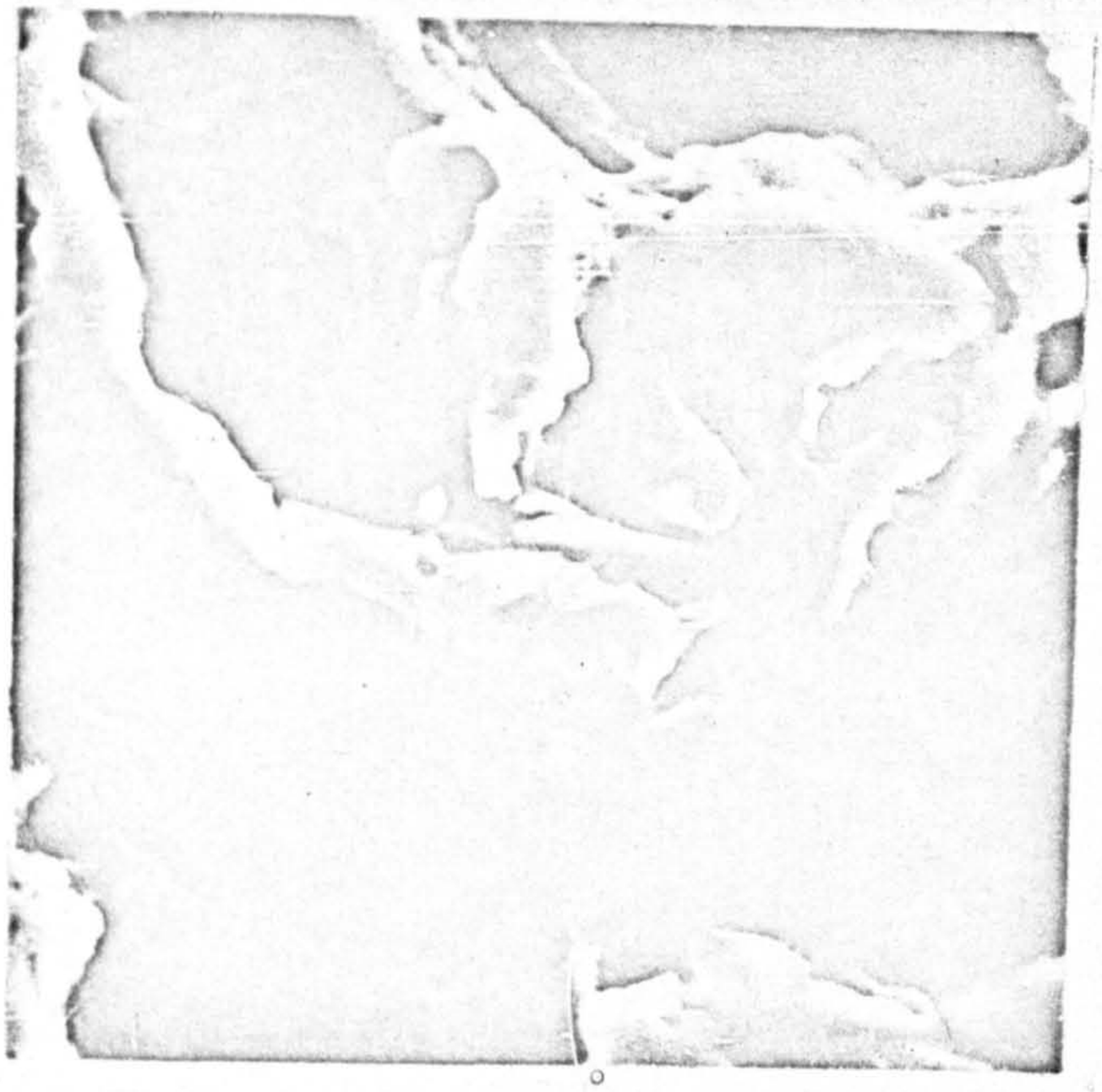

Fig.65. Alloy B Cast+250hrs./725°C Fractured 25°C x2700

Fig.66. Alloy B As-Rolled Fractured 25°C x2000

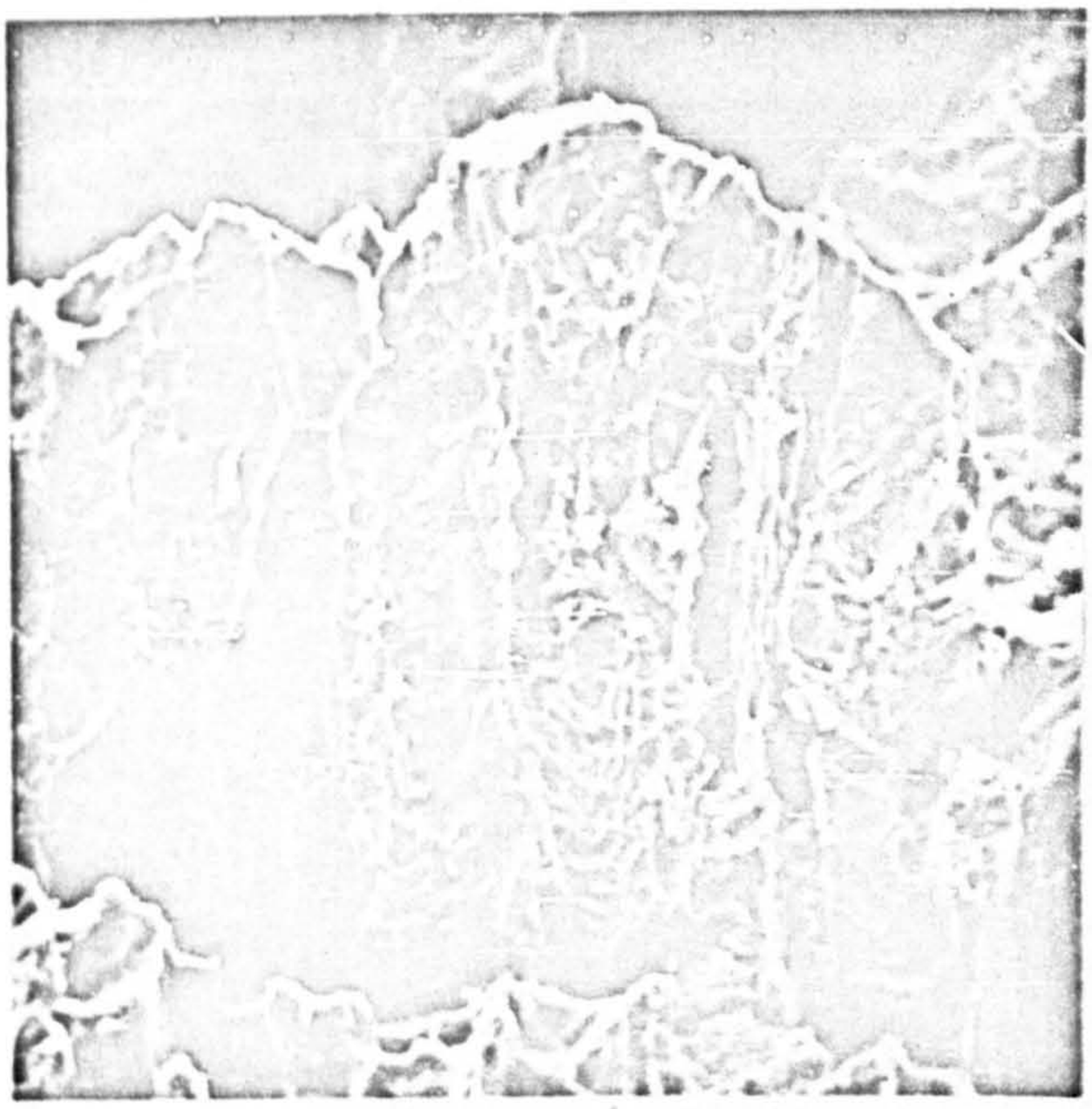

Fig.67. Alloy B As-Rolled Fractured 25°C x530

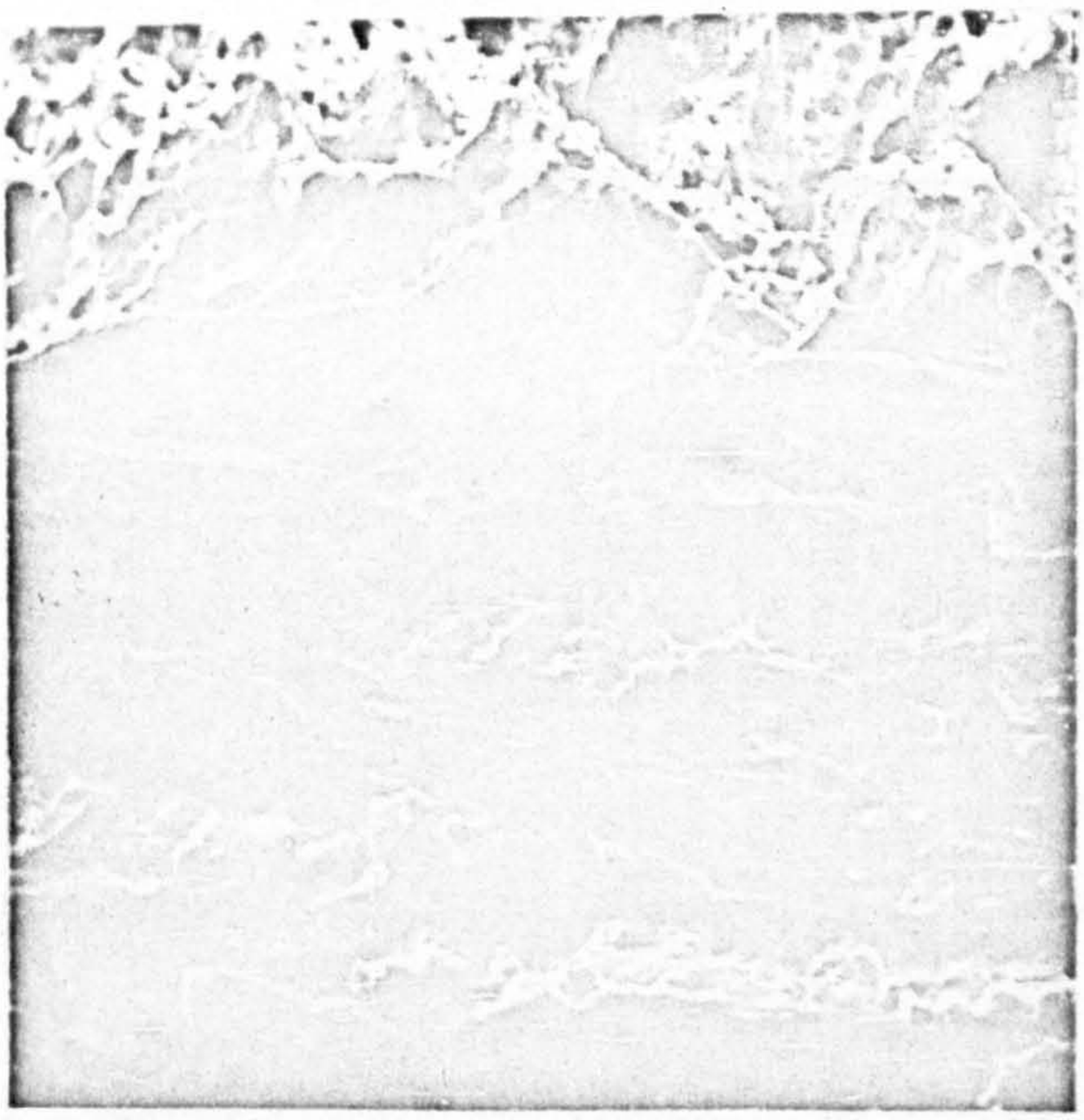

Fig.68. Alloy A Rolled+50hrs./725°C Fractured 25°C x250

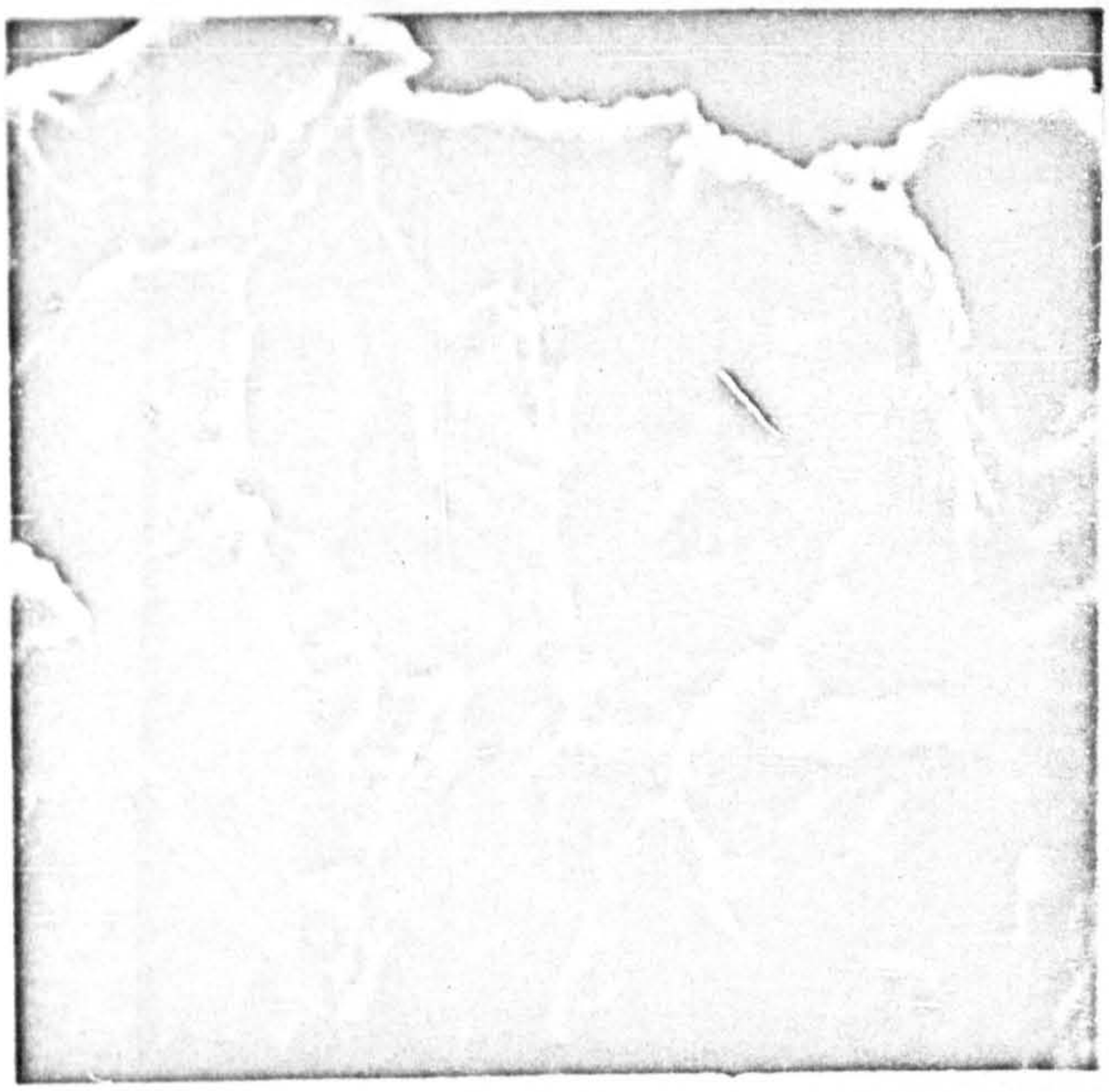

Alloy B

Fig.69. Rolled+1000hrs./725°C Fractured 25°C x2100

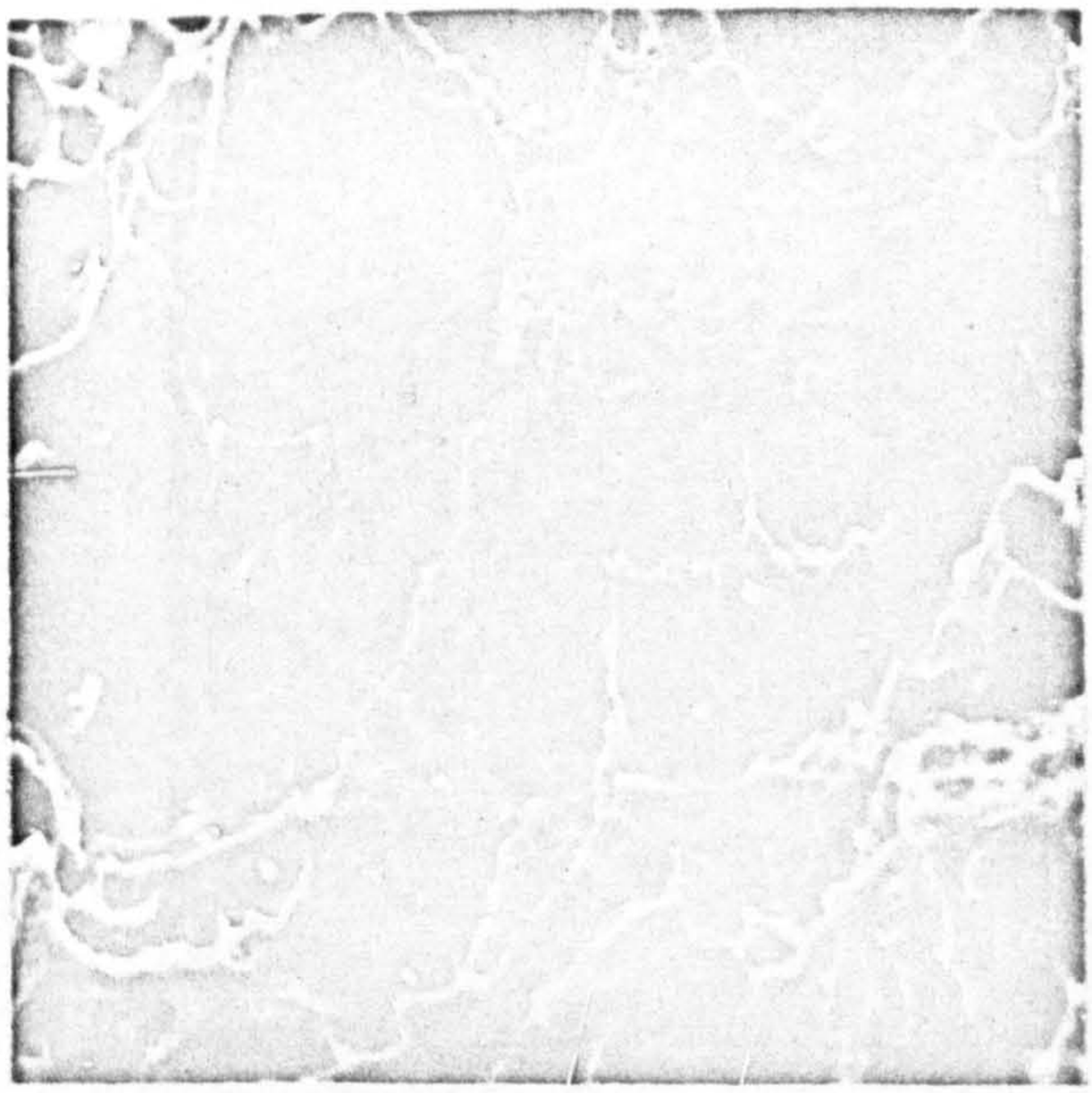

Fig.70. Alloy A As-Forged Fractured 25°C x675

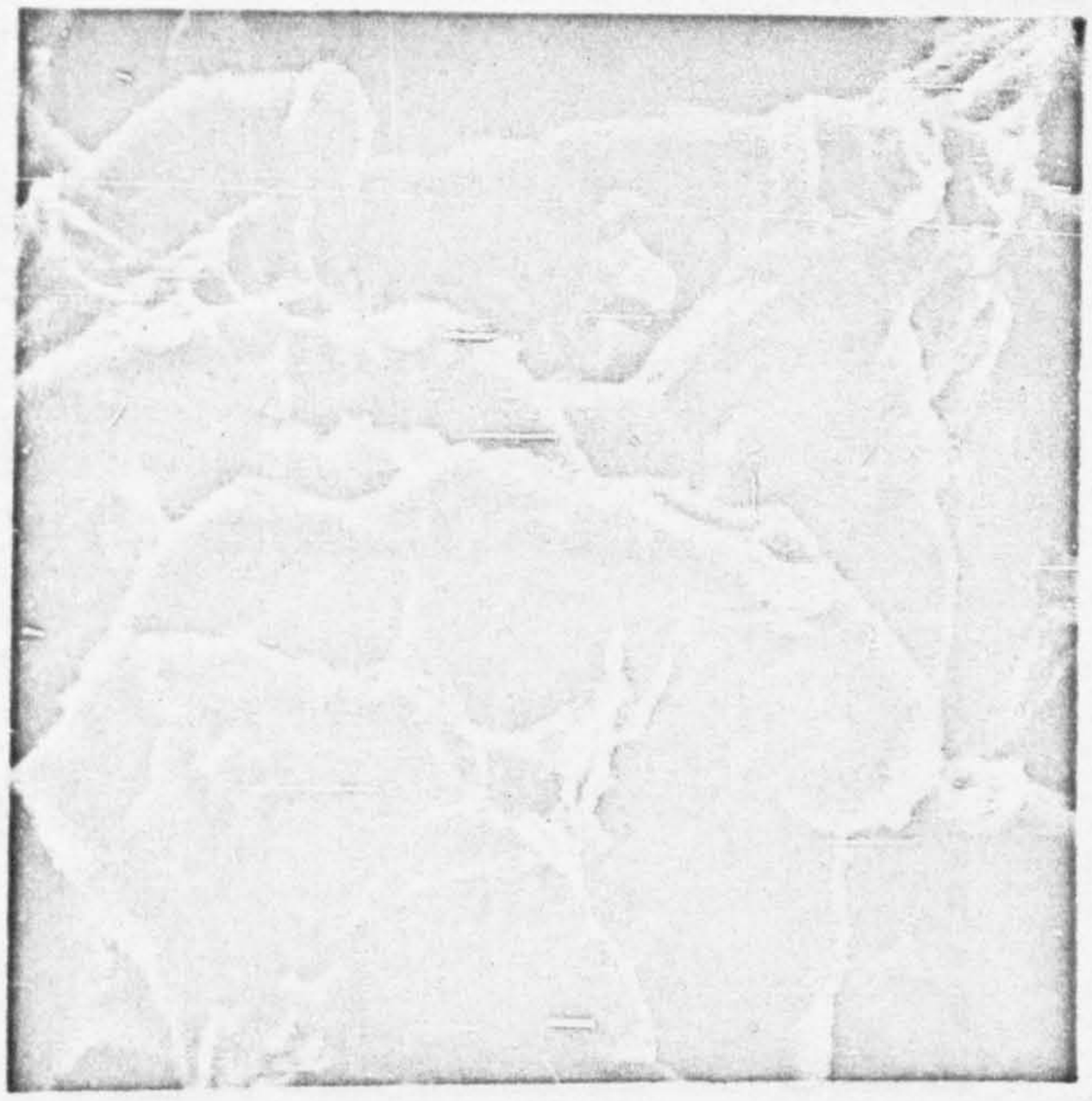

Fig.71. Alloy B As-Forged Fractured 25°C x2200

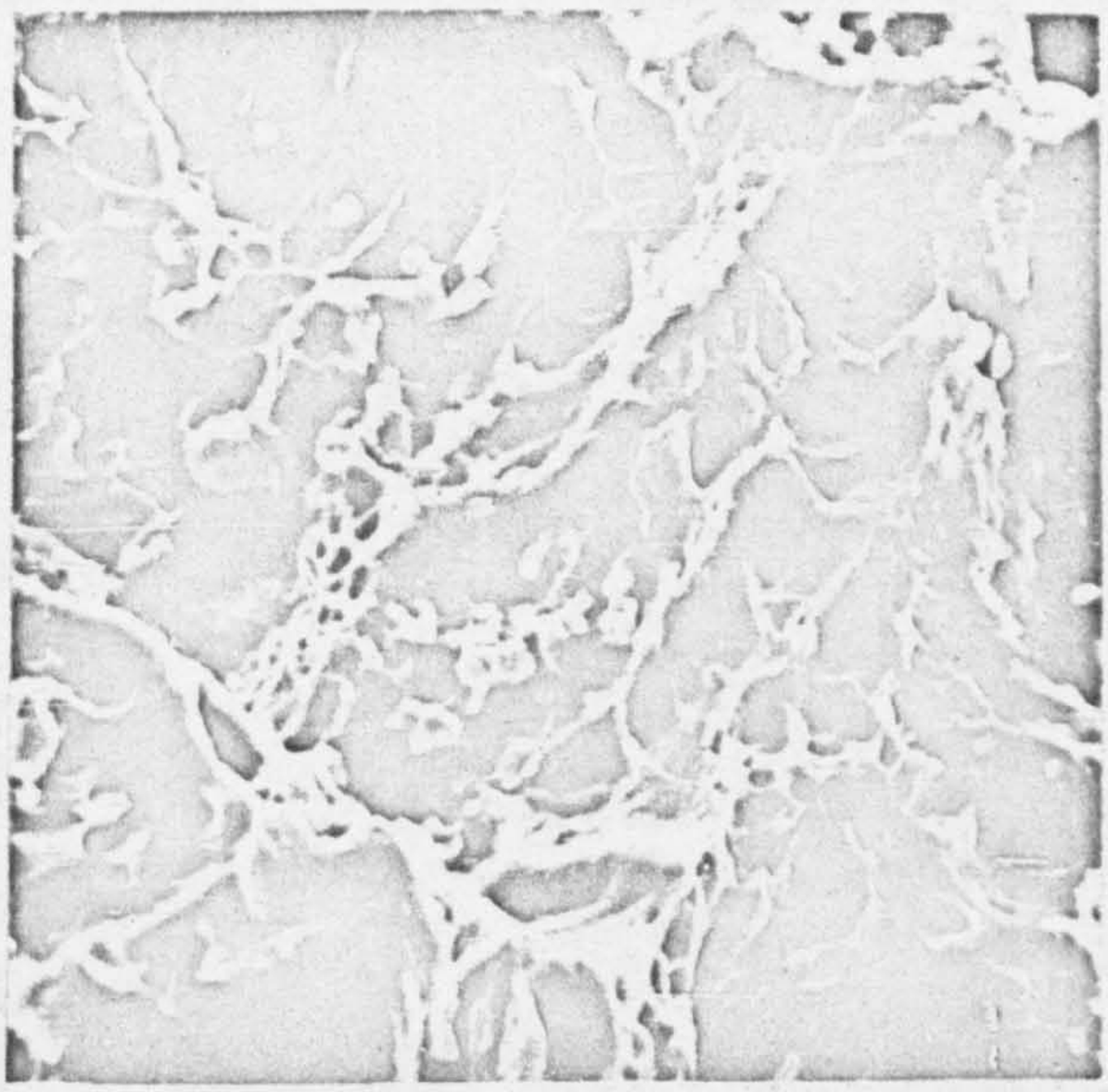

Fig.72. Alloy A Forged+2000hrs./725°C Fractured 25°C x2500

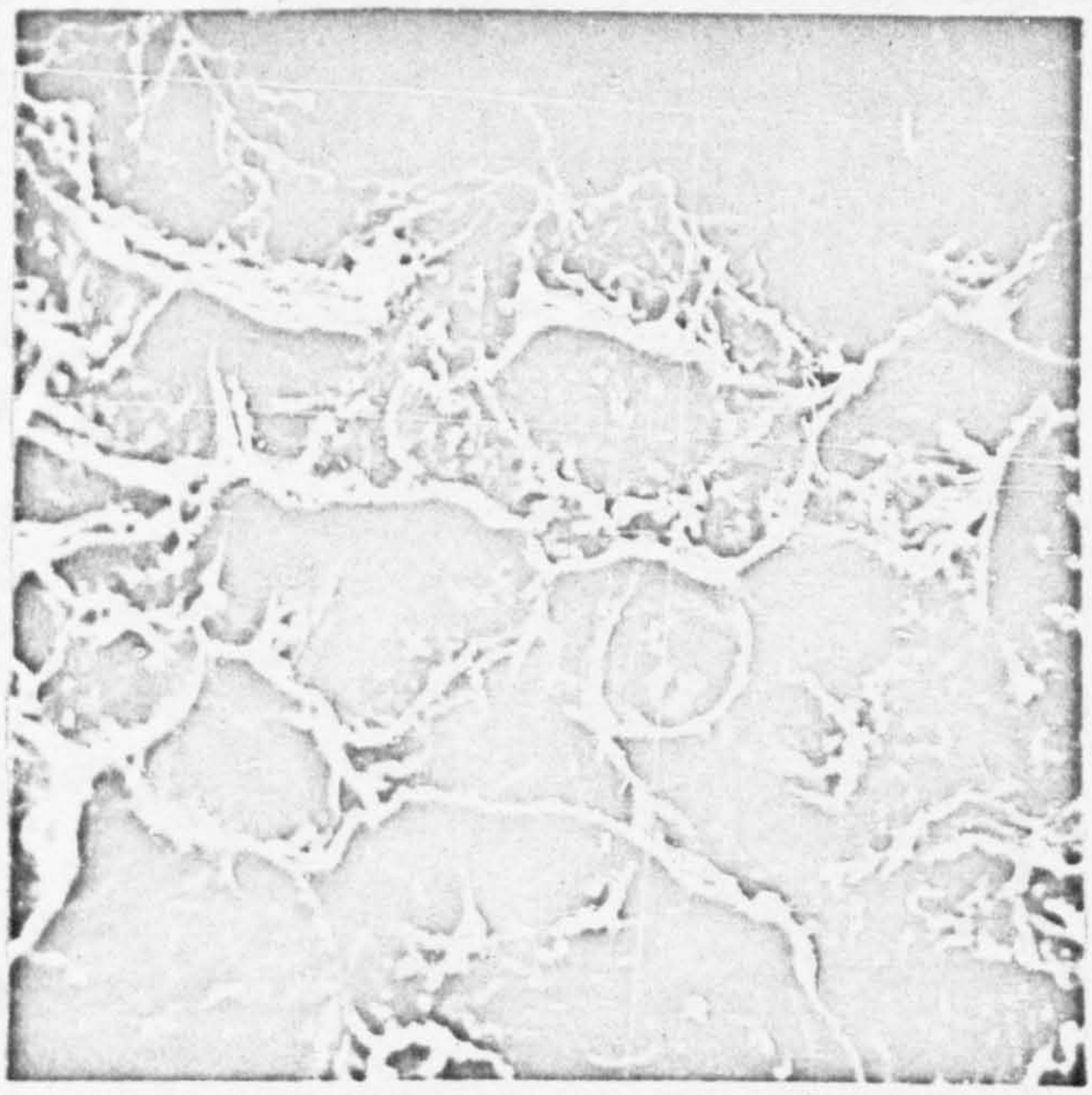

Fig.73. Alloy A As-Cast Fractured 725°C in Impact x600

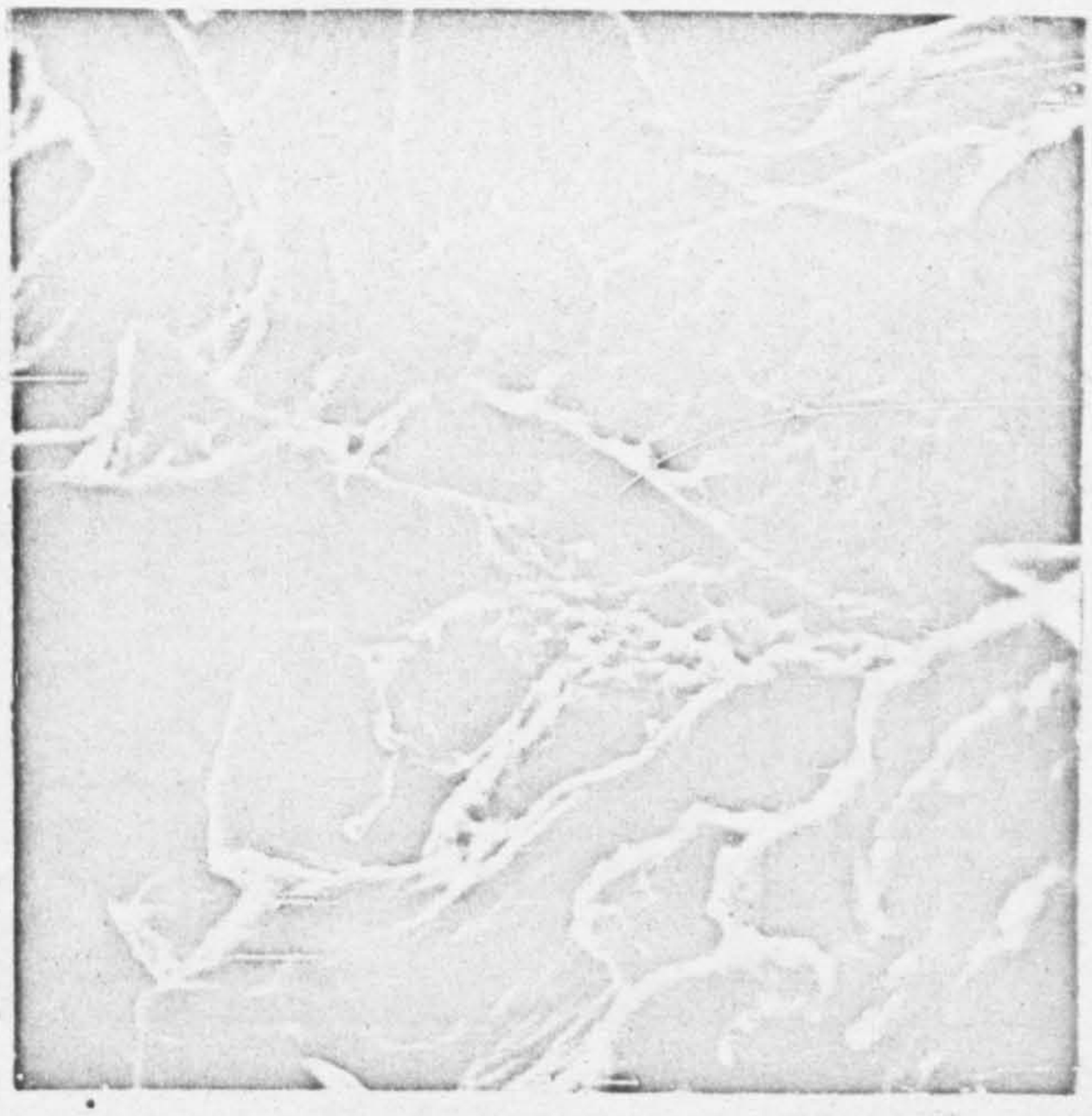

Fig.74. Alloy B As-Cast Fractured 725°C in Impact x1250

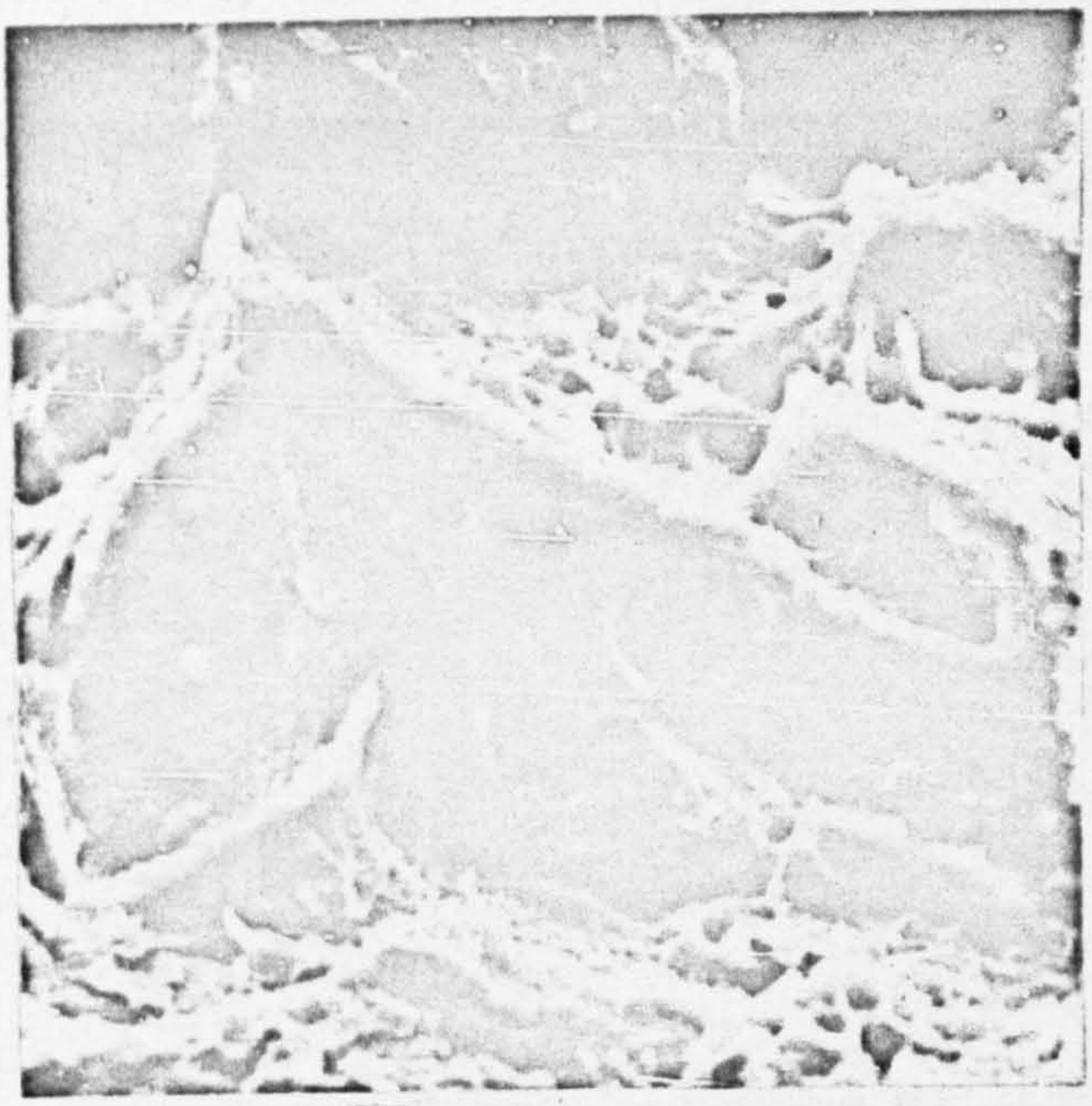

Alloy A
Fig.75. As-Cast Fractured 725°C in Slow Bend x1300

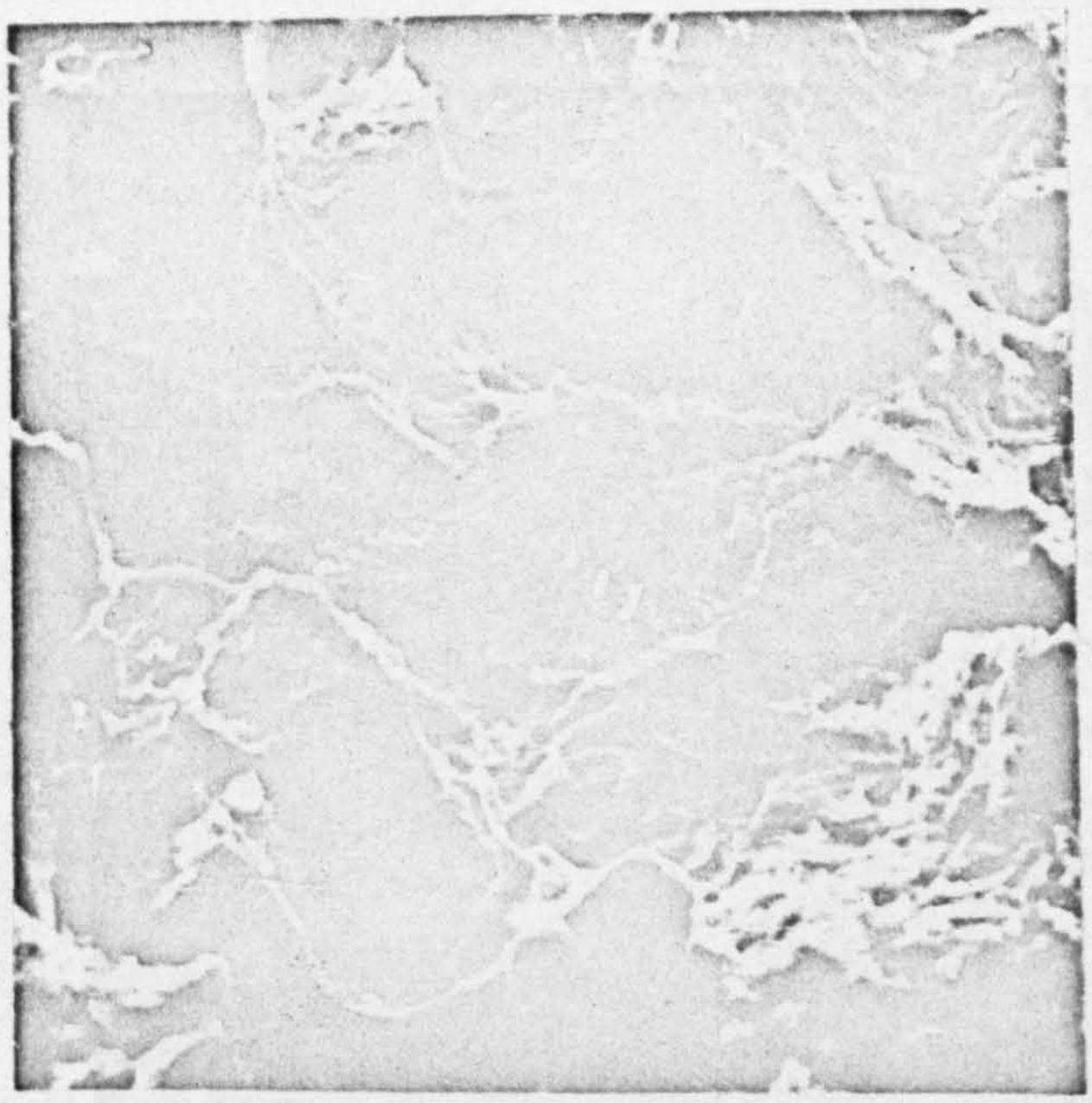

Alloy A
Fig. As-Cast Fractured 725°C in Slow Bend x650

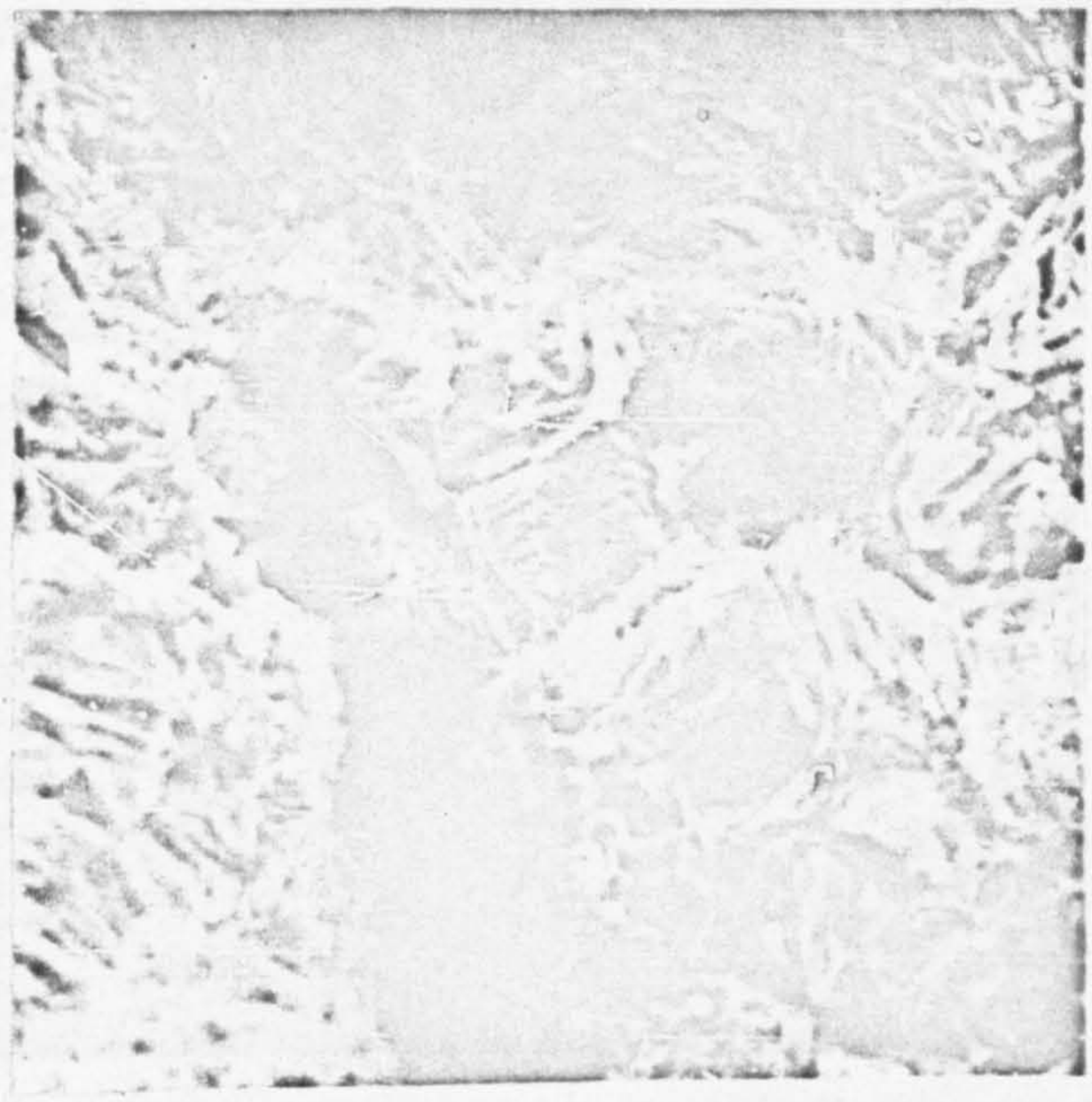

Alloy B
Fig.77. As-Cast Fractured 725°C in Slow Bend x650

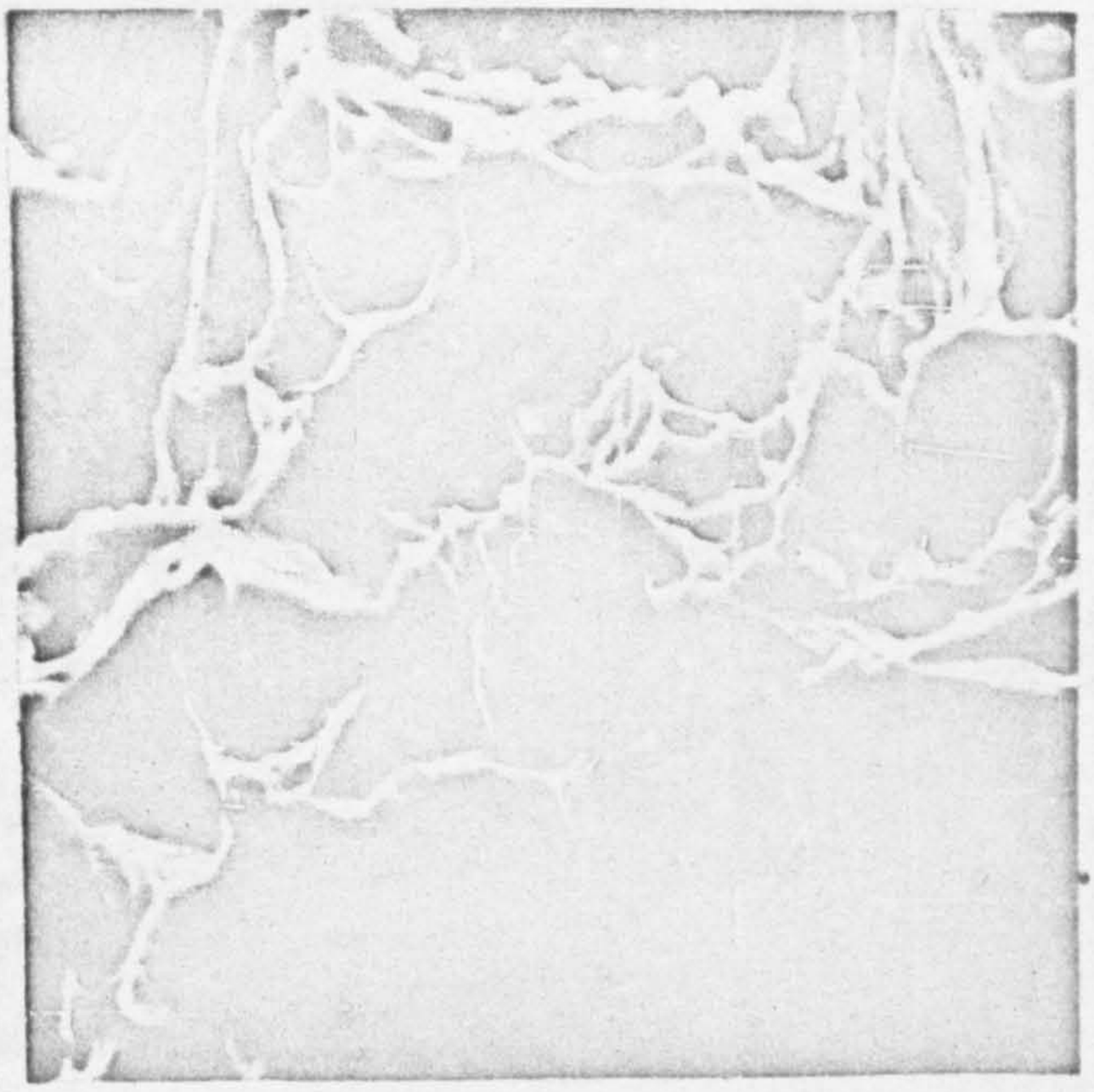

Alloy A
Fig.78. As-Forged Fractured 725°C in Impact x1300

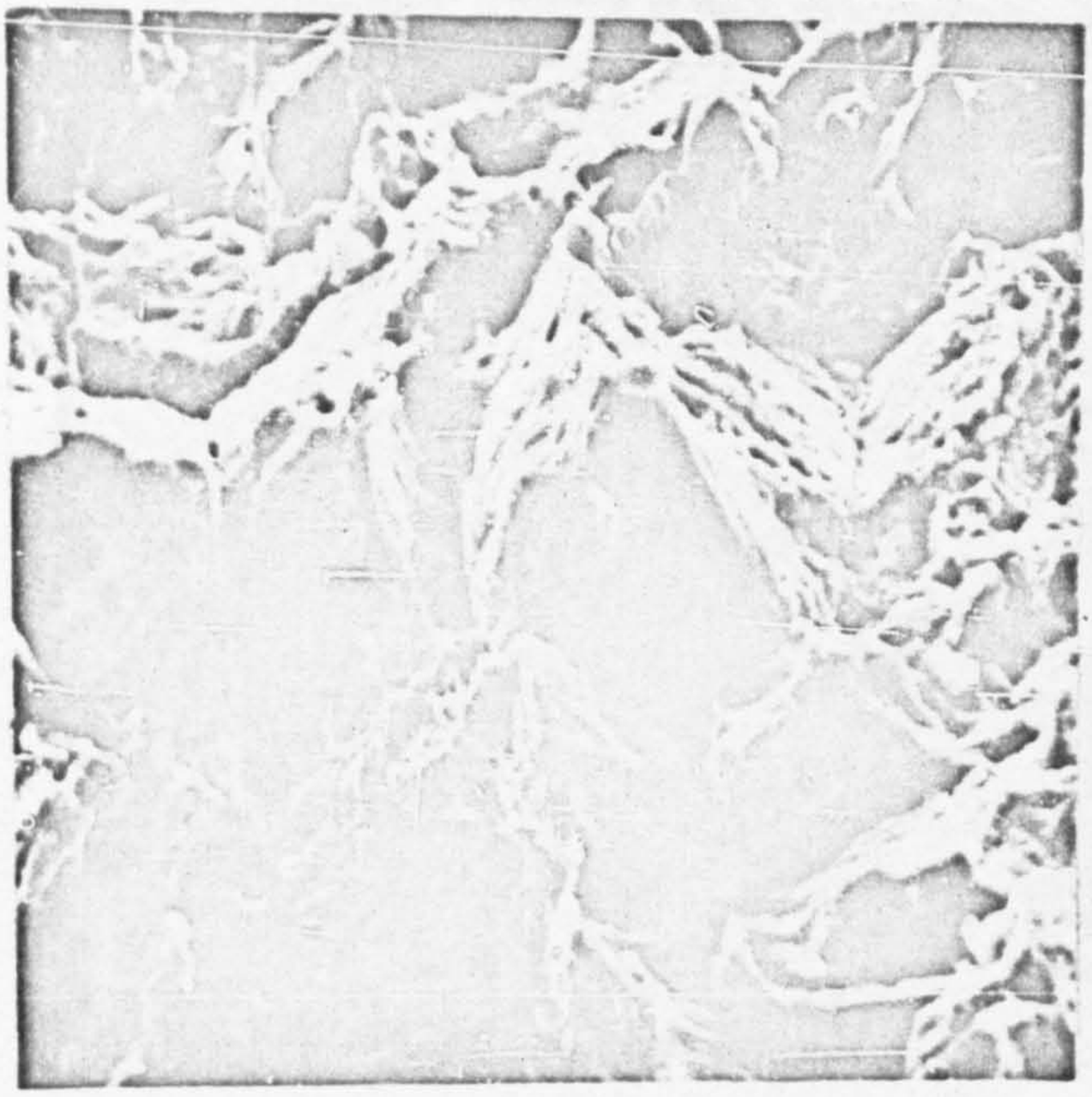

Alloy A
Fig.79. As-Forged Fractured 725°C in Slow Bend x625

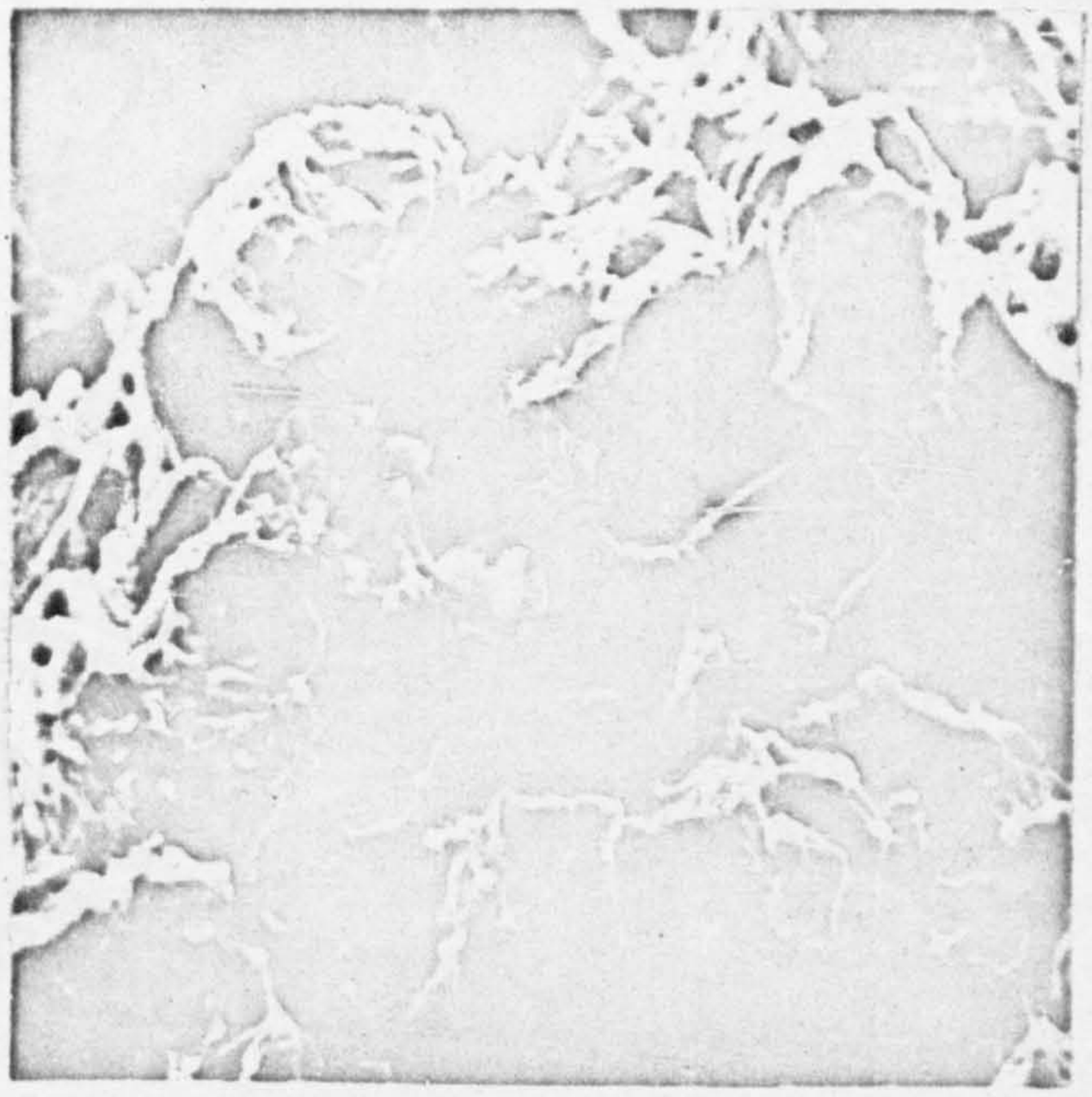

Alloy A
Fig.80. As-Forged Fractured 725°C in Slow Bend x625

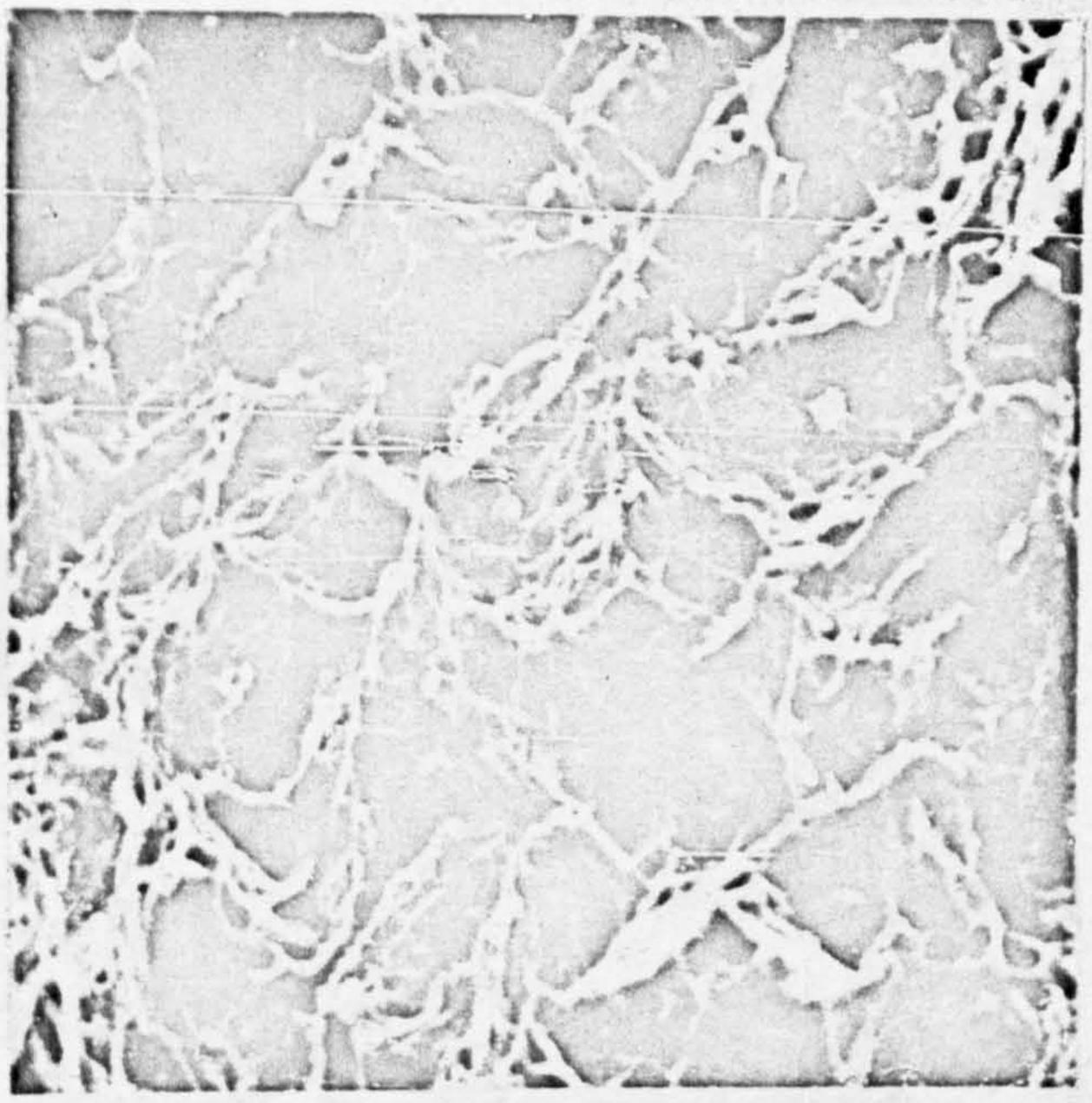

Alloy B
Fig.81. As-Forged Fractured 725°C in Slow Bend x650

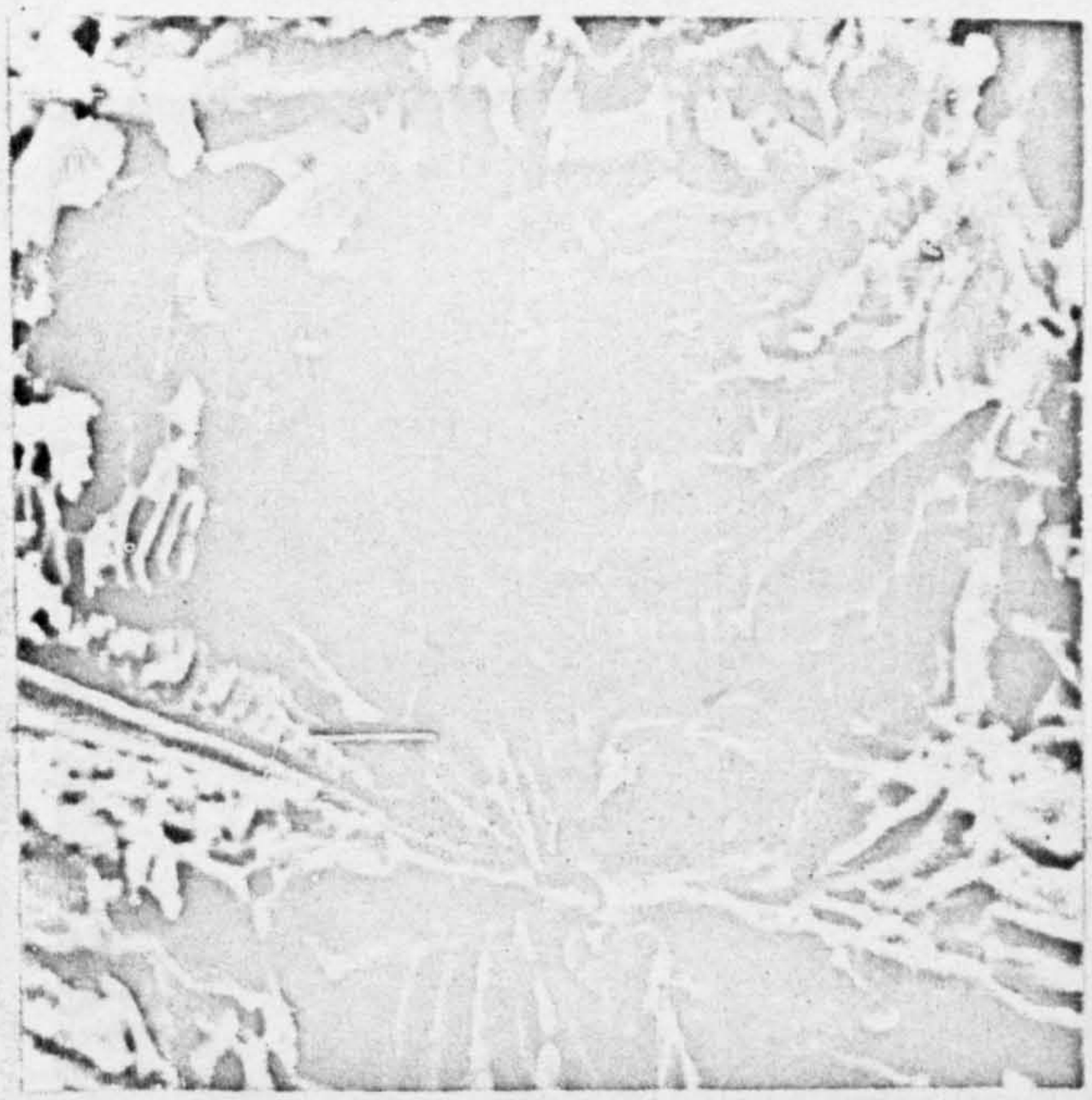

Alloy B Cast+50hrs./725°C
Fig.82. Fractured 725°C in Slow Bend x700

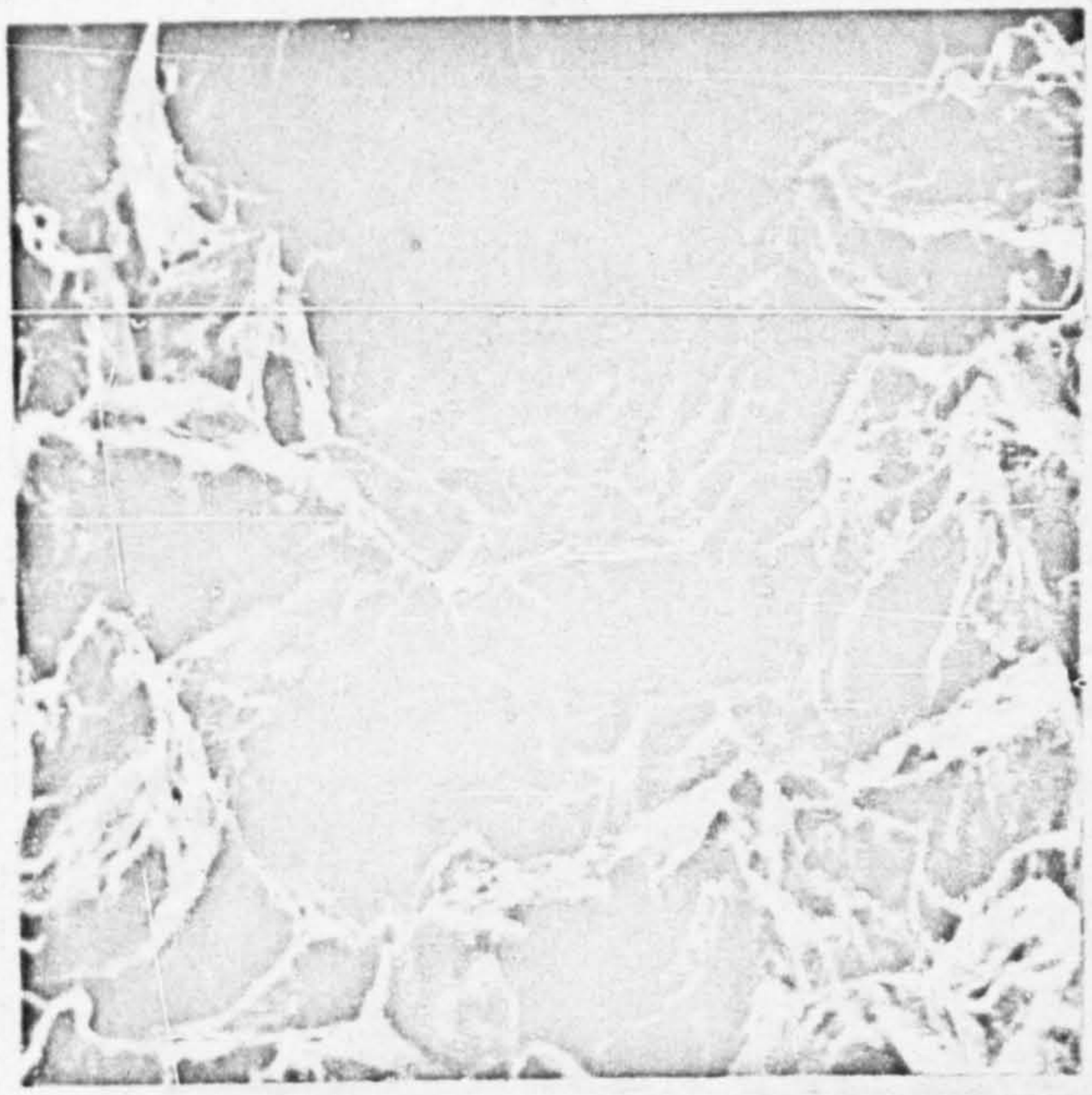

Fig.83. Alloy A Forged+50hrs./725°C
Fractured 725°C in Slow Bend x600

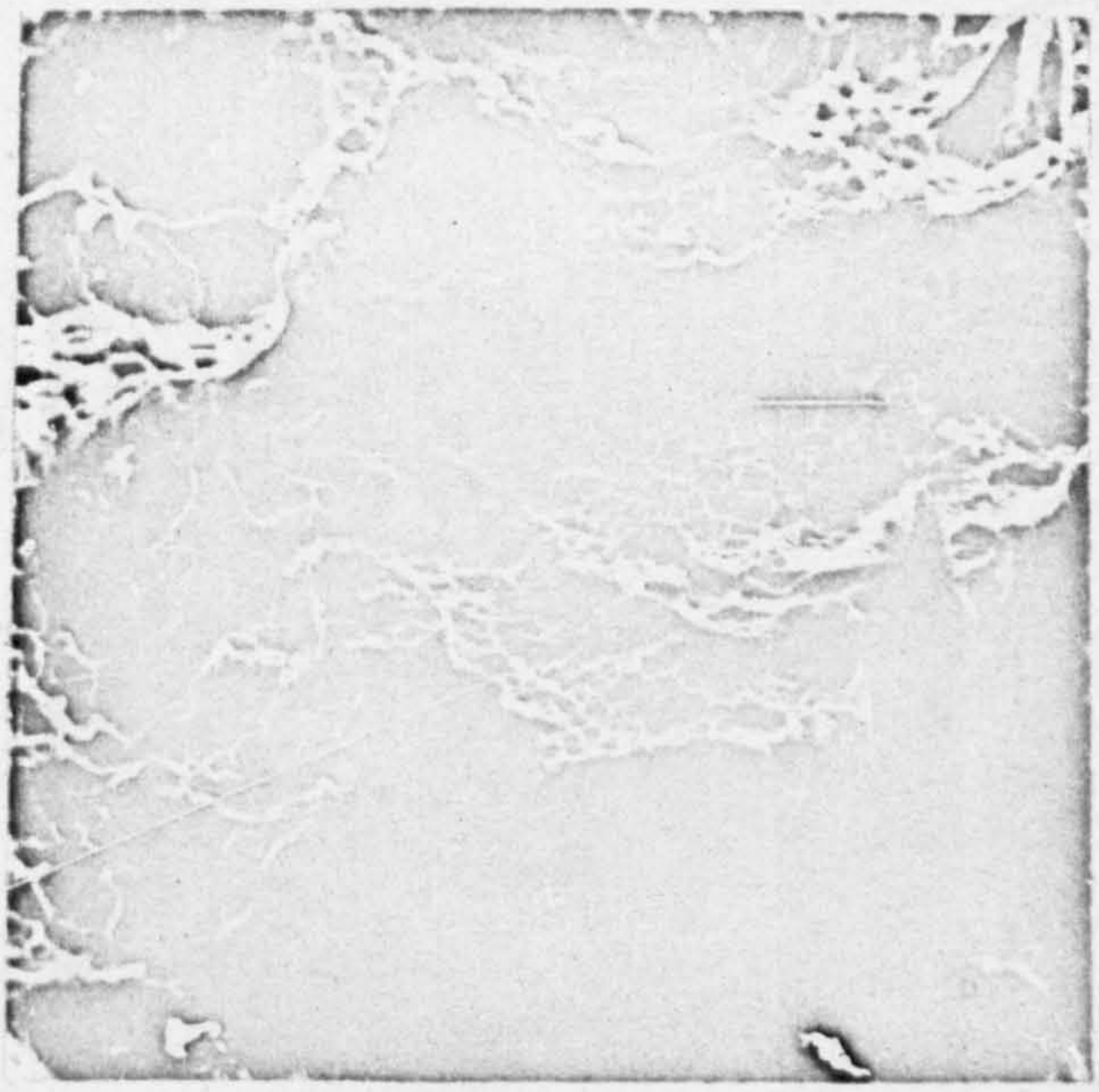

Fig.84. Alloy A Cast+50hrs./725°C
Fractured 725°C in Slow Bend x575

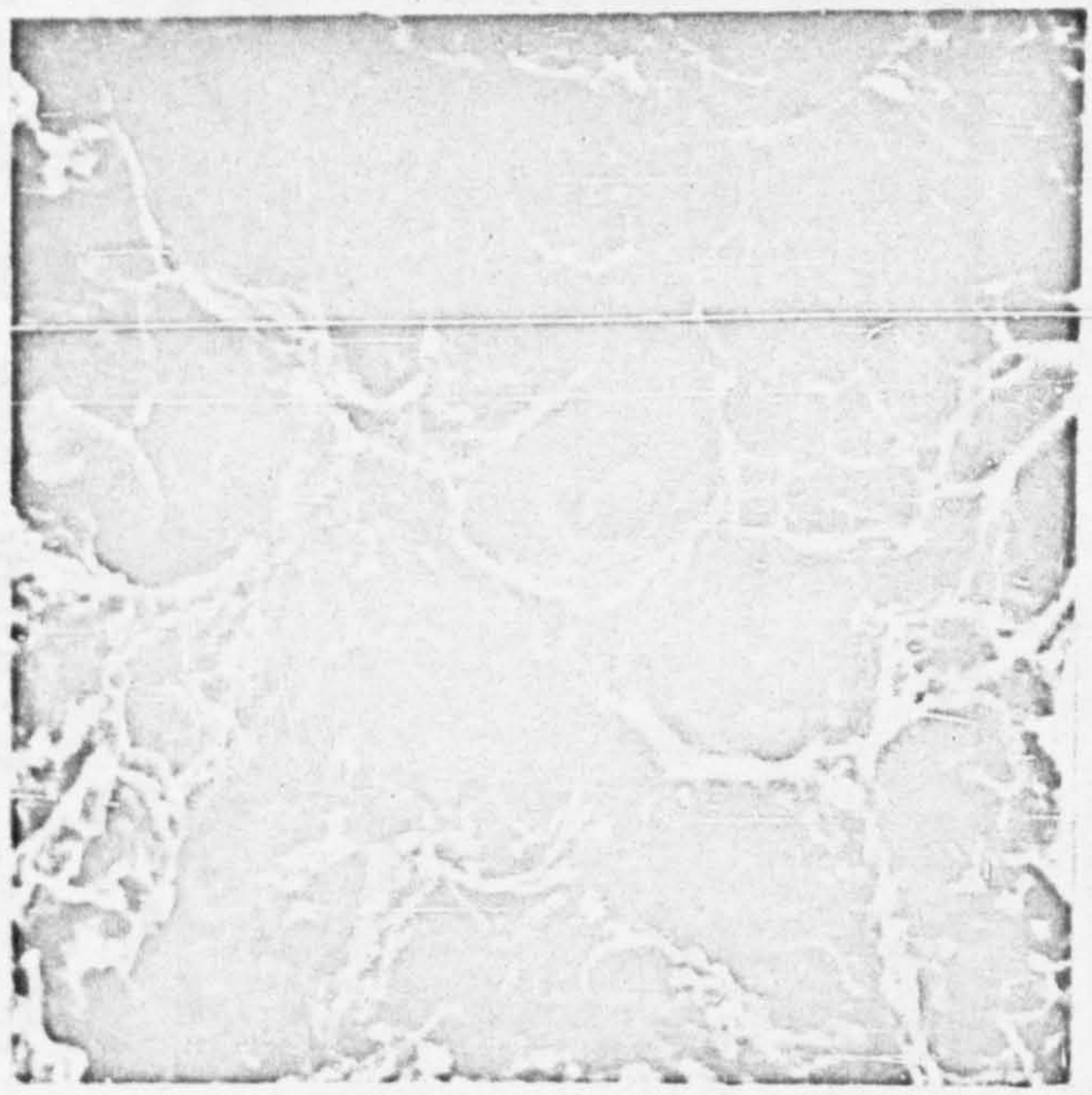

Fig.85. Alloy A Cast+50hrs./725°C Fractured 725°C in Slow Bend x1200

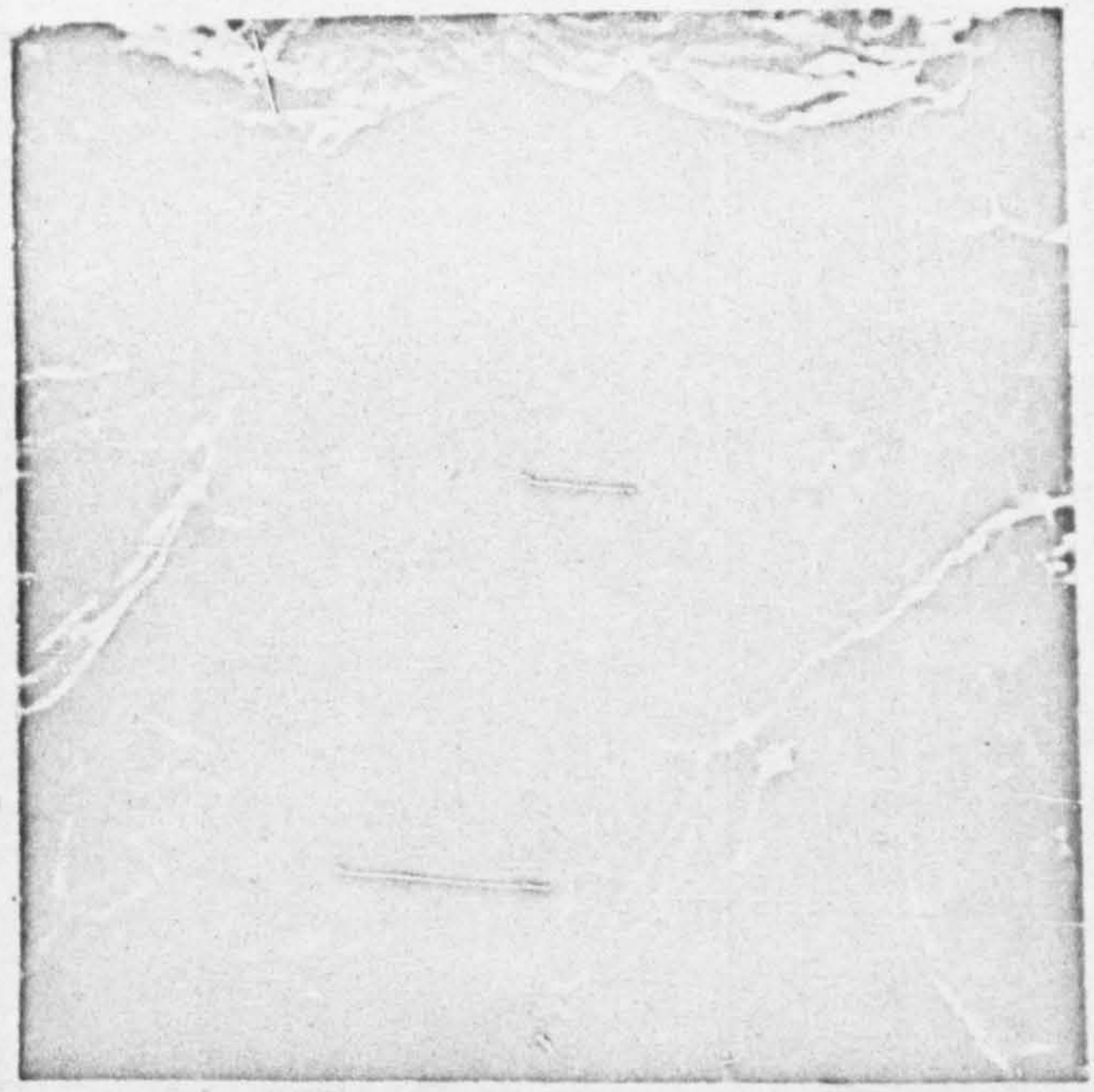

Fig.86. Alloy A Cast+50hrs./725°C Fractured 375°C in Slow Bend x700

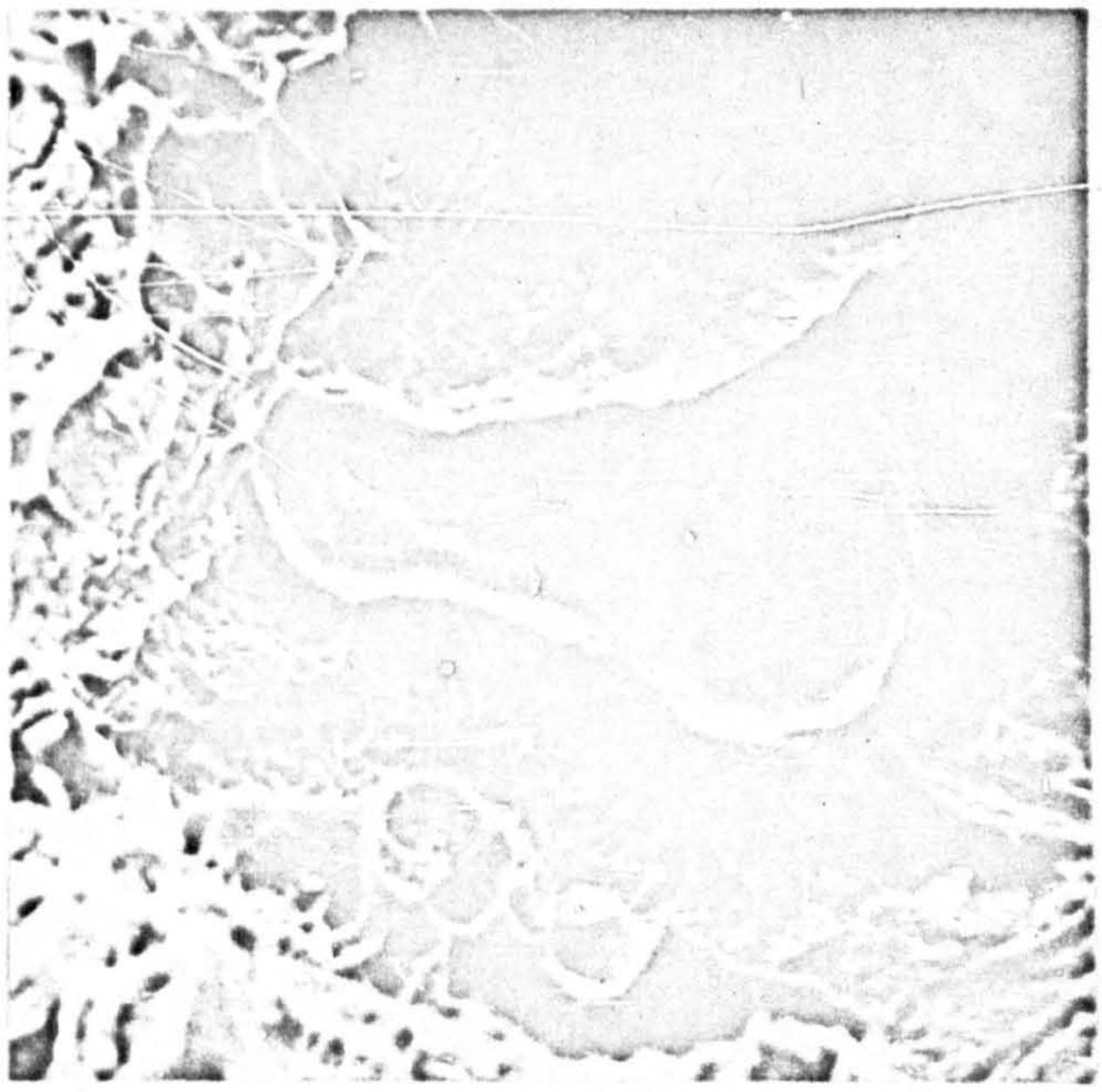

Fig.87. Alloy A Cast+50hrs./725°C Fractured 375°C in Slow Bend x700

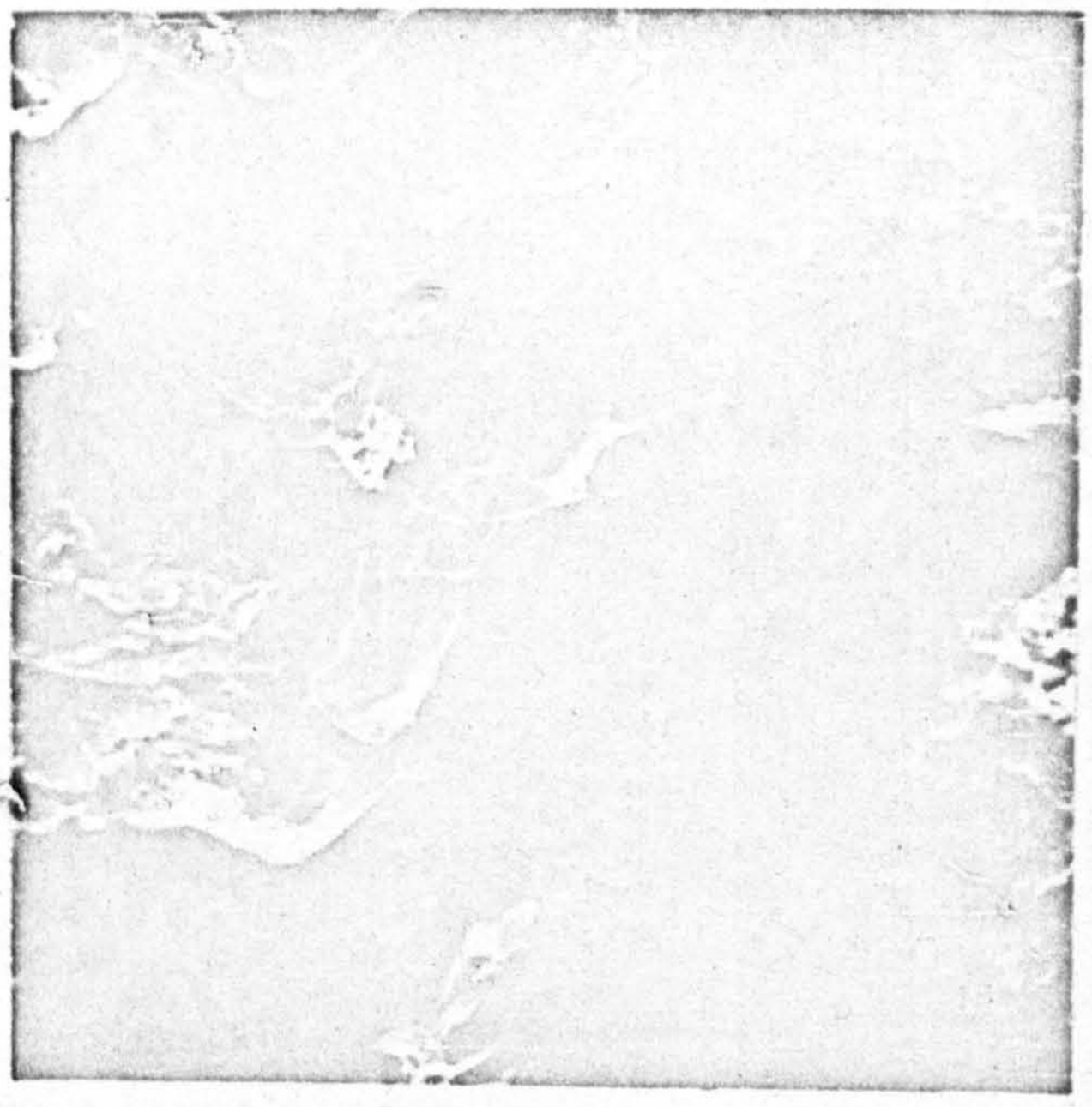

Fig.88. Alloy A Cast+50hrs./725°C Fractured 375°C in Slow Bend x280

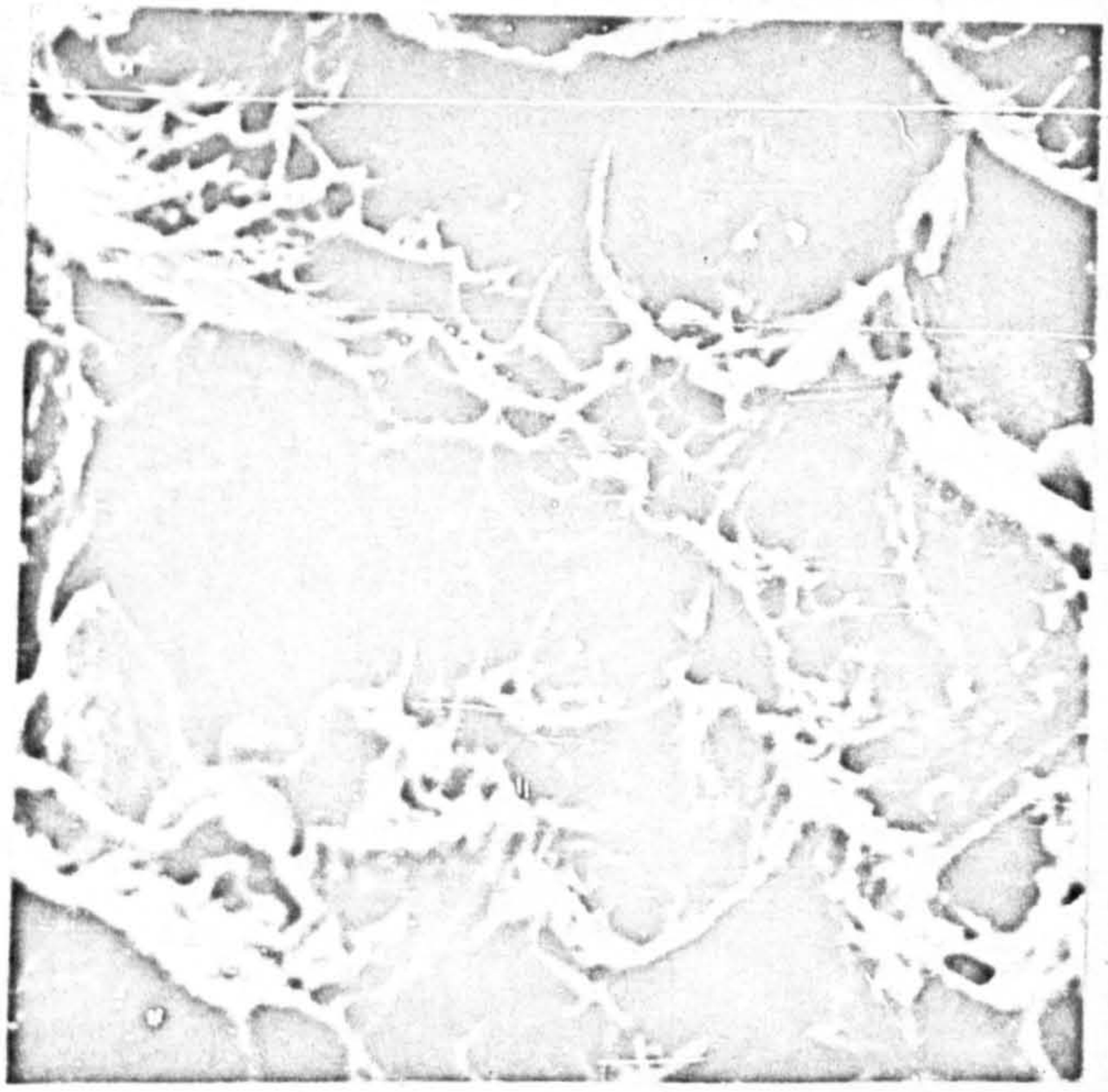

Fig.89. Alloy A Cast+50hrs./725°C Fractured 670°C in Slow Bend x650

Fig.90. Alloy B Cast+50hrs./725°C Fractured 500°C in Slow Bend x650

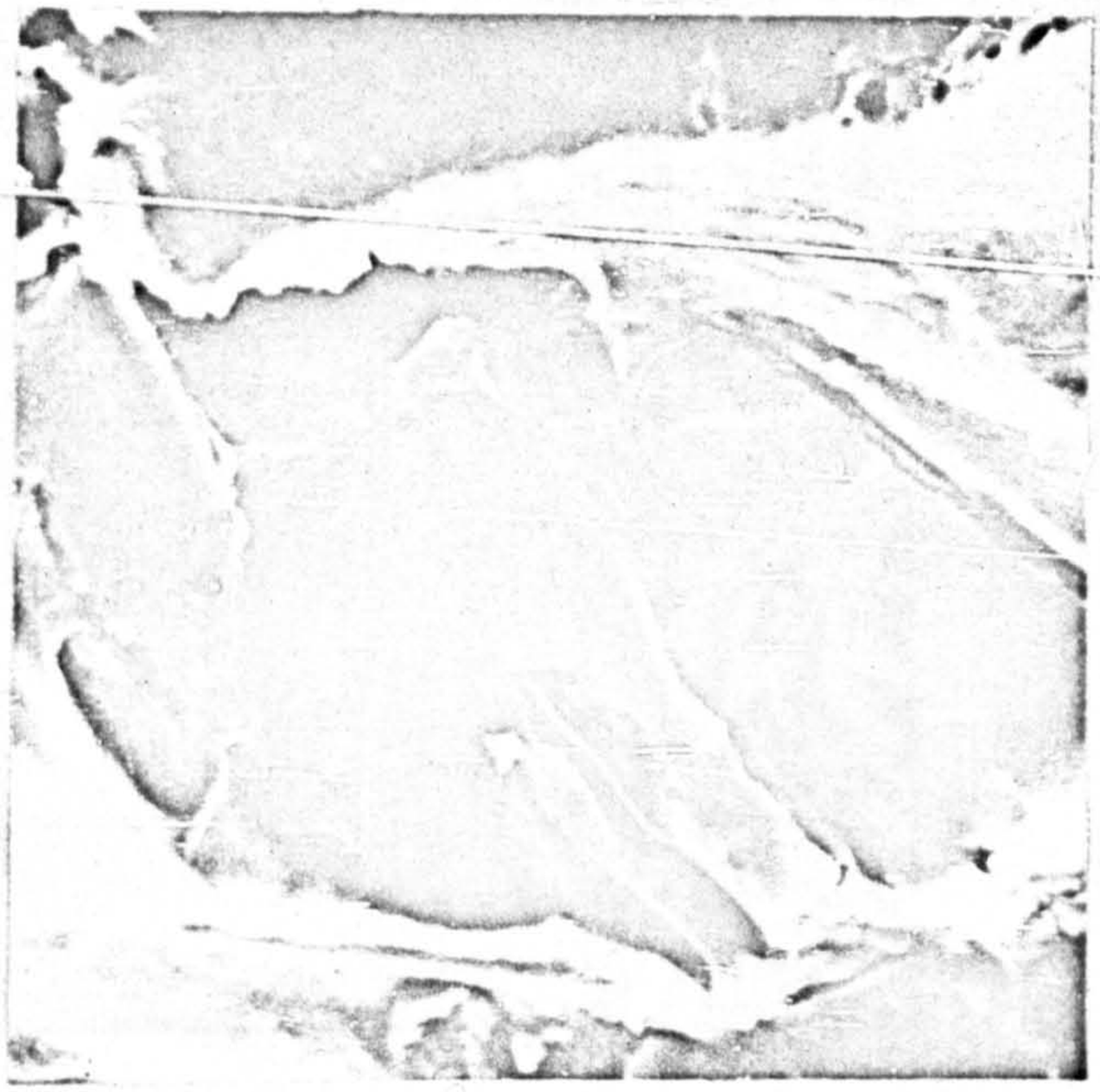

Fig.91. Alloy B Cast+50hrs./725°C Fractured 550°C in Slow Bend x1350

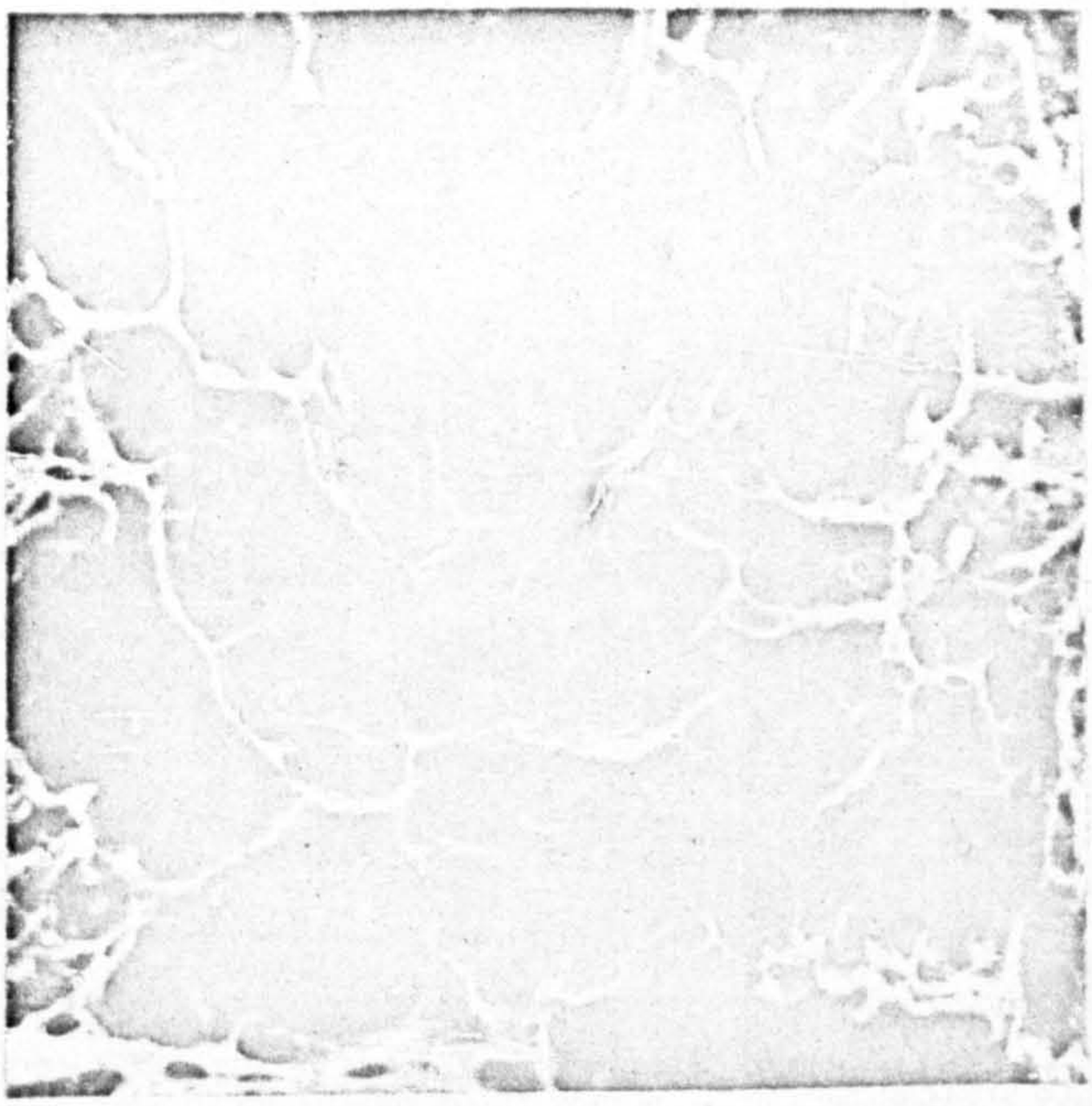

Fig.92. Alloy A Forged+50hrs./725°C Fractured 550°C in Slow Bend x1250

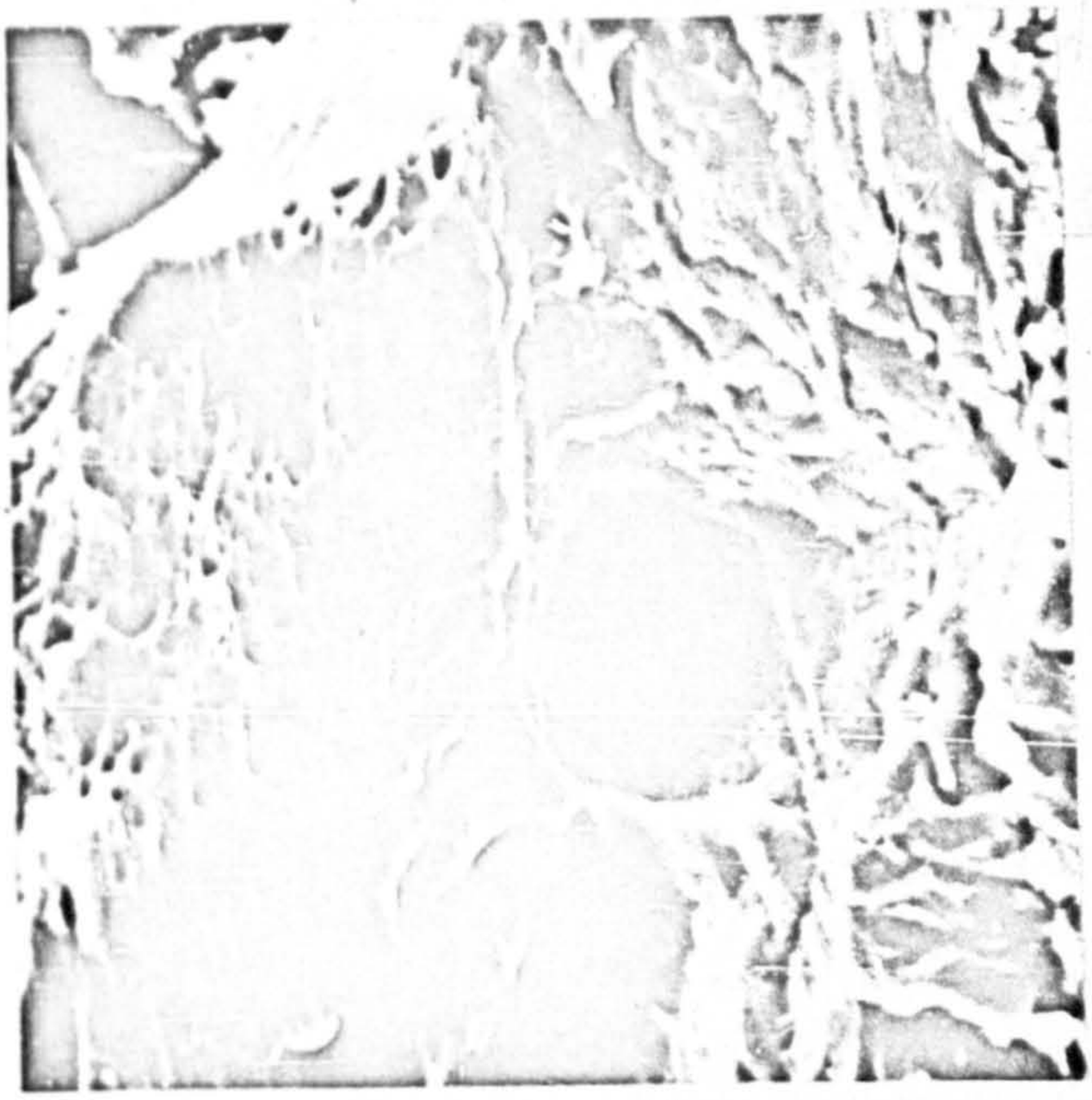

Alloy B Cast+50hrs./725°C
Fig.93. Fractured 500°C in Slow Bend x1300

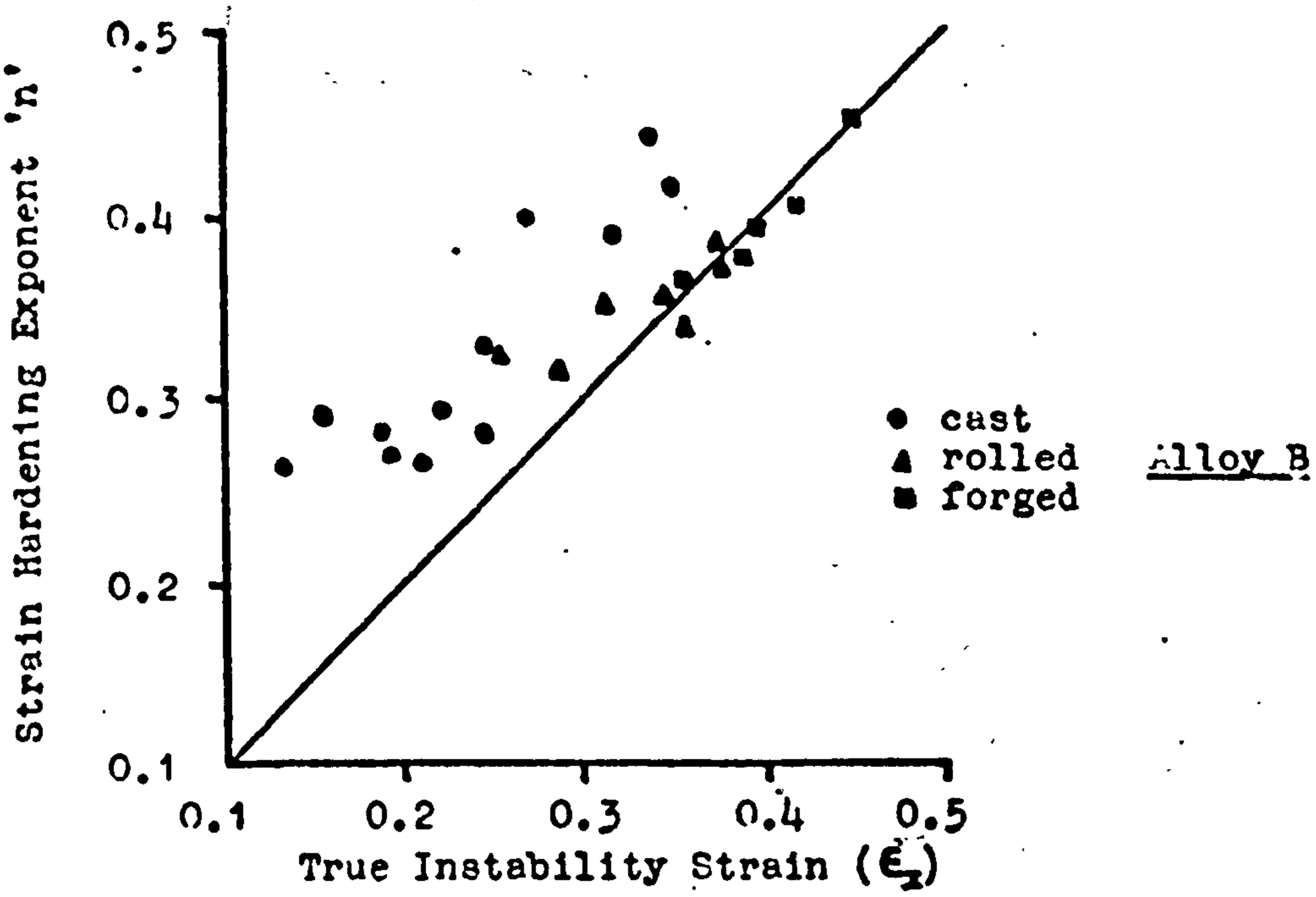

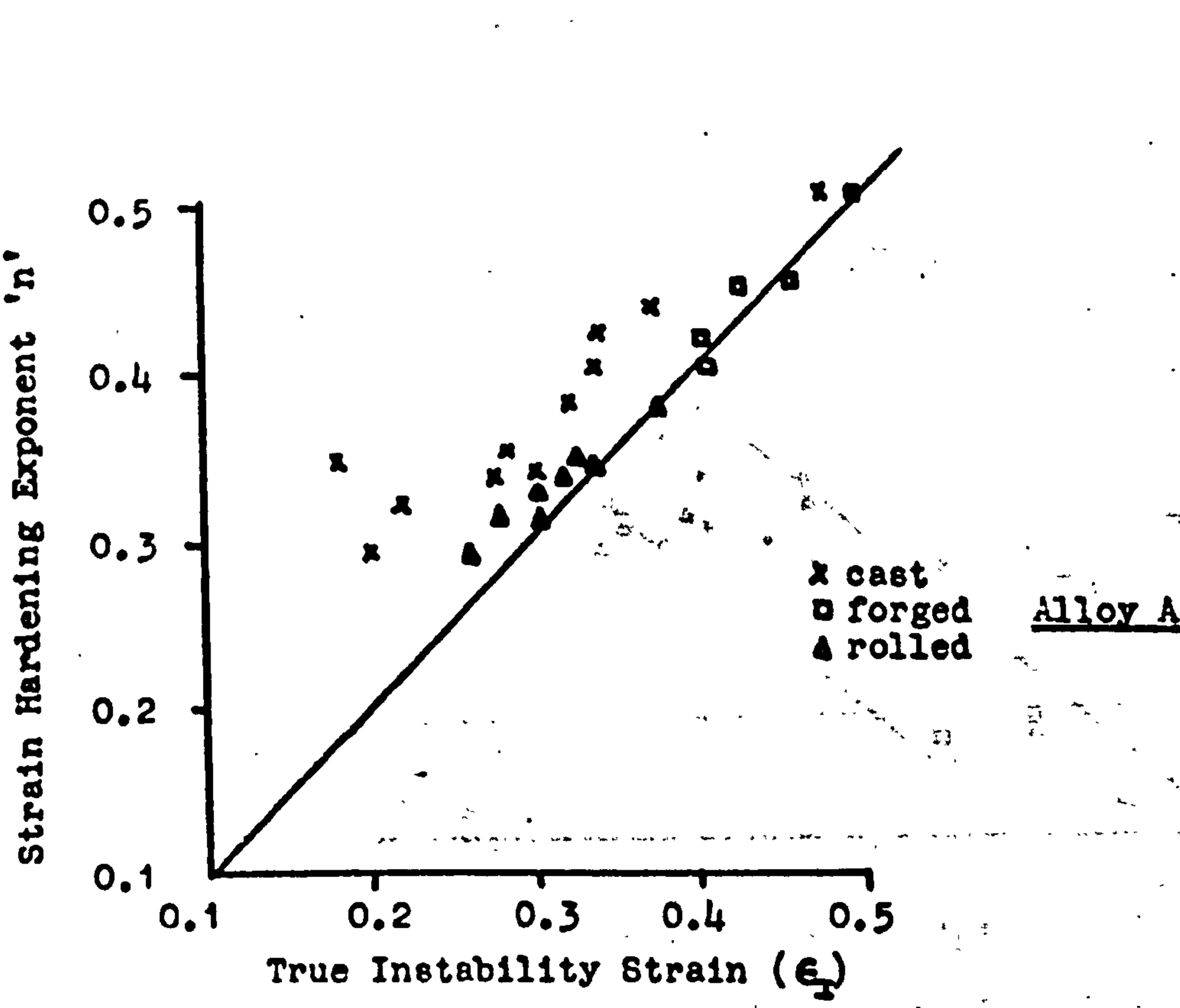

Fig 94. Effect of Manufacturing Process on the Discrepancy Between Strain Hardening Exponent and True Strain at Instability.

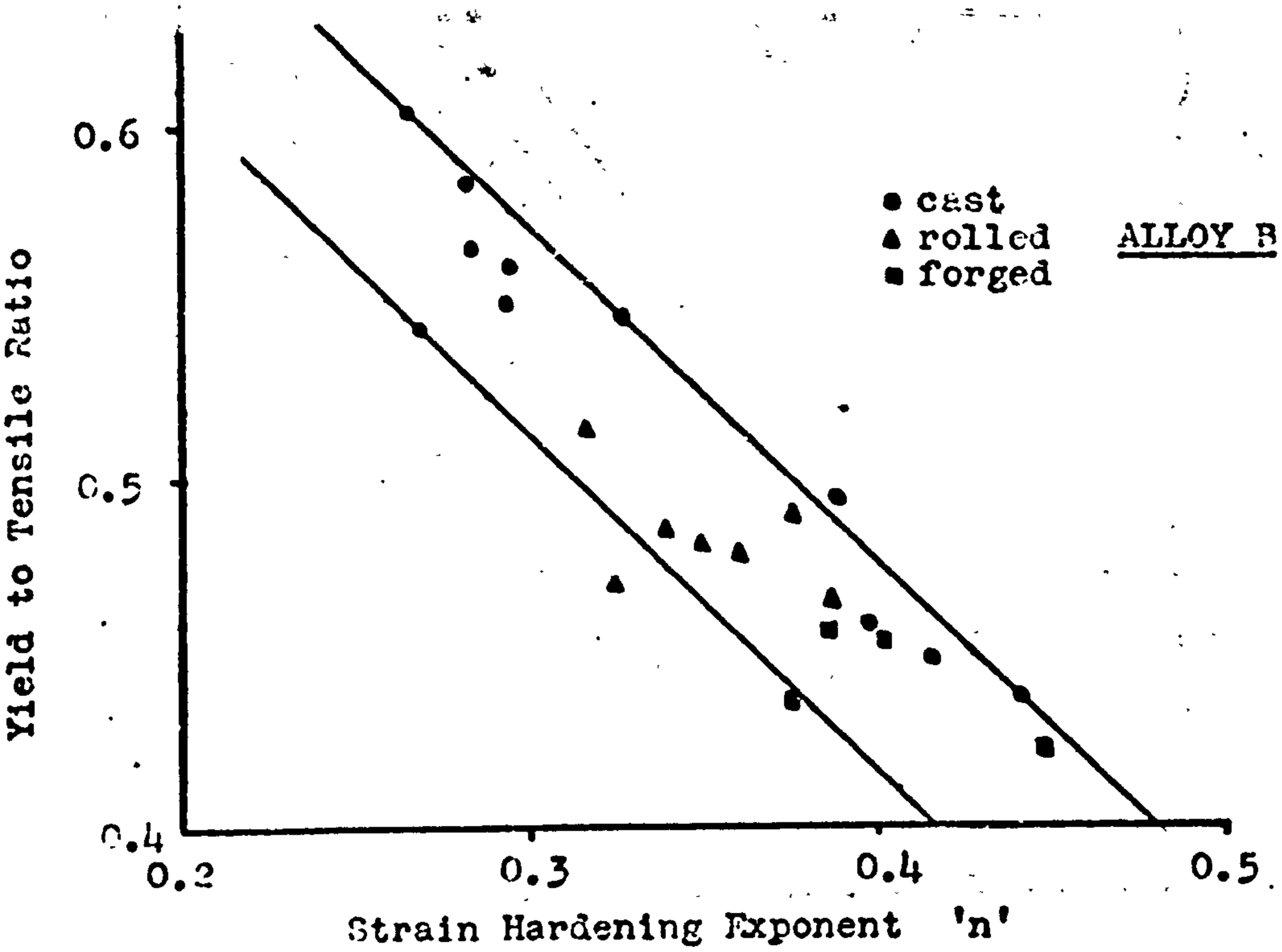

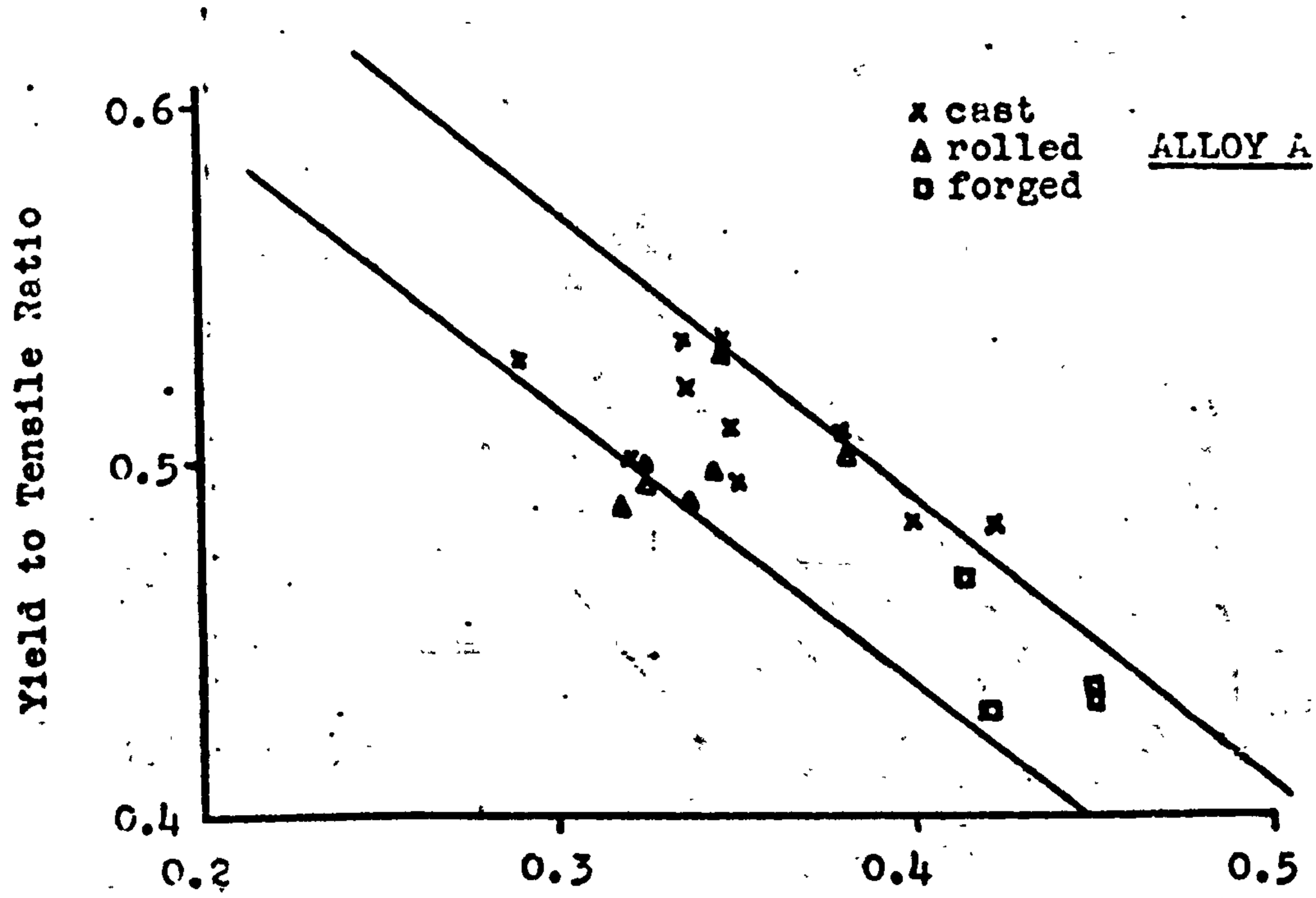

Fig 95. Relationship Between Yield to Tensile Ratio and Strain Hardening Exponent.

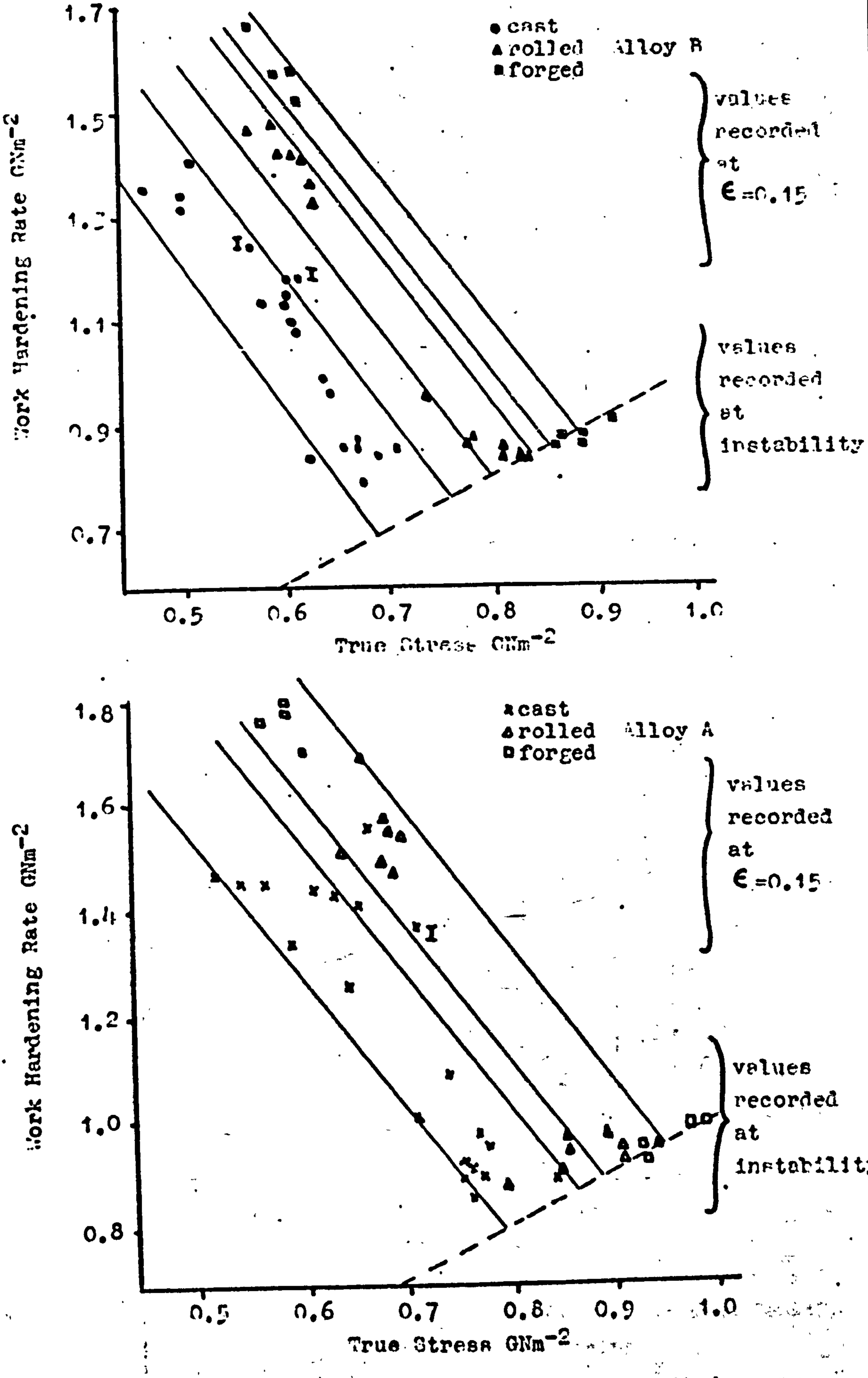

Figs 96 & 97. Effect of Manufacturing Process on Work Hardening Rate at 25°C.

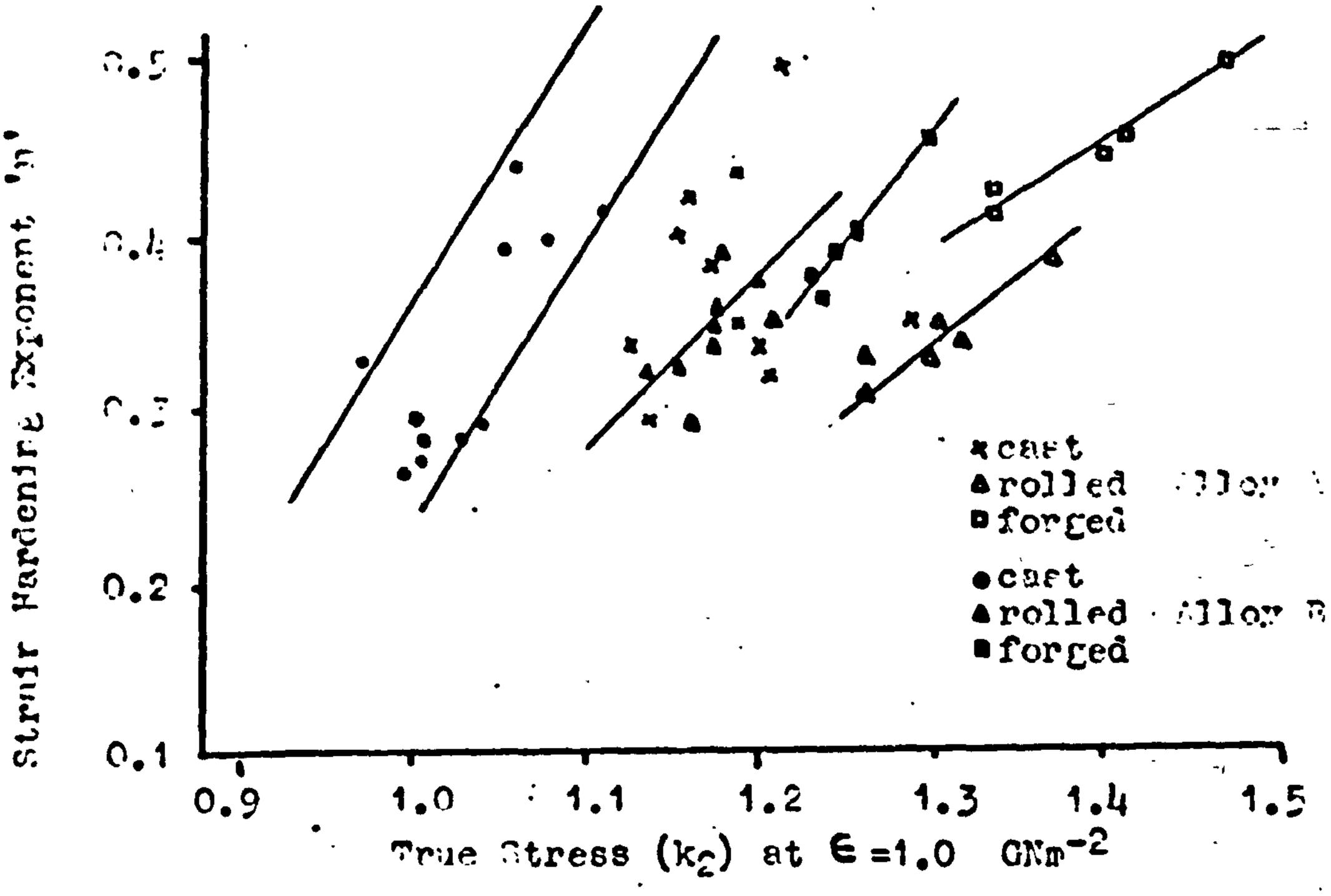

Fig 98. Variation of Strain Hardening Exponent with k_2 as a Function of Microstructure.

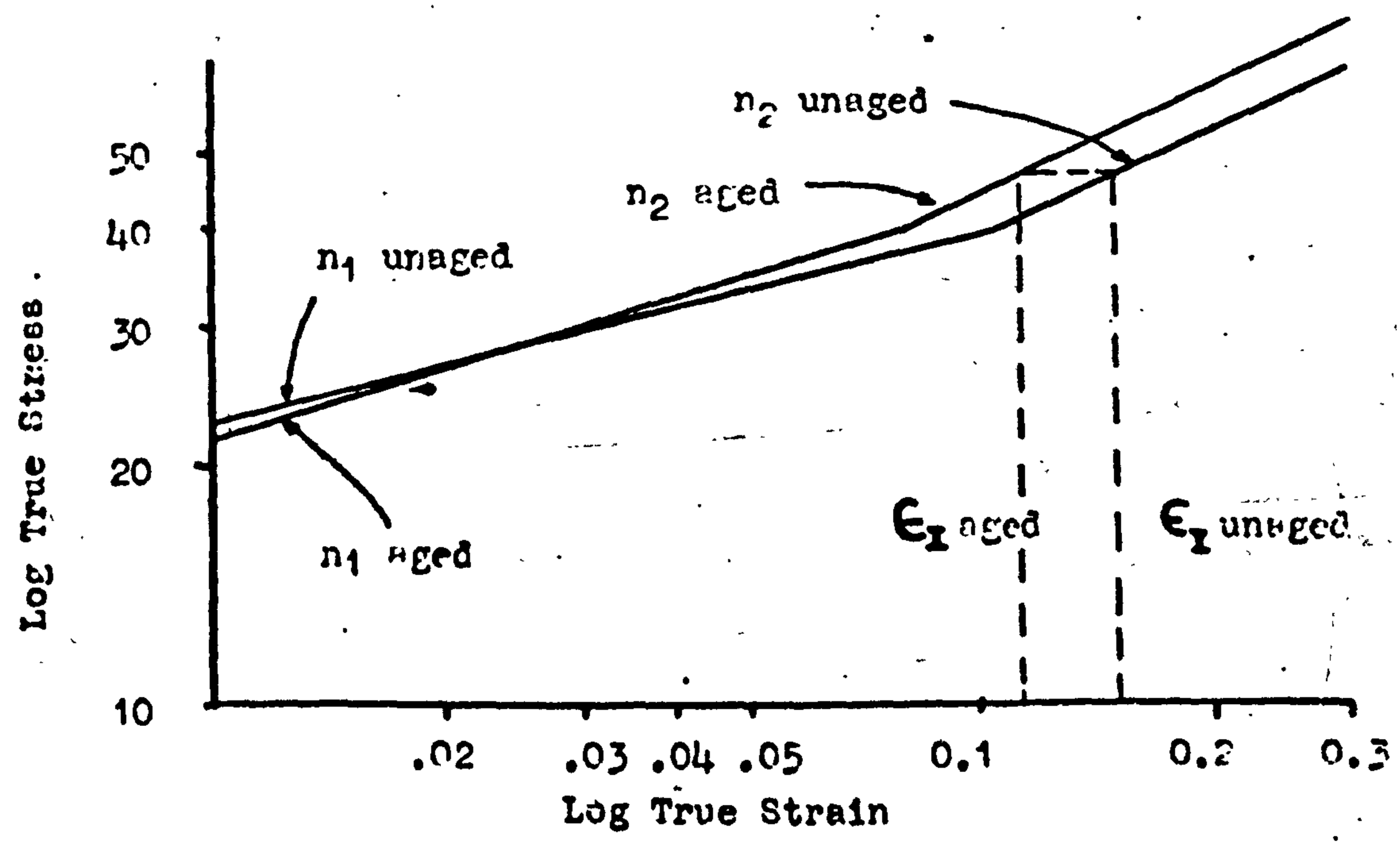

Fig 99. Effect of Double-'n' Behaviour in Reducing Instability Strains and Work Hardening Rates for Constant Tensile Strength after Ageing